UNIVERSITA' DEGLI STUDI DI PADOVA

Sede Amministrativa: Università degli Studi di Padova

Dipartimento di Principi e Impianti di Ingegneria Chimica “I. Sorgato”

SCUOLA DI DOTTORATO DI RICERCA IN INGEGNERIA INDUSTRIALE
INDIRIZZO: INGEGNERIA CHIMICA
CICLO XXI

TITOLO TESI

DESIGN AND DEVELOPMENT OF MICROSCALE TECHNOLOGIES AND MICROFLUIDIC PLATFORMS FOR THE IN VITRO CULTURE OF STEM CELLS

Direttore della Scuola: Ch.mo Prof. Paolo Bariani
Supervisore: Ch.mo Prof. Nicola Elvassore
Co-Supervisore: Ch.mo Prof. Gordana Vunjak-Novakovic

Dottoranda: Elisa Cimetta

Table of contents

Sommario

Le impellenti necessità legate allo sviluppo di nuovi farmaci e di terapie innovative per la cura di malattie dell'apparato muscolare, quali ad esempio la Distrofia Muscolare di Duchenne o l'infarto miocardico, hanno portato alla crescente domanda di nuovi metodi e tecnologie. E' chiaro inoltre come le cellule staminali possano costituire una risorsa fondamentale per la generazione di tessuti umani artificiali da impiegare in tali processi. Tale prospettiva, richiederebbe da un lato strumenti sofisticati per il controllo e il differenziamento delle cellule staminali e dell'altro, l'integrazione di questi all'interno di procedure in grado di soddisfare i requisiti fondamentali dei modelli sui quali operare per lo sviluppo di nuovi farmaci o strategie terapeutiche. Tra i requisiti fondamentali da rispettare si citano quindi: micronizzazione, versatilità, basso costo e highthroughput.

Obiettivo fondamentale di questa tesi sono stati la progettazione, sviluppo e fabbricazione di tecnologie su scala micrometrica in grado di riprodurre una stimolazione biomimetica ispirata al microambiente cellulare *in vivo* e, nello stesso tempo, di rispondere ai requisiti tecnologici descritti sopra.

E' stata effettuata un'analisi semi quantitativa basata sull'analisi dei tempi caratteristi dei fenomeni su microscala, che ha portato alla produzione di diagrammi operativi da impiegarsi nelle fasi di progettazione e sviluppo di tali strategie sperimentali. Sono stati sviluppati microbioreattori all'interno di piattaforme microfluidiche applicate poi allo studio di sistemi cellulari. In particolare, sono stati effettuati studi biologi sull'effetto di gradienti di concentrazione all'interno dell'importante signaling cellulare del Wnt.

E' stata realizzata una tecnica per l'organizzazione topologica su microscala di colture cellulari su substrati in hydrogel dalle proprietà meccaniche definite. Le tecnologie sviluppate sono state impiegate per casi studio dall'elevato valore scientifico e sono state interfacciate con colture di particolare interesse quali mioblasti umani distrofici e cellule cardiache derivate da staminali embrionali umane.

Infine, è stato proposto un prototipo di piattaforma microfluidica in grado di accoppiare le stimolazioni di tipo topologico al controllo dell'ambiente solubile su colture cellulari.

I risultati ottenuti aprono nuove ed interessanti prospettive sia per lo sviluppo di nuovi farmaci che di strategie terapeutiche volti alla cura di patologie ed allo studio approfondito della complessità dei sistemi biologici.

Introduzione

Al giorno d'oggi, molti sforzi sono rivolti allo sviluppo di terapie e farmaci innovativi per la cura di specifiche malattie. La strada che porta i benefici di questa ricerca al paziente è lunga e irta di ostacoli, ed il cosiddetto passaggio "*from bench to bed*" non è mai immediato. Un'altra limitazione è data dal fatto che il processo per lo sviluppo di nuovi farmaci o terapie deve rispondere a rigide regolamentazioni ad affrontare costi estremamente elevati per un lungo periodo di tempo e senza la certezza di successo.

In quest'ottica, l'implementazione di metodi innovativi che possano ridurre i tempi e i costi per lo sviluppo di nuovi farmaci, nonché facilitare il processo decisionale all'interno di tali processi, risulta estremamente rilevante e desiderabile. Un primo passo in tale direzione potrebbe essere l'adottare tecniche quali screening "highthroughput" ed una gestione automatizzata dei dati.

Al contempo, è emerso con sempre maggiore importanza come i test basati sull'utilizzo di cellule umane come elemento sensibile possano essere uno strumento fondamentale per studiare in modo rapido e rilevante l'effetto di determinate sostanze su di un campione che possa effettivamente essere rappresentativo di una determinata condizione patologica. Tuttavia, le metodologie standard di coltura cellulare si distaccano drammaticamente da quella che è la complessità dei tessuti naturali *in vivo* e possono per tale motivo dare dei risultati fuorvianti e non predittivi di quelle che possono essere le effettive risposte del sistema reale.

Per tale motivo, le tecnologie innovative sviluppate negli ultimi anni cercano di imitare il più da vicino possibile il naturale microambiente cellulare questo si effettua attraverso un accurato controllo e l'imitazione delle complesse cascate di segnali regolatori che si riscontrano *in vivo* seguendo il cosiddetto "approccio biomimetico", una nuova prospettiva attraverso la quale ottenere una visione più reale dei sistemi biologici.

Tale principio ha sotteso tutta la ricerca che si è effettuata durante questo dottorato, guidando il raggiungimento degli scopi principali, focalizzati al tentativo di mimare la nicchia staminale e raggiungere un elevato grado di controllo sui sistemi biologici studiati. Nel pieno rispetto di ciò, siamo stati focalizzati alla progettazione e realizzazione di

tecnologie *ad hoc* per la produzione di piattaforme da essere impiegate all'interno di processi di screening farmacologi o per lo sviluppo di terapie innovative.
Tali piattaforme devono soddisfare a molteplici requisiti, tra i quali:

- ricreare il microambiente cellulare;
- essere integrabili con sistemi biologici di elevata rilevanza;
- avere caratteristiche "highthroughput";
- consentire un elevato controllo sulla microscala;
- essere miniaturizzati.

Questi ultimi aspetti assumono una particolare importanza in quanto la miniaturizzazione ed il controllo sulla microscala sono stati un tema comune di tutta la ricerca che è stata qui sviluppata.

Nel primo capitolo verrà presentato lo stato dell'arte sull'utilizzo di tecnologie innovative per la coltura e lo studio di cellule staminali, con una particolare attenzione alla rilevanza biologica della fonte cellulare e alle limitazioni delle tecnologie esistenti.

Nel secondo capitolo verrà presentata una razionalizzazione attraverso un approccio matematico dei principali fenomeni, delle variabili in gioco e della loro relativa importanza, all'interno dei sistemi che si andranno poi a sviluppare.

I capitoli 3 e 4 presenteranno invece le tecniche e apparecchiature che sono state sviluppate e prodotte all'interno di questo studio. Avranno una struttura simile, presentando lo stato dell'arte sull'argomento specifico, ed approfondendo i casi studio più rilevanti con attenzione alle loro motivazioni, metodi e risultati principali. In particolare, il capitolo 3 sarà incentrato sullo sviluppo di strategie per ottenere un controllo topologico del microambiente e sull'ottimizzazione del substrato per le colture cellulari. Il capitolo 4 invece presenterà in dettaglio i risultati relativi alle applicazioni in campo microfluidico.

Il capitolo 5 infine, descriverà le potenzialità di una piattaforma integrata che fornisca sia il controllo topologico che la microfluidica. Verrà presentato un primo caso studio e saranno discusse le sue limitazioni. In conseguenza a ciò, proporremo un nuovo sviluppo che si presenta come soluzione tecnologica alle limitazioni emerse. Tale soluzione tecnologica verrà presentata con un prototipo di piattaforma integrata e dalla sua validazione.

I principali risultati degli studi effettuati sono rappresentati dalle 7 pubblicazioni riportate nelle appendici e dai 2 lavori in fase di sottomissione inclusi.

Summary

The impelling needs related to the processes of drug and therapy development for the cure of diseases such as Duchenne Muscular Dystrophy or myocardial infarction, led to an increasing demand for the development of innovative methods and strategies. It is also clear how stem cells could represent a fundamental source for the production of artificial human tissues to be employed in such processes. This perspective, would require both sophisticated tools for the control of stem cells differentiation and their integration within procedures apt to satisfy the fundamental requirements for obtaining tissue-model on which perform pharmacological or therapeutic studies. Among the fundamental requisites are: micronization, versatility, low-cost and highthroughput.

The main aims of this thesis have been the design, development and fabrication of microscale technologies capable of both reproducing a biomimetic stimulation inspired to the *in vivo* cell microenvironment and responding to the above mentioned technological requirements.

We performed a semi-quantitative analysis of the characteristic times of microscale phenomena that lead to the generation of operative diagrams that would prove useful in the design and development phases of experimental strategies. We developed microfluidic microbioreactors that have been used for biological studies involving cell cultures. In particular, we investigated the role and effect of concentration gradients on the fundamental Wnt signaling pathway.

We developed techniques for obtaining a topological control at the microscale of cell cultures on hydrogels with tunable mechanical properties. These techniques were successfully applied and interfaced with relevant biological systems such as primary human myoblasts from dystrophic patients and human embryonic stem cells-derived cardiomyocytes.

We finally proposed a prototype of an integrated microfluidic platform capable of coupling the topological stimulations to the control of the soluble microenvironment on cell cultures.

The obtained results open new and interesting perspectives for both de efficient development of drugs or therapies for defined diseases and for gaining deeper insights into the complexity of biological systems.

Introduction

Nowadays, huge efforts are invested in trying to develop novel therapies and drugs to treat specific diseases. In order to bring benefit to the final end user -the patient-, the road is long and steep, and the so-called translation “from bench to bed” is never easy. The process of development of new therapeutic strategies is characterized by many specific requirements and by high costs incurred over a period of several years before even having any feedback on their potential success or failure.

Within this scenario, there is a great interest in implementing innovative methods that would reduce the development times and costs, and would facilitate the processes of decision−making giving more insight into the studied processes themselves. A first step in this direction would be to adopt technologies such as highthroughput screenings and electronic data acquisition.

In parallel, it has emerged that primary human cell systems and cell-based testing can be both a valuable tool to quickly explore toxic and non functional compound and a representative model of human disease biology. However, the traditional cell models are dramatically different from the complex functional tissues *in vivo* and may give unsatisfactory, misleading and non-predictive data for the actual response.

For this reason, novel cell culture technologies developed in recent years try to mimic *in vitro* the *in vivo* cellular microenvironments with an increasing fidelity, through improved control and provision of cascades of multiple regulatory factors. This is the so-called “biomimetic approach”, a new perspective through which gain a closer view of biological systems.

All the work that has been performed in this study was sustained by this principle, and the attention paid at the goal of mimicking the stem cell niche and controlling biological systems with a biomimetic approach have always been primary aims. In the respect of these aspects, we focused on the design and development of *ad hoc* techniques and technologies for the production of platforms to be used in drug screening processes and therapy development.

Such technology platforms must respond to many specific requirements, the main of which can be summarized in:

- recapitulating the cell microenvironment;
- allowing interface with relevant biological systems;
- possessing highthroughput characteristics;
- allowing control at the microscale level;
- being miniaturized.

These last aspects are of particular relevance, as miniaturization and microscale-control will be a common theme for all the technology development that will be described here.

Chapter 1 will review the state of the art with regards to the use of advanced technologies for stem cell culture, with particular attention to the biological relevance of the cell sources and to the current limitations and technology perspectives.

Chapter 2 will present a rationalization of the potential applications of the techniques that will be developed; a mathematical approach will help understanding the variables and the main phenomena in the system and their relative importance.

Chapter 3 and 4 will describe the techniques and devices that have been developed in this study. They will both briefly describe the state of the art and then treat the most relevant case studies with their motivations, methods and main results. Chapter 3 will be focused on the development of strategies for the topological control of the microenvironment and the optimization of the substrates for our cell cultures. Chapter 4 will treat in detail the achievement reached within the field of microfluidics.

Chapter 5, finally, will describe the potentialities of an integrated device comprising the two individual components (topological control and microfluidics) that have been described above. A first case study will be presented and its limitations discussed. The second and last part will present the technology developments that promise to be the technical solution to the previously mentioned limitations. This technical solution is presented as a prototype of an integrated platform and by its validation.

The main achievements of the performed studies are represented by the 7 published papers (6 research articles and a congress report) reported in the Appendixes. In addition, two other papers to be soon submitted are enclosed.

Foreword

After these three years of intense research, I am well aware of the priceless opportunity that I've been given. I've learned how to exploit the engineering tools in a variety of problems, and to specifically apply them in sought of improvements in the field of biomedical research. I thus gratefully acknowledge my supervisor, Prof. Elvassore, for giving me this chance and always believing in me, and my co-supervisor Prof. Vunjak-Novakovic, for the great opportunity of working in her laboratory.

The work of this PhD program was performed at the Department of Chemical Engineering Principles and Practice "I. Sorgato" of Padua University. Part of the experimental section was carried out at the Department of Biomedical Engineering of Columbia University.

The author is grateful to Fondazione Cariparo, Ministero Italiana dell'Università e della Ricerca (MIUR), Università di Padova, Regione Veneto for Azione Biotech II and III, Città della Speranza and Telethon for the financial support to the research activity and to Columbia University for the financial support of the research activity abroad.

During this PhD program the following publications have been produced:

1. E Cimetta, E Figallo, C Cannizzaro, N Elvassore, G Vunjak-Novakovic. "Micro-bioreactor arrays for controlling cellular environments: Design principles for human embryonic stem cell applications". Tissue Engineering: Methods. 2009 47: 81–89.

2. E Cimetta, S Pizzato, S Bollini, E Serena, P De Coppi, N Elvassore. "Production of arrays of cardiac and skeletal muscle myofibers by micropatterning techniques on a soft substrate". Biomed Microdevices. 2008 Nov 6. [Epub ahead of print].

3. E Cimetta, M Flaibani, M Mella, E Serena, L Boldrin, P De Coppi, N Elvassore. "Enhancement of viability of muscle precursor cells on 3D scaffold in a perfusion bioreactor". Int J Artif Organs. 2007 May;30(5):415-28.

4. M Flaibani, L Boldrin, E Cimetta, M Piccoli, P De Coppi, N Elvassore. "Muscle differentiation and myotubes alignment is influenced by micro-patterned surfaces and exogenous electrical stimulation". In press on Tissue Eng.

5. L Boldrin, A Malerba, L Vitiello, E Cimetta, M Piccoli, C Messina, PG Gamba, N Elvassore, P De Coppi. “Efficient delivery of human single fiber-derived muscle precursor cells via biocompatible scaffold”. Cell Transplant. 2008;17(5):577-84.

6. L Boldrin, N Elvassore, A Malerba, M Flaibani, E Cimetta, M Piccoli, D Baroni, C Messina, PG Gamba, L Vitiello, P De Coppi. “Satellite cells delivered by micro-patterned scaffolds: a new strategy for cell transplantation in muscle diseases”. Tissue Eng. 2007 Feb;13(2):253-62.

7. E Serena, E Cimetta and M Zagallo. “Financing for research on embryonic stem cells: The situation in Italy and its origins” Report on 3rd Italian National Congress of the Group of Italian Researchers on Embryonic Stem Cells (IES Group) Rome, 1st July 2008. Notizie di Politeia. Rivista di Etica e Scelte Pubbliche” Vol. 91/Anno XXIV, 2008, pp. 110-113.

Numerous abstracts were submitted to several international conferences during the PhD program, including: The American Institute of Chemical Engineers (AIChE), Biomedical Engineering Society (BMES), Keystone Symposia, Tissue & Cell Engineering Society (TERMIS-EU), International Society for Stem Cell Research (ISSCR).

In addition, the following works are being considered for publication:

a. E Cimetta, S Cagnin, A Volpatti, G Lanfranchi, N Elvassore. “Dynamic culture of bubble-confined cell arrays”. Submitted to Biotechnology Progress.

b. E Cimetta, C Cannizzaro, R James, RT Moon, G Vunjak-Novakovic, N Elvassore. “Microfluidics-generated Wnt3a gradients induce a proportionate response in β-catenin signaling in HEK cells”. To be submitted to Langmuir.

Chapter 1
Advanced technologies for stem cell culture

After introducing the issue and importance of stem cells and of the research activity in this field, this chapter will review the fundamental technologies for stem cell culture, highlighting the current limitations and thus introducing the technology perspective that guided the work that has been done and that will be presented in the following chapters.

1.1 Stem cells

The international scientific community and the whole society recognize huge potentiality to the applications of stem cells for disease therapy. Over the past several decades a number of highly successful treatments employing stem cells (in particular haematopoietic stem cells (Goldstein et al. 2006, Gussoni et al. 1999)) have been developed.

The main properties defining stem cells are (Orkin and Morrison 2002, Watt and Hogan 2000):

- the potential to produce more stem cells for their unlimited or prolonged self-renewal;
- the potential to differentiate generating highly specialized cell types (plasticity).

Usually, between the stem cell and its terminally differentiated progeny there are intermediate populations of committed progenitors with a limited capacity for proliferation

and a more restricted differentiation potential. In Figure 1.1 is reported an exemplifying schematization (adapted from a NIH report) highlighting the plasticity of bone marrow-derived stem cells.

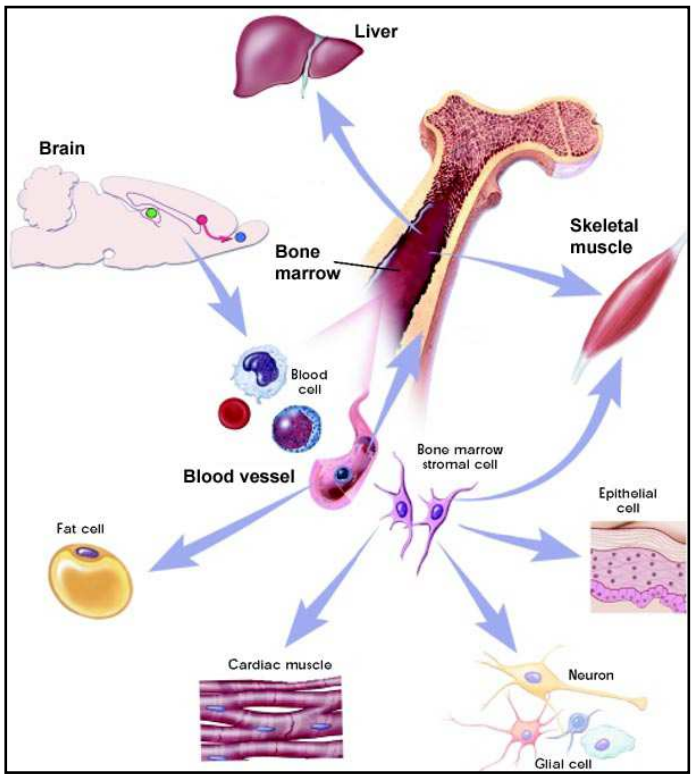

Figure 1.1. *Schematic representation of stem cell plasticity. Adapted from NIH report.*

Until recently, it was thought that tissue-specific stem cells could only differentiate into cells of the tissue of origin; however, recent studies suggested that tissue-specific stem cells can differentiate into lineages other than the tissue of origin (Jiang et al. 2002).

Stem cells come in different varieties, relating to when and where they are produced during development and where they reside within tissues. Stem cells are also present in tissues that normally undergo very limited regeneration or turnover, such as the brain and liver.

This huge attention on stem cells related issues, has revealed gaps in our knowledge, especially for what concerns the proper culture techniques. Consequently, in order to be able to fully exploit the potential of such cells for treating degenerative diseases such as Parkinson's disease and muscular dystrophy, we need to fill those gaps.

What thus emerges, is a strong need for gaining insights into the intrinsic and extrinsic mechanisms that control stem cells fate (i.e. maintain their undifferentiated state or direct

them along particular differentiation pathways). Such mechanisms are strictly dependent on the microenvironment, or niche, where stem cells normally reside, as we will more deeply discuss in the following sections.

1.1.1 Adult and embryonic stem cells

Stem cells also exist in most tissues of adult organisms. However, some limitations in the above mentioned potentials exists.

Stem cells collected from tissues of adults or older embryos are typically more restricted in their developmental potential and ability to proliferate, if compared with embryonic cells. For this reason, much attention has been lately focused on studying the behavior and potential application of embryonic cells.

Embryonic stem cells (ESC) are pluripotent stem cell lines that have the potential to give rise to every cell type in the body. ESCs are derived from the inner cell mass (ICM) cells of the blastocyst at a pre-impantation stage in the developing mammalian embryo. The outer layer of the blastocyst, the trophoectoderm, is removed and the ICM cells isolated; such cells are then plated on a mitotically inactivated mouse embryonic fibroblast (MEF) feeder layer where they form colonies, which are then selected, passaged, and expanded (Figure 1.2 A). The first derivation of mouse ESC (mESC) is dated 1981 (Evans and Kaufman 1981, Martin 1981), while the first human ESC (hESC) line was obtained years later, in 1998 (Thomson et al. 1998). These human cell lines were derived from the ICM of the blastocysts of human embryos, generated by *in vitro* fertilization (IVF) for clinical purposes, and donated by individuals after informed consent and after institutional review board approval.

When removed from the MEF feeder layer and cultivated in suspension, hESC tend to spontaneously form three-dimensional differentiating cell clusters (Figure 1.2B) named embryoid bodies (EBs), which contain cell derivatives of endoderm, mesoderm, and ectoderm origin (Andrews and al. 2005). The proof of this property opened new and promising perspectives in fields such as developmental biology, genomics, patho-physiological studies, drug screening and development. It worth underlying how many of the most common diseases (heart failure, neurodegenerative disorders, diabetes, etc.) result from cellular deficiencies or dysfunctions. In this sight, having the possibility of generating

relevant numbers of defined cell populations, may allow the development of novel cell therapies or, in parallel, to perform studies on specialized human cells that would permit the obtainment of more significant data aimed at the development of the necessary therapeutic strategies.

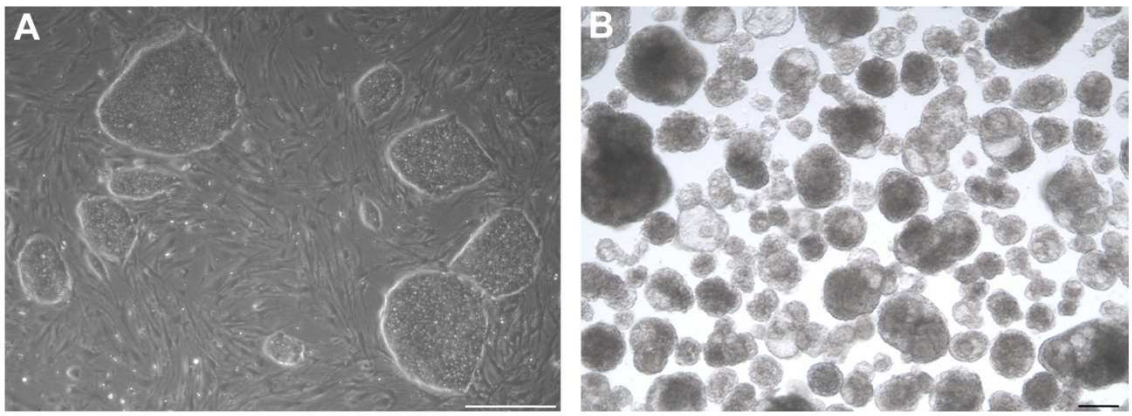

Figure 1.2. *Human embryonic stem cells in culture. In A: colonies adhering to a mouse embryonic fibroblasts (MEF) feeder layer. In B: embryoid bodies growing in suspension culture. Scale bars 500 µm.*

Nowadays, the number of hESC lines that have been derived has notably increased; in order to assess the similarities and differences in the expression of commonly used markers of hESC and to identify a set of well-validated markers to establish hESC identity of newly derived lines, the International Stem Cell Initiative (ISCI) (Andrews and al. 2005) was appointed by the International Stem Cell Forum the task to perform a comparative study of a large and diverse set of hESC lines (The-International-Stem-Cell-Initiative 2008). Such study identified lists of the most common markers of both pluripotency (undifferentiated state) and differentiation in terms of surface antigens and expressed genes that could be used to assess the properties of the cell line of interest.

The hESC lines that have been used in this study were purchased from the WiCell Research Institute (Madison, Wisconsin, USA) after filing all the required documentation and authorization, in complete accordance with the Italian legislation.

It is fundamental to underline how the Italian legislation with regards to the use of stem cells is defined by the 40/2004 law. This legislation forbid whatsoever experimentation on human embryos, human cloning, and on genetic alteration of human embryos. However, as it is forbidden to work on human embryos and directly derive cell lines from such embryos, it is possible to perform experimentations on cell lines that have been derived in other

countries. The confirmation of that came from the Italian *"Comitato Nazionale di Bioetica"* that expressed its approval within the *"European Centre for the Validation of Alternative Methods"*.

Interested on these bioethical debates, our research group actively participated to the 3rd Italian National Congress of the Group of Italian Researchers on Embryonic Stem Cells (IES Group) in 2008. The leading theme was: "Financing for research on embryonic stem cells: The situation in Italy and its origins"; our report of the event (Serena et al. 2008) has been published on the Italian journal "Notizie di Politeia. Rivista di Etica e Scelte Pubbliche" and on the newsletter for Estools (the largest grouping of human embryonic stem cell researchers in Europe). The complete report is in Appendix I.

1.1.2 Induced pluripotent stem cells (iPS)

The ethical issues centered on the use of embryos for the obtainment of human embryonic cells, have been a driving force towards the development of alternative strategies for obtaining similar and such powerful cells.

Since 2007 (Yamanaka 2007) researchers reported that they had found a possible way around the practical and ethical questions surrounding embryonic stem cells (ES). By introducing just four genes into somatic cells growing in a lab dish, they could produce cells that looked and acted very much like ES cells. They called these cells induced pluripotent stem (iPS) cells. The reprogramming technique was soon extended and adapted to human cells (Park et al. 2008a, Takahashi et al. 2007) and the scientific importance of this was awarded by Science journal, that defined iPS cells as the Breakthrough of the 2008 Year discovery (Vogel 2008).

In Figure 1.3, a cartoon adapted from the work of Jaenisch et al. (Jaenisch and Young 2008) schematizes the process for obtaining iPS cells via viral infection.

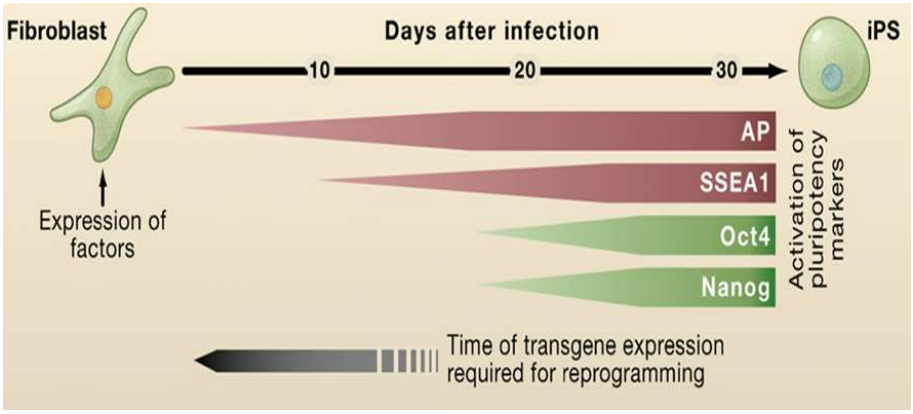

Figure 1.3. *Schematic representation of the obtainment of iPS cells via viral infection. Adapted from Jaenisch et al.2008.*

Scientists already derived patient-specific iPS cell lines (usually starting from skin cells) and were able to induce their directed differentiation into specialized cells. Notably, have been derived iPS cell lines for different diseases including muscular dystrophy, type 1 diabetes, and Down syndrome. Many of these diseases are difficult or impossible to study in animal models; thus the reprogrammed cells would give scientists a new tool for studying their genetic and molecular basis on a much relevant model. In this sight, iPS cells may also prove useful in screens for potential drugs.

It is fundamental to underline here how all the technologies and studies that have been performed and will be presented in this thesis, could be easily transferred and applied to iPS cells.

In this way, it would be possible to exploit the full potentiality of both the advanced technologies and the cell source. To summarize, iPS can prove as useful as hESC but with the advantage of avoiding all possible ethical issues.

1.1.3 Stem cell niche and microenvironment

The nowadays scientific community is becoming more and more aware of the importance of the concept of stem cell *niche* (Powell 2005). The term *niche* has been at first borrowed from ecology, where it identifies where an organism lives, what it does, and how it interacts with its environment, and then translated into biology.

Cells in their native tissues reside in an extremely complex environment constituted of other cell types, extracellular matrix proteins (ECM), and structural templates guiding their orientation and maintaining the three-dimensional (3D) architecture. Not to mention the intricate network of short and long range communication between single cells and/or tissues that occurs through an enormous cascade of signaling pathways and regulates their behavior (Metallo et al. 2007).

Novel cell culture technologies developed in recent years mimic the *in vivo* cellular microenvironments with an increasing fidelity (Kaplan et al. 2005), through improved control and the provision of cascades of multiple regulatory factors, as we will treat more in detail in the following sections.

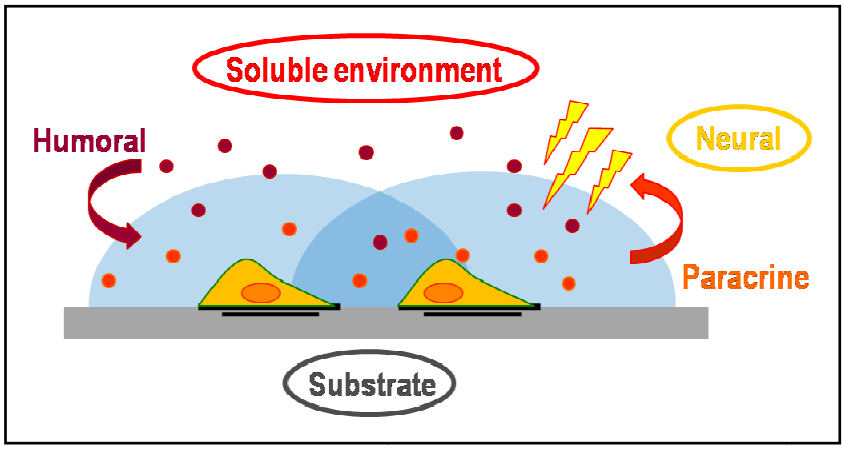

Figure 1.4. *Schematic representation of the stem cell niche.*

Figure 1.4 shows a simple schematization of the components of the cell microenvironment constituting the so-called *niche*. Two cells are adhering to a specific substrate, which is defined by a set of mechanical and chemical-physical properties. The cells are immersed in a soluble environment composed by a complex ensemble of factors that can be either produced by the cells themselves or by other cells in the surroundings. Finally, another important component is given by the electro-physiological activity of the neural system.

During this past three years, the center of the presented work has been mostly focused on the first two aspects (soluble environment and substrate), while the electrical component has represented an activity that has been performed in the first phases, as a completion of a pre-existing study that led to the publication reported in Appendix D. What thus will follow in this chapter will be a more detailed analysis of the state of the art on the first two aspects.

1.1.4 Potential applications

Recent studies suggest that primary human cell systems can be designed to model many aspects of disease biology and that robust and automated assays can be engineered to detect and discriminate disease relevant mechanisms and potential therapies. The human cell-based testing has proven to be a valuable tool to quickly explore toxic and non functional compounds. The low-cost and high-speed testing of compounds in cell culture, and the obvious advantages of using intact cells as a first representation of the living patients, would make the cell-based testing a key component on therapy discovery programs.

Concerning the obtainment of clinically-oriented products, it would be required to develop *in vivo* models, an aspect that has been the primary aim of this work (some experimentations have been performed during the first phases and led to the publications in Appendixes E and F).

However, whenever directing the efforts towards pharmaceutical companies and research laboratories in general, the need for strong and reliable *in vitro* testing emerges. Such *in vitro* systems would greatly benefit from the improvements that could derive from our studies.

1.1.5 Current limitations and technology perspective

The traditional cell-based approaches yielded relevant results but are however hindered by the actual numbers that are at stake: there is the need for enormous numbers of cells for each patient and, contemporarily, a huge number of patients may need such treatments.

The most recent strategies are thus aimed at applying engineering tools and different approaches to the problem-solving of the posed obstacles.

Novel technologies are constantly motivated by those strong needs and they design and development phases tend to be accomplished with an ever-increasing awareness of the specific requirements for their ultimate applications.

To be effective, cell therapy bioprocess design and optimization needs to incorporate a few basic criteria (Kirouac and Zandstra 2008):

- assessment of relevant cell properties;
- measurement and control of key parameters;

- robust predictive strategies for interrogating and evaluating the many parameters that may impact the culture output;
- approaches to test the many different parameters that may impact cell output in a high throughput and scale-relevant manner.

In addition, many individuals in the industry and academic community would argue that traditional cell models may give unsatisfactory, misleading and non-predictive data for the actual response of a complex functional tissue. In this sight, the developed technologies must always incorporate cell-level parameters such as heterogeneity, endogenously produced factors, and the local physicochemical microenvironment, trying to rationalize and closely reproduce the biological systems and their phenomena.

These will be key factors sustaining all the research work that will be presented in this thesis.

1.2 Tissue Engineering perspective

Tissue engineering has been defined as “an interdisciplinary field that applies the principles of engineering and the life sciences toward the development of biological substitutes that restore, maintain or improve tissue function” (Langer and Vacanti 1993).

This field is in continuous expansion and progress, facing and trying to overcome the many challenges that it offers (Griffith and Naughton 2002) and applying many of the state-of-the-art technologies.

Key features are the use and interplay between cells, biomaterials and bioreactors. As cells have already been introduced in section 1.1, the other two aspects will be briefly reviewed in what follows.

Biomaterials and scaffolds

"A Biomaterial is a nonviable material used in medical device, so its intended to interact with a biological systems" (Williams 1987); this is one of the first definitions given to biomaterials. Biomaterial scaffolds provide a critical means of controlling engineered tissue architecture and mechanical properties (Peppas and Langer 1994, Hubbel 1995, Langer and Tirrell 2004).

Biomaterials must respond to many specific requirements; here we list some of the most relevant and interesting for the performed research activity of this study:

- possess defined mechanical properties and performance requirements
- reproduce the structure of functional tissues and of pathological tissues;
- be biocompatibile;
- eventually be biodegradable.

Scaffolds and biomaterials for Tissue Engineering applications have been an object of study in the initial phases of this work, and the related and more detailed descriptions are treated in the already mentioned publications in Appendix D, E and F.

Bioreactors for tissue engineering

The advent of tissue engineering has been motivated by the challenge to produce tissue substitutes that could restore the structural features and physiological functions of natural tissues *in vivo*. To do this, many efforts have been put in obtaining such tissue constructs by growing isolated cells on polymer scaffolds using various *in vitro* culture bioreactors. Since the beginning, it has clearly emerged how the key feature was the necessity to capture the complexity of natural tissues *in vivo* displaying their structural and functional characteristics (Ingber et al. 2006).

Numerous extensive articles review the more relevant findings and the adopted techniques (Bilodeau and Mantovani 2006, Freed et al. 2006, Freed and Vunjak-Novakovic 1998, Kretlow and Mikos 2008, Park et al. 2008b). As an example, we underline how, driven by the enormous clinical need, myocardial tissue engineering has become a prime focus of research within the field of tissue engineering (Chen et al. 2008, Davis et al. 2005).

In parallel with the development of functional tissue substitutes, the use of stem cells in cell therapies or in other tissue engineering applications, requires extremely large number of cells (Chai and Leong 2007, Cabral 2001); a goal that -again- can impractically be accomplished using the standard culture techniques. Bioreactors, thus, have also found large application for cell expansion applications (Luni 2009).

A the beginning of this study, experimentations on a bioreactor for the perfused culture of 3D cellularized scaffold led to the publication reported in Appendix C (Cimetta et al. 2007).

1.2.1 Current limitations and technology perspective

Despite many interesting outcomes and undeniable progresses in improving the ultimate tissue engineered products, only few of them could effectively be available for clinical use, and significant challenges still remain in the successful long-term repair of biomechanically functional tissues. Animal studies and preclinical trials explain some of this failure's reasons, mostly imputable to a combination of fundamental biological and mechanical cues that failed to be reproduced in artificial grafts and are however present under physiologic conditions.

What is gaining much attention, thought, is the fact that the methodologies developed by tissue engineering and regenerative medicine are becoming powerful tools for studying tissues and diseases physiology in a controlled environment (Baar 2005) and for basic studies on tissue development and cell functions in response to genetic alterations, drugs and physiological stimuli (Gerecht-Nir et al. 2006).

In this sight, it is becoming more and more clear how cells are extremely sensitive to the local environment in terms of chemistry, physics and topography, on scales that differ from the sole "macro" one (Stevens and George 2005). For these and other reasons, much of the more recent efforts have been spent in facing the research with the so-called "biomimetic approach". Thus, novel technologies aim at gaining a bioactive control of the microenvironment (Dellatore et al. 2008, Lutolf and Hubbel 2005), able to overcome the afore mentioned limitations and -most important- able to give more insight in the actual functionality and requirements of the studied tissues or biological systems more in general.

In this context, microscale technologies can represent a powerful tool capable of giving answers to such questions and of gaining knowledge at a different, and extremely biologically- (and for future clinically-) relevant, scale. In addition, microscale technologies opened new perspectives in exploring other fields than tissue engineering such as: drug development, pharmacological and toxicological screenings, gene therapy and therapy development, and so on.

1.3 Microscale technologies

Novel cell culture technologies developed in recent years mimic the *in vivo* cellular microenvironments with an increasing fidelity, through improved control and the provision of cascades of multiple regulatory factors. It is now evident how living cell-arrays can offer unique advantages when used as the sensing element for biological assays or in drug development and differentiation studies (Flaim et al. 2005). To this aim, miniaturization of the culture systems is an important step towards accurate control of the cultured cells and tissues (Weibel et al. 2007, Folch and Toner 2000, Khademhosseini et al. 2006). In addition, another major advantage introduced by microscale technologies resides in the possibility of simultaneously acquiring vast amounts of information (Chen and Davis 2006, Kozarova et al. 2006), thus increasing the highthroughput characteristics of the system.

Sections 1.3.1 and 1.3.2 will briefly review the state of the art in the two main (and strictly correlates) aspects of the field of microscale technologies: microfabrication and lithography, and microfluidics.

1.3.1 Microfabrication and lithography

Microfabrication techniques are numerous and are used for different applications ranging from micropatterning, microfluidics, microelectronics and micro electro-mechanical systems (MEMS). All these techniques are described in detail in the book of Madou (Madou 2002). Extensive literature exists, giving many different examples of both fabrication methods and applications (Richards-Grayson et al. 2004, McCreedy 2000, McDonald et al. 2000).

For what concerns the present study, we would be focused on the optimization and application of polymer-based micromachining aimed at obtaining high-aspect-ratio structures. Specifically, we employed thick resist photolithography using SU-8 resin. In addition, within soft lithographic techniques, another fundamental method for our purposes was micromolding using polydimethylsiloxane (PDMS), enabling the production of polymeric devices with high accuracy and yield.

While Figure 1.5 schematizes the fundamental steps of the above mentioned techniques, for a more detailed description the review of Xia et al. is recommended (Xia and Whitesides 1998).

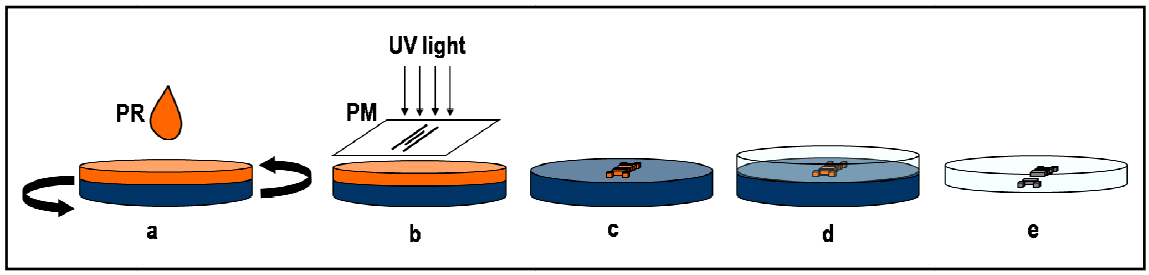

Figure 1.5. *Schematic representation of the photolithographic and micromolding techniques. In a. an uniform layer of photoresist resin (PR) is deposited onto a silicon wafer (blue disk) surface using a spin coater. Following precise thermal treatments, the photoresist is exposed to UV light interposing a selective photomask (PM). The wafer is then developed with the appropriate solvents which remove the un-polymerized resin and leave the polymerized resin representing the desired structure, in c. the following steps, d. and e., show the micromolding of PDMS that polymerizes on the wafer allowing the obtainment of a negative replica of the original master.*

1.3.2 Microfluidics

Microfluidics can be de fined as a broad discipline, with applications spanning from chemistry to biology, medicine and physical sciences, that deals with fluids within small-scale (typically sub-millimeter) channels or devices.

Besides the advantages in terms of the obtainable highthroughput characteristics of a system, the optimization and accurate use of microfluidic platforms allows for a precise control and manipulation of the fluids, thus opening new perspectives in studying the complex biological systems that we're interested in (Dittrich and Manz 2006).

At the relevant scale for microflows, meaning inside the microchannels and culture chambers of microfluidic devices, the dominating forces change and differ from the most known, macroscale ones. Several excellent reviews (Beebe et al. 2002, Squires and Quake 2005, Stone et al. 2004, Whitesides 2006, Stone and Kim 2001), as well as books (Berthier and Silberzan 2005, Nguyen and Wereley 2002) extensively analyze the physics of fluids at the micro and nano scale and illustrate the most relevant applications giving insights into the operating principles for system configurations of possible interest.

Chemical engineering classically dwells with the fluid physics of large-scale plants or pilot reactors, which strongly differ from that at the microscale. The numerous phenomena which rules microfluidic devices may thus not be intuitive. What is thus needed, is a comprehensive study of those phenomena in a given system, and the best and most intuitive way to do this is analyzing the dimensionless numbers expressing the ratio of competing phenomena and thus giving information on their relative importance.

Among the dimensionless numbers used in classical chemical engineering, the most important and informative for our studies are:

- the Reynolds number (Re), relating inertial forces to viscous forces:
- the Péclet number (Pe), relating convection to diffusion
- the Damköhler numbers (Da), relating chemical reaction timescale to other phenomena occurring in a system.

The first and most common feature of microfluidic devices is the fact that flow is always laminar (Reynolds numbers are well below the turbulence threshold, and in most cases $Re < 10$), the inertial forces are therefore dominated by viscous forces, and the transport is dominated by molecular diffusion or by convective regime of well-defined hydrodynamic profile. The laminarity of flows and exclusion of the nonlinearities and turbulence carried by inertia allows for precise calculation of mass transport and of the convective flow profiles as a function of channel geometry, pressure drops or flow rates and of the fluid properties. In addition, due to the very short transport distances which are in turn associated with shorter time constants, biological responses could are not always and only limited by the slow kinetics of physical phenomena.

Moreover, as in laminar flows the streamlines remain constant over time and mixing occurs primarily by diffusion, the feasible control over the operating parameters allows to apply precise, localized as well as spatially and temporally dynamic perturbations, as we will see in Chapter 3.

1.3.3 Applications

Within biological systems, microfabrication and lithography are the main techniques by which means to obtain topological control over substrates and adhesion of cells. To guide cell adhesion, many patterning techniques have been proposed and widely reviewed over the last few years (Falconnet et al. 2006, Chen et al. 1998, Fink et al. 2007, Kane et al. 1999, Ruiz and Chen 2007, Revzin et al. 2004).
A more detailed description will be given in Chapter 4.

Since its first appearance decades ago, microfluidics have been adapted to a multiplicity of different applications. Microscale technologies were designed for applications ranging from studies at a single cell level (DiCarlo et al. 2006) to the recreation of more complex 3D structures (Chiu et al. 2000, Gottwald et al. 2007, Kim et al. 2007) and the development of diagnostics platforms (Linder 2007, Toner and Irimia 2005). High-tech platforms involving integrated microdevices such as micro-valves, injectors, pumps or mixers (Melin and Quake 2007) are also being considered for use in live cell experimentation. The most interesting and relevant recent applications, have seen the use of microfluidic devices in studies on human embryonic stem cells (Figallo et al. 2007, Zhong et al. 2008), which importance and promise in clinical and pharmaceutical experimentation as already been discussed.

To this end, it should however be underlined how the biological relevance of many other research articles tends to be low and sacrificial in favor of more “simple” proof-of-concepts. Similar interesting considerations have also been made in a recent article (Paguirigan and Beebe 2008), highlighting a novel impelling need in trying to integrate microfluidics and microdevices as common tools in biological laboratories.

1.4 Motivations and aim of the thesis

The process of development of new therapeutic strategies is characterized by high costs incurred over a period of several years before any returns from the developmental efforts of the researchers are realized (Grabowski 2008, Grabowski et al. 2006).

The actual driving force towards further innovations is a strong need for:

- processing and screening large number of potential therapies;
- identifying the ones having the highest probability of becoming social, clinical and, also economical, sustainable in the shortest time possible;
- reducing the timeline of therapy development;
- completely avoiding the risk of chronic pathological or side effects after their clinical approve.

Within this scenario, there is a great interest in initiating and managing practices that reduce the development times, facilitate development decision−making and adopt technologies such as highthroughput screenings and electronic data acquisition which hold the promise of lowering the cost of therapy discovery and development. It is worth to underline that implementing improvements and alternative methodology that facilitates the therapy development process resulting in a lower cost, should ultimately bring therapies to the patients with an enormous benefit for the entire society.

This is where this work is find its basis and strong motivations: in the development of advanced technologies for the *in vitro* culture of stem cells, aimed at responding to the specific needs and requirements listed here.

1.5 References

G. Goldstein, A. Toren and A. Nagler, Human umbilical cord blood biology, transplantation and plasticity. *Current Medicinal Chemistry*, 2006, **13**, 1249-59.

E. Gussoni, Y. Soneoka, C. D. Strickland, E. A. Buzney, M. K. Khan, A. F. Flint, L. M. Kunkel and R. C. Mulligan, Dystrophin expression in the mdx mouse restored by stem cell transplantation. *Nature*, 1999, **401**, 390-394.

S. H. Orkin and S. J. Morrison, Stem-cell competition. *Nature*, 2002, **418**, 25-27.

F. M. Watt and B. L. M. Hogan, Out of Eden: Stem Cells and Their Niches. *Science*, 2000, **287**, 1427-1430.

M. J. Evans and M. H. Kaufman, Establishment in culture of pluripotential cells from mouse embryos. *Nature* 1981, **292**, 154-156.

G. Martin, Isolation of a pluripotent cell line from early mouse embryos cultured in medium conditioned by teratocarcinoma stem cells. *Proc Natl Acad Sci U S A*, 1981, **78**, 7635.

J. A. Thomson, J. Itskovitz-Eldor, S. S. Shapiro, M. A. Waknitz, J. J. Swiergiel, V. S. Marshall and J. M. Jones, Embryonic Stem Cell Lines Derived from Human Blastocysts. *Science*, 1998, **282**, 1145-1147.

P. W. Andrews and e. al., The International Stem Cell Initiative: toward benchmarks for human embryonic stem cell research. *Nature Biotechnology*, 2005, **23**, 795-797.

The-International-Stem-Cell-Initiative, Characterization of human embryonic stem cell lines by the International Stem Cell Initiative. *Nature Biotechnology*, 2008.

E. Serena, E. Cimetta and M. Zagallo, Financing for research on embryonic stem cells: The situation in Italy and its origins. Report of the 3rd Italian National Congress of the Group of Italian Researchers on Embryonic Stem Cells (IES Group). *Notizie di Politeia. Rivista di Etica e Scelte Pubbliche*, 2008, **91**, 110-113.

S. Yamanaka, Strategies and New Developments in the Generation of Patient-Specific Pluripotent Stem Cells. *Cell Stem Cell*, 2007, **1**, 39-49.

I. H. Park, R. Zhao, J. A. West, A. Yabuuchi, H. G. Huo, T. A. Ince, P. H. Lerou, M. W. Lensch and G. Q. Daley, Reprogramming of human somatic cells to pluripotency with defined factors. *Nature*, 2008a, **451**, 141-U1.

K. Takahashi, K. T. K, M. Ohnuki, M. Narita, T. Ichisaka, K. Tomoda and S. Yamanaka, Induction of pluripotent stem cells from adult human fibroblasts by defined factors. *Cell*, 2007, **131**, 861-872.

G. Vogel, Breakthrough of the year: Reprogramming Cells. *Science*, 2008, **322**, 1766-1767.

R. Jaenisch and R. Young, Stem Cells, the Molecular Circuitry of Pluripotency and Nuclear Reprogramming. *Cell*, 2008, **132**, 567–582.

K. Powell, It's the ecology, stupid! *Nature*, 2005, **435**, 268-270.

C. M. Metallo, J. C. Mohr, C. J. Detzel, J. J. DePablo, B. J. VanWie and S. P. Palecek, Engineering the Stem Cell Microenvironment. *Biotechnology Progress*, 2007, **23**, 18-23.

D. Kaplan, R. T. Moon and G. Vunjak-Novakovic, It takes a village to grow a tissue. *Nat Biotechnol*, 2005, **23**, 1237-1239.

D. C. Kirouac and P. W. Zandstra, The Systematic Production of Cells for Cell Therapies. *Cell Stem Cell*, 2008, **3**, 369-381.

R. Langer and J. P. Vacanti, Tissue Engineering. *Science*, 1993, **260**, 920-926.

L. G. Griffith and G. Naughton, Tissue Engineering - Current Challenges and Expanding Opportunities. *Science*, 2002, **295**, 1009-1016.

D. F. Williams, *Definitions in Biomaterials: Proceedings of a Consensus Conference of the European Society for Biomaterials, Chester, England, March 3-5, 1986*, Elsevier Publishing Company, 1987.

N. A. Peppas and R. Langer, New Challenges in Biomaterials. *Science*, 1994, **263**, 1715-1720.

J. A. Hubbel, Biomaterials in Tissue Engineering *Biotechnology*, 1995, **13**, 565-575.

R. Langer and D. A. Tirrell, Designing materials for biology and medicine. *Nature*, 2004, **428**, 487-492.

D. E. Ingber, V. C. Mow, D. Butler, L. Niklason, J. Huard, J. Mao, I. Yannas, D. Kaplan and G. Vunjak-Novakovic, Tissue Engineering and Developmental Biology: Going Biomimetic. *Tissue Engineering*, 2006, **12**.

K. Bilodeau and D. Mantovani, Bioreactors for Tissue Engineering: Focus on Mechanical Constraints. A Comparative Review. *Tissue Engineering*, 2006, **12**, 2367-2383.

L. E. Freed, F. Guilak, E. Guo, M. L. Gray, R. Tranquillo, J. W. Holmes, M. Radisic, M. V. Sefton, D. Kaplan and G. Vunjak-Novakovic, Advanced Tools for Tissue Engineering: Scaffolds, Bioreactors, and Signaling. *Tissue Engineering*, 2006, **12**, 3285-3305.

L. E. Freed and G. Vunjak-Novakovic, Culture of organized cell communities. *Advanced Drug Delivery Reviews*, 1998, **33**, 15–30.

J. D. Kretlow and A. G. Mikos, From Material to Tissue: Biomaterial Development, Scaffold Fabrication, and Tissue Engineering. *AIChE Journal*, 2008, **54**, 3048-3067.

D. H. Park, C. V. Borlongan, D. J. Eve and P. R. Sanberg, The emerging field of cell and tissue engineering. *Medical Science Monitor*, 2008b, **14**, RA206-220.

Q. Z. Chen, S. E. Harding, N. N. Ali, A. R. Lyon and A. R. Boccaccini, Biomaterials in cardiac tissue engineering: Ten years of research survey. *Materials Science and Engineering*, 2008, **R 59** 1–37.

M. E. Davis, P. C. H. Hsieh, A. J. Grodzinsky and R. T. Lee, Custom Design of the Cardiac Microenvironment With Biomaterials. *Circulation Research*, 2005, **97**, 8-15.

C. Chai and K. W. Leong, Biomaterials Approach to Expand and Direct Differentiation of Stem Cells. *Molecular Therapy*, 2007, **15**, 467–480.

J. M. S. Cabral, Ex vivo expansion of hematopoietic stem cells in bioreactors. *Biotechnology Letters*, 2001, **23**, 741–751.

C. Luni, Development of cell culture technology for the expansion of homogeneous populations of human stem cells. *PhD thesis*. Dipartimento di Principi e Impianti di Ingegneria Chimica “I. Sorgato”, University of Padova, 2009.

E. Cimetta, M. Flaibani, M. Mella, E. Serena, L. Boldrin, P. D. Coppi and N. Elvassore, Enhancement of viability of muscle precursor cells on 3D scaffold in a perfusion bioreactor. *The International Journal of Artificial Organs*, 2007, **30**, 220-226.

K. Baar, New dimensions in tissue engineering: possible models for human physiology. *Experimental Physiology*, 2005, **90**, 799-806.

S. Gerecht-Nir, M. Radisic, H. Park, C. Cannizzaro, J. Boublik, R. Langer and G. Vunjak-Novakovic, Biophysical regulation during cardiac development and application to tissue engineering. *International Journal of Developmental Biology*, 2006, **50**, 233-43.

M. M. Stevens and J. H. George, Exploring and Engineering the Cell Surface Interface. *Science*, 2005, **310**, 1135-1138.

S. M. Dellatore, A. S. Garcia and W. M. Miller, Mimicking stem cell niches to increase stem cell expansion. *Current Opinion in Biotechnology*, 2008, **19**, 534–540.

M. P. Lutolf and J. A. Hubbel, Synthetic biomaterials as instructive extracellular microenvironments for morphogenesis in tissue engineering. *Nature Biotechnology*, 2005, **23**, 47-55.

C. J. Flaim, S. Chien and S. N. Bhatia, An extracellular matrix microarray for probing cellular differentiation. *Nature Methods*, 2005, **2**, 119-125.

D. B. Weibel, W. R. DiLuzio and G. M. Whitesides, Microfabrication meets microbiology. *Nature Reviews - Microbiology*, 2007, 209-218.

A. Folch and M. Toner, Microengineering of cellular interactions. *Annu. Rev. Biomed. Eng.*, 2000, **2**, 227–56.

A. Khademhosseini, R. Langer, J. Borenstein and J. P. Vacanti, Microscale technologies for tissue engineering and biology. *PNAS*, 2006, **103**, 2480–2487.

D. S. Chen and M. M. Davis, Molecular and functional analysis using live cell microarrays. *Curr Opin Chem Biol* 2006, **10**, 28-34.

A. Kozarova, S. Petrinac, A. Ali and J. W. Hudson, Array of informatics: applications in modern research. *J Proteome Res*, 2006, **5**, 1051-1059.

A. C. Richards-Grayson, R. S. Shawgo, A. M. Johnoson, N. T. Flynn, Y. Li, M. J. Cima and R. Langer, A BioMEMS Review: MEMS Technology for Physiologically Integrated Devices. *Proceedings of the IEEE*, 2004, **92**, 6-21.

T. McCreedy, Fabrication techniques and materials commonly used for the production of microreactors and micro total analytical systems. *Trends in analytical chemistry*, 2000, **19**, 396-401.

J. C. McDonald, D. C. Duffy, J. R. Anderson, D. T. Chiu, H. K. Wu, O. J. A. Schueller and G. M. Whitesides, Fabrication of microfluidic systems in poly(dimethylsiloxane). *Electrophoresis*, 2000, **21**, 27-40

Y. Xia and G. M. Whitesides, Soft lithography. *Angew Chem Int Ed*, 1998, **37**, 550-575.

P. S. Dittrich and A. Manz, Lab-on-a-chip: microfluidics in drug discovery. *Nature Reviews - Drug Discovery*, 2006, **5**, 210-218.

D. J. Beebe, G. A. Mensing and G. MWalker, Physics and applications of microfluidics in biology. *Annu. Rev. Biomed. Eng.*, 2002, **4**, 261–86.

T. M. Squires and S. R. Quake, Microfluidics: Fluid physics at the nanoliter scale. *Reviews of Modern Physics*, 2005, **77**, 977-1016.

H. A. Stone, A. D. Stroock and A. Ajdari, Engineering Flows in Small Devices: Microfluidics Toward a Lab-on-a-Chip. *Annual Review of Fluid Mechanics*, 2004, **36**, 381–411.

G. M. Whitesides, The origins and the future of microfluidics. *Nature*, 2006, **442**, 368-373.

H. A. Stone and S. Kim, Microfluidics: Basic Issues, Applications, and Challenges. *AIChE Journal*, 2001, **47**, 1250-1254.

J. Berthier and P. Silberzan, *Microfluidics for Biotechnology*, Artech House Publishers, 2005.

N.-T. Nguyen and S. Wereley, *Fundamentals and Applications of Microfluidics*, Artech House Publishers, 2002.

D. Falconnet, G. Csucs, H. M. Grandin and M. Textor, Surface engineering approaches to micropattern surfaces for cell-based assays. *Biomat* 2006, **27**, 3044-3063.

C. S. Chen, M. Mrksich, S. Huang, G. M. Whitesides and D. E. Ingber, Micropatterned Surfaces for Control of Cell Shape, Position, and Function. *Biotechnology Progress*, 1998, **14**, 356-363.

J. Fink, M. Thery, A. Azioune, R. Dupont, F. Chatelain, M. Bornensa and M. Piel, Comparative study and improvement of current cell micro-patterning techniques. *Lab on a Chip*, 2007, **7**, 672-680.

R. S. Kane, S. Takayama, E. Ostuni, D. E. Ingber and G. M. Whitesides, Patterning proteins and cells using soft lithography. *Biomaterials*, 1999, **20**, 2363-2376.

S. A. Ruiz and C. S. Chen, Microcontact printing: A tool to pattern. *Soft Matter* 2007, **3**, 1–11.

A. Revzin, P. Rajagopalan, A. W. Tilles, F. Berthiaume, M. L. Yarmush and M. Toner, Designing a Hepatocellular Microenvironment with Protein Microarraying and Poly(ethylene glycol) Photolithography. *Langmuir*, 2004, **20**, 2999-3005.

D. DiCarlo, L. Y. Wu and L. P. Lee, Dynamic single cell culture array. *Lab on a Chip*, 2006, **6**, 1445–1449.

D. T. Chiu, N. L. Jeon, S. Huang, R. S. Kane, C. J. Wargo, I. S. Choi, D. E. Ingber and G. M. Whitesides, Patterned deposition of cells and proteins onto surfaces by using three-dimensional microfluidic systems. *PNAS*, 2000, **97**, 2408–2413.

E. Gottwald, S. Giselbrecht, C. Augspurger, B. Lahni, N. Dambrowsky, R. Truckenmuller, V. Piotter, T. Gietzelt, O. Wendt, W. Pfleging, A. Welle, A. Rolletschek, A. M. Wobus and K. F. Weibezahn, A chip-based platform for the in vitro generation of tissues in three-dimensional organization. *Lab on a Chip*, 2007, **7**, 777–785.

M. S. Kim, J. H. Yeon and J. K. Park, A microfluidic platform for 3-dimensional cell culture and cell-based assays. *Biomedical Microdevices*, 2007, **9**, 25-34.

V. Linder, Microfluidics at the crossroad with point-of-care diagnostics. *The Analyst*, 2007, **132**, 1186–1192.

M. Toner and D. Irimia, Blood-on-a-Chip. *Annu. Rev. Biomed. Eng.*, 2005, **7**, 77–103.

J. Melin and S. R. Quake, Microfluidic Large-Scale Integration: The Evolution of Design Rules for Biological Automation. *Annual Review of Biophysics and Biomolecular Structure*, 2007, **36**, 213–31.

E. Figallo, C. Cannizzaro, S. Gerecht, J. A. Burdick, R. Langer, N. Elvassore and G. Vunjak-Novakovic, Micro-bioreactor array for controlling cellular microenvironments. *Lab on a Chip*, 2007, **7**, 710-719.

J. F. Zhong, Y. Chen, J. S. Marcus, A. Scherer, S. R. Quake, C. R. Taylor and L. P. Weinera, A microfluidic processor for gene expression profiling of single human embryonic stem cells. *Lab on a Chip*, 2008, **8**, 68–74.

A. L. Paguirigan and D. J. Beebe, Microfluidics meet cell biology: bridging the gap by validation and application of microscale techniques for cell biological assays. *BioEssays*, 2008, **30**, 811–821.

H. Grabowski, Follow-on biologics: data exclusivity and the balance between innovation and competition. *Nature Reviews: Drug Discovery*, 2008, **7**, 479-488.

H. Grabowski, I. Cockburn and G. Long, The market for follow-on biologics: how will it evolve? *Health affairs (Project Hope)*, 2006, **25**, 1291-301.

Chapter 2
Principles for designing stem cell culture technologies

This chapter is aimed at analyzing the rationale beneath the use and application of advanced cell culture technologies in order to catch the complexity of biological systems. This is a fundamental step in sight of the obtainment of valuable and reliable data in studying and guiding cells behavior. A major interest will be focused on the topics of perfusion and topological control.

2.1 Scaling biological phenomena

Biological phenomena cannot be simply considered as the sum of small “building blocks” whose final structure recapitulates the function or behavior of a cell or tissue. When dealing with biological phenomena, one must at first acknowledge how they arise from a dense network of interactions between the cell’s numerous constituents and their distinct biological components. Short and long range communication between single cells and/or tissues occurs through an enormous cascade of signaling pathways, most of which involve mechanisms, intermediate steps and connections that are not fully understood. In addition, these interactions often involve numerous and different processes (e.g. gene regulation, signal transduction etc) which are not only determined by steady-state characteristics of the systems, but also possess inherent dynamic properties (Barabási and Oltvai 2004, Hartwell et al. 1999, Oltvai and Barabási 2002, Xiong et al. 2008).

Such complexity of cellular functions and their response to internal events and environmental perturbations or stimuli, develop in both time and space with scales characteristically spanning over orders of magnitude (Jamshidi and Palsson 2008, Cervinka et al. 2008).

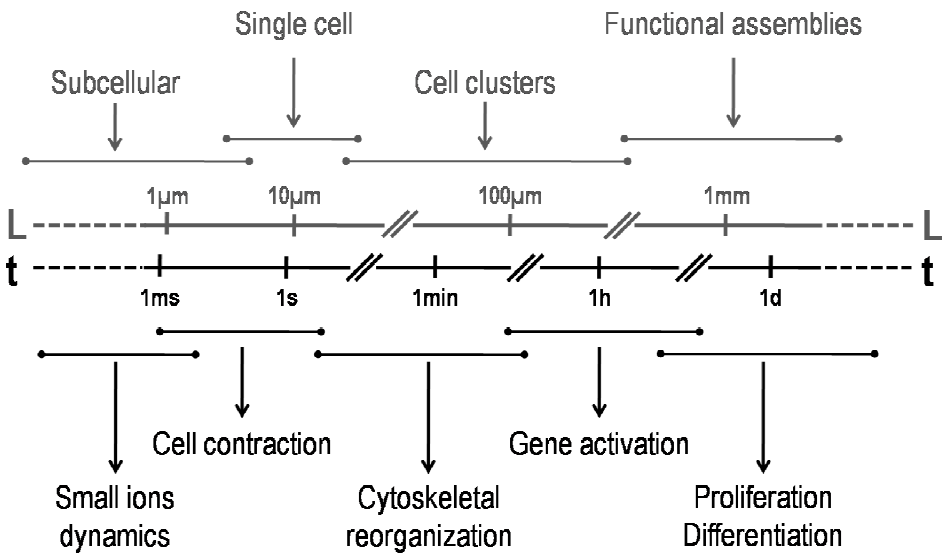

Figure 2.1. *Length and time scales for some relevant biological phenomena.*

Figure 2.1 represents a schematization showing approximated ranges for both space and time scales of some relevant biological phenomena. It is now clear how each "level" is tightly interconnected with all the others and how phenomena occurring on smaller scales influences the subsequent ones. For example, intracellular events such as small ions dynamics can affect the whole cell, or cell cluster, behavior in terms of contractile properties and/or gene activation.

Noteworthy, another clear evidence is the fact that when it comes to scaling to the biologically relevant lengths and time scales, the conventional methodologies of the so-called ''flat biology" fail.

Standard culture methods involving cell culture in Petri dishes cannot be representative of the real state of physiologic systems and therefore often result in unrealistic and uncontrollable biological readouts. The relatively large volume of medium in contact with cells and the batch-wise operation associated with the periodic medium exchange does not allow for the generation and control of precise patterns of stimulation in space and time.

These observations lead to the impelling necessity for the researchers to develop novel technologies, adequate data acquisition methodologies and analysis techniques that could be interfaced with biological systems. The ultimate goal would be that of more closely reproducing the natural events occurring in living cells and tissues, strictly controlling and manipulating the recreated artificial environment and thus being able to study the complex biological phenomena in a more realistic manner. Ideally, biological studies should be performed under conditions that are controllable and at the same time capture the complexity of the native environment.

To answer to the many specific requirements that such systems must satisfy, solutions that will be more in detail discussed in the following paragraphs and chapters have been developed.

2.2 Phenomenological description of microscaled perfusion systems (MPS)

Standard culture systems such as Petri dishes have the advantage of ensuring spatial uniform conditions, at a given time, throughout the entire culture in terms of metabolite and growth factor concentrations and mass fluxes. Besides that, they can be compared to batch reactors in which conditions are precisely defined only at time zero, and then continuously vary until next medium exchange. Batch processes have unpredictable time scales, are diffusion-limited and, most important, are intrinsically uncontrollable. This strong limitation can be overcome by the use of perfused systems, as they offer the advantage of working under well defined and stable steady-state conditions.

Before going into more detail concerning microscaled systems, lets first analyze perfused systems in a more general perspective.

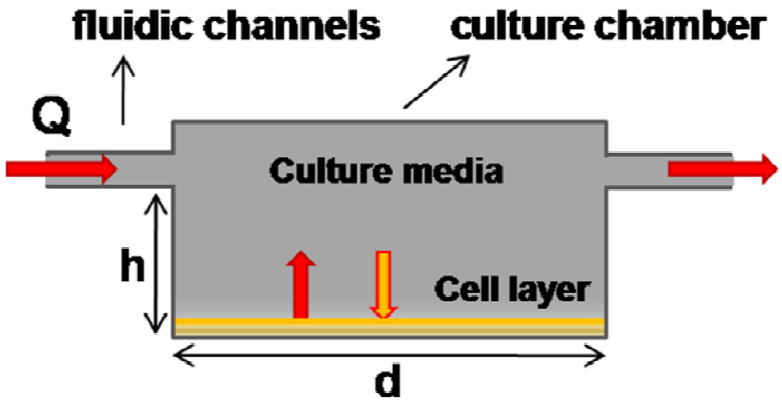

Figure 2.2. *Schematic representation of a typical culture chamber with the fluidic channels for fluid perfusion. The characteristic dimensions are the width d and the height h, distance between the bottom of the chamber and the fluidic channels.*

Figure 2.2 shows a schematic representation of a perfused culture chamber, inspired from what has been described elsewhere (Cimetta et al. 2009, Figallo et al. 2007). The culture chamber, usually a cylindrical well, is characterized by two fundamental geometrical parameters (that will be discussed more in detail in the following sections): its characteristic width *d* and the height *h*, the distance between the bottom of the well and the fluidic channels. The culture chamber is filled with culture media and cells are adhering to its bottom at a defined surface density. A stationary flow rate *Q* perfuse the chamber entering and exiting from the fluidic channels. The above mentioned parameters can have a strong (and predictable) influence on the phenomena happening within the cell layer.

It is important to underline how a perfused chamber works at steady state conditions, meaning that average properties are constant with time. The only exception could happen at the microscale where cell density may vary due to proliferation, thus affecting the absolute values of fluxes (uptake and release).

However, another crucial point is the observation that the convective transport is parallel to the cell surface, which is characterized by normal mass flux. This is an important phenomena that needs to be taken into account and discussed.

In this sight, it will be important to identify which differences in geometrical configuration, at defined transport regimes, will increase or reduce the above mentioned heterogeneities; it seems obvious that the upstream culture section, with respect to the downstream section, could experience very different conditions in terms of solute concentration.

The following sections will treat in more detail such systems, analyzing the dominant phenomena, giving the design specifications for important operating parameters and the principles for their optimization at the microscale level.

In the following sections we will treat in detail the described systems with different aims:

- first of all, we will perform an analysis of the characteristic dimensionless numbers for the identification of averaged properties of the system;
- secondarily, we will perform computational simulations to catch the heterogeneities within the system.

These results are based on the analysis of transport rates and characteristic times of the involved phenomena.

2.2.1 Characteristic times and dimensionless parameters analysis

The detailed description of this study is reported in the publication “Micro-bioreactor arrays for controlling cellular environments: Design principles for human embryonic stem cell applications” (Cimetta et al. 2009) in Appendix A.

At the microscale -inside the microchannels and culture chambers- the dominating forces change and differ from the most known, macroscale ones. Flow is always laminar (Reynolds numbers are well below the turbulence threshold, and in most cases $Re < 10$) the inertial forces are therefore dominated by viscous forces, and the transport is dominated by molecular diffusion or by convective regime of well-defined hydrodynamic profile. Reducing the characteristic dimensions to a microscale level allows a more rigorous control of the operating parameters involved, due to the very short transport distances, which are in turn associated with very short time constants. As a result, biological responses are not anymore always limited by the slow kinetics of physical phenomena.

It is often necessary to accurately modulate transients in space and time to recreate precise stimulation patterns in the form of concentration gradients, and deliver particular signals. Working with small volumes (order of a few µL) generally leads to fast-response systems. This means that the switch between defined sets of conditions can be fast and still controllable. For example, operating parameters can be changed by a simple variation of the

medium flow rate. At the microscale, one can design the system to provide tightly controlled, orderly conditions of flow and mass transport.

Another fundamental aspect deriving from the application of microscale perfusion, is the increased degree of control over the system. Due to the well-defined geometry, short transport distances, and fast transients, transport phenomena occurring in microdevices can be more easily subjected to theoretical analysis and precise control than those in larger scale systems. Accurate predictions of the velocity gradients and shear stresses are indeed very important because of the profound effects of flow environment on biological systems. Again, the versatility of microscaled systems, allows decoupling the effects of mass transport phenomena such as the generation of specific concentration patterns from physical phenomena such as the application of mechanical forces.

2.2.2 Tuning operational parameters

The operational parameters affecting the pool of variables in the cell micro-environment can be divided into two categories:

- the initial parameters that are normally set before the experiment such as:
    - the characteristic dimensions of the culture chamber,
    - the cell seeding density
    - the medium composition;
- operative parameters that can be controlled during the experiment such as:
    - the medium flow rate.

For sake of clarity, Table 1 summarizes all the relevant parameters involved and their main targets within the system.

Table 1. *Parameters involved, notification, description and main targets within the culture system..*

Parameter	Symbols	Description	Main Target
Geometrical	**L_g**	Gas exchange channel length	- Gas concentration
	h	Chamber height	- Mass transfer
	d	Chamber diameter	- Total number of cells
	h·d	Chamber cross section	- Velocity field - Mass transport
Operative	**ρ**	Seeding density	- Total uptake and release rates
	Q	Total flow rate	- Velocity field - Shear stress - Mass transfer

In this section, we discuss the principles guiding the selection of the optimal variables and their values through the analysis of characteristic times of fundamental phenomena such as cellular uptake and release, and diffusional and convective mass transport rates.

We considered two representative species, oxygen and albumin, representative of a small metabolite and a larger growth factor respectively.

Before going into detail, it is necessary to clarify the notations used and to list the values of the parameters at play. Table 2 shows a complete list of the parameters values used in the calculations of the characteristic times.

Table 2. *Parameters used. The table reports a list of the parameters and variables used for the performed calculations with their values and ranges.*

Variable	Values	Units
D_{02}	3.30E−09	m^2/s
D_{Alb}	7.00E-11	m^2/s
h	$0 < h < 0.004$	m
ρ_c	$1.0E + 7 < \rho_c < 4.0E + 10$	cells/m^2
k_{on}	1.00E + 07	l/Ms
$[R]$	1000	Molecules/cell
μ	0.0007	Pas
d	0.004	m
Q	$0 < Q < 2.3E-10$	m^3/s

The ratio of the time scales of uptake at the bottom of the culture chamber (by cultured cells) τ_{UP}, to species diffusion from the medium, τ_D, can be estimated. For example, assuming a maximum uptake reaction rate expressed by a mass action law for a ligand-receptor association kinetics (Lauffenburger and Linderman 1993), the above mentioned time scale ratio can be expressed by:

$$\frac{\tau_{UP}}{\tau_D} = \frac{D}{h\rho_C k_{on}[R]} \qquad 1.$$

where D is the diffusion coefficient of the chemical species, h is the height of the culture chamber, k_{on} is the ligand-receptor association rate constant, $[R]$ is the number of receptors on cell surface and ρ_C is the surface cell density.

In this context, the most important variable that can be precisely controlled is the medium flow rate; thus giving importance to the mass transport due to convection.

The analysis of the influence of the medium flow rate on mass transport is carried as follows. The ratio of the time scales of diffusion in the culture chamber, τ_D, to convection, τ_C (residence time of the medium in the culture chamber), can be defined as:

$$\frac{\tau_D}{\tau_C} = \frac{hQ}{Dd^2} \qquad 3.$$

where D is the diffusion coefficient of the chemical species, h is the height of the culture chamber, Q is the medium flow rate and d is the culture chamber diameter.

Figure 2.3 summarizes the results of the analyses on these characteristic times.

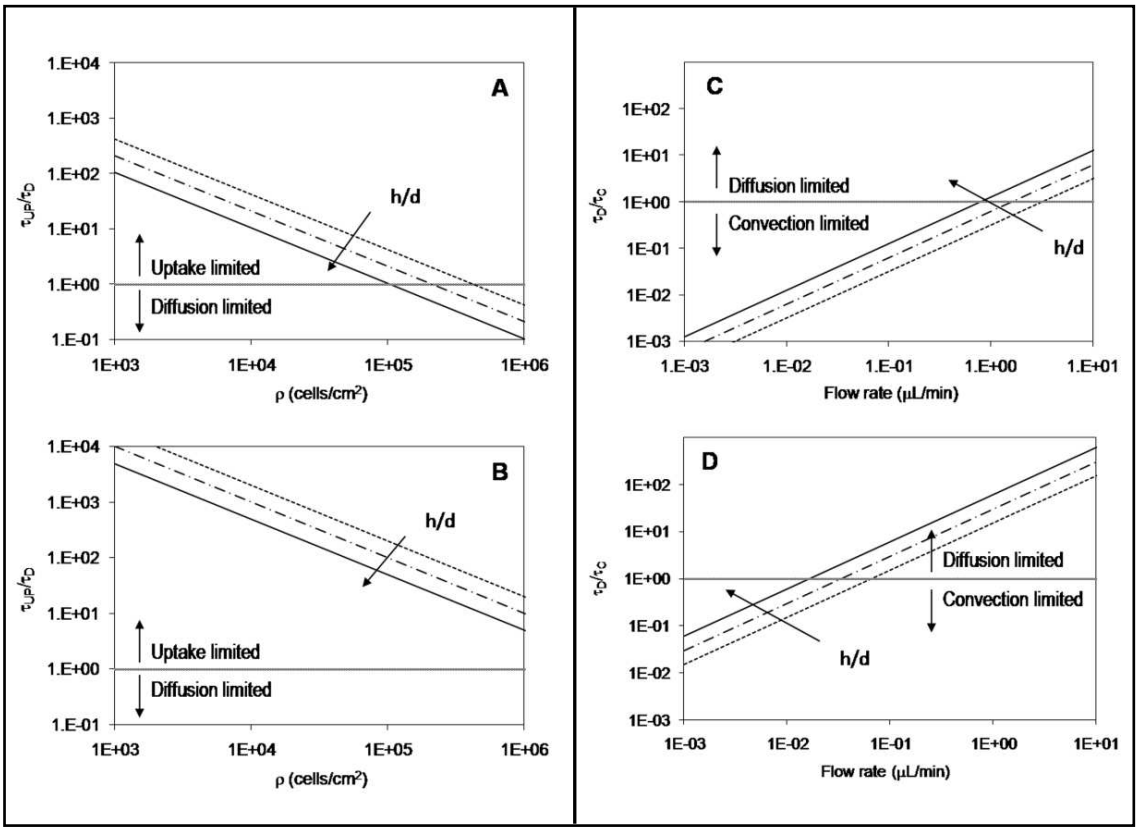

Figure 2.3. *On the left: diffusion and reaction time constants as a function of cell density and culture chamber geometry. The ratio of characteristic times of uptake reactions and molecular diffusion, τ_{UP}/τ_D, is shown as a function of the cell density, for three values of the culture chamber height: h = 1, 2 and 4 mm; d = 4 mm.. On the right: diffusion and convection time constants as a function of medium flow rate and culture chamber geometry. The ratio of characteristic times of molecular diffusion and convection, τ_D/τ_C, is shown as a function of medium flow rate, for the same three values of the culture chamber height. Panels A and C shows data for a small metabolite such as oxygen while B and D shows data for albumin representative of large growth factors. The values for all parameters used are listed in Table 1.*

Figure 2.3 A and B show the calculated ratio of the time constants at the bottom of the culture chamber between the reaction, τ_{UP}, and diffusion, τ_D, as a function of cell seeding density. The ratio is shown for two representative molecules: oxygen (the most important upon small molecules, panel A) and albumin (a protein representative of larger growth factors, panel B). At low cell densities, the characteristic time scale for reaction is longer than that for diffusion. Therefore, mass transport at low cell densities is dominated by uptake reaction rates. As cell density increases up to its maximum value (i.e. at confluence), the time constant for diffusion becomes comparable with that for reaction. It is interesting to note that the height of the culture chamber only slightly influences the ratio of the two time

constants. This semi-quantitative analysis suggests that for higher cell seeding densities, medium perfusion is required to enhance mass transport rates and establish a kinetic-limited operating regime.

Similarly, Figure 2.3 B and C show the ratio of the time scales of diffusion to convection as a function of medium flow rate, for different heights of the culture chamber. In the presented logarithmic graphs, values greater than 1 represent culture conditions that are reaction controlled, whereas <1 values correspond to the convection-limited regimes, and values of ~1 indicate the competition between the two rates. From these graphs we can conclude that for small metabolites with high diffusion rates in the 4 mm diameter culture chamber, flow rates >1 μL/min are necessary to cross from a diffusion- to a convection-controlled regime. In addition, it is possible to adjust the mass transport phenomena at a given flow rate by changing the height of the culture chamber. The chamber geometry thus provides an additional degree of freedom for setting the proper culture conditions (Table 2).

Table 2. *Parameters involved and their main targets. The main geometrical and operative parameters are summarized in the table, listing also the corresponding symbols and the main targets of their variations.*

Parameter	Symbol	Description	Phenomena
Design	L_g	Channel length	Gas-liquid mass transfer
	h	Chamber height	Cell-liquid mass transfer
	d	Chamber diameter	Total number of cells
	$h \times d$	Chamber cross section	Velocity field; Mass transport
Operation	ρ_c	Seeding density	Total uptake and release rates
	Q	Total flow rate	Velocity field; Shear stress; Mass transfer

Finally, we wanted to determine the distance z from the bottom of the culture chamber at which the diffusion and convection time scale were comparable as a function of the flow rate. Introducing the above mentioned variable z, and traducing the flow rate Q in terms of the linear velocity v_z, the following equation for the ratio of τ_D and τ_C was obtained.

$$\frac{\tau_D}{\tau_C} = \frac{(h-z)^2}{D}\frac{v_z}{d} \qquad 4.$$

Assuming that the flow profile would be well-approximated by parallel-plate Poiseuille flow, v_z can be expressed as:

$$v_z = 1.5\langle v \rangle (1 - (z/h)^2) \quad 5.$$

where $\langle v \rangle$ is the mean channel velocity.

The results obtained simultaneously solving equations 4 and 5 for $\tau_D/\tau_C = 1$ are presented in Figure 2.4.

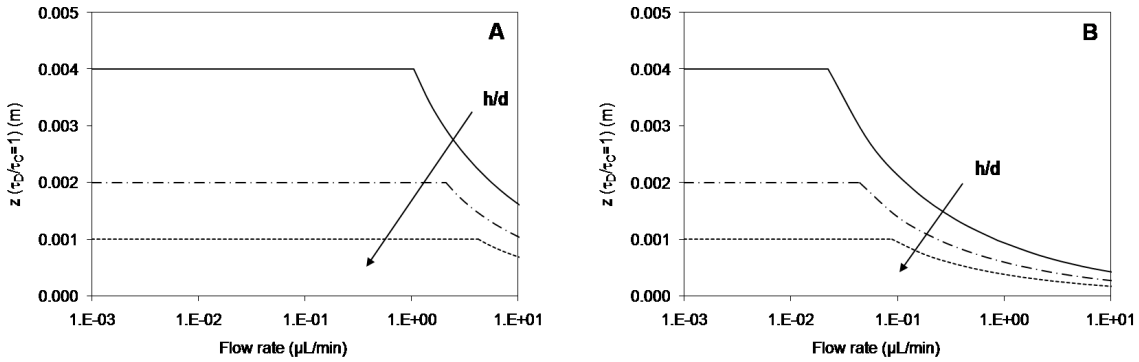

Figure 2.4. *Characteristic length scale as a function of medium flow rate and culture chamber geometry. The distance from the bottom of the culture chamber at which the ratio of the diffusion and convection time constants is equal to one is shown as a function of the flow rate and culture chamber geometry h = 1, 2 and 4 mm; d = 4 mm. Panel A shows data for a small metabolite, such as oxygen while panel B shows data for albumin representative of large growth factors.*

At low flow rates, the values of *z* correspond to the height of the culture chamber, indicating that diffusion dominates at all levels. By increasing the flow rate, *z* decreases and takes values between the top and bottom of the chamber. In turn, increasing the height of the culture chamber decreases the transport rates at the cell culture surface and thereby decreases the wash-out of endogenous factors. This latter aspect can be relevant to cultures of stem cells, where the preservation and recreation of the natural diffusion-limited cell *niche* is of fundamental importance.

However, in this study we didn't took into account any of the heterogeneity that we recognized within these systems; this reason mainly supported and determined the follow up of this work, that will be presented here in the next paragraph.

2.3 Computational modeling and dimensionless parameters on MPS

As briefly described in section 2.2, conventional culture systems can be treated as batch systems in which the variables of interest vary with time. In particular, the concentration of metabolites or growth factors that are continuously consumed by cultures, decreases in a manner dependent on the uptake rates of the cells.

These culture conditions, thought varying with time, are always spatially uniform throughout the system, while the sole spatial heterogeneity could be encountered in the close proximity of the culture chamber's walls.

The answer to the need of increasing the mass transport is given by the introduction of a convective component; this is usually done perfusing the system, thus setting the fluid in motion controlling its flow rate. Within microscaled perfusion systems (MPS), as seen in Figure 2.2, the given configuration usually results in a convective flux orthogonal to the diffusive one.

The first and fundamental difference between batch and perfused systems is the establishment of well defined and stable steady state conditions. In addition, the use of perfusion allows for an additional degree of freedom in tuning the mass transport via regulation of the convective flux.

It is needed to underline the possible cons of perfusion, which are mainly derived from the establishment of spatial disuniformities and heterogeneity within the system and, eventually, from the introduction of potentially damaging shear stresses.

The experimental design and the choice of all operational and geometrical parameters, as seen above, play a key role in dictating the system behavior and the final outcomes. What is thus required is an analysis based on the interplay between diffusion, convection and reaction, the fundamental phenomena acting on the system, and aimed at identifying the dominating regime.

A similar issue has been treated in a recent research article (Squires et al. 2008), focused on biomolecular detection and surface-based sensors. Squires and coworkers proposed a simple yet complete study exploring the distinct behaviors of systems with varying properties (in terms of characteristic dimensions, transport regimes etc.) and developed intuitive methods

to derive order-of-magnitude estimates for fundamental quantities of interest to determine the system behavior.

The study that will be presented in this section had a fundamental difference with the one presented in section 2.2, where the properties were described as averaged values; in the treatment that will follow, we were also aimed at capturing the heterogeneity within the system.

In order to capture this heterogeneity, we used computational modeling and based the study of the relevant phenomena utilizing dimensionless variables.

In particular we considered:

- Concentration: c/c^*, where c^* is the initial bulk value.
- Time: t/t^*, where t^* is the initial bulk value defined as: $t^* = 1/(k_{on}c)$, and k_{on} is as in Table 2.
- Flux: N/N_{max}, with: $N = k_{on}[R]\rho_c c$, where k_{on} and $[R]$ are as in Table 2.
  For N_{max} we used the value of c^*.
- Velocity: v/v_{max}, where v_{max} is the maximum velocity value within the chamber.
- Chamber geometry:
  - x/L, where x is the x-axis coordinate and L is the chamber length;
  - z/H, where z is the z-axis coordinate and H is the chamber height;
- Peclet number, defined as $Pe = vH/D$, where v is the velocity, and D the diffusion coefficient.
- The mean absolute deviation (**MAD**) of the values was evaluated as follows:
  $MAD = \Sigma|m - \bar{m}|/\mathrm{n}$ 6.
  where m is the measure, and n the total number of measurements.

Averaged values of the defined properties and variables will be indicated in brackets (< >).

To accomplish the task, extensive studies involving two-dimensional (2D) mathematical modeling of a representative microbioreactor was performed.

The Navier-Stokes equations for incompressible fluids were numerically solved using the finite elements method implemented in Comsol Multiphysics (Burlington, MA). The 2D domain of the culture chamber was geometrically modeled and a non-structured mesh was automatically generated with triangular elements. Then, to ensure independency of the solution from the spatial discretization, grid refinements were required. No-slip boundary conditions were used for the chamber and microfluidic conduits walls, a fixed velocity for the inlet channel and finally zero pressure for the outlet. The fluid properties viscosity and density were taken from the literature.

To obtain concentration profiles within the chambers, the mass balance equations for a convective-diffusive regime were solved again using Comsol Multiphysics software (Burlington, MA, USA). Fluid velocity profiles were obtained from the Navier-Stokes solutions. A defined concentration was used as initial condition within the chamber and as boundary condition at the inlet; convective flux at the outlet; a specific flux at the cell layer adhering at the bottom of the chamber (as will be clarified) and insulation/symmetry elsewhere.

All results were obtained generating a script from the Comsol file that was then integrated and compiled in MATLAB (The MathWorks), allowing for the addition of routines and data analysis.

The solutions were evaluated for the 3 different 2D chamber geometries shown in Figure 2.5.

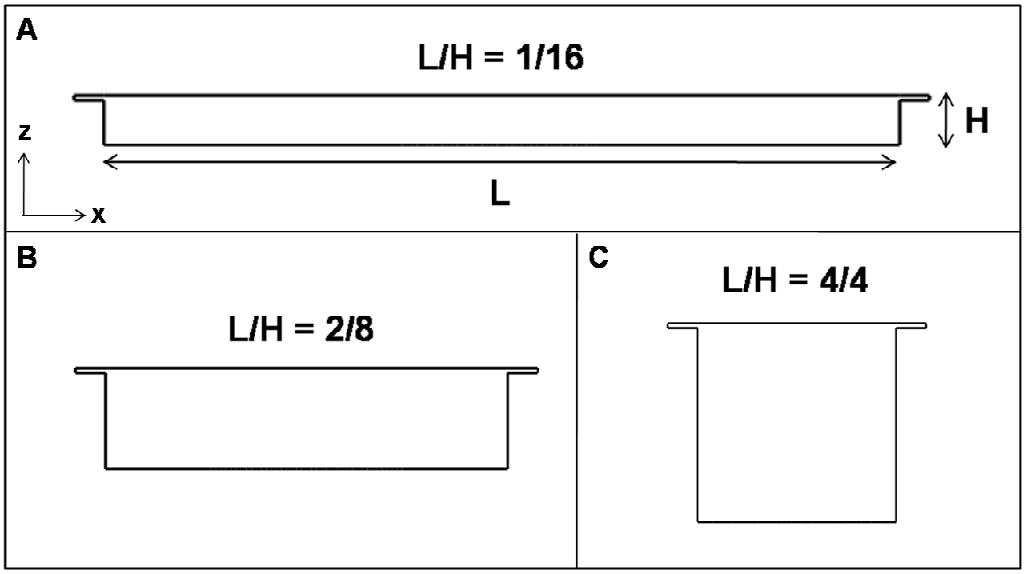

Figure 2.5. *Schematic representation of the modeled culture chamber. The characteristic geometric dimensions are its length L and height H. The microfluidic channels entering and exiting the chamber have a fixed height of 100 µm. Panels* ***A.*** ***B.*** *and* ***C.*** *show the three configurations used for the modeling which are represented by the varying ratio L/H, while L·H remains constant.*

With the primary aim of deriving estimates for fundamental parameters identifying the dominating phenomena, the outputs of our modeling were:

- the concentration values at the steady state;
- the "availability" of molecules (metabolites) at the cells surface in terms of dimensionless fluxes.

As said before, the cultured cells are adhering to the bottom of the chamber with a maximum density that is dictated by the available surface. Cell density is an important variable that has been analyzed and discussed in section 2.2 of this chapter. In this section, we considered a cell layer covering the entire available surface of the "4/4" configuration. This length of the cell layer was used for all configurations.

2.3.1 Transient analysis on conventional batch cultures

The three configurations of Figure 2.5 have also been modeled as batch systems, studying an appropriate temporal transient aimed at evaluating the concentration profiles and fluxes. Again, a cell layer was adhering to the bottom of the chamber and was characterized by a defined uptake rate for a given metabolite. The results of this analysis are reported in Figure 2.6.

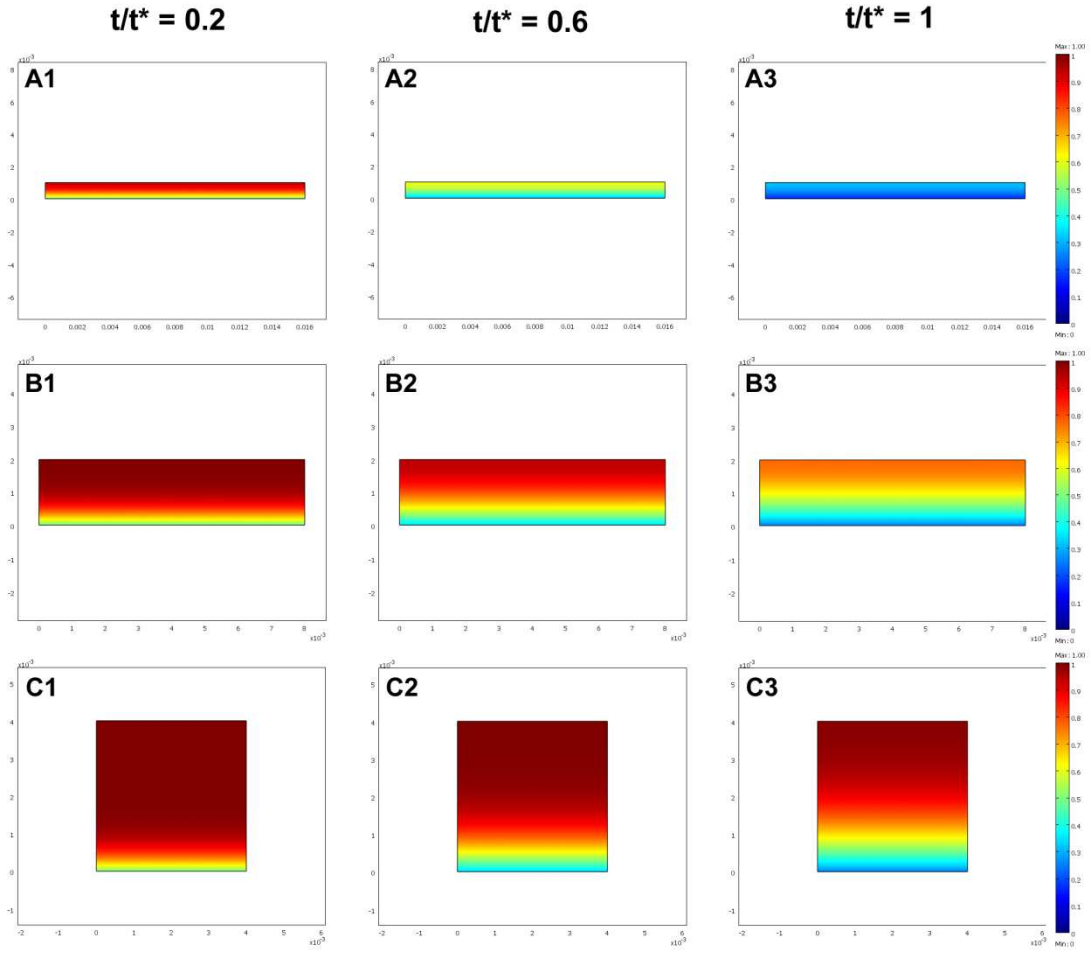

Figure 2.6. *Simulated transients on the three chamber configurations. The color coded bars on the right are valid for each of the represented dimensionless times and indicate the value of the ratio c/c*.* ***A. B.*** *and* ***C.*** *represents the configurations for H/L of 1/16, 2/8, and 4/4 respectively.*

The columns of Figure 2.6 show snapshots taken at representative dimensionless times of the analyzed transient; colors corresponded to a specific value for the ratio c/c*. It can be noticed how at the first times (first column), the varying geometric configurations have little or no effect on the concentration gradient that is established. Only at later time points, the formation of a depletion zone at the cell layer is differentially developed in the 3 configurations.

Another fundamental observation that can derive from these images is the effective spatial uniformity of conditions on cell surface (here in terms of flat concentration profiles) on sections parallel to the bottom of the chamber (on the z axis).

Figure 2.7 shows the results of the analysis of the dimensionless concentration profiles and dimensionless fluxes on representative sections of the culture chambers.

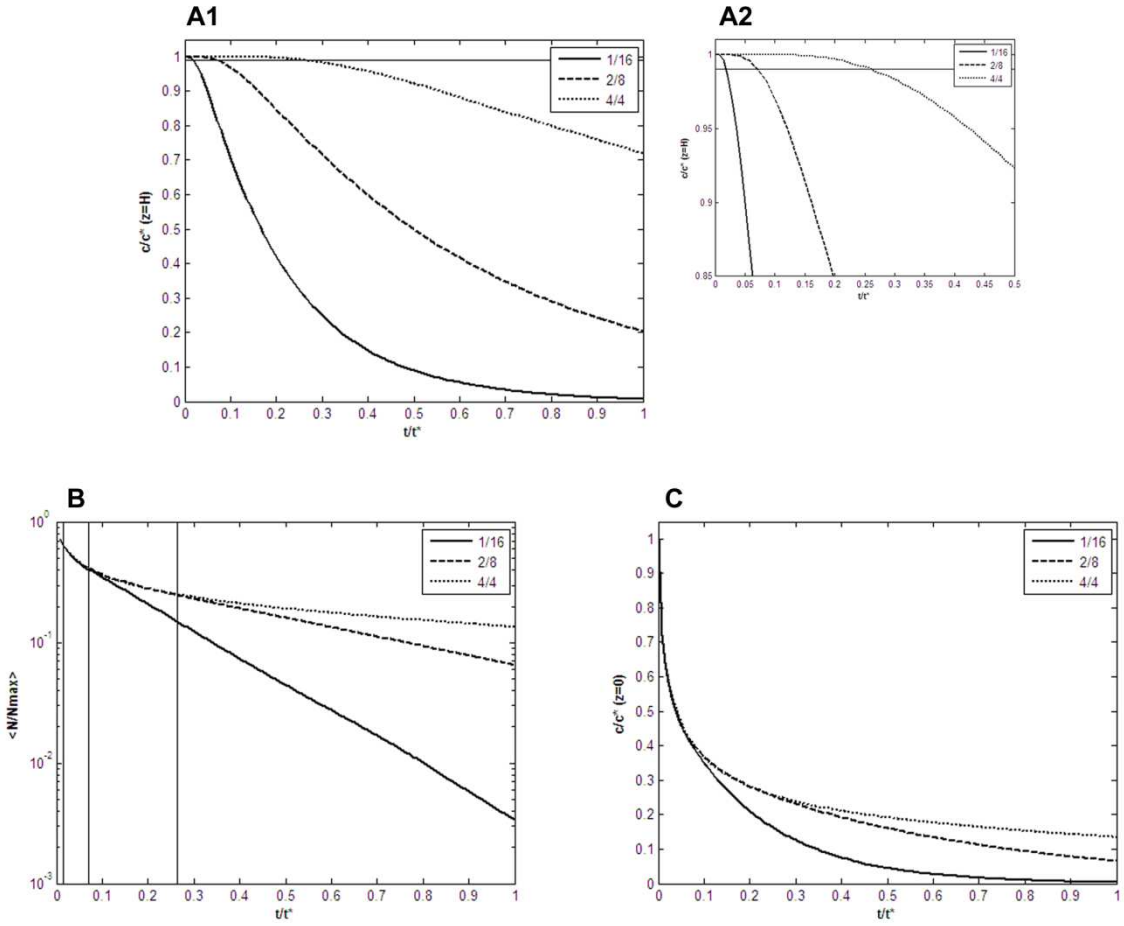

Figure 2.7. *Transient analysis on batch cultures: concentration profiles and fluxes for the three chamber configurations.* ***A1.*** *concentration profiles at the top of the chamber. Horizontal line is set at 99% of the initial concentration value. Zoomed image in* ***A2*** *allows for a better identification of the characteristic times at which this decrease occurs.* ***B.*** *dimensionless fluxes on the same section. Vertical lines mark the above mentioned times.* ***C.*** *concentration profiles at the cell layer (z=0).*

From the concentration profiles evaluated at the top of the chamber shown in panel A1 it is possible to estimate the times at which *c/c** decrease below the threshold set at 0.99. The magnification of the area of interest in panel A2 allows for an easier identification of such times and for a clearer understanding of the different behaviors of all three configurations. As can be noticed, the concentration profile for the configuration with the highest aspect

ratio (“1/16”) showed a more rapid decrease at earlier time if compared with the others. In particular, the “4/4” configuration initiated the concentration decrease at much later times.

The importance of identifying the times at which this decrease occurs resides also in the consequent shift in the fluxes regime, as can be noticed from the graph in panel B. This transition, that can be translated in a linear behavior (in semi-logarithmic terms), had its starting point at that time in which the decrease in concentration within the chamber “reached” the top section at $z=H$.

Figure 2.8 reports additional graphs of the concentration profiles on vertical sections on the z-axis direction.

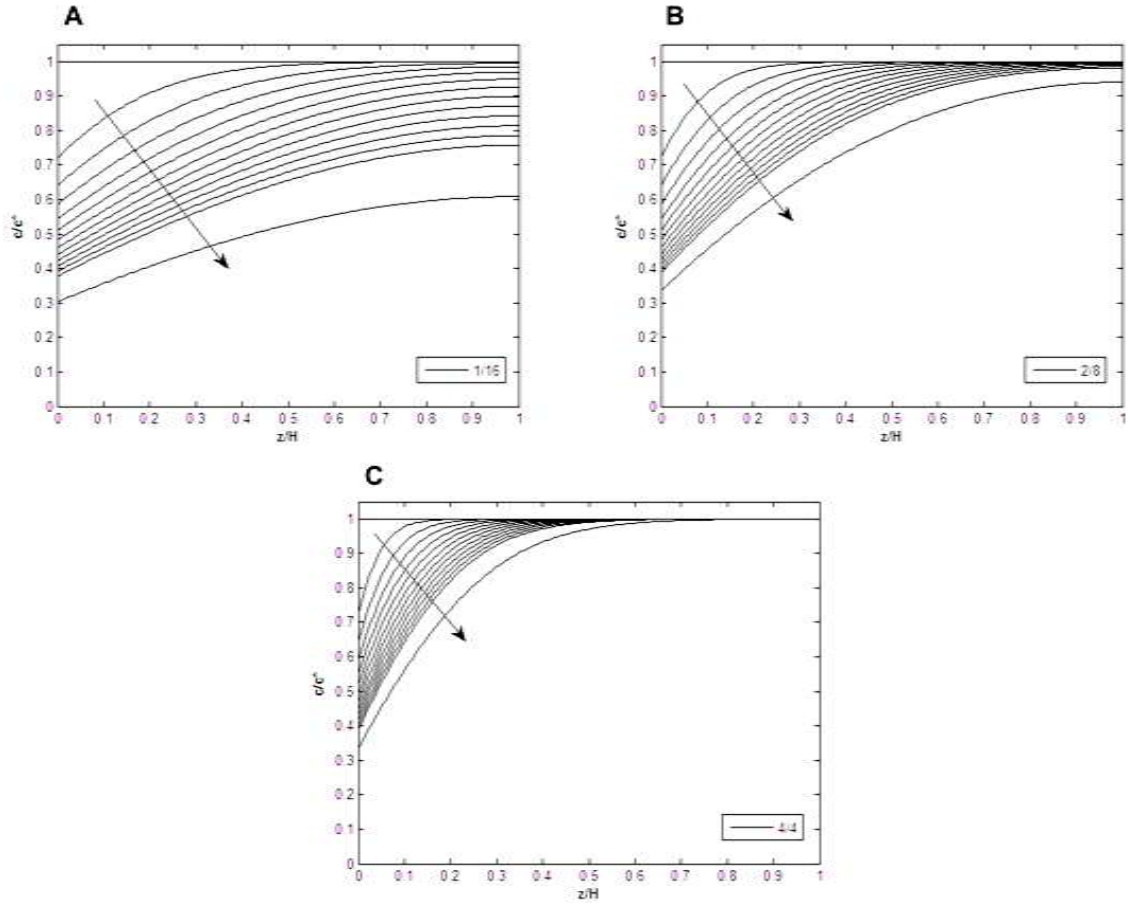

Figure 2.8. *Transient analysis on batch cultures: concentration profiles along the z-axis of the chamber at different times. Profiles were evaluated for each configuration (“1/16” in A., “2/8” an B., and “4/4” in C.) at values of t/t* from 0 to 0.12 with 0.01 intervals, and finally at 0.18. Arrows identify the increasing times direction.*

From these images, it is straightforward to observe how the “1/16” configuration (Figure 2.8 A), resulted in a sudden drop in concentration starting from the first time steps. The “2/8” configuration (Figure 2.8 B), showed a slightly different behavior with a delayed decrease in concentration; finally, this decrease was absent, in the analyzed time course, for the “4/4” configuration (Figure 2.8 C).

The next step would then be to study the effects of introducing perfusion in the above discussed configurations together with the need to capture the heterogeneity that may consequently be generated within the system.

2.3.2 Steady state analysis on perfused cultures

As mentioned before, the study has been performed trying to obtain generalized description of the system that could eventually be extended to different configurations. in this sight, we based the analysis on dimensionless variables such as the Peclet number. The complete list has been listed in section 2.3.

A convective regime was induced introducing perfusion within the system; with a fluid in motion entering the chamber from the microfluidic channels from the upper left corner of the chamber (see Figure 2.2).

The qualitative analysis in Figure 2.9 allows to identify the different fluidodynamic behavior of the 3 simulated culture chambers.

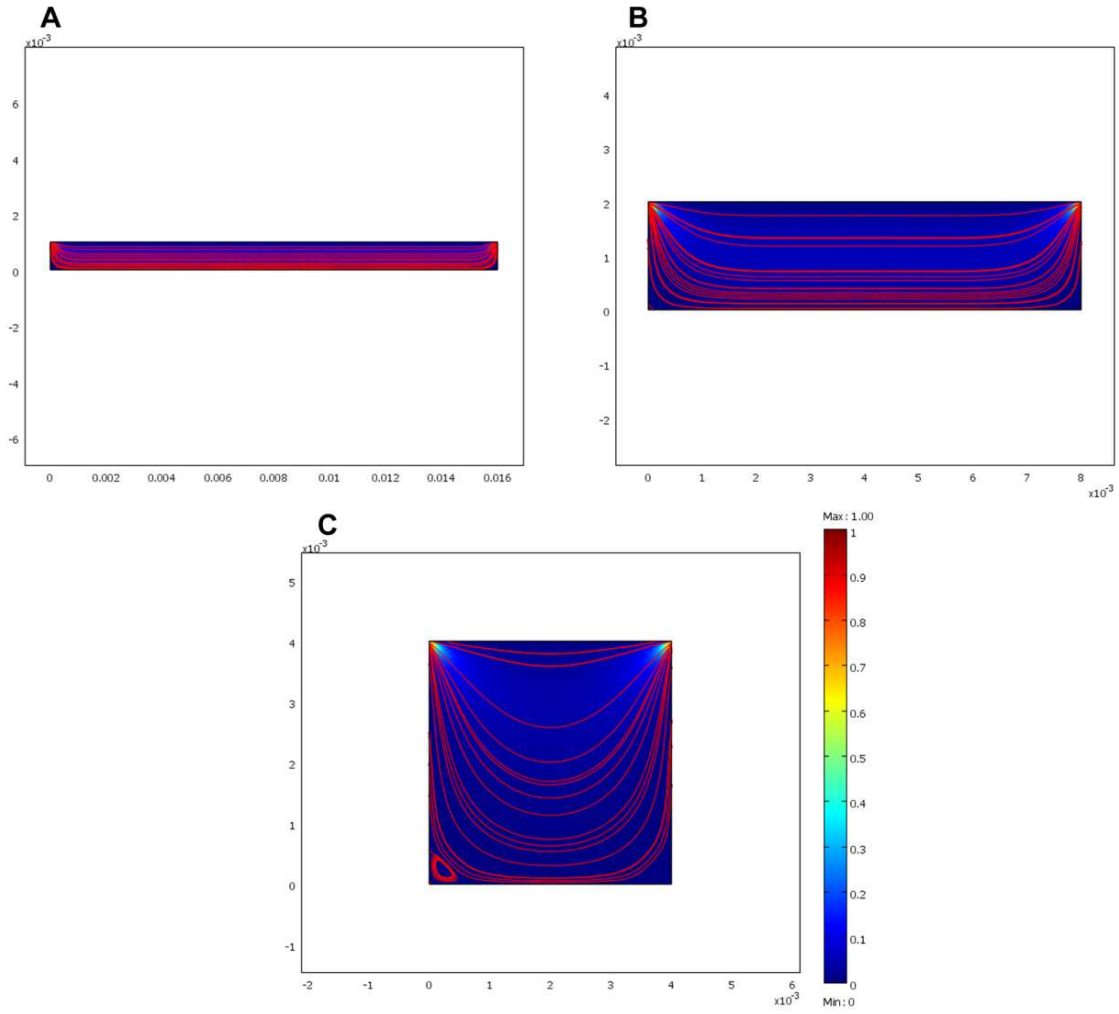

Figure 2.9. *Streamlines and velocity fields. The color coded bar is valid for each simulated configuration and represents the dimensionless velocities values, v/v_{Max}, where v_{Max} is the maximum velocity developed within the chamber.*

The velocity field identified by the streamlines in the configurations with the higher aspect ratios ("1/16" and "2/8") were parallel to the bottom of the chamber (where cells would adhere) and were uniform in almost the entire section. Considering the last configuration, the disuniformities are more evident and are highlighted by the dead volume on the corner at the bottom of the chamber.

Figure 2.10 shows the velocity profiles, v/v_{max} measured at the cells layer level for the 3 configurations. The representative section for the cell layer was chosen at 50µm from the bottom of the chamber.

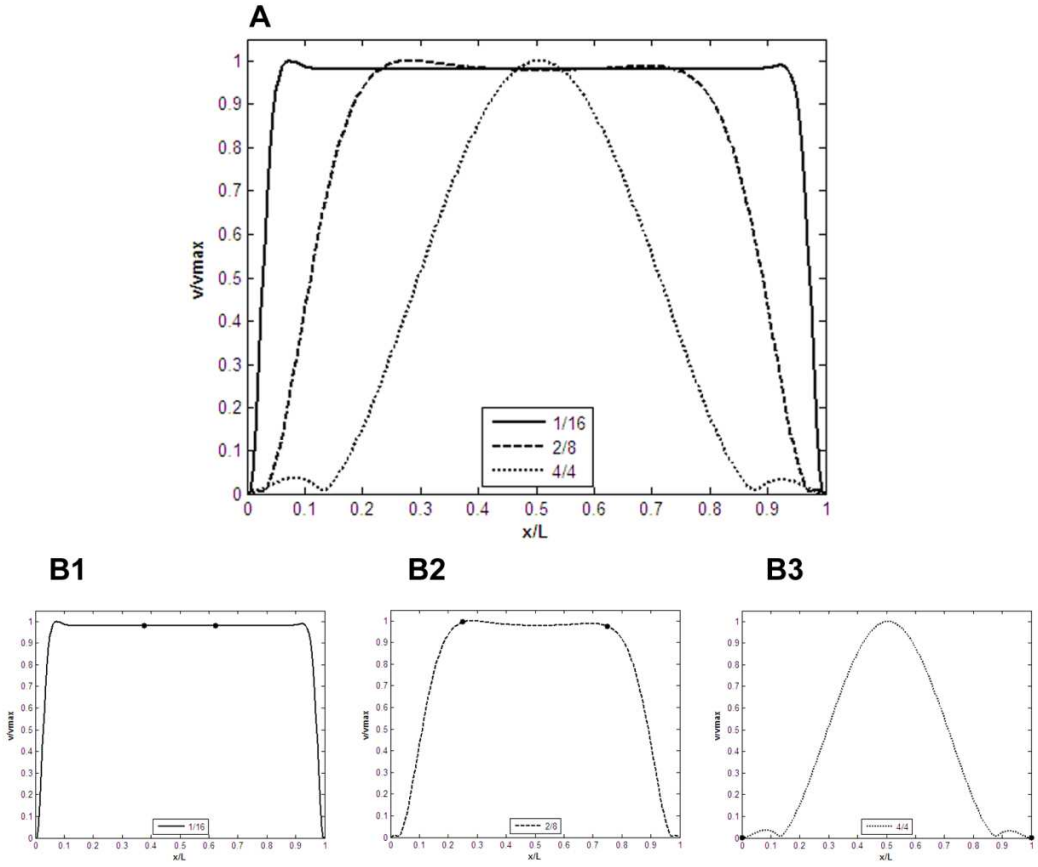

Figure 2.10. *Velocity profiles. A. The dimensionless velocity profiles at the cell layer were evaluated along the dimensionless chamber coordinate. B1-3 show the individual profiles and the dots highlights the positions between which cells would be adhering in each configuration (4 mm in all cases).*

Figure 2.10 A, highlights the differences in the velocity profiles at the cells layer. Decreasing the aspect ratio *H/L* from 1/16 to 4/4, the velocity profiles changed from an almost perfect flat profile to a parabolic one. The direct consequence of this behavior is the fact that cells adhering to the bottom of a "1/16" chamber experienced uniform and constant velocities, similarly to what happened in the "2/8" configuration. In parallel, cells on the "4/4" configuration would be exposed to the entire and heterogeneous range of velocities developed in the parabolic profile.

The dots in Figure 2.12 B1-3 allow to visualize the exact location of the cells along the chamber coordinate and to determine the above mentioned range of velocities.

Figure 2.11 show some relevant results obtained studying the concentration profiles at the steady state, simulating all the Pe within the defined range, for each configuration.

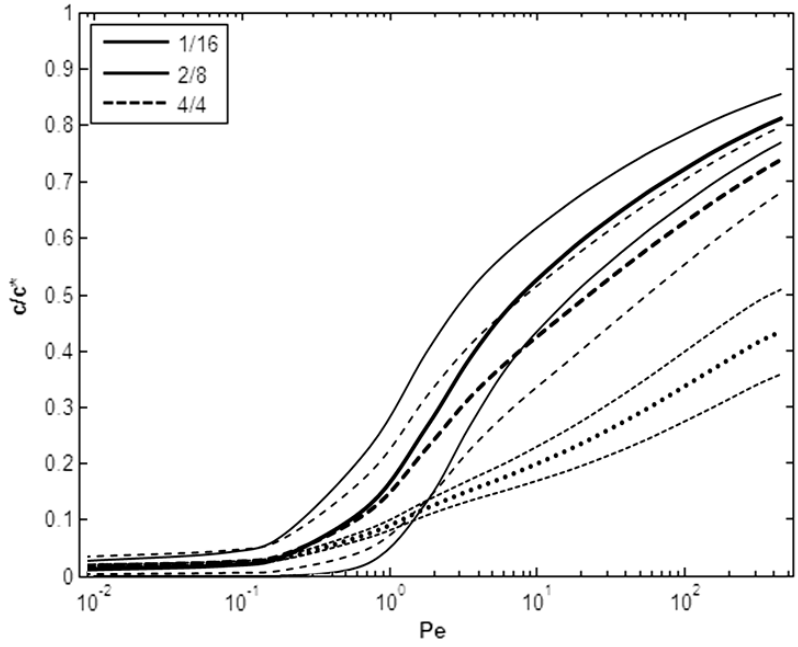

Figure 2.11. *Average concentrations and standard deviations. For each configuration, thick curves represent <c/c*> while thin curves identify the standard deviations of the c/c* values.*

First of all, the differences in terms of mean c/c* increased with increasing Pe. At lower Pe, the dimensionless concentration was almost constant while the first differences started to emerge for Pe~1. We can thus conclude that the variations in concentration, both within each configuration and between the different configurations, could be detected depending on the passage from a diffusive (Pe<1) to a convective (Pe>1) regime.

Related to that, it was evident that the convective regime lead to increased differences between the three configurations. Increasing Pe determined more dramatic differences in the "1/16" case if compared with the others.

Thin curves represent the values of $c/c^* \pm \sigma$, where σ is the standard deviation; increasing distances of these values from the thick curve (representing the mean) translates into increased heterogeneity of behavior within the cell layer along the x coordinate.

Figure 2.12 shows the dimensionless concentration profiles as a function of the dimensionless x coordinate at 3 different representative Pe values:

- *Pe = 0.001*: diffusion-limited regime;
- *Pe = 1*: competition between convection and diffusion;
- *Pe = 100*: convection-dominated regime.

In addition, for the same Pe values we reported the results of the simulations giving a color coded representation of the dimensionless concentrations for the entire chamber.

In Figure 2.12 a, are represented the results of the analysis at the lower Pe. The graph on the left highlights how the “1/16” and “2/8” configurations displayed a high degree of heterogeneity, if compared with the flat profile of the “4/4”. In this diffusion-limited regime, the exponential decrease encountered in the first two could be explained considering the fact that in higher aspect-ratio configurations, the diffusion along the x-axis plays a relevant role in determining a heterogeneity in conditions, while in the “4/4” configuration the diffusion occurs mostly in the z axis direction, giving more uniformity.

In Figure 2.12b, *Pe = 1* determines a competition between convection and diffusion, with an overall effect similar to the one observed in 2.12a, even thought a major difference resided in the much higher absolute values of c/c* for all configurations. Being the effects of convection more relevant in the “1/16” and “2/8” configurations, their profiles changed (in terms of a less steep decrease) significantly.

Finally, in Figure 2.12c a convection-dominated regime increased the differences between “1/16” and “2/8” if compared with “4/4”. Nevertheless, this regime notably reduced the heterogeneity within the cell culture for the first two configurations. On the contrary, there is an increase in heterogeneity in “4/4” due to the un-uniform velocity field developed at the bottom of the chamber (see Figure 2.9).

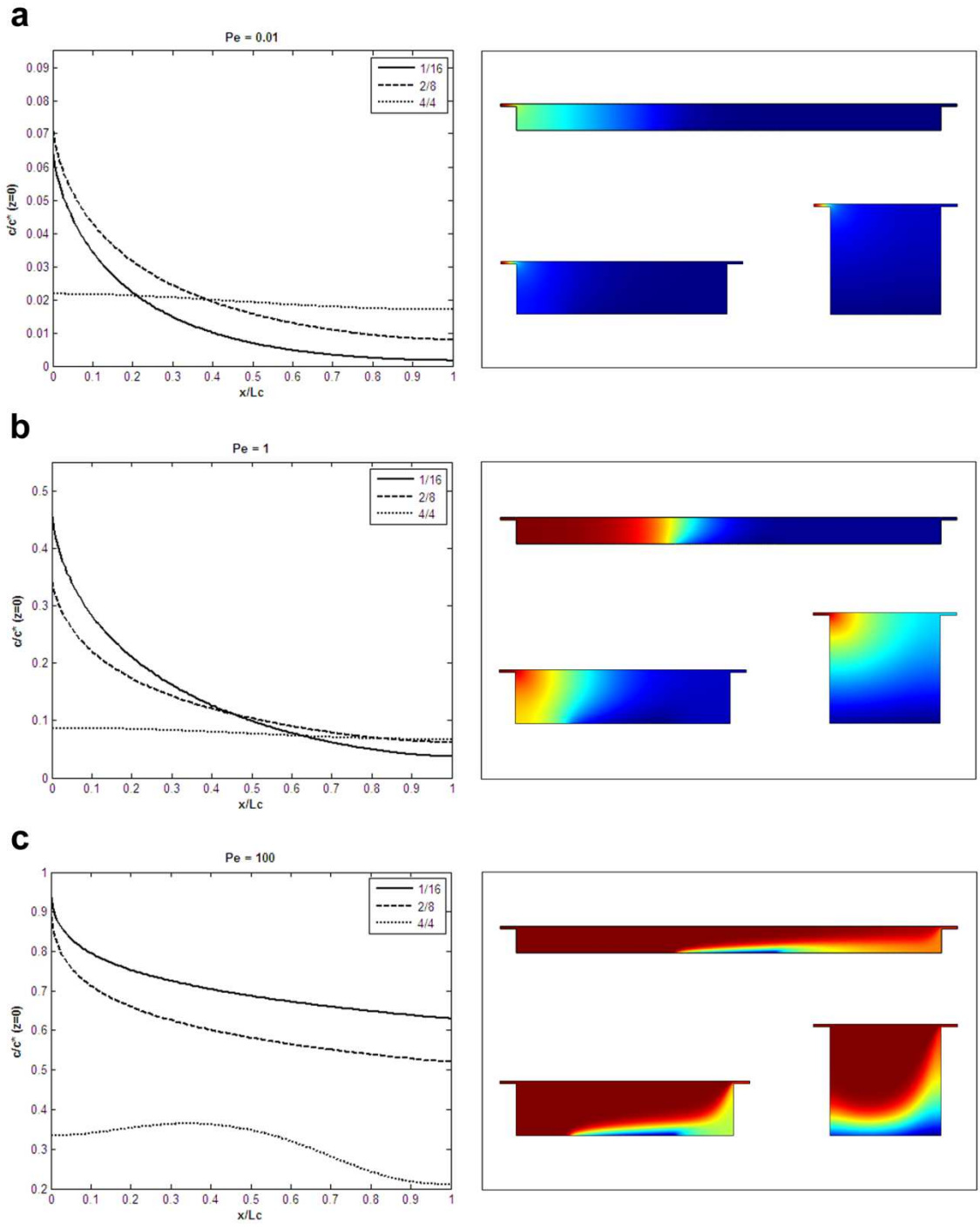

Figure 2.12. *Dimensionless concentration profiles at the cell layer and color coded representations of the dimensionless concentrations for the entire chamber of the three configurations evaluated at defined Pe values (Pe = 0.01, 1, and 100).*

Another measure of the systems heterogeneity as a function of Pe number, is given in Figure 2.13 with a plot of the mean absolute deviation (MAD).

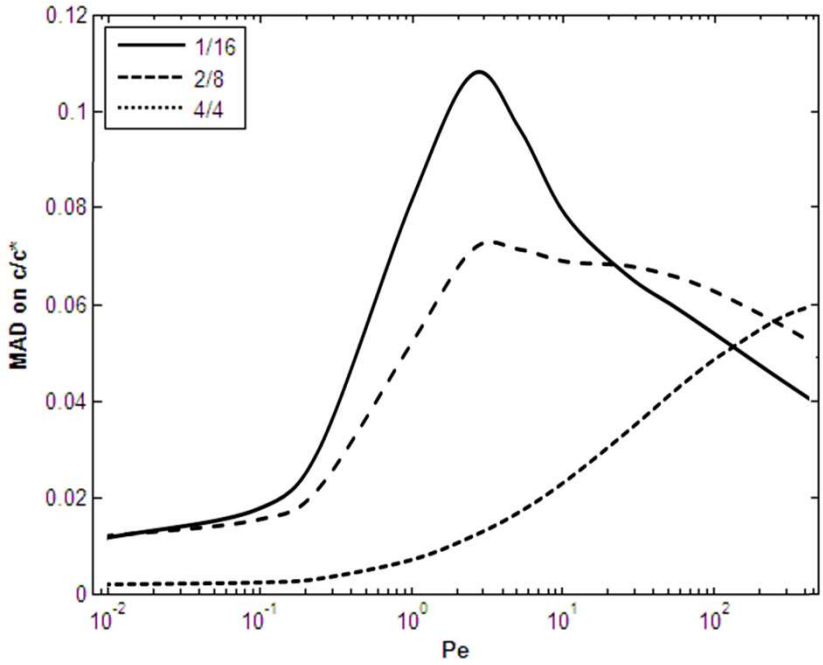

Figure 2.13. *Mean absolute deviation (MAD) of c/c* values as a function of Pe for each configuration.*

From this plot we could highlight how the highest heterogeneity was encountered near Pe = 1 and for the "1/16" and "2/8" configurations. On the contrary, for the above explained reasons, while for these configurations the heterogeneity decreased for further Pe increases, an increase in Pe determined a higher heterogeneity in the "4/4" configuration.

Thus, the configuration that minimizes the heterogeneity of conditions as a function of the configuration geometry and of the operational parameters should be accurately chosen taking all these phenomena into account.

2.4 Computational modeling and dimensionless parameters on MPS with patterned surfaces

The concept of topological control over cells has already been introduced together with its fundamental role in guiding cell adhesion to obtain organized cellular structural templates so to drive differentiation and allow expression of cells correct phenotype. However, in this section we won't discuss these aspects but will instead focus on the phenomenological consequences of confining cells within controlled areas.

The same theoretical and operative path of section 2.3 has been followed here, with the sole difference of having introduced the topological control in the cell layer.

In this study, the fact of spatially organizing cells via micropatterning techniques, didn't modify the local cell density but only altered its global value. The concepts of global and local density are clarified in the following figure.

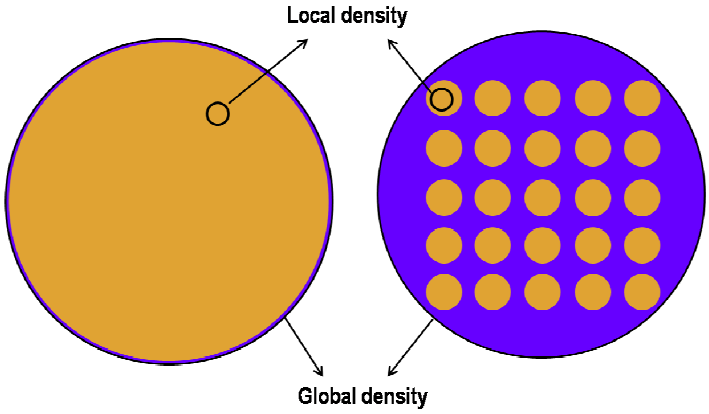

Figure 2.14.*Cell density values. The concepts of global and local cell density are schematized. The global density was evaluated as an average on the entire available area of the culture chamber, while the local value was measured on a smaller area (i.e. the patterned regions).*

Again, cells have been considered adhering to the central area of the bottom of the culture chamber, with a linear extension of 4 mm. A cartoon clarifying the configuration follows.

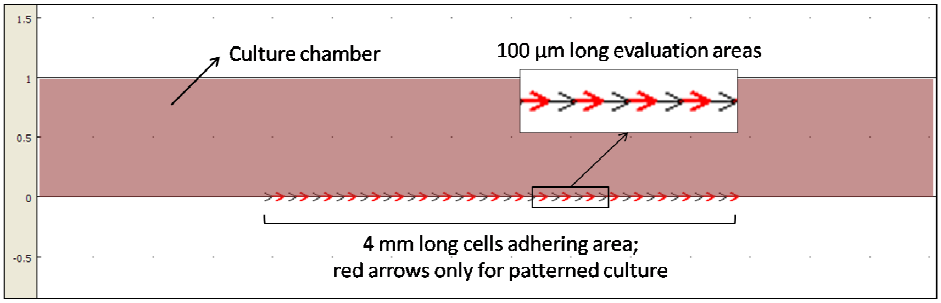

Figure 2.15. *Schematic representation of the modeled culture chamber with the characteristic dimensions introduced in section 2.3.*

Accordingly to this description, the model presented in section 2.3 has been modified taking into account this different cell topology, with cells adhering to defined areas alternated with equivalent empty areas. This translated into different boundary conditions for the bottom plane of the modeled chamber: a specific flux (same as in the case in section 2.3) for the patterned sections with adhering cells and insulation/symmetry for the empty areas.

Figure 2.16, similarly to Figure 2.12, shows the dimensionless concentration profiles at the cell layer and the color coded representations of the dimensionless concentrations for the entire chamber of the three configurations evaluated at defined Pe values (Pe = 0.01, 1, and 100). The global behavior in terms of profiles trend, doesn't differ significantly from the case of a continuous layer of cells. What is evident is the different wave-like characteristic of the profiles (left side of Figure 2.16) and of the depletion zones at the bottom of the chambers (more easily detectable at high Pe on images in the right side), following the pattern of the adhering cells.

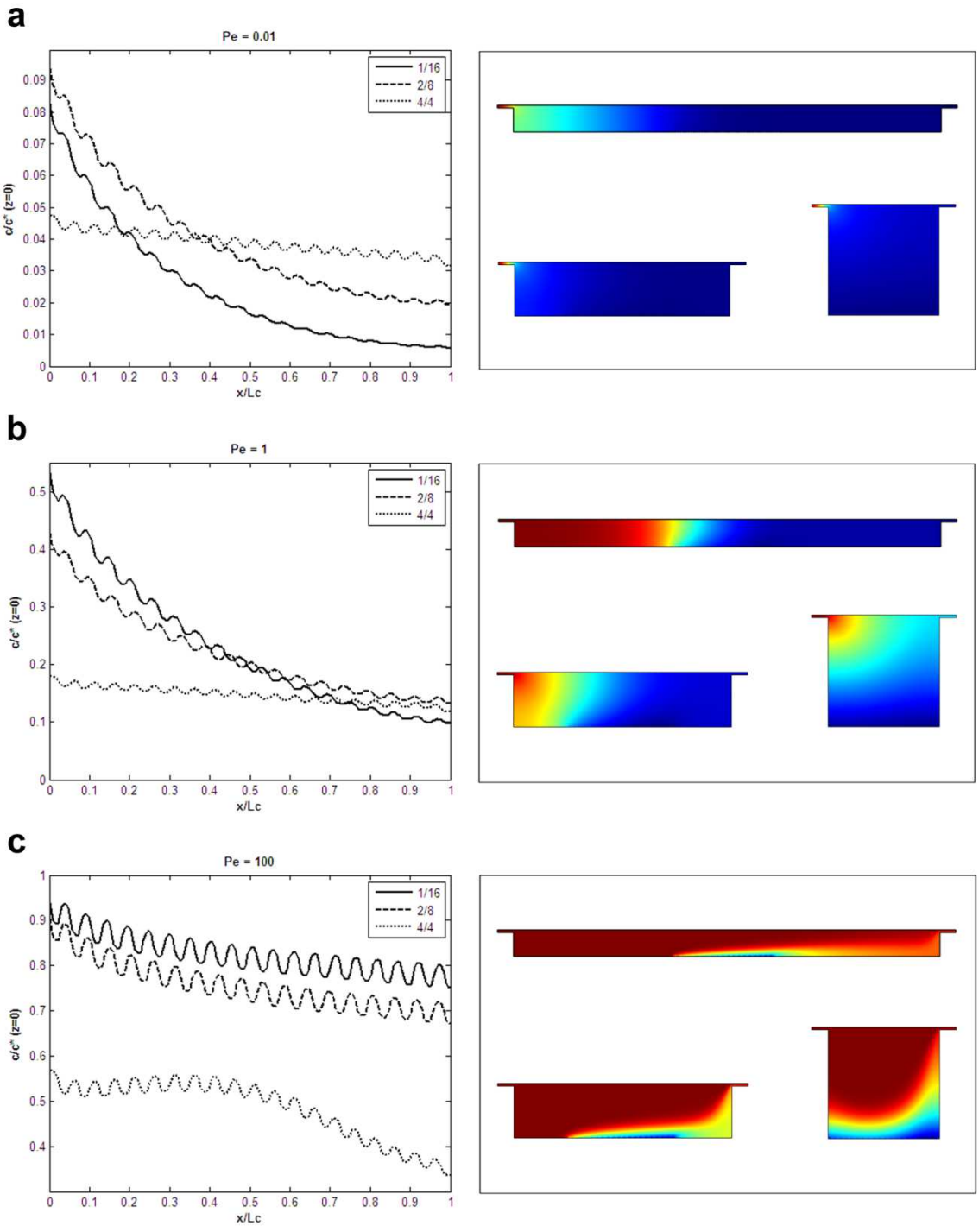

Figure 2.16. *Dimensionless concentration profiles at the patterned cell layer and color coded representations of the dimensionless concentrations for the entire chamber of the three configurations evaluated at defined Pe values (Pe = 0.01, 1, and 100).*

Figure 2.17 and 2.18 reports the graphs of the standard deviations and mean absolute deviations for *c/c**. Similar curves were obtained for the fluxes calculations. Analogous observations to those in section 2.3 could be made.

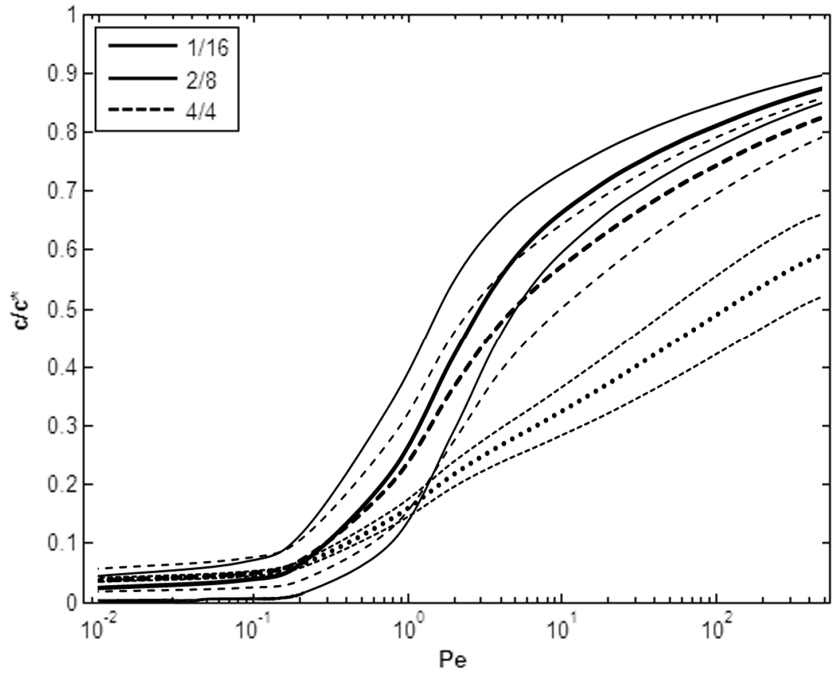

Figure 2.17. *Average dimensionless concentrations their standard deviations. For each configuration, thick curves represent the mean values of c/c* while thin curves identify their standard deviations.*

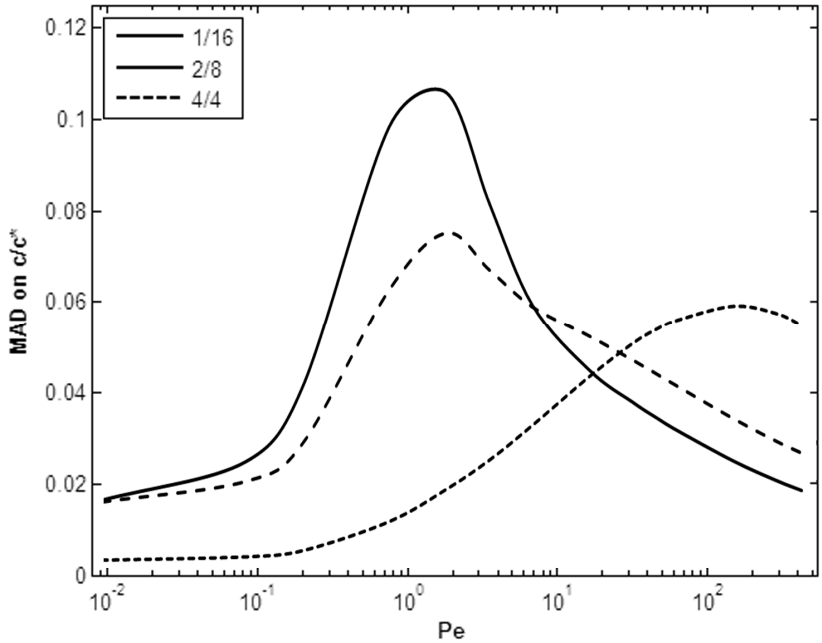

Figure 2.18. *Mean absolute deviation (MAD) of c/c* values as a function of Pe for each configuration.*

Interestingly, we could observe how for a patterned cell layer also the “4/4” configuration reached its maximum MAD value within the studied Pe range. This happened at high Pe convection-dominated regimes, were the velocity field could ensure more uniform conditions even in this configuration.

2.5 References

A. L. Barabási and Z. N. Oltvai, Network biology: understanding the cell's functional organization. *Nature Reviews Genetics*, 2004, **5**, 101-113.

L. H. Hartwell, J. J. Hopfield, S. Leibler and A. W. Murray, From molecular to modular cell biology. *Nature*, 1999, **402**.

Z. N. Oltvai and A. L. Barabási, Life's Complexity Pyramid. *Science*, 2002, **298**, 763-764.

M. Xiong, F. C. Arnett, X. Guo, H. Xiong and X. Zhou, Differential Dynamic Properties of Scleroderma Fibroblasts in Response to Perturbation of Environmental Stimuli. *PLoS Computational Biology*, 2008, **3**.

N. Jamshidi and B. Ø. Palsson, Top-Down Analysis of Temporal Hierarchy in Biochemical Reaction Networks. *PLoS Computational Biology*, 2008, **4**.

M. Cervinka, Z. Cervinkova and E. Rudolf, The role of time-lapse fluorescent microscopy in the characterization of toxic effects in cell populations cultivated in vitro. *Toxicology in Vitro*, 2008, **22**, 1382-1386

E. Cimetta, E. Figallo, C. Cannizzaro, N. Elvassore and G. Vunjak-Novakovic, Micro-bioreactor arrays for controlling cellular environments: Design principles for human embryonic stem cell applications. *Methods*, 2009, **47**, 81-89.

E. Figallo, C. Cannizzaro, S. Gerecht, J. A. Burdick, R. Langer, N. Elvassore and G. Vunjak-Novakovic, Micro-bioreactor array for controlling cellular microenvironments. *Lab on a Chip*, 2007, **7**, 710-719.

D. A. Lauffenburger and J. Linderman, *Receptors - Models for binding, trafficking, and signaling*, Oxford University Press, 1993.

T. M. Squires, R. J. Messinger and S. R. Manalis, Making it stick: convection, reaction and diffusion in surface-based biosensors. *Nature Biotechnology*, 2008, **26**, 417-426.

Chapter 3
Microscale bioreactors: microfluidics

In this chapter we will discuss the design, development and fabrication of microfluidic microbioreactors. In particular we will analyze in more detail the key issue generating spatial and spatial-temporal concentration gradients within cell cultures. The theoretical aspects seen in Chapter 2 guided the choice of the proper operative and geometrical parameters while the observations in Chapter 1 helped the establishment of the optimal coupling with the biological system of interest.

3.1 Motivations

Examples of applications of microfluidic platforms for lab-on-a-chip applications have been extensively reviewed (Breslauer et al. 2006, Haeberle and Zengerle 2007, Hong et al. 2008) and point at the advantages deriving from the miniaturization, integration and automation of biochemical assays. Recent literature reflects increased interest in interfacing microfluidic devices with biological systems (Amarie et al. 2007, Jeon et al. 2000, Keenan and Folch 2007, Whitesides 2006).

As already discussed, relevant outcomes would for example derive from the use of microfluidic platforms in drug discovery process (Dittrich and Manz 2006, Wen and Yang 2008), molecular detection (Piorek et al. 2007), and in clinical and medical research.

Concerning a specific application for this latter aspect, Toner and Irimia (Toner and Irimia 2005) have reviewed the use such devices for blood manipulation at the microscale, highlighting the importance of having small, portable, highthroughput but yet reliable and ready-to-use instruments for specific blood analysis tasks.

In addition, microfluidics has been adopted also for tissue engineering purposes, and examples exist in applications involving basal lamina, vascular tissue, liver, bone, cartilage and neurons (Andersson and van den Berg 2004). Again, microfluidics can greatly contribute to novel achievements in this field as it allows for a better control of the microenvironment, thus generating in vitro systems apt to be used as physiological models for the study of the complexity of biological phenomena.

Many other interesting review can be cited, some of which give more insights also in the fabrication processes and properties of the materials that are typically used (McDonald et al. 2000, Sia and Whitesides 2003, Whitesides et al. 2001).

As already introduced in Chapter 1 and extensively discussed in Chapter 2, it is fundamental to gain a deep knowledge of the physics of phenomena and of fluid flows at the microscale. Excellent descriptions can be found in the literature (Beebe et al. 2002, Squires and Quake 2005).

3.2 Materials and methods

Microfabrication is a well established technique and the protocols and procedures that must be followed are extremely rigid. No relevant modifications can be made, so for what concerns the material and methods for the effective fabrication of microfluidic platforms, we refer to the cited literature and to the corresponding sections of the publications that are reported in the Appendixes, and in particular in Appendix A, B, and G.

In the following paragraphs we will describe the application of microfluidic technologies to 3 case studies and report the most relevant results. Specific and informative materials and methods sections will be enclosed for each case study in the relative paragraph.

3.3 Effects of glucose and hydrodynamic shear on Primary Mouse Aortic Endothelial Cells

At the core of this study was the huge relevance of the Advanced Glycation End products (AGEs) which are implicated in microvascular and macrovascular complications related to diabetes, renal failure, inflammation, neurodegenerative disorders and natural aging. The receptor for AGEs (RAGE) is minimally expressed in normal tissues and vasculature and upregulated in diabetic tissues, thus determining the above mentioned consequences (Goldin et al. 2006).

The main aim of this study was thus to test the impact of RAGE ligands on primary mouse aortic endothelial cell (PMAEC) shape and release of secreted factors that determine processes such as inflammation, under different conditions involving dynamic or static culture.

Our role in this study was to develop and test a simple device allowing to culture endothelial cells in perfused conditions and to simultaneously analyze the effects of different factors.

As seen in Chapter 1, in order to obtain valuable data in biological studies it is important to recapitulate the cell *niche*; for this reason the experimental plan has been based on the attempt of mimicking the physiology. We thus imitated:

- normal and diabetics tissues using different glucose concentrations in the culture medium;
- blood flow shear stress using a microfluidic device.

For this reason we designed and realized an array of parallel microfluidic channels that would allow a sufficient degree of parallelization, and thus consenting to test multiple conditions within the same platform and during the same experimental run. (Figure 3.1) The overall dimensions were chosen to ensure compatibility with standard glass slides, while the those of each channel to have a statically significant number of cells for the downstream analyses and within any observation field at the microscope. The internal volume of each channel was 2.7 μL. The system allowed to collect the discarded medium during culture, and such volume was sufficient to perform quantitative analysis.

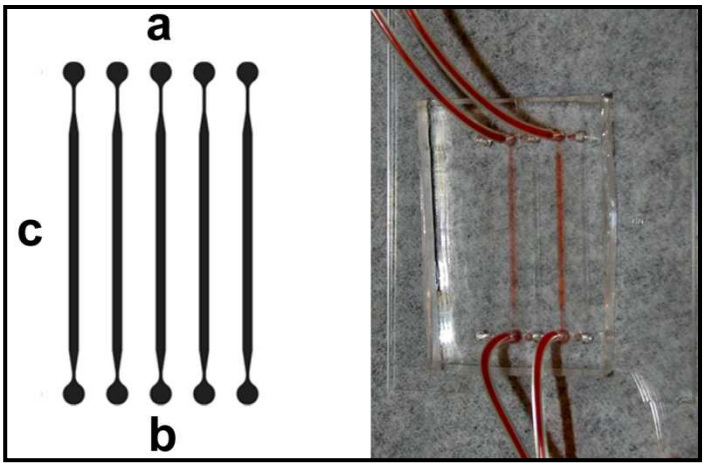

Figure 3.1. *Schematization and image of the microchannel array. On the schematics on the left, inlets and outlets are denoted by a and b, respectively. c indicates the culture section of the channel. Each microchannel was 30 mm long, 900 μm wide and 100 μm high.*

The two variables, glucose concentration and shear stress level, were initially established for the preliminary experiments; in particular:

- Glucose concentration in culture medium on three levels:
  - CTRL: 5.5 mM D-glucose,
  - L-GLU: 5.5 mM D-glucose + 9.5 mM L-glucose,
  - HIGH: 15 mM D-glucose (3 times higher than the physiological level);
- Shear stress by means of fluid flow:
  - Static culture: 0 dyne/cm^2,
  - Dynamic culture: constant flow: 0.001 dyne/cm^2.

The microfluidic channels were coated with 20 μg/mL fibronectin prior to cell seeding; an optimal cell seeding density has been determined in order to obtain a confluent monolayer since the first stages of the experiments. After seeding, all cultures underwent a "preconditioning" stage with the defined culture medium for 4 days before starting perfusion.

The analysis performed on the cultured cells have been:

- Viability by Live & Dead assay;
- Morphology by immunofluorescence;
- AGEs and methylglyoxal (MG, a precursor of AGEs) release by ELISA and HPLC.

3.3.1 Results and discussion

A more detailed description of the biological data can be found in (Serena 2009).

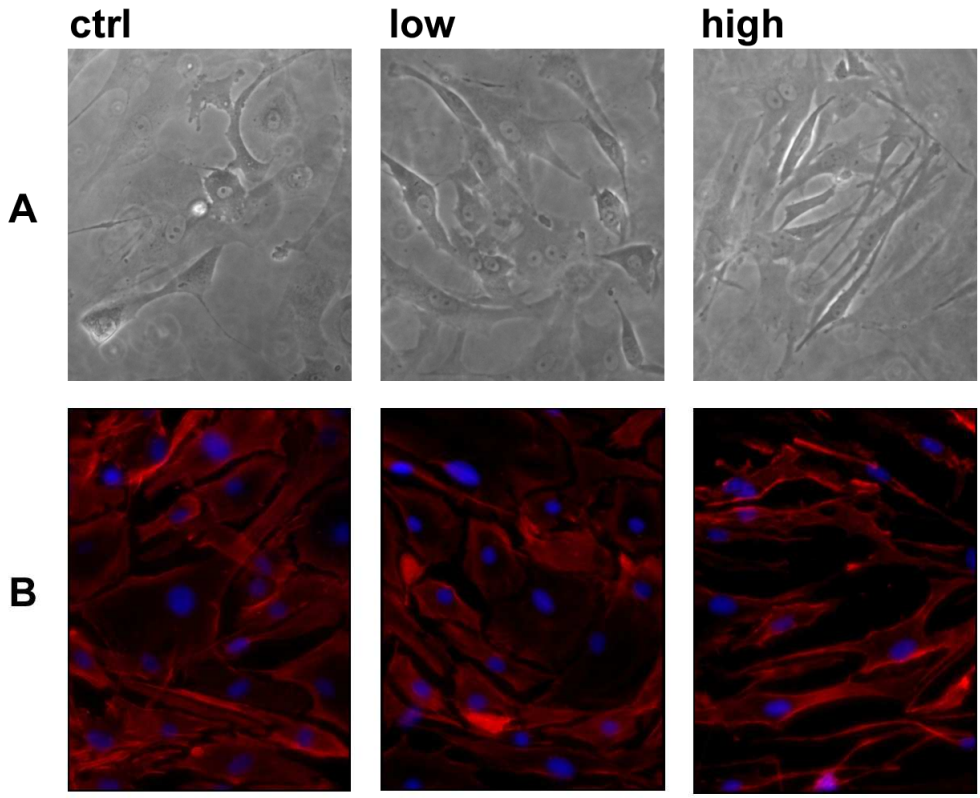

Figure 3.2. *Effect of glucose concentration on wild type PMAEC cells cultured in microfluidic channels. Bright field images are in the first row (A), while second row (2) reports the results of an immunostaining for Actin, protein marking the cytoskeleton. This staining allows to better notice the morphological differences between the varying conditions.*

It was evident (Figure 3.2) how high levels of glucose in the culture medium induced changes in morphology: cells looked more stressed and elongated, with several pseudopodia that could be observed both with bright field imaging (Figure 3.4A) and with immunofluorescence for Actin (Figure 3.4B).

We report some results deriving from the quantification of AGEs in the culture medium during culture.

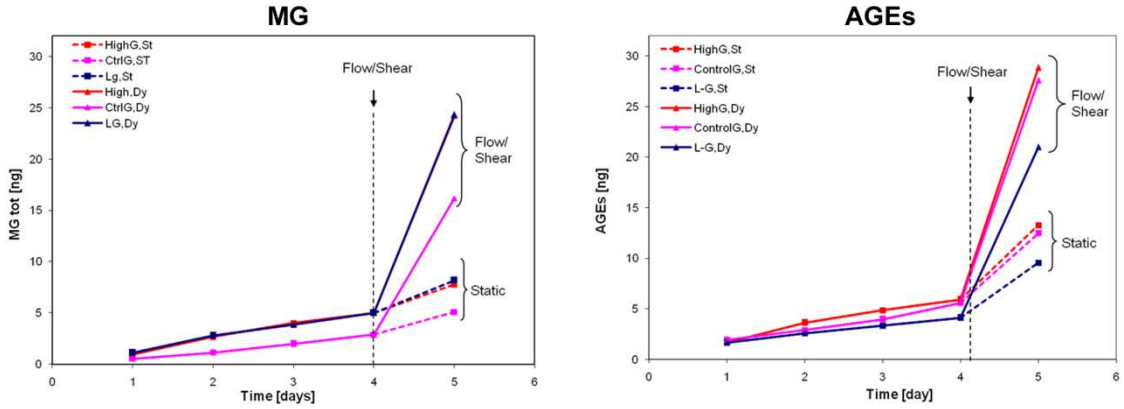

Figure 3.3. *Effect of glucose concentration and of shear stress induced by fluid flow on wild type PMAEC cells cultured in microfluidic channels. The application of flow, with extremely low shear stress, induces an increase in MG and AGEs release in the culture media.*

It is evident how the effects of perfusion dramatically increased the release of AGEs and MG by the cultured cells. This effect overcome the one due to the different concentrations of glucose in the culture medium, which could not be assessed for this particular combination of variables.

Similar experiments were performed using a particular RAGE-KO (knock-out) cell line, giving similar results in terms of enhanced release of MG and AGEs in the culture medium but with less effects in terms of changes in morphology following exposition to increasing glucose levels (Serena 2009).

Those preliminary results were promising in sight of the final goal of the study, and contributed rising new questions on which the dominating phenomena could be and which combination of factors and variables could lead to the more dramatic results.

3.4 Microfluidics-generated spatial concentration gradients: Wnt3a and response in β-catenin signaling pathway

The relevance of this study (reported in detail in Appendix G) is related to the extreme importance of the molecules of the Wnt family and their signaling pathways. Much efforts in the nowadays scientific community are directed towards deeply studying and comprehending the mechanisms, causes and effects related to Wnts functions.

Wnt proteins are a family of powerful macromolecules involved in a multitude of biological phenomena ranging from early-stage cell fate specification, to embryo development, cell proliferation, differentiation and tumorigenesis (Clevers 2006, Logan and Nusse 2004, Moon 2005, Moon et al. 2002, Moon et al. 2004). Of particular interest is the pattern by which the Wnt signals are presented to the cells, though concentration gradients on a short and long range (Aulehla et al. 2008, Bartscherer and Boutros 2008). However, surprisingly little is known about the effects of Wnt gradients on cell populations and the quantitative data have not been reported.

Microfluidic devices offer the possibility of generating complex and well defined patterns of stimulation, via tight control of fluid dynamics on a micrometer scale.

Because of the laminar regime that is inherent to fluid flow in micro-channels, the geometry of the micro-device and the flow rates can be tuned to establish desired patterns of flow and molecular transport. The utilization of flow rates that are in the range of few μL/min enables generation of well-defined, diffusion-independent concentration profiles. Examples include studies of chemotaxis in cell culture systems utilizing hydrogels of differential compositions, (Burdick et al. 2004) short-term perfusion of graded concentrations of regulatory factors over seeded cells (Saadi et al. 2006), and the assembly of membrane-based diffusion chips (Diao et al. 2006).

However, the use of such microfluidic gradient generators is generally associated with hydrodynamic shear stresses exerted on cultured cells, that arise from the small characteristic dimensions of microfluidic channels (Chisti 2001). For studies of most cells, control of hydrodynamic shear is vital for the maintenance of the cell well-being during cultivation (Cimetta et al. 2009).

Our study was focused on β-catenin signaling in response to Wnt3a concentration gradients.

With this aim, we designed, fabricated and validated a microfluidic device enabling the generation of stable and controlled Wnt3a gradients under cell-protective conditions of low hydrodynamic shear, and thus prolonged culture of cells necessary to cover the time span required for gene activation. We used a cell line specifically created for this study: HEK 293T cells stably expressing pBARVS (Biechele and Moon 2008), a Wnt/β-catenin reporter driving the fluorescent expression of Venus.

The device consisted of three 500 µm wide channels aligned in parallel, where the middle channel served as the cell culture space (Figure 3.4). The three channels were connected by an array of smaller channels (25 µm wide x 50 µm deep, spaced at 50 µm) perpendicular to the three larger channels, enabling diffusion of molecular species without significant convective flux. This configuration allowed the obtainment of sharp and stable concentration gradients inside the middle channel, by the diffusion of species between the two outer larger channels.

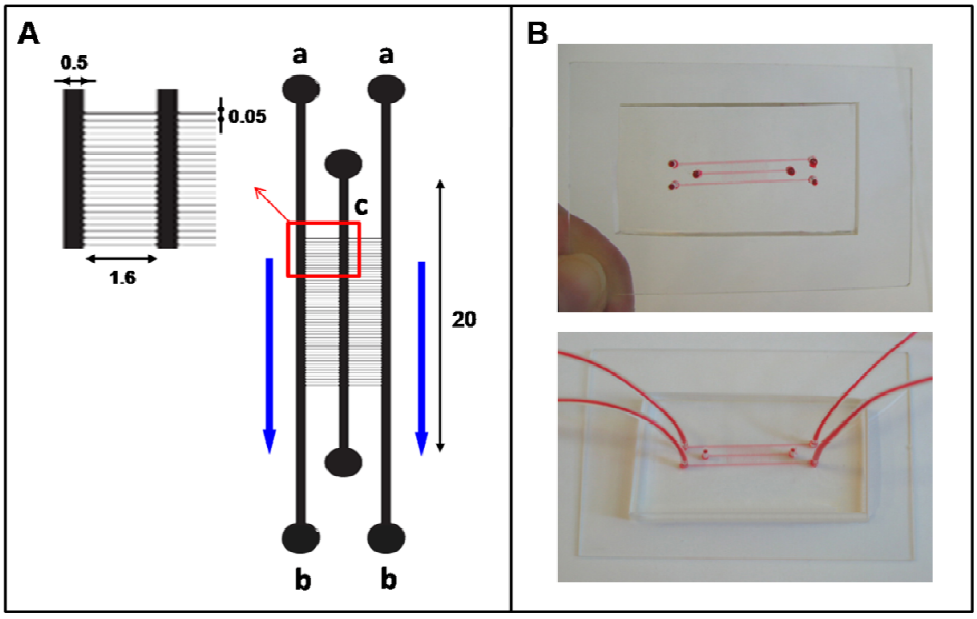

Figure 3.4. *Microfluidic device. The microfluidic bioreactor (panel A) was composed of two flow channels with inlets in a and outlets in b, that flank the culture channel c. Lateral arrows identify the main flow direction. The reported dimensions are in mm. The height of the microbioreactor is 50 µm. Images in panel B are top views of the microbioreactor in which the fluidic channels are filled with a color tracer; the inlet and outlet tubing connecting the assembled device to the syringe pump is shown in the lower image.*

In order to predict the flow regimes and the concentration profiles within the microbioreactor culture channel, we performed a mathematical modeling with a two-dimensional (2D) geometry of our microbioreactor (top view of the microfluidic channels). The Navier-Stokes equations for incompressible flow, modified for taking into account a surface forces-related component, and the convection-diffusion equation were numerically solved using a finite element analysis solver (Comsol Multiphysics).

To validate the model predictions, the resulting Wnt3a concentration profiles were compared with experimentally measured profiles of fluorescently labeled dextrans of defined diffusion coefficient, used as color tracers flowing into the microbioreactor.

After choosing the optimal operative variables, cells were seeded inside the culture channels of the microbioreactors and cultured under both static or perfused conditions under a stable Wnt3a concentration gradient.

The evaluation of the cell response to Wnt3a concentration gradients was performed on live cell cultures by measuring the presence and the distribution of the fluorescent signal resulting from the activation of the targeted Venus-tagged reporter gene. The quantification of fluorescence images was performed in two ways: (i) by evaluating the mean grey value (MGV) of the image, thus measuring the averaged fluorescence intensity; (ii) by evaluating the fraction of cells expressing Venus signal, determined as the ratio between the area of cells expressing Venus signal and the total area covered by cells. The developed script containing the chosen operations was run with Matlab.

3.4.1 Results and discussion

Establishment of concentration gradients: effects of flow velocity and diffusion coefficient

The capability of the microbioreactor to generate predictable concentration gradients of soluble molecules was theoretically tested via mathematical modeling, for a range of fluid flow rates and diffusion coefficients. Experimental data for concentration gradients were obtained using fluorescent dextrans as molecular-weight tracers for proteins of interest in cell culture studies, and compared with the corresponding gradients predicted by a rigorous mathematical model of momentum and mass transport (results are reported in Appendix G).

Both the experimental and model-predicted concentration profiles showed that at low flow rates and for low molecular weight chemical species (i.e., higher diffusion coefficients) molecular diffusion becomes the dominating transport regime, and that these conditions lead to dissipation of the concentration gradient. On the contrary, flow rates as low as 1 µL/min and species with approximate sizes of 40 KDa (corresponding to the molecular weight of Wnt3a) and higher, are sufficient for obtaining a sharp and stable concentration gradient along the entire culture channel length.

Experimental conditions analysis

Based on the results obtained from the above described experiments and considering the fact that the value of $6 \cdot 10^{-11}$ m^2/s could be used as Wnt3a diffusion coefficient, the appropriate culture conditions were set choosing a flow rate of 1 µL/min. Figure 3.5 shows mathematical analysis of (i) concentration gradients, (ii) velocity profiles, and (iii) hydrodynamic shear stress for the microfluidic device operating with Wnt3a as the diffusing molecule at a flow rate of 1 µL/min.

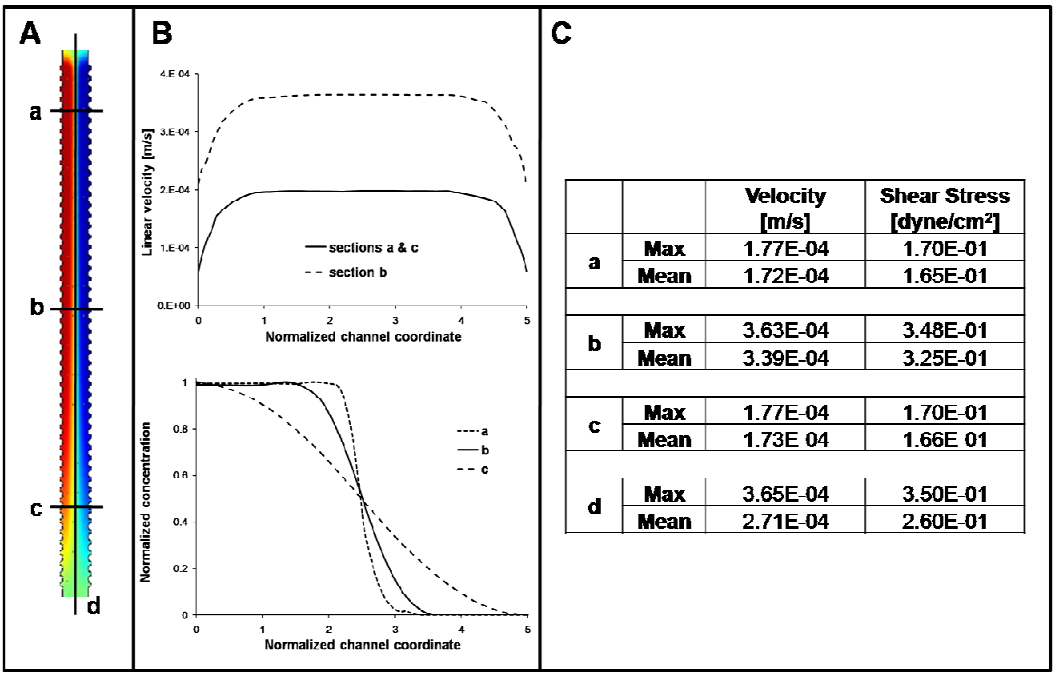

		Velocity [m/s]	Shear Stress [dyne/cm²]
a	Max	1.77E-04	1.70E-01
	Mean	1.72E-04	1.65E-01
b	Max	3.63E-04	3.48E-01
	Mean	3.39E-04	3.25E-01
c	Max	1.77E-04	1.70E-01
	Mean	1.73E 04	1.66E 01
d	Max	3.65E-04	3.50E-01
	Mean	2.71E-04	2.60E-01

Figure 3.5. *Experimental conditions: concentration, velocity, and shear stress. Using the Wnt3a diffusion coefficient of $6e^{-11}$ m^2/s and the flow rate of 1 µL/min, we evaluated the flow characteristics of 4 sections of the culture channel highlighted in A. Panel B shows the plug-like velocity profiles in the chosen cross sections (upper graph) and the curves representing the concentration profiles on the same sections (bottom graph).The table in panel C summarizes the maximum and minimum values for the velocity and shear stress in the 4 sections of the culture channel.*

Panel A shows again the color-coded representation of the Wnt3a concentration gradient inside the culture channel, where a-d letters mark the sections in which further analyses were carried. Panel B, upper graph, shows the modeled plug-like velocity profiles in the chosen cross sections while the curves representing the normalized values of Wnt3a concentration on the same sections are reported in the bottom graph. Finally, the table in panel C summarizes the calculated maximum and minimum values for the velocity and shear stress in the 4 sections of the culture channel.

We can conclude that the system was able to generate predictable and stable concentration gradients with flat and uniform velocity profiles within the culture channel, thus exposing the adhering cells to very low values of both velocity and shear stress (which averaged values were $2.63 \cdot 10^{-4} \pm 8.74 \cdot 10^{-5}$ m/s and $2.53 \cdot 10^{-1} \pm 8.39 \cdot 10^{-2}$ dyne/cm^2 respectively).

Activation of the canonical β-catenin pathway in response to Wnt3a

First of all, we evaluated the behavior of cell populations in terms of β-catenin pathway activation when statically cultured with Wnt3a conditioned medium at defined dilutions. The extent of the Venus-related pathway activation was evaluated by the quantification of fluorescence images as described above. The expression of Venus signal showed statistically significant increases with increasing Wnt3a concentration.

Cells were successfully cultured inside the microbioreactor for up to 3 days total (static and perfused culture). Figure 3.6 reports representative bright field and fluorescence images (first and second row respectively) of cells cultured inside the microbioreactor both in static (left) and perfused conditions (right). The reported static control experiment was performed filling the microbioreactor with Wnt3a conditioned medium at the dilution chosen for the perfused experiments. In the case of perfused microbioreactors, the Wnt3a conditioned medium was injected from the right inlet port.

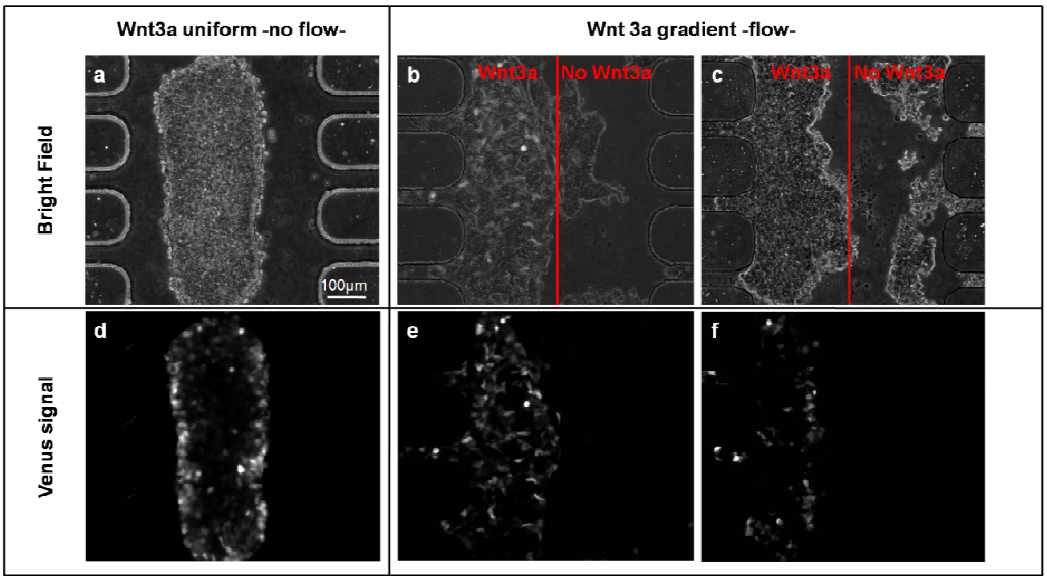

Figure 3.6. *Differential activation of the canonical Wnt3a/β-catenin pathway: perfused experiments. Upper part of panel shows bright field images (a-c), while the lower one shows the fluorescent Venus signal (d-f). The control results in a random activation of cells (panels a and d); while cells cultured under a Wnt3a gradient show a differential activation, in accordance with the imposed concentration gradient.*

Cells cultured inside the microbioreactor were exposed for 24 h to a microfluidic-generated Wnt3a gradient. During perfusion, a Wnt3a concentration gradient was soon established, thus exposing the cells adhering on the right side of the channel to a defined ligand concentration. The vertical line in the images divides the channel in two halves, helping the visualization approximately identifying the areas in which the Wnt3a ligand is present. As can be noticed from the fluorescent images reported in the second row of Figure 3.6, the Venus expression was detectable only on the cell population fraction that was exposed to the Wnt3a conditioned media. Cells of the control experiments showed a more uniform expression on the entire population.

The quantification of the obtained images was performed as described above, on an average of 20 images per condition, and led to the results reported in Figure 3.7.

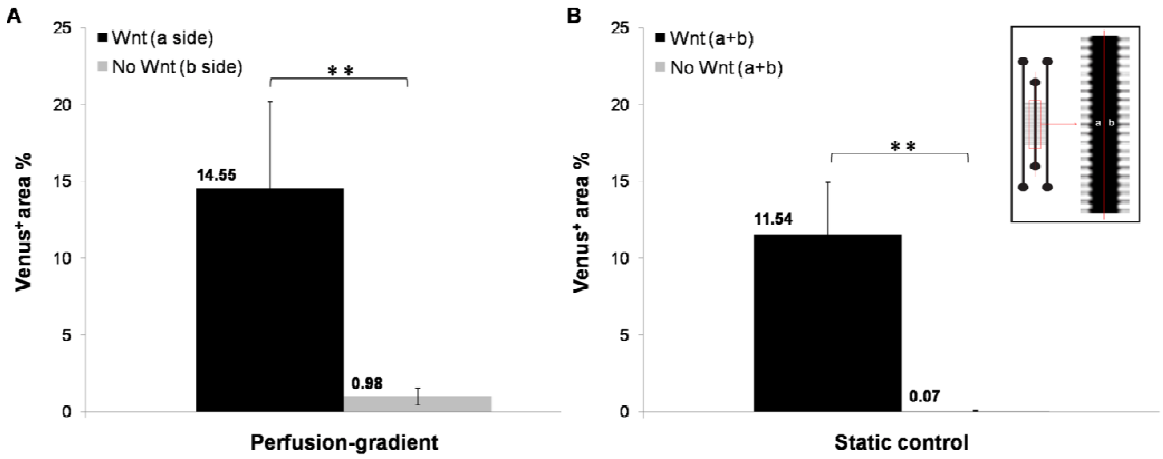

Figure 3.7. *Differential activation of the canonical Wnt3a/β-catenin pathway: data evaluation for perfused experiments. Panel A reports results of the perfused experiments; a: area exposed to Wnt3a conditioned medium and b: exposed to control medium (no Wnt3a). Panel B summarizes the outcomes of the static experiments, performed evaluating the images of the entire channel section (a+b). Results are reported for two sets of control experiments where cells were exposed to a defined and uniform Wnt3a concentration or exposed to control medium with no Wnt3a. **p<0.001*

Panel A shows the results of the perfused experiments. Quantification was performed on the two halves of the channel evaluating the fraction of cells expressing Venus signal, determined as the ratio between the area of cells expressing Venus signal and the total area covered by cells. The microfluidics-generated Wnt3a gradient dictated its presence in the right side of the channel (b side), while the left side of the channel (a side) had no Wnt3a. The fraction of cells expressing Venus signal evaluated on the cell populations adhering on the right side of the channel was 15 fold higher than that on cells on the left side. Panel B summarizes the outcomes of the static experiments, performed evaluating the images of the entire channel section (identified in the graph by the notation "(a+b)"). Two sets of control experiments were performed: one where cells were exposed to control medium with no Wnt3a and the other where cells were uniformly exposed to a defined and uniform Wnt3a concentration. Both results are presented and a 11 fold increase in the fraction of GPF positive cells was encountered in cells exposed to Wnt3a when compared with those with no Wnt3a.

These results prove the effective and statistically significant differential activation of the cell population fraction exposed to the microfluidic-generated Wnt3a gradient.

In this study, a microfluidic microbioreactor capable of generating well characterized concentration gradients under low shear stress conditions was designed, developed and validated. The capability of effectively proving the spatio-temporal stability of the imposed gradient is of paramount importance, and in the microfluidic device presented in this work, extremely predictable behaviors in accordance with the results of the mathematical modeling could be developed.

The system allowed prolonged culture of cells both under static and perfused conditions and proved its efficacy in generating and maintaining stable Wnt3a concentration gradients. In addition, from the quantification of the static multiwell experiments we could observe how the Wnt reporter expression followed more of a threshold-like behavior rather than a graded response.

These results, specifically applied to the extremely relevant family of Wnt3a molecules, are promising in sight of further applications aimed at exploring the role of concentration gradients on cell populations.

3.5 Microfluidic-generated spatial-temporal concentration gradients

In this section we report the design, development and validation of a system capable of generating controlled concentration gradients both in time and space.

The importance of having spatial-temporal gradients within cell cultures is paramount. An example above all can be found in the recent work of Murry and Keller (Murry and Keller 2008), clearly explaining how the processes leading from an uncommitted embryonic stem cell to a fully differentiated and committed cell develop through a cascade of regulatory factors that act on both temporal and spatial scales.

Graded signals are thus fundamental in many, if not all, signaling pathways and their intervention also follows specific temporal patterns.

These are the motivations that led us to the development of this prototype, that has so far been validated with color tracers but has not yet been interfaced with a biological system.

In order to generate spatial-temporal concentration gradients within a microfluidic system, it was necessary to develop an automated platform integrating various components.

The fundamental units were:

- automated control system;
- microfluidic platforms;
- control valves and connectors;

The core of the system, where the spatial-temporal control of the concentration of a defined factor had to be performed, was the microfluidic bioreactor described in section 3.4 and reported here in Figure 3.8 (“NN” configuration). For clarity and simplicity we reported in Figure 3.8 all the microfluidic bioreactors used here, with the corresponding acronyms.

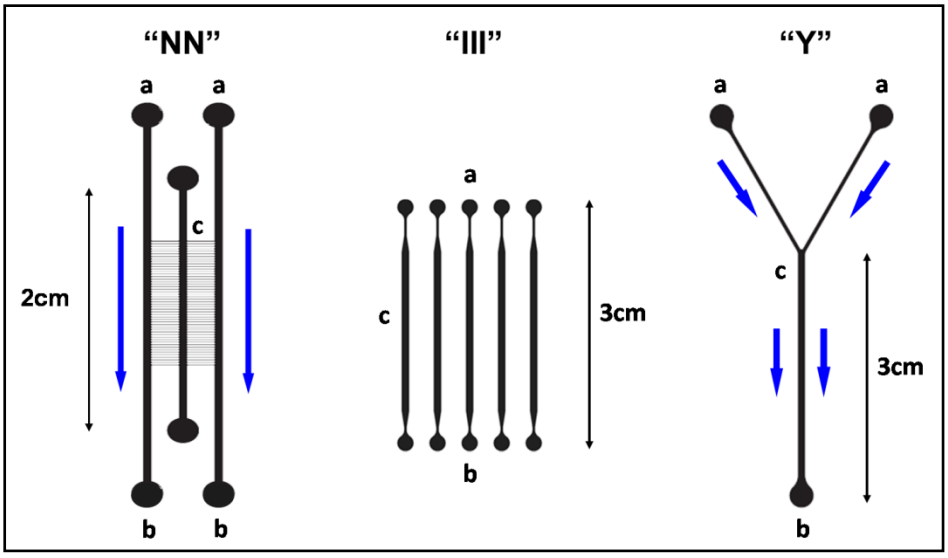

Figure 3.8. *Schematics of the microfluidic microbioreactors used in this study and their acronyms. Inlets are denoted by a letters and outlets by b; main channels and culture channels are denoted by c. Lateral arrows identify the main flow direction. Dimensions are not on scale.*

The overall system, reported in figure 3.9, was composed, from an upstream to downstream view, by a syringe pump controlling the fluid motion of three syringes which were connected to the different microfluidic platforms.

It is worth underlying how all fluidic paths needed to be accurately calculated in order to ensure a perfect and equalized distribution of head-losses along each of them. The different configurations of the microfluidic platforms were used also for allowing an even distribution of head-losses, as will be described in what follows.

In detail, following the schematics of the entire apparatus in Figure 3.9 we had that:

- one of the syringes was connected to the so-called "continuous path", delivering a fluid through a "Y" microbioreactor and to the left inlet of the final "NN" microbioreactor;
- the other two syringes delivered fluids to the "discontinuous path" through the 4 electro-valves controlled by the developed data acquisition (DAQ) system. At the first tee split, regulated downstream by the first two valves we had that:
    - one branch led to a discard collector following a defined number of passages in the "III" channels (depending on the tubings length and calculated so to equalize head-losses),
    - the other led to one of the inlets of a "Y" microbioreactor;

- the second syringe followed a symmetric path, controlled by the last two electro-valves;

- the fluid finally exiting from the b port of the “Y” microbioreactor was delivered to the second inlet of the “NN”.

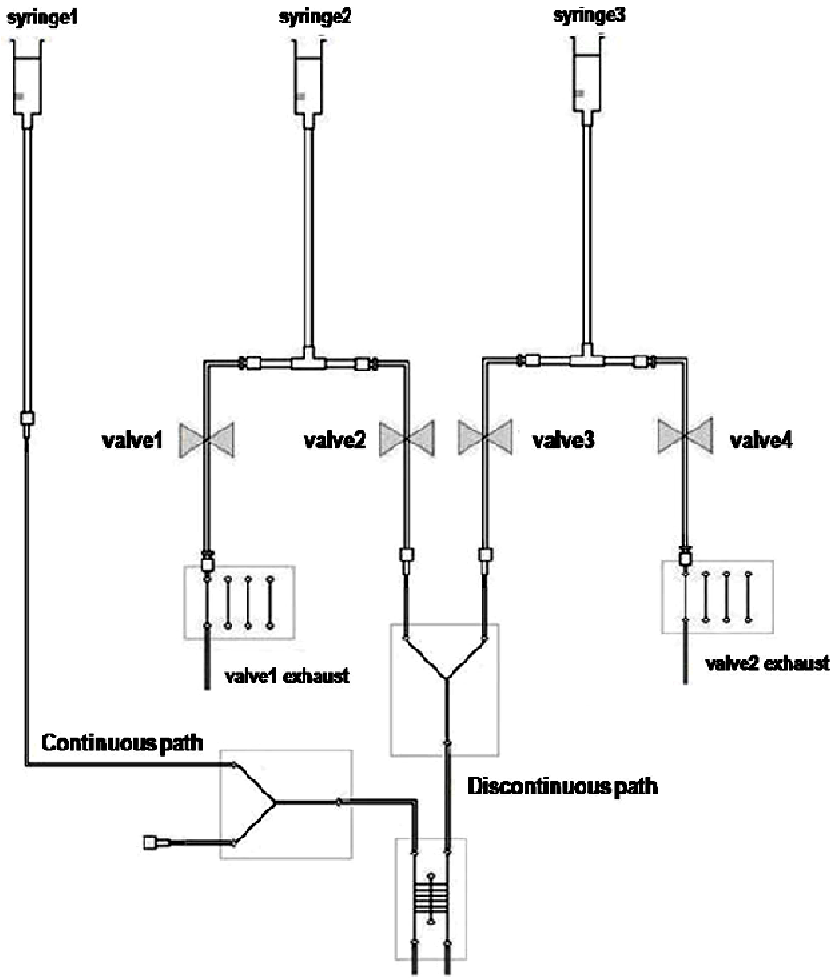

Figure 3.9. *Schematics of the developed apparatus comprising a set of solenoid electro-valves controlling the selective delivery of fluids through defined flow paths constituted by microfluidic bioreactors connected via Tygon tubings and connectors.*

To control the valves opening/closing, an external system was built and formed by an I/O connector block for DAQ devices with 68-Pin Connectors (SCB-68) and a static and waveform analog output board (NI PCI-6722, both from National Instruments). This allowed the interface with a software (LabView) running the actual routines regulating the ON/OFF operations of the valves and, importantly ,it consented to manage all valves in parallel.

The output signal of the DAQ system needed to be amplified in order to correctly operate the solenoid valves and thus an appropriate electrical circuit was built. This circuit comprised also the power relays that effectively controlled the opening and closing of the electro-valves.

3.5.1 Results and discussion

This system was validated using color tracers and we have been able to obtain:

- different dilutions of the fluids contained in the second and third syringes, which underwent controlled mixing while passing through the c channel of the "Y" microbioreactor. The extent of mixing depended on:
    - residence time in the channel (flow rates-related),
    - diffusion coefficient of the considered species.
- concentration gradients as described in section 3.7, in the c channel of the "NN" microbioreactor;
- above all, was the possibility of controlling such gradients in time with a proper operation of the upstream solenoid valves.

Figures 3.10 and 3.11 report the results obtained applying a flow rate of 10 μL/min.

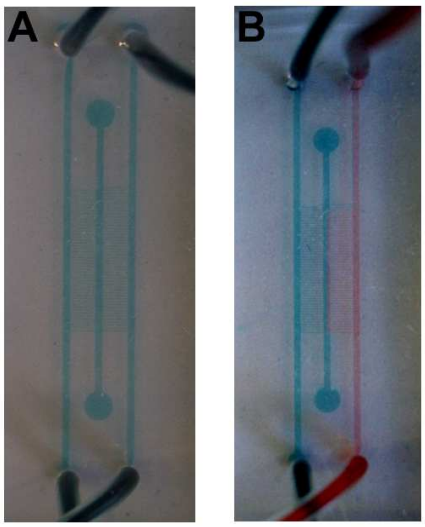

Figure 3.10. *Pictures demonstrating the formation of a spatial-temporal concentration gradient within the "NN" microbioreactor using color-tracer fluids. Panel A reports an image taken at time zero, while B after 1 minute.*

Further validation derived from the quantification of the fluorescent images at the microscope, as shown in Figure 3.11.

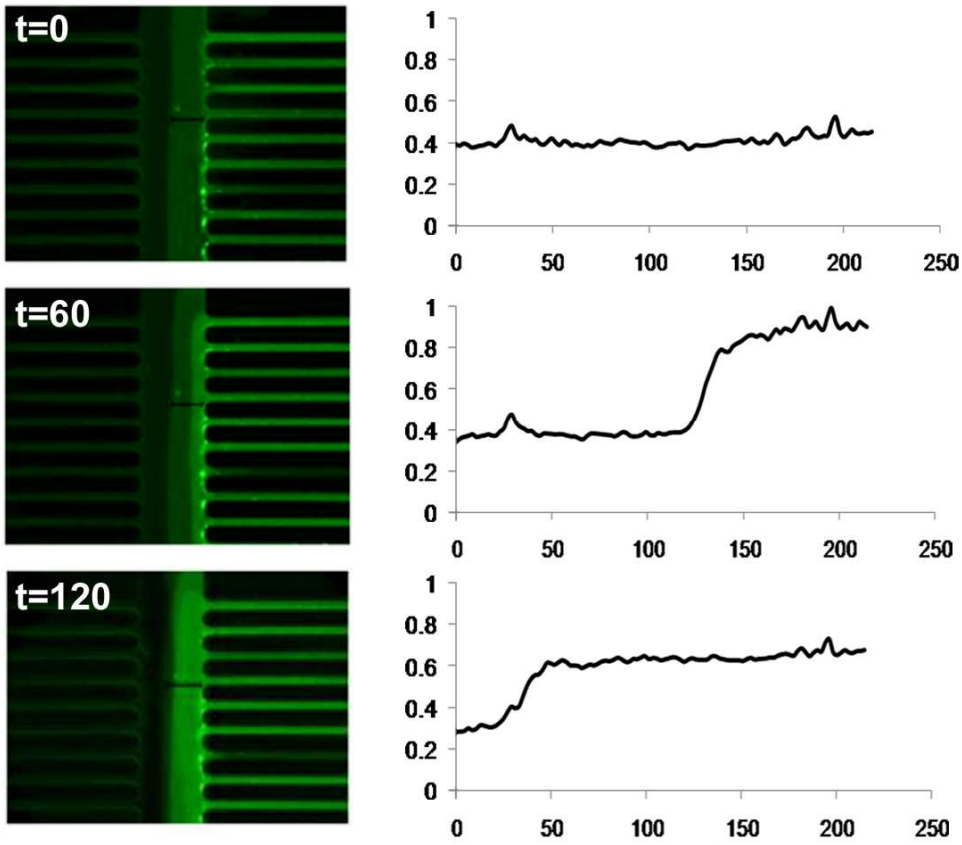

Figure 3.11. *Fluorescent images on the left pat of the panel were taken at the top section of the c channel of the "NN" microbioreactor at the indicated times (unit: seconds). On the right we reported the quantification of the fluorescent signal evaluated along the horizontal lines (in black) in the corresponding images. X-axes report the horizontal coordinates, with zero centered at the mid of the channel, while y-axes correspond to the dimensionless fluorescence intensity.*

With the developed system we were able to obtain fast-switch and extremely controlled spatial-temporal concentration gradients within a microfluidic bioreactor.

This work would prove extremely useful in its future interface with biological systems, thus fully exploiting its potentialities in studying the behavior of a cell population when exposed to defined signals that can be modulated with extreme flexibility trying to mimic the way in which they are presented *in vivo*.

For example, this prototype could also be useful for testing different physio-pathological conditions (i.e. ischemia in heart failure)which typically undergo spatial and temporal phenomena.

3.6 References

D. N. Breslauer, P. J. Lee and L. P. Lee, Microfluidics-based systems biology. *Mol. BioSyst.*, 2006, **2**, 97-112.

S. Haeberle and R. Zengerle, Microfluidic platforms for lab-on-a-chip applications. *Lab on a Chip*, 2007, **7**, 1094–1110.

J. Hong, J. B. Edel and A. J. Demello, Micro- and nanofluidic systems for high-throughput biological screenin. *Drug Discovery Today* 2008, Epub ahead of print.

D. Amarie, J. A. Glazier and S. C. Jacobson, Compact Microfluidic Structures for Generating Spatial and Temporal Gradients. *Analytical Chemistry*, 2007.

N. L. Jeon, S. K. W. Dertinger, D. T. Chiu, I. S. Choi, A. D. Stroock and G. M. Whitesides, Generation of Solution and Surface Gradients Using Microfluidic Systems. *Langmuir*, 2000, **16**, 8311-8316.

T. M. Keenan and A. Folch, Biomolecular gradients in cell culture systems. *Lab on a Chip*, 2007, **8**, 34–57.

G. M. Whitesides, The origins and the future of microfluidics. *Nature*, 2006, **442**, 368-373.

P. S. Dittrich and A. Manz, Lab-on-a-chip: microfluidics in drug discovery. *Nature Reviews - Drug Discovery*, 2006, **5**, 210-218.

Y. Wen and S. T. Yang, The future of microfluidic assays in drug development. *Expert Opinion on Drug Discovery*, 2008, **3**, 1237 -1253.

B. D. Piorek, S. J. Lee, J. G. Santiago, M. Moskovits, S. Banerjee and C. D. Meinhart, Free-surface microfluidic control of surface-enhanced Raman spectroscopy for the optimized detection of airborne molecules. *Proceedings Of The National Academy Of Sciences Of The United States Of America*, 2007, **104**, 18898-18901.

M. Toner and D. Irimia, Blood-on-a-Chip. *Annu. Rev. Biomed. Eng.*, 2005, **7**, 77–103.

H. Andersson and A. van den Berg, Microfabrication and microfluidics for tissue engineering: state of the art and future opportunities. *Lab On A Chip*, 2004, **4**, 98-103.

J. C. McDonald, D. C. Duffy, J. R. Anderson, D. T. Chiu, H. K. Wu, O. J. A. Schueller and G. M. Whitesides, Fabrication of microfluidic systems in poly(dimethylsiloxane). *Electrophoresis*, 2000, **21**, 27-40

S. K. Sia and G. M. Whitesides, Microfluidic devices fabricated in poly(dimethylsiloxane) for biological studies. *Electrophoresis*, 2003, **24**, 3563–3576.

G. M. Whitesides, E. Ostuni, S. Takayama, X. Jiang and D. E. Ingber, Soft lithography in biology and biochemistry. *Annual Review of Biomedical Engineering*, 2001, **3**, 335–73.

D. J. Beebe, G. A. Mensing and G. MWalker, Physics and applications of microfluidics in biology. *Annu. Rev. Biomed. Eng.*, 2002, **4**, 261–86.

T. M. Squires and S. R. Quake, Microfluidics: Fluid physics at the nanoliter scale. *Reviews of Modern Physics*, 2005, **77**, 977-1016.

A. Goldin, J. A. Beckman, A. M. Schmidt and M. A. Creager, Advanced Glycation End Products Sparking the Development of Diabetic Vascular Injury. *Circulation*, 2006, **114**, 597-605.

E. Serena, Microscale tissue engineering of human skeletal and cardiac muscles for in vitro applications. *PhD thesis*. Dipartimento di Principi e Impianti di Ingegneria Chimica “I. Sorgato”, University of Padova, 2009.

H. Clevers, Wnt/β-Catenin Signaling in Development and Disease. *Cell*, 2006, **127**, 469-480.

C. Y. Logan and R. Nusse, The Wnt signaling pathway in development and disease. *Annu. Rev. Cell Dev. Biol.*, 2004, **20**, 781–810.

R. T. Moon, Wnt/ß-Catenin Pathway. *Science Signaling*, 2005, **2005**.

R. T. Moon, B. Bowerman, M. Boutros and N. Perrimon, The Promise and Perils of Wnt Signaling Through b-Catenin. *Science*, 2002, **296**, 1644-1646.

R. T. Moon, A. D. Kohn, G. V. DeFerrari and A. Kaykas, Wnt and b-cat signalling diseases and therapies. *Nature Reviews Genetics*, 2004, **5**, 689-699.

A. Aulehla, W. Wiegraebe, V. Baubet, M. B. Wahl, C. Deng, M. Taketo, M. Lewandoski and O. Pourquié, A β-catenin gradient links the clock and wavefront systems in mouse embryo segmentation. *Nature Cell Biology*, 2008, **10**, 186-193.

K. Bartscherer and M. Boutros, Regulation of Wnt protein secretion and its role in gradient formation. *European Molecular Biology Organization*, 2008, **9**, 977-982.

J. A. Burdick, A. Khademhosseini and R. Langer, Fabrication of gradient hydrogels using a microfluidics/photopolymerization process. *Langmuir* 2004, **20**, 5153-5156.

W. Saadi, S. J. Wang, F. Lin and N. L. Jeon, A parallel-gradient microfluidic chamber for quantitative analysis of breast cancer cell chemotaxis. *Biomed Microdevices*, 2006, **8**, 109–118.

J. Diao, L. Young, S. Kim, E. A. Fogarty, S. M. Heilman, P. Zhou, M. L. Shuler, M. Wu and M. P. DeLisa, A three-channel microfluidic device for generating static linear gradients and its application to the quantitative analysis of bacterial chemotaxis. *Lab on a Chip*, 2006, **6**, 381–388.

Y. Chisti, Hydrodynamic Damage to Animal Cells. *Critical Reviews in Biotechnology*, 2001, **21**, 67-110.

E. Cimetta, E. Figallo, C. Cannizzaro, N. Elvassore and G. Vunjak-Novakovic, Micro-bioreactor arrays for controlling cellular environments: Design principles for human embryonic stem cell applications. *Methods*, 2009, **47**, 81-89.

T. L. Biechele and R. T. Moon, Assaying beta-catenin/TCF transcription with beta-catenin/TCF transcription-based reporter constructs. *Methods in molecular biology*, 2008, **468**, 99 -110.

C. E. Murry and G. Keller, Differentiation of Embryonic Stem Cells to Clinically Relevant Populations: Lessons from Embryonic Development. *Cell* 2008, **132**, 661-680.

Chapter 4
Topological control of cell cultures

This chapter will present the obtained results with regards to the topological control of cell cultures. The important aspects of the choice and design of the optimal substrates together with the optimization of the techniques aimed at spatially guiding cell adhesion will be analyzed.

Two of the most relevant case studies treated will be presented in more detail.

4.1 Motivations

Driven by the strong need of obtaining organized structures mimicking the *in vivo* physiology of natural muscle and by the necessity of developing highthroughput technologies helping the processes of drug development or pharmacological screenings, the aspect of spatially organizing our cell cultures has caught much attention.

Recent studies suggest that primary cell systems can be designed to model many aspects of disease biology and that robust and automated assays can be engineered to detect and discriminate disease relevant mechanisms and potential therapies (Liu et al. 2007).

The human cell−based testing has proven to be a valuable tool to quickly explore toxic and non functional compounds. The low−cost and high−speed testing of compounds in cell

culture, and the obvious advantages of using intact cells as a first representation of the living patients, would make the cell−based testing a key component on therapy discovery programs. However, many individuals in the industry and academic community would argue that cell models may give unsatisfactory, misleading and non−predictive data for the actual response of a complex functional tissue.

There is strong evidence of the fact that a principal component of this failure is the quality of the cell culture conditions *in vitro*, such as the lack of structural and topological cues, the different mechanical and chemical properties of the substrate used *in vitro* or the unpredictable spatial−temporal combination of different soluble factors or and cell−cell interactions in conventional cell culture systems (Albrecht et al. 2006, Jang and Schaffer 2006, Kaplan et al. 2005, Vunjak-Novakovic and Freed 1998). On the other hand, the animal model based assays show two main limitations. First, the current animal−genetic−focused methods of target validation cannot reliably predict human biology; even if a model can be predictive of human target biology, it cannot predict human drug biology or therapy response. Second, the target−specific approach is exceedingly slow as only a few targets can be screened at a time; this approach lacks of complexity and of the multi−interacted processes of diseases.

To achieve this goal, first of all, we need to rationally understand how the cells respond to the micro−environmental stimulations, thus defining structure/function relationships for skeletal muscle tissues and diseases. In particular, we need to succeed in reproducing *in vitro* the *in vivo* responses of individual cells, clusters of cells and tissue−like structures; such events are regulated by spatial−temporal cues that reside in the local, surrounding microenvironment and include: the extracellular matrix, the presence of neighboring cell, soluble factors, physical forces and, eventually, electrical stimuli, all intrinsically expressed and interplaying in a defined context.

In this sight, a relevant part of the presented work has dealt with the development of the proper substrates and techniques aimed at ultimately obtaining human derived tissue−based assays and technologies which should:

- provide robust and reproducible biological and functional data representative of human physiology;

- be integrated with technological platforms for highthroughput screenings and development of new therapeutic strategies at large scale;
- easily transferable to research laboratory for facilitating the therapy development process in reduced time and at lower cost.

At the beginning of this study, we performed studies using microfabricated microstructured polymeric membranes as substrate for mouse and rat muscle cells growth and differentiation. The results are presented in the publications in Appendix D, E, and F.
An example is shown in Figure 4.1.

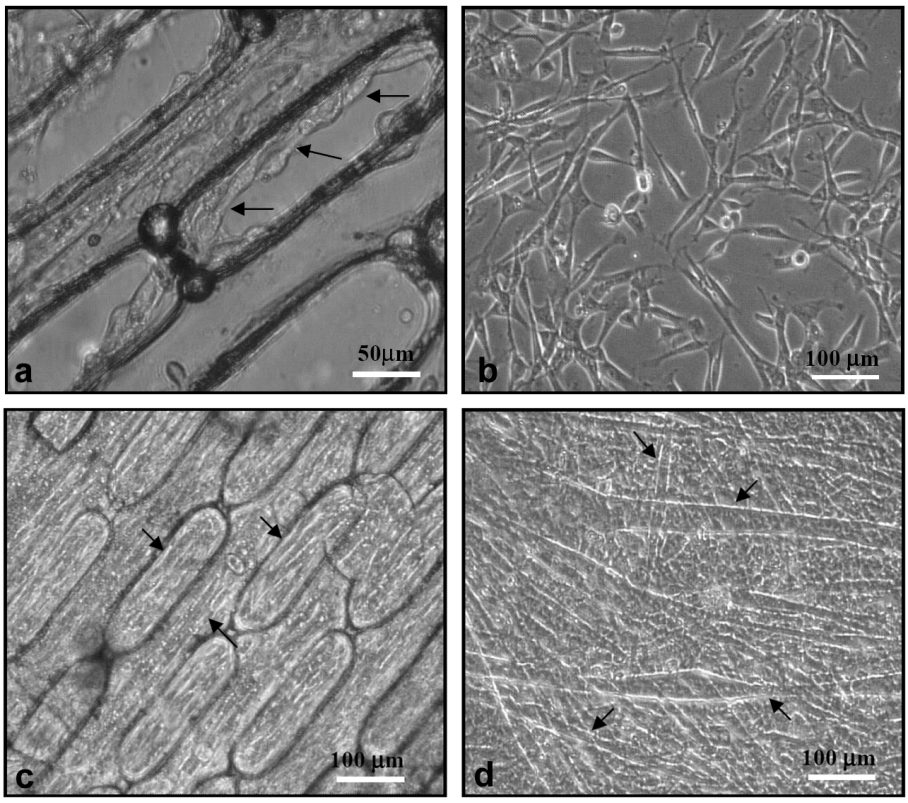

Figure 4.1. *Mouse satellite cells cultured on microstructured (a, c) and smooth (b, d) polymeric membranes. The differences in the topology of adhesion are visible since day 1 after seeding (a, b) and more dramatic after 7 days (c, d): the myotubes formed on the microstructured substrate are perfectly oriented (arrows) while those on smooth surfaces have no preferential orientation.*

What needed to be acknowledged, and drove us to the development that will soon be described, was the fact that, besides guiding cell adhesion and promoting correct differentiation of such muscle cells into contractile myotubes, these substrates lacked of most of the necessary tissue-like properties of which we stressed the extreme importance. In addition, they tended to guide cell adhesion but failed in maintaining a prolonged

confinements of the cultures, thus loosing the potentialities deriving from the use of arrayed systems.

In the following sections we will treat more in detail the developed technologies and focus on the two most relevant case studies.

4.2 Technology development: substrate and topological control of cell adhesion

With reference to the publication reported in Appendix B, in this section we will briefly describe the rationale and the steps the lead to the development and optimization of the key features and techniques that will then be applied to the case studies presented in the following sections. In particular we will describe and discuss:

- the production of the optimal substrate;
- the obtainment of topological control of cell adhesion.

Two-dimensional arrays of single cells or clusters of cells can provide appropriate culture conditions for adherent cells, however, the lack of structural and topological cues may alter cell behavior and phenotype expression. As already seen, mammalian cells integrate and respond to a combination of factors in the microscale environment, such as chemical and mechanical properties, shape, organization and cell-cell interactions. These aspects are particularly important for cell phenotypes such as cardiac, skeletal, and smooth muscular, which are highly dependent on three-dimensional (3D) cell organization (Motlagh et al. 2003) and on the surface mechanical properties (Ingber 2002, Khatiwala et al. 2006, Engler et al. 2004a) which translates into the coupling to a soft or stiff substrate.

Among soft substrates, hydrogels have recently captured attention in the field of tissue engineering because of their high water content, biocompatibility and elastic properties, resembling those of native tissues. In recent years many kinds of hydrogels, especially poly(ethylene glycol) (PEG) and derivatives (Britton-Keys et al. 1998, Burdick et al. 2004, Lin-Gibson et al. 2005), have been widely used for encapsulating living cells or as substrates for cell culture. A wide variety of copolymers, composed of a synthetic backbone

and grafted biomolecules (or *vice versa*) such as fibrinogen (Almany and Seliktar 2005) and hyaluronic acid (Leach et al. 2003, Leach and Schmidt 2005) or short peptides sequences such as RGD (Hern and Hubbell 1998), was proposed and tested to develop substrates with the biological cues required for cell attachment. In addition, the elastic properties can be controlled and modulated by changing the amount of polymer and crosslinker, thus obtaining stiff or soft gels with a different influence on cell behavior at the cytoskeletal level (Engler et al. 2004b, Peyton and Putnam 2005), as we will see in more detail in the following sections.

Strictly related, emerges the issue of the topological control.

To guide cell adhesion, many patterning techniques have been proposed and widely reviewed over the last few years (Falconnet et al. 2006, Xia and Whitesides 1998). Various lithographic techniques have been used to guide cell adhesion and orientation onto different substrates (Karp et al. 2006, Rohr et al. 1991, Suh et al. 2004) while microfluidics have been employed to pattern cardiomyocites on PDMS or glass substrates (Gopalan et al. 2003, Khademhosseini et al. 2007). Muscle cells have been studied on surfaces comprising nanopatterned gratings, microgrooves and microtextures (Motlagh et al. 2003, Vernon et al. 2005, Yim et al. 2005). Patterns of proteins have been created on glass or polystyrene surfaces via micro-contact printing (μCP) (Ruiz and Chen 2007) and laminin lanes have been patterned using the same technique on polimeric films for the subsequent adhesion of cardiomyocytes (McDevitt et al. 2002, McDevitt et al. 2003).

The major limitations of the enumerated techniques are related to the stiffness of the substrates used - gold, silver, metal or metal-oxide, glass and polystyrene - on the one hand and to the difficulties encountered while producing controlled patterning on soft materials on the other.

For these reasons we centered our attention in the development of a hydrogel substrate that would respond to specific needs and requirements. All the phases leading to the final product and some exemplifying applications will be treated in detail in the next sections. The most relevant case studies will be presented in sections 4.3 and 4.4.

4.2.1 Substrate design

More detailed descriptions of the procedures reported here can be found in Appendix B (Cimetta et al. 2008).

A polyacrylamide (PA) based hydrogel was used as the substrate for cell culture because of its elastic properties, which are particularly suitable for muscle cell culture. Moreover, this hydrogel is easy to produce, inexpensive, biocompatible, and optically transparent; the latter being an important prerequisite for performing optical image analyses. PA hydrogel can be produced as a thin film and covalently bonded to a functionalized glass slide showing long term stability in culture. Figure 4.2 shows an image of a circular hydrogel film adhered to a glass coverslip and covered with culture medium. A 35 mm Petri dish contains the system.

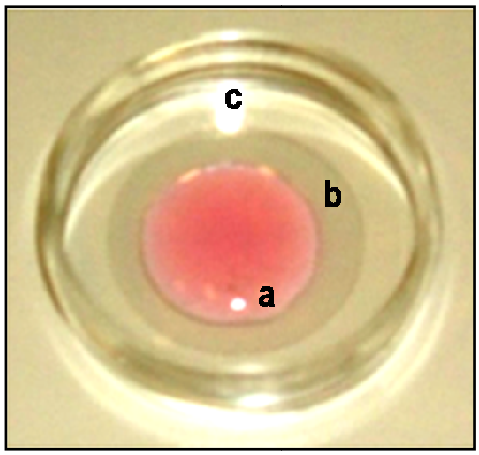

Figure 4.2. *Photograph of an hydrogel disk covered with culture medium (a) adhering to a 25 mm diameter glass coverslip (b) and placed in a standard 35 mm Petri dish.*

As PA hydrogel is a non-fouling material, and thus doesn't consent proper cell adhesion without the necessary cues. Thus, an adhesion-protein pattern was micro-contact printed onto the PA surface; this technique was chosen for being a simple and versatile method to pattern adhesion proteins with a resolution of ~1 μm. The immobilization on the surface occurred through physical adsorption and allowed proteins to maintain their activity without suffering from major denaturation phenomena. In addition, patterning proteins on hydrogel films enabled microscope observations on the same focal plane of the substrate.

Summarizing, polyacrylamide hydrogels have the following characteristic properties that contribute to their election as optimal substrates for our purposes:

- mechanical properties:
    - tissue-like tunable stiffness;
- biochemical properties:
    - biocompatibility,
    - persistence in culture;
- chemical-physical properties:
    - photo-polymerizable,
    - high water content,
    - allows adsorption of compounds,
    - gas permeability,
    - high hydrophilicity.

Briefly, Figure 4.3 show examples of how these hydrogels were utilized in our first experimentations. The fact that the hydrogel was photo-polymerizable was exploited by means of photolithographic techniques (specifically: microtransfer molding). A photomask was interposed, as described above, to obtain a defined “macroscopic” shape (i.e. circular pads of 5 mm diameter); in addition, the use of a microstructured PDMS stamp placed above the liquid pre-polymer solution, allowed to shape the hydrogel at the microscale level obtaining a replica of the features imposed by the PDMS stamp.

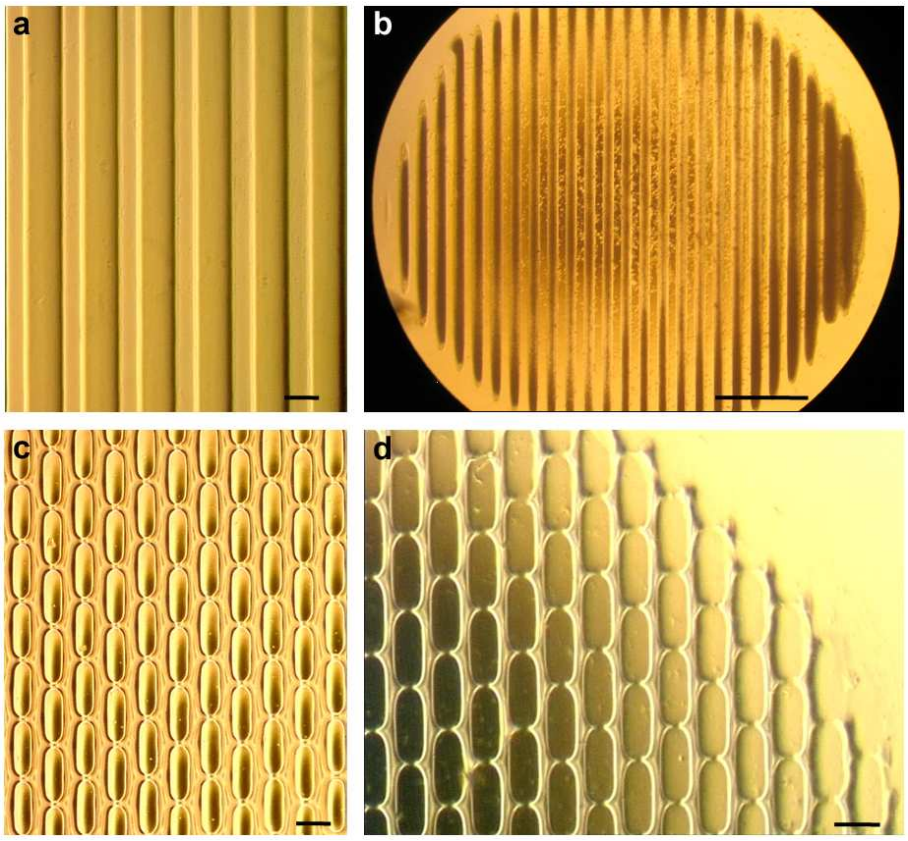

Figure 4.3. *Images of microstructured polyacrylamide hydrogels obtained via microtransfer molding. In a: a pattern of parallel lanes 75 µm wide and 100 µm spaced was created on hydrogel circles of 5 mm diameter (b). Panels c and d show a different geometry: a matrix of rectangles of 50 µm width and 200 µm length. Scale bars on a, c, and d: 100 µm; on: b 1mm.*

The limitation of this technique derives from the fact that the subsequent control in cell adhesion occurred primarily because of the physical constraint created by the microstructures walls. Hydrogel worked as a barrier, and not as a substrate to which cells attached (following proper coating with adhesion proteins); cells preferentially adhered to the glass slide over which the hydrogel was covalently bonded.

We thus decided to adopt the micro-contact printing technique, as will be described in section 4.2.2.

4.2.2 Topological control

Once chosen the optimal substrate and considering the limitations of the above presented technique for controlling cells spatial organization, we decided to directly guide the topology of cell adhesion using defined patterns of adhesion proteins. This was done optimizing the micro-contact printing techniques on a soft substrate such as PA hydrogel.

Again, Appendix B reports all details of the performed operations.

Figure 4.4 reports cartoons identifying the main steps of the developed procedure.

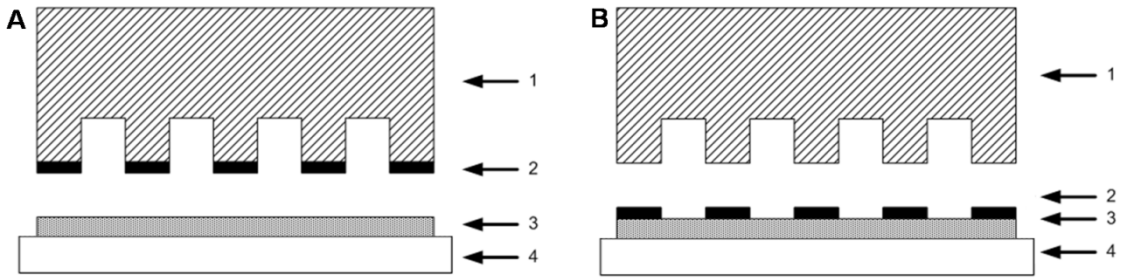

Figure 4.4. *Schematic representation of the micro-contact printing (μCP) technique. Panel A exemplifies the microstructured PDMS stamp (1) with a monolayer of protein solution (2) adsorbed on its surface. A thin film of PA hydrogel (3) is covalently bonded to a glass slide (4). Panel B schematically represents the result of the protein printing: the protein solution (2) previously adsorbed on the PDMS stamp surface (1) has been transferred onto the PA hydrogel surface (3) adhered on the glass slide (4).*

Solutions of adhesion proteins at the desired concentration were printed on smooth hydrogel surfaces via μCP technique using a PDMS stamp carrying the desired micropattern. Specifically, the stamp was inked in the protein solution for a few seconds, and then the excess solution was removed. Conformal contact between the dry hydrogel surface and the stamp was then achieved by applying a gentle pressure, thus transferring the desired protein microstructured pattern on the substrate.

It is worth underlying how this general procedure has been easily optimized and adapted to multiple cell types.

Figure 4.4 briefly summarizes the cell seeding procedures.

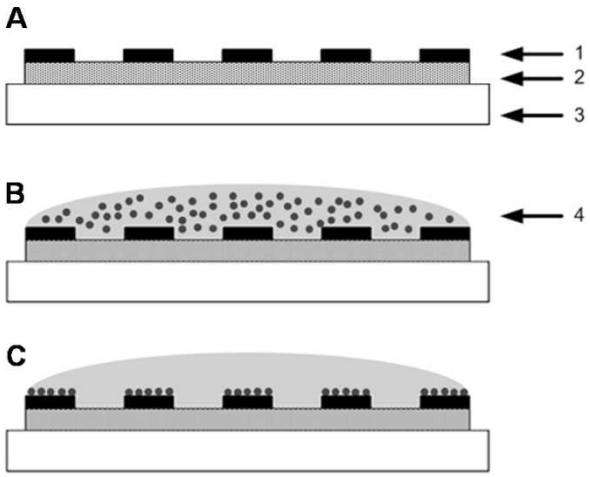

Figure 4.5. *Schematic representation of the cell seeding procedures onto patterned PA hydrogels. Panel A shows the starting point: protein solution (1) has been adsorbed following μCP onto the hydrogel surface (2), the hydrogel is covalently bonded to a glass coverslip (3). A cell suspension (4) is uniformly distributed over the patterned hydrogel; after a few hours, all cells are selectively adhering only on the protein patterned areas.*

On the obtained substrates and with the optimized micropatterning techniques, we were able to create extremely selective deposition of adhesion proteins on the typically non-fouling polyacrylamide hydrogel surfaces. Consequently, seeding an uniform cell suspension resulted in a well defined and persistent control over the topology of cell adhesion.

These techniques have been validated using multiple cell types and for different applications. For example, we used:

- murine muscle cell lines C2C12;
- neonatal rat cardiomyocytes (Figure 4.6);
- murine satellite cells;
- human-derived hepatocarcinoma cell lines HepG2 (Figure 4.7 and 4.8);

Figure 4.6-8 demonstrate some exemplifying results.

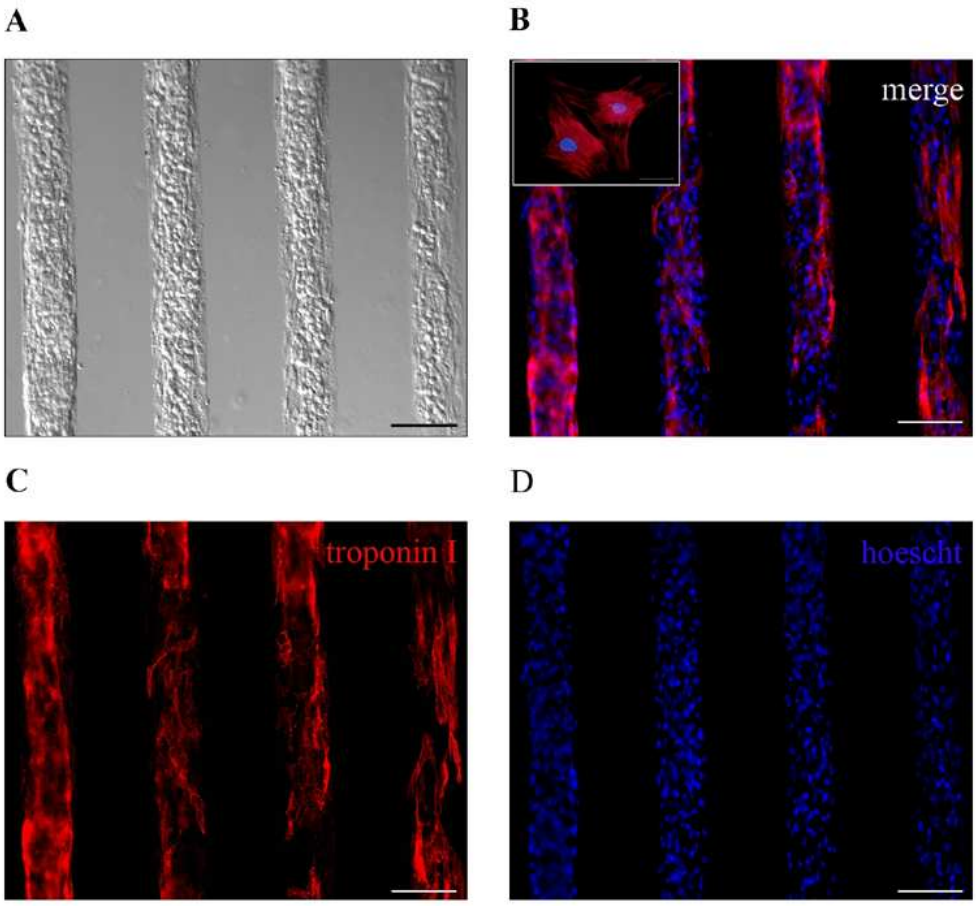

Figure 4.6. *Neonatal rat cardiomyocytes cultured on patterned polyacrylamide hydrogel. The controlled topology was designed as lanes 100 μm wide and 1 mm long, spaced by 100 μm horizontally and 300 μm vertically. Images were taken at 10x magnification. (A): bright field image of cardiomyocytes after 4 days in culture; (B): cultured cardiomyocytes express troponin I (red), a typical cardiomyocytes marker; nuclei were counterstained with Hoechst (blue). Unmerged images are reported in panels C and D (scale bars=100μm). Immunostaining for troponin I represented in the inset of picture B shows at higher magnification (40x) a developed contractile apparatus (scale bar=75 μm).*

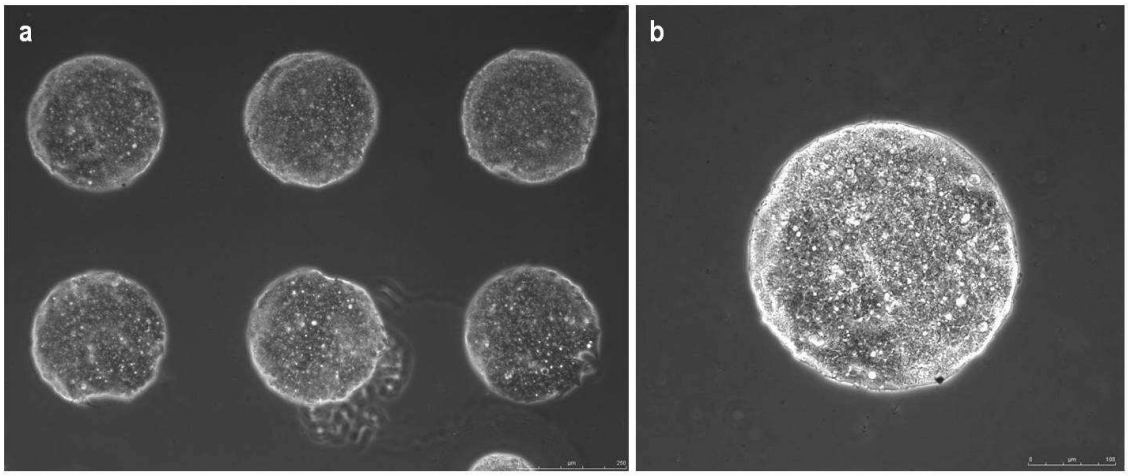

Figure 4.7. *Micropatterned human-derived hepatocarcinoma cell lines. Micropatterning of 300 μm diameter islands with 100 μg/ml Fibronectin solution on polyacrylamide hydrogels guides cell adhesion with an extreme selectivity. Hepatocytes adhere and cluster only on the protein patterned circular areas. Panel a reports a 10x magnification, while in Panel b a 20x magnification represents in detail a single cluster of cells. It is noticeable how, after 48 h of culture, confluent cells confined in the circular islands appear vital and no outgrowths extend from the micropatterned regions.*

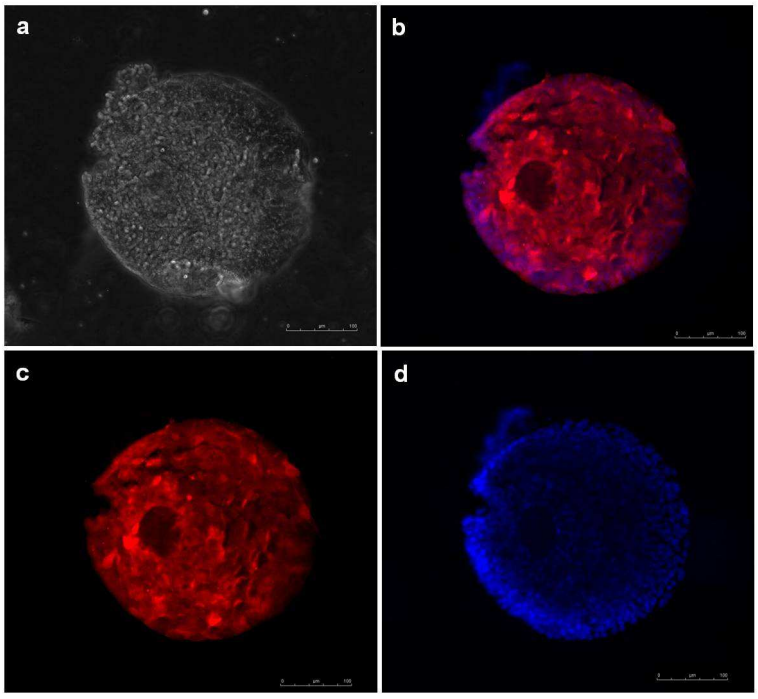

Figure 4.8. *Biological validation on micropatterned human-derived hepatocarcinoma cell lines. 20x magnification images of HepG2 cells cultured on micropatterned island onto hydrogel substrates. The correct maintenance of the expression of the Squamous Cell Carcinoma Antigen (SCCA) was proven and the signal clearly detectable. Panel a: bright field image, panel b: merged image of the staining for SCCA (panel c) and for DAPI, marking all nuclei (panel d). Scale bars 100 μm.*

The following sections will present two relevant case studies based on the generation of human models for muscle dystrophy (section 4.3) and cardiac diseases (section 4.4).

4.3 Development of an *in vitro* model of Human Duchenne Muscular Dystrophy

This study, centered on the development of an *in vitro* model for a specific disease, Duchenne Muscular Dystrophy (DMD), found its motivations on both the necessity of generating tissue substitutes closely mimicking *in vivo* muscle physiology in order to perform pharmacological studies and/or therapy development and on the relevance of the disease itself. More details on the biophysical description of this study are reported in the PhD thesis of Serena (Serena 2009).

In general, therapeutic strategies for muscle dystrophy can be classified into three groups based on their approach: (a) gene therapy, (b) cell therapy (myoblasts and stem cells), and (c) pharmacological therapy. Unfortunately today, after almost 20 years since the discovery of the gene, an effective therapy that could mitigate the dystrophic process is yet to be found (Cossu and Sampaolesi 2007).

Although numerous current studies are showing promising potential, many suffer from a variety of weaknesses. It is likely that the development of therapeutic strategies, based on accurate studies on the progressive and multi−factorial nature of muscle dystrophy, may only be achieved through a combination of different approaches.

The process of skeletal myoblast differentiation *in vitro* has been widely investigated over the last years (Bach et al. 2007, Bassel-Duby and Olson 2006, Collins et al. 2005) and several cell sources and different substrates (standard Petri dishes, natural or synthetic scaffolds, etc) have been used. Besides the increased level of knowledge in the fields of myofibrillogenesis and skeletal muscle tissue engineering that these studies brought, only few of them were based on the use of human myoblasts as cell source (Barberi et al. 2007, Thorrez et al. 2008). It is of paramount importance to stress the fact that, aimed at ultimately reaching clinical applications and patient-specific therapies, the use of a human cell source would be required.

Besides the use of the “not optimal” cell source, most studies and clinical trials failed to succeed in reproducing the actual human muscle physiology because of the methodologies used for cell culture *in vitro*. As extensively reported here and in Chapter 1, the recognition of the complexity of the *in vivo* microenvironment, renders standard *in vitro* cultures extremely lacking in its recapitulation. To capture the above mentioned complexity, it is thus necessary to develop and implement new strategies.

In particular, among the different properties required to closely reproduce the *in vivo* environment, surface mechanical properties are of particular relevance for the functionality of contractile cells such as skeletal muscle cells (Ingber 2002, Engler et al. 2004a, Beningo and Wang 2002, Ingber 2005); consequently, the coupling to soft or stiff substrate is extremely important. As a demonstration, Engler and colleagues (Engler et al. 2004a) showed that after one week of culture, myosin/actin striations necessary for functional muscle activity, developed only on C2C12 myoblasts cultured on polyacrylamide gels with the same stiffness as that of native muscle.

In this work we thus:

- cultured human dystrophic myoblasts (from DMD-affected patients) on a polyacrylamide based hydrogel to more closely mimic the mechanical physiological properties of *in vivo* muscle;
- performed micro−contact printing of adhesion proteins on the hydrogel surface, in order to:
    - obtain a topological control over cell adhesion.
    - direct their alignment and drive differentiation into functional myotubes,
    - mimic the structure of a natural muscular fiber.

The micro−contact printing techniques have been described in detail in section 4.2.

Within this study, we exploited the possibility of tuning the mechanical properties of the hydrogel substrate. For this reason, using different amount of acrylamide mixture in the prepolymer solution, we obtained hydrogels with elastic modulus (Young modulus) covering the range from 10 to 20 kPa. Figure 4.9 shows the results of the mechanical tests performed on hydrogel samples of different composition.

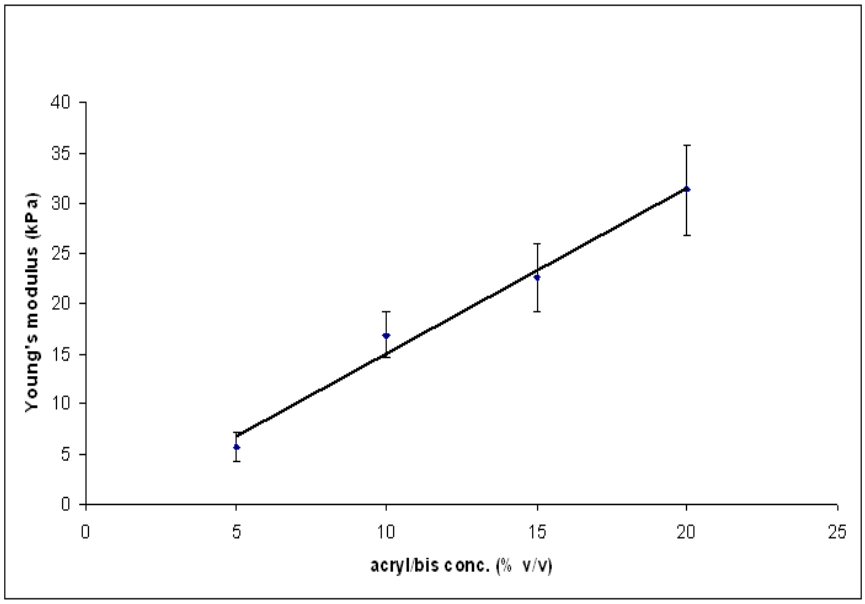

Figure 4.9. *Young's modulus of polyacrylamide hydrogels. Elastic moduli were quantitatively measured through standard compression tests for four different hydrogel compositions, i.e. 5-10-15-20% (v/v) acrylamide/bis-acrylamide 29:1 mixture in the prepolymer solution.*

Concerning micro-patterning for the control of cell adhesion, we chose a geometry composed of parallel lanes with a 75 μm width and 100 μm spacing.

In addition, we tested the effects of different adhesion proteins on the myoblast cultures, verifying both the persistence of the pattern (at least 7 days of culture were required) and the correct differentiation and maturation of the newly-formed myotubes.
In particular we used:

- laminin and fibronectin (100 μg/mL);
- Matrigel 2.5%.

Immunofluorescence analyses were used to assess the expression of the correct myogenic markers such as desmin, and the sarcomeric organization (sign of functional differentiation) though myosin heavy chain (MHC) and α-actinin detection. Cell nuclei were stained with DAPI in order to facilitate cell counts for the fusion index evaluation.

4.3.1 Results and discussion

Figure 4.10 shows a representative comparison between the time course of adhesion of human myoblasts adhering to uniformly coated standard culture surfaces and to micropatterned PA hydrogels.

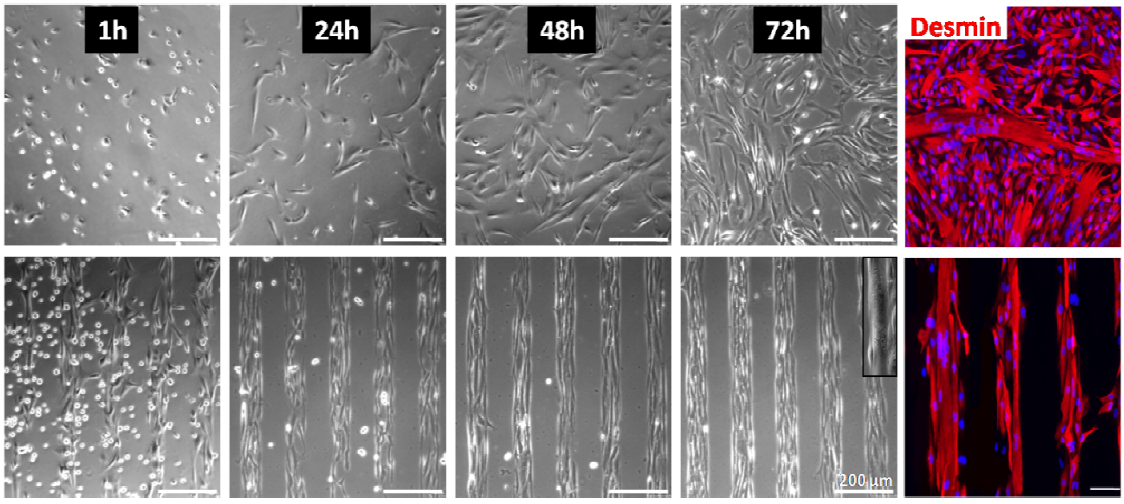

Figure 4.10. *Time course of adhesion of human DMD myoblasts on uniformly coated surfaces (first row) versus cells adhering to hydrogel surfaces with protein micropattern (second row). Uniform coating induced cells to randomly adhere on the available area, while cells on micropatterned lanes adhered only to the protein coated areas. The alignment and the degree of confluence that was soon reached, favored the differentiation into functional myotubes. This was further confirmed by immunofluorescence analyses(last column): cells on standard surfaces fused without any preferential orientation (top image) while those onto micropatterned hydrogels differentiated precociously and into parallel-oriented myotubes. Scale bars 200 µm.*

Figure 4.11 reports the results of the striated myotubes count on hydrogels of varying stiffness and patterned with different adhesion proteins.

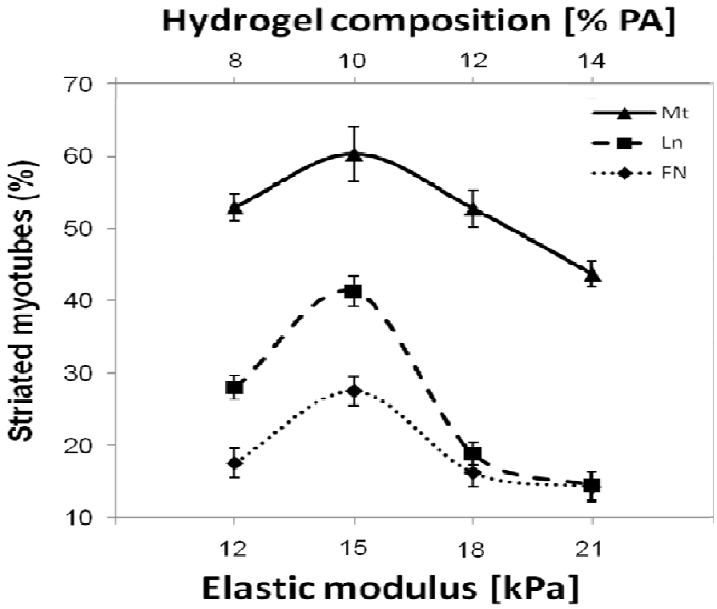

Figure 4.11. *Analysis of the percentage of striated myotubes on hydrogels of varying stiffness after 7 days of culture. Different proteins were used to create the adhesive areas on the substrates: Matrigel 2.5%, laminin and fibronectin 100 µg/mL.*

The results in Figure 4.11 pointed at Matrigel 2.5% as the optimal promoter for the adhesion and differentiation of human myoblasts from DMD patients. Most intriguingly, all adhesion proteins displayed their maximum value in terms of striated (and so physiologically mature) myotubes at an elastic modulus value of ~ 15 kPa, corresponding to the stiffness of skeletal muscle *in vivo*.

For these reasons, for the following experimentations we chose to micro-pattern Matrigel 2.5% onto hydrogels with an elastic modulus ~ 15 kPa (acrylamide/bis-acrylamide 29:1 40% solution to a final value of 10% (v/v) in the prepolymer solution).

Figure 4.12 reports the extremely relevant results obtained. Images derive from the above mentioned immunofluorescence analyses.

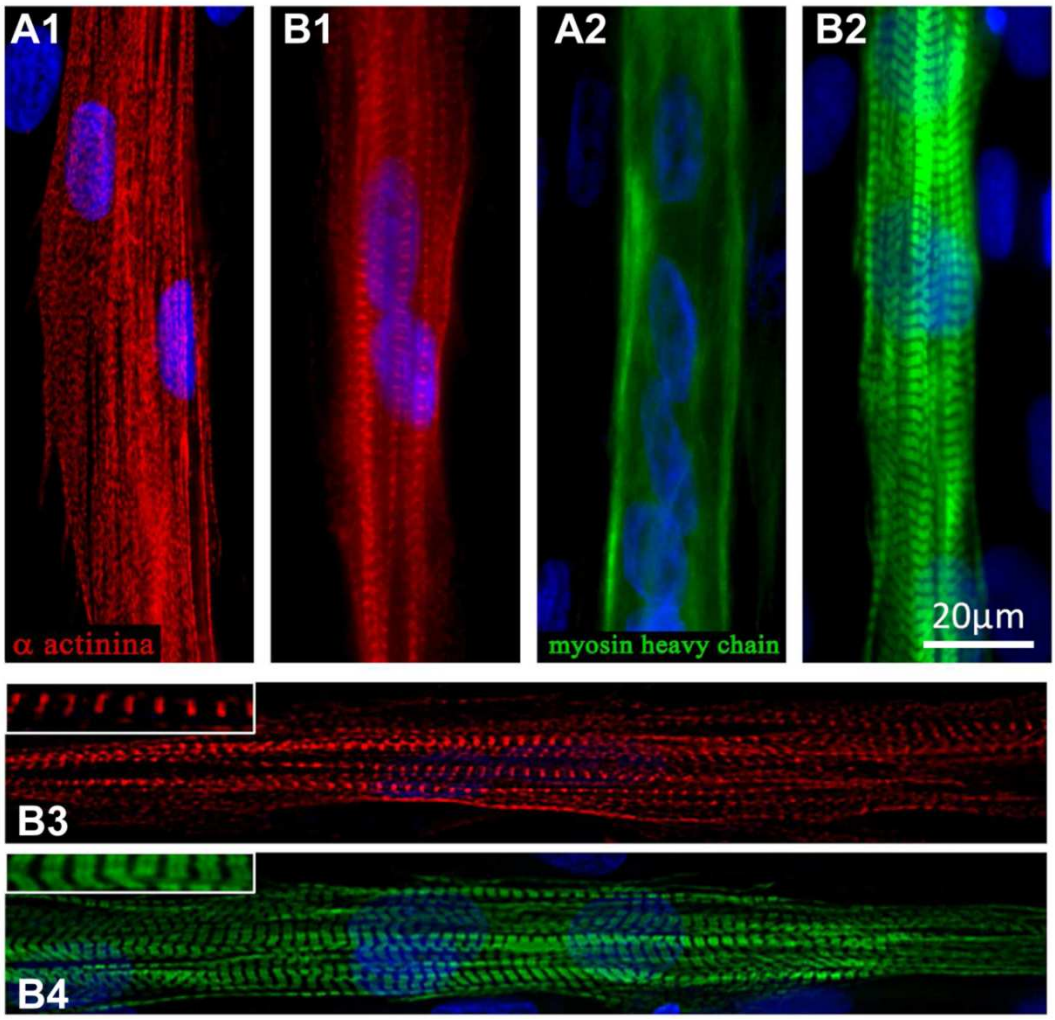

Figure 4.12. *Biological validation of the maturation of the myotubes obtained from the differentiation of human myoblasts from DMD patients. Images denoted by A letters referred to myotubes formed onto standard glass surfaces while B indicated myotubes formed on micropatterned hydrogels.*

From the images in Figure 4.12 we could observe how myotubes formed on standard glass (and thus stiff) substrates didn't show sarcomeric organization, as from the immunofluorescence analysis for α-actinin and MHC, we could observe a diffuse and not organized cytoplasmic signal (Panel A1 and A2). In such cases, only few sarcomeric striations were observed, and they covered only part of the the length of the myotubes. On the contrary, myotubes formed on hydrogel surfaces showed the typical sarcomeric striations of Z-disk and A-band for the entire length of the myotubes (Panel B1-4 and magnifications in insets). In addition, the dimensions of the entire sarcomere (distance between Z-disks) and the A-band was consistent with physiological values: 2-2.5 μm between Z-lines and A-band of 1.2 μm.

We could further observe that in most cases, the striated myotubes that formed onto standard stiff substrates were adhering to a layer myoblasts that acted as a soft supporting material. In addition, such myotubes formed at later time points if compared with myotubes grown on hydrogels.

All experiments presented here were also successfully replicated using myoblasts from healthy patients. In this case, we could detect a significant and defined membrane-expression of dystrophin in myotubes after 11 days of culture.

With the aim of developing an *in vitro* model for human disease, and specifically of Duchenne Muscular Dystrophy, in this study we proved that:

- the percentage of striated myotubes was strongly dependent on substrates stiffness;
- a substrate with tissue-like mechanical properties (E≈15kPa) induced more rapid and spontaneous human myoblast differentiation into functional myotubes.

These results, together with the detected remarkable dystrophin expression on myotubes from healthy patients, open relevant and promising perspectives in the application of our methodologies for:

- performing highthroughput screenings of defined drugs or compounds;
- test the feasibility of cell- or gene-therapy *in vitro* before the *in vivo* trials.

It is important to underline how those studies would benefit of the fact that they would be performed on an *in vitro* model that would be much closer to the real *in vivo* physiology than most of the pre-existing ones. This *in vitro* model, was obtained with simple, robust and repeatable techniques, that could be easily transferred to other research laboratories and adapted to different applications and cell types.

4.4 Development of an *in vitro* array of human-derived beating cardiomyocytes

Heart failure following ischemic heart disease, hypertension, and myocardial infarction is a common cause of death in developed countries. The incidence of cardiac-related diseases is ever-increasing and gaining much attention from the scientific community.

In this sight, the derivation of cardiomyocytes from human embryonic stem cells (hESC) would offer unlimited advantages for myocardial cell therapy and engineered cardiac patch. Moreover, the development of an *in vitro* model, reproducing at least the morphological and physiological features of human cardiac tissue, would be of great value for physiological studies or drug and therapies development, as discussed in section 4.3.

The aim of this study was to assess the compatibility of our technologies with the culture of hESC-derived cardiomyocytes and the maintenance of their correct phenotype following from the application of such different culture conditions and techniques.

In our perspective, a model of human functional cardiomyocytes could for example provide a relevant tool to study the effects of new or existing drugs on cardiomyocytes physiology and functionality and to develop novel and alternative therapeutic strategies.

At the moment, the most efficient protocol for cardiomyocytes derivation from hESC has been established by Professor Gordon Keller (Toronto University) and his research group. Adopting the strategy of mimicking as close as possible the events happening *in vivo* during embryo development, the methodology developed by Dr. Keller and coworkers tries to recapitulate *in vitro* the natural steps leading to the ultimate cardiac differentiation of uncommitted progenitors (Murry and Keller 2008). To do this, they have been well aware of the fact that the effects of the multiple and specific soluble factors acted in a precise spatial-temporal sequence and in a concentration-dependent manner.

The first studies have been performed using mouse embryonic stem cells (Kattman et al. 2006) but the great urge of having human-based models, promoted the optimization of the protocol also for the embryoid bodies (EBs) obtained from human embryonic stem cells cultures (Yang et al. 2008).

A schematization of the protocol is shown in Figure 4.13; the fundamental stages involved in the directed differentiation of the EBs are: *i.* the formation of a primitive streak-like population, *ii.* the induction and specification of cardiac mesoderm, and *iii.* the expansion of the obtained cardiovascular lineages. More details can be found in Serena (Serena 2009).

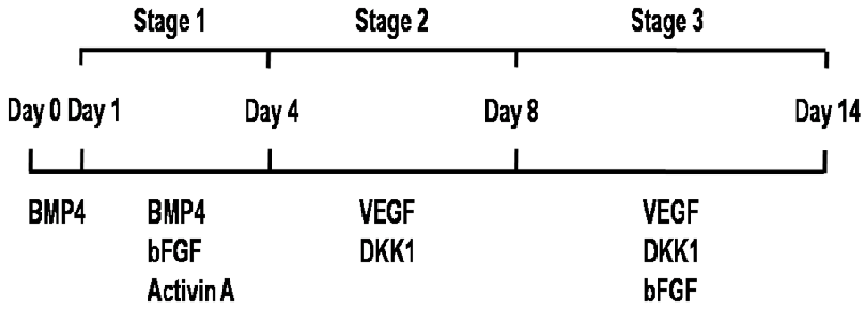

Figure 4.13. *Schematization of the protocol developed by Dr. Keller and coworkers for the specification of the cardiac lineage from hESC.*

At the end of these phases, after day 17, the EBs population showed extensive and diffused contractile activity, a clear sign of correct cardiac differentiation. For our experimentations we thus used cells obtained from the dissociation of these differentiated EBs.

Thus, adapting the microscale techniques previously developed and applied to other cell types (sections 4.2 and 4.3), we produced an array of hESC-derived cardiomyocytes adhering onto polyacrylamide hydrogel surfaces.

Again, the hydrogel ensured the establishment of a more physiological environment in terms of its effect of mimicking the mechanical properties of striated muscles *in vivo* (with elastic modulus ~10-15 kPa).

In addition, the topological control of cell adhesion at the microscale allowed us to study the most favorable geometry that would optimally adapt to the cardiac phenotype. Other preliminary experiments were aimed at identifying the optimal adhesion protein for this cardiac-enriched population.

This set of preliminary experiments led us to the choice of an array of circular dots with 300 µm diameter and 700 µm center to center spacing; the entire array covered a 8x8 mm area at the center of the hydrogel disk. The circular shape of the pattern allowed to obtain a more stable configuration with regards to the characteristic contractile activity of cardiac cells: a circular arrangement resulted in a more uniform distribution of the mechanical stresses

developed during contractions, without the generation of critical-tensions in localized edges of the geometry that would result in unwanted cell detachments.

With this geometry we thus performed the micro-contact printing technique on PA hydrogel surfaces transferring solutions of laminin 100 µg/mL.

Cell seeding was performed optimizing the general procedures presented in section 4.2.2. In particular, the critical parameter of cell seeding density was set at $6.2 \cdot 10^4$ cells/cm^2.

The maintenance of the correct expression of cardiac markers and the degree of differentiation were verified on the arrayed cultures between 5 and 7 days of evaluating the expression of Connexin 43 (Cx43), cardiac Troponin T (cTnT) and Integrin β1D (Intβ1D) by immunofluorescence analysis.

In addition, in order to assess the functionality of the human-derived cardiomyocytes after culture onto the hydrogel surfaces, spontaneously contracting dots array were electrically stimulated trying to pace their beating. We were thus aimed at inducing a coupling between the spontaneous contractions and the electrical stimulation. The square-wave impulse was modulated trying to find the optimal values in terms of amplitude, duration and frequency capable to elicit that coupling.

The optimal results were obtained with square waves of $5 \cdot 10^3$ mV amplitude and 10 ms duration. Their frequency was varied during the experiments in a range from 1 to 2 Hz.

The system allowed on line observations at the microscope, thus allowing live capture of the contractile activity. The obtained movies were thus post-processed via image analysis for the quantification of the recorded contractions.

It is worth noticing how on a single observation field (and thus in each movie-frame) we had at least 5 individual beating dots to analyze, demonstrating the consistency and valuable statistical significance of the obtained data.

Briefly, movies were converted into stacked frames and several 5 µm diameter regions of interest (ROIs) were positioned in appropriate areas of the contracting cell-dots (so that their color intensity changed during contraction). An automated routine then measured the average intensity of each ROI and for all images in the stack. From such intensity values, graphs representing the cells contractions could be built.

4.4.1 Results and discussion

First of all, the PA-based hydrogels proved to be completely biocompatible with regards to the hESC-derived cardiomyocytes, which selectively adhered with high efficiency to the micropatterned areas. This, in parallel, confirmed the feasibility of the application of the developed techniques also to this extremely delicate cell type.

We confirmed how the chosen configuration and experimental parameters resulted in an homogenous array in the entire patterned surface and in cells maintaining the correct cardiac marker Troponin T expression even after several days of culture.

As can be seen from the images at increasing magnification in Figure 4.14, row 1, we obtained an uniform array of circular cell-dots covering a 8x8 mm area and adhering with extreme selectively onto the protein patterned areas, with only few outgrowths. In addition, Troponin T was clearly detectable and extensively expressed by the majority of cells.

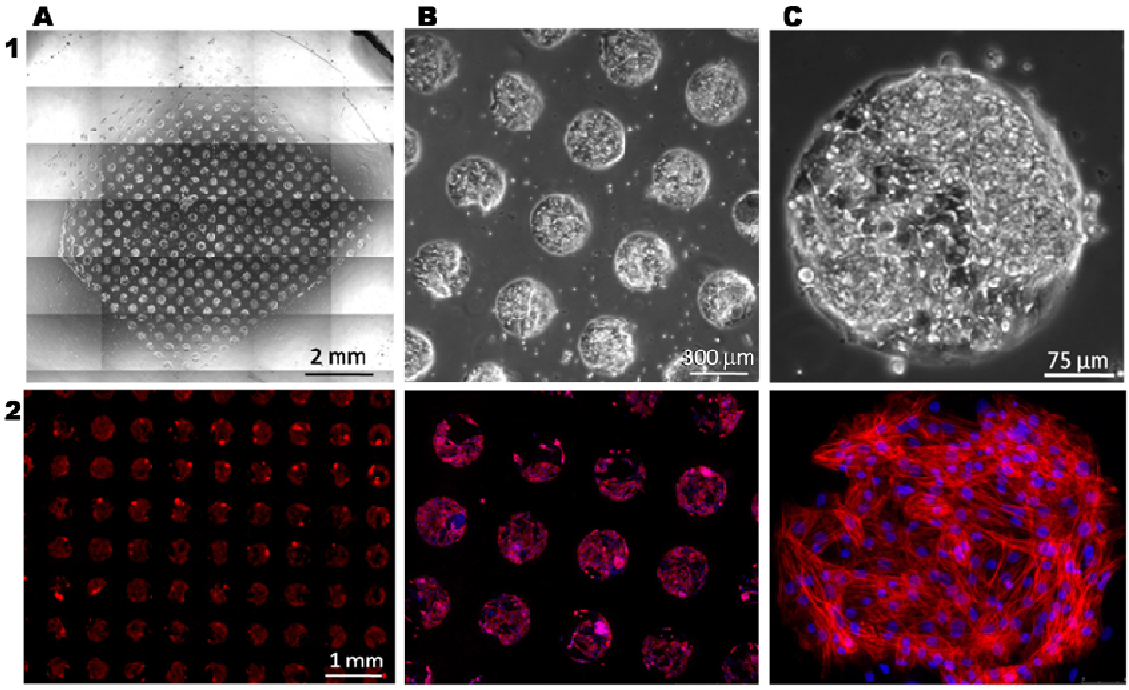

Figure 4.14. *Bright field images (row 1) and cardiac Troponin T (red in row 2) immunofluorescence of the cardiomyocytes array. Nuclei were counterstained with DAPI (blue). Image A1 shows the entire surface of the 8x8 mm array of circular dots, obtained merging individual images. Higher magnifications are reported in B and C.*

Further results are reported in Figure 4.15, proving the correct maturation of the cardiac cell population expressing Connexin 43 (Cx43), again cardiac Troponin T (cTnT) and Integrin β1D (Intβ1D).

Connexin 43 is a typical protein found in gap junctions; its expression would thus prove the correct coupling between the cytoplasms of neighboring cells establishing proper communication in terms of signal transmission during contraction.

Integrin β1D mediate cell-matrix adhesion and is exclusively found in cardiac and skeletal muscle; its expression would thus further prove the correct cardiac phenotype of the cultured cells besides their proper coupling to the substrate-matrix formed by the protein-patterned hydrogel.

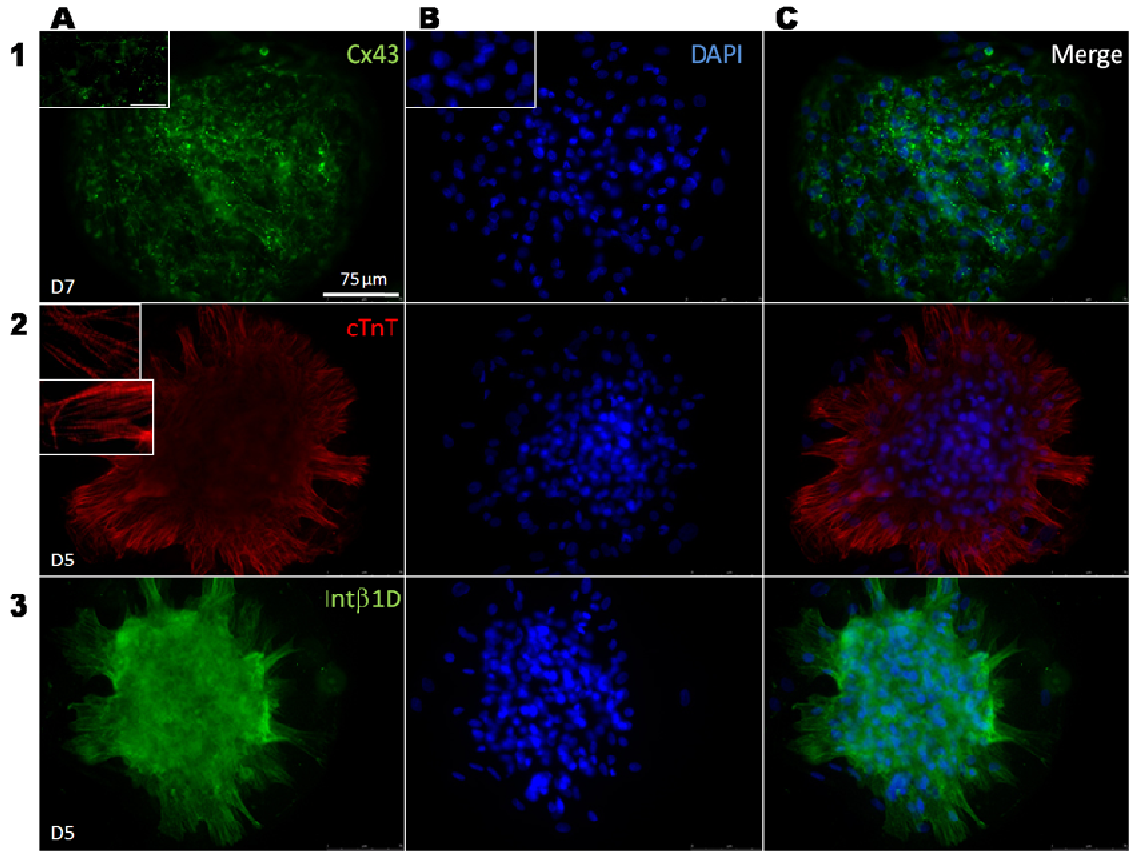

Figure 4.15. *The maintenance of the correct expression of cardiac markers and the degree of differentiation were verified evaluating the expression of Connexin 43 (Cx43), cardiac Troponin T (cTnT) and Integrin β1D (Intβ1D) by immunofluorescence analysis. Row 1 reports Cx43 expression by cells on patterned dots after 7 days of culture: individual stain in A1, corresponding DAPI (marking all nuclei) in B1 and merged image in C1. Rows 2 and 3 repot results on arrays after 5 days of culture. In A2 cTnT expression shows remarkable organization in terms of characteristic striations (higher magnification insets) while row 3 demonstrate the diffuse expression of Intβ1D.*

Finally, with regards to the application of an external electrical stimulation, table 4.1 summarizes an example of the applied stimuli and the results of the analyzed movies.

In parallel, non-stimulated control cultures were monitored and their spontaneous contractions were recorded and analyzed.

We underline again how the data for each movie derived from averaged values evaluated on at least 5 individual contracting cell-dots.

Table 4.1. *Results of the electrical stimulation on spontaneously contracting cell-dots. The contraction frequency recorded after application of the described stimuli is reported in the last column.*

Movie nr	Voltage [mV]	Duration [msec]	Interval [msec]	Frequency [Hz]	Contraction frequency [Hz]
1	5000	10	1000	1.0	1.3±0.1
2			750	1.3	1.7±0.1
3			500	2.0	2.0±0.0

When ramping from a 1 Hz frequency to 2 Hz, cell-dots clearly tended to follow the applied electrical stimulation, beating at a rate closely resembling the frequency of the external stimulus. In particular, at 2 Hz we could observe the obtainment of a perfect excitation-contraction coupling.

The graphs in Figure 4.16 report exemplifying traces obtained from the above described quantification of the contractile activity on both stimulated and spontaneously contracting cell-dots.

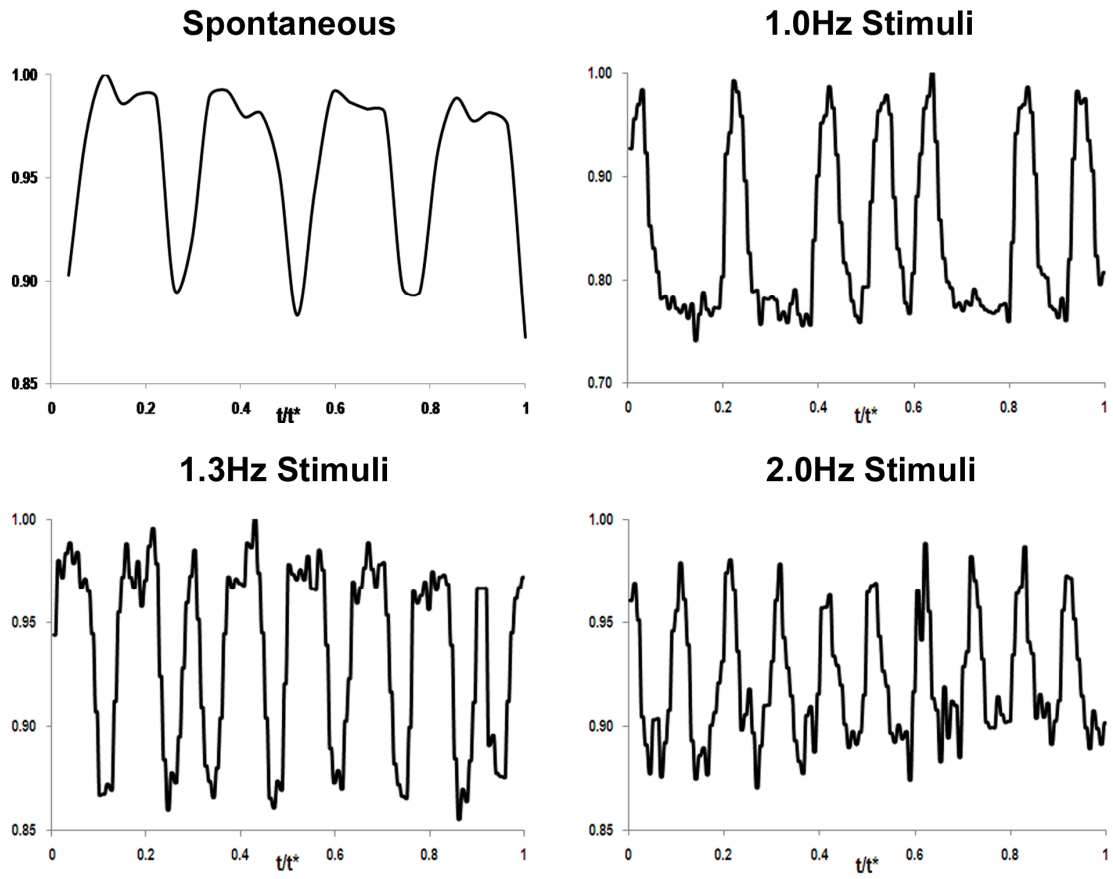

Figure 4.16. *Graphs representing the cells contractions have been obtained though image analysis of the recorded movies. Contractions of randomly chosen cell-dots are shown for each condition. The first trace represents a spontaneous contraction. In the other traces, the applied external electrical stimulation had the reported values. The dimensionless extent of contraction is represented as a function of dimensionless time.*

From these trace-graphs, it is clear how the individual dots experiencing electrical stimulation, tended to contract synchronously and at frequencies dictated by the electrical stimulation, with a perfect coupling at a stimuli frequency of 2Hz.

On the contrary, not-stimulated dots had a lower “basal” beating rate and, from the comparison between multiple traces, had a more heterogeneous behavior and didn’t presented synchronous contractions.

With this study, we proved that the developed technologies could effectively be adapted and applied to another relevant cell source: human embryonic stem cells-derived cardiac populations with the primary aim of obtaining physiological models of human functional cardiomyocytes.

The developed technologies, could for example provide a relevant tool to perform pharmacological studies on a relevant biological system representative of human cardiac physiology and functionality.

This would prove useful in both testing the effects of existing drugs or of new compounds in their development phases, to assess their potential toxicity or their pharmacological activity on cardiac human tissue substitutes and on the development of novel and alternative therapeutic strategies for treating cardiac diseases.

Another interesting aspect that have not been treated in detail here and is object of ongoing studies in our laboratories, is the fact that working with a substrate such as polyacrylamide hydrogel with tunable mechanical properties, would for example allow to perform studies in a microenvironment mimicking the increased stiffness of the fibrotic tissue in infracted heart. The perspectives that similar studies would open are extremely valuable for the insights that they could give in the effective processes acting in such tissues, and consequently plan and test the most proper interventions and therapies.

4.5 References

Q. Liu, H. Huang, H. Cai, Y. Xua, Y. Li, R. Li and P. Wang, Embryonic stem cells as a novel cell source of cell-based biosensors. *Biosensors and Bioelectronics*, 2007, **22**, 810–815.

D. R. Albrecht, G. H. Underhill, T. B. Wassermann, R. L. Sah and S. N. Bhatia, Probing the role of multicellular organization in three-dimensional microenvironments. *Nat Methods*, 2006, **3**, 369-375.

J. H. Jang and D. V. Schaffer, Microarraying the cellular microenvironment. *Mol Syst Biol*, 2006, **2**.

D. Kaplan, R. T. Moon and G. Vunjak-Novakovic, It takes a village to grow a tissue. *Nat Biotechnol*, 2005, **23**, 1237-1239.

G. Vunjak-Novakovic and L. E. Freed, Culture of organized cell communities. *Adv Drug Deliv Rev*, 1998, **33**, 15-30.

D. Motlagh, S. E. Senyo, T. A. Desai and B. Russell, Microtextured substrata alter gene expression, protein localization and the shape of cardiac myocytes. *Biomaterials* 2003, **24**, 2463 76.

D. E. Ingber, Mechanical signaling and the cellular response to extracellular matrix in angiogenesis and cardiovascular physiology. *Circ Res*, 2002, **91**, 877-887.

C. B. Khatiwala, S. R. Peyton and A. J. Putnam, Intrinsic mechanical properties of the extracellular matrix affect the behavior of pre-osteoblastic MC3T3-E1 cells. *Am J Physiol Cell Physiol*, 2006, **290**, C1640-1650.

A. J. Engler, M. A. Griffin, S. Sen, C. G. Bönnemann, H. L. Sweeney and D. E. Discher, Myotubes differentiate optimally on substrates with tissue-like stiffness: pathological implications for soft or stiff microenvironments. *The Journal of Cell Biology*, 2004a, **166**, 877-887.

K. Britton-Keys, F. M. Andreopoulos and N. Peppas, Poly(ethylene glycol) star polymer hydrogels. *Macromolecules* 1998, **31**, 8149-8156.

J. A. Burdick, A. Khademhosseini and R. Langer, Fabrication of gradient hydrogels using a microfluidics/photopolymerization process. *Langmuir* 2004, **20**, 5153-5156.

S. Lin-Gibson, R. L. Jones, N. R. Washburn and F. Horkay, Structure-property relationships of photopolymerizable poly(ethylene glycol) dimethacrylate hydrogels. *Macromolecules* 2005, **38**, 2897-2902.

L. Almany and D. Seliktar, Biosynthetic hydrogel scaffolds made from fibrinogen and polyethylene glycol for 3D cell cultures. *Biomat* 2005, **26**, 2467-2477.

J. B. Leach, K. A. Bivens, C. W. Patrick and C. E. Schmidt, Photocrosslinked hyaluronic acid hydrogels: natural, biodegradable tissue engineering scaffolds. *Biotechnol Bioeng*, 2003, **82**, 578-5.

J. B. Leach and C. E. Schmidt, Characterization of protein release from photocrosslinkable hyaluronic acid-polyethylene glycol hydrogel tissue engineering scaffolds. *Biomat* 2005, **26**, 125-135.

D. Hern and J. A. Hubbell, Incorporation of adhesion peptides into nonadhesive hydrogels useful for tissue resurfacing. *J Biomed Mater Res*, 1998, **39**, 266-276.

A. Engler, L. Bacakova, C. Newman, A. Hategan, M. Griffin and D. Discher, Substrate compliance versus ligand density in cell on gel responses. *Biophys J*, 2004b, **86**, 617-628.

S. R. Peyton and A. J. Putnam, Extracellular matrix rigidity governs smooth muscle cell motility in a biphasic fashion. *J Cell Physiol* 2005, **204**, 198-209.

D. Falconnet, G. Csucs, H. M. Grandin and M. Textor, Surface engineering approaches to micropattern surfaces for cell-based assays. *Biomat* 2006, **27**, 3044-3063.

Y. Xia and G. M. Whitesides, Soft lithography. *Angew Chem Int Ed*, 1998, **37**, 550-575.

J. M. Karp, Y. Yeo, W. Geng, C. Cannizarro, K. Yan, D. S. Kohane, G. Vunjak-Novakovic, R. S. Langer and M. Radisic, A photolithographic method to create cellular micropatterns. *Biomat* 2006, **27**, 4755-4764.

S. Rohr, D. M. Scholly and A. G. Kleber, Patterned growth of neonatal rat heart cells in culture. Morphological and electrophysiological characterization. *Circ Res*, 1991, **68**, 114-130.

K. Y. Suh, J. Seong, A. Khademhosseini, P. E. Laibinis and R. Langer, A simple soft lithographic route to fabrication of poly(ethylene glycol) microstructures for protein and cell patterning. *Biomat* 2004, **25**, 557-563.

S. M. Gopalan, C. Flaim, S. N. Bhatia, M. Hoshijima, R. Knoell, K. R. Chien, J. H. Omens and A. D. McCulloch, Anisotropic stretch-induced hypertrophy in neonatal ventricular myocytes micropatterned on deformable elastomers. *Biotechnol Bioeng*, 2003, **81**, 578-587.

A. Khademhosseini, G. Eng, J. Yeh, P. A. Kucharczyk, R. Langer, G. Vunjak-Novakovic and M. Radisic, Microfluidic patterning for fabrication of contractile cardiac organoids. *Biomed Microdevices*, 2007, **9**, 149-157.

R. B. Vernon, M. D. Gooden, S. L. Lara and T. N. Wight, Microgrooved fibrillar collagen membranes as scaffolds for cell support and alignment. *Biomat* 2005, **26**, 3131-3140.

E. K. F. Yim, R. M. Reano, S. W. Pang, A. F. Yee, C. S. Chen and K. W. Leon, Nanopattern-induced changes in morphology and motility of smooth muscle cells. *Biomat* 2005 **26**, 5405-5413.

S. A. Ruiz and C. S. Chen, Microcontact printing: A tool to pattern. *Soft Matter* 2007, **3**, 1–11.

T. C. McDevitt, J. C. Angello, M. L. Whitney, H. Reinecke, S. D. Hauschka, C. E. Murry and P. S. Stayton, In vitro generation of differentiated cardiac myofibers on micropatterned laminin surfaces. *Journal of biomedical materials research* 2002, **60**, 472-479.

T. C. McDevitt, K. A. Woodhouse, S. D. Hauschka and C. E. Murry, Spatially organized layers of cardiomyocytes on biodegradable polyurethane films for myocardial repair. *J Biomed Mater Res*, 2003, **66A**, 586-595.

E. Cimetta, S. Pizzato, S. Bollini, E. Serena, P. DeCoppi and N. Elvassore, Production of arrays of cardiac and skeletal muscle myofibers by micropatterning techniques on a soft substrate. *Biomedical Microdevices*, 2008, Epub ahead of print.

E. Serena, Microscale tissue engineering of human skeletal and cardiac muscles for in vitro applications. *PhD thesis*. Dipartimento di Principi e Impianti di Ingegneria Chimica "I. Sorgato", University of Padova, 2009.

G. Cossu and M. Sampaolesi, New therapies for Duchenne muscular dystrophy: challenges, prospects and clinical trials. *Trends in Molecular Medicine*, 2007, **13**, 520-6.

A. D. Bach, J. P. Beier, J. Stern-Staeter and R. E. Horch, Skeletal muscle tissue engineering. *Journal of Cellular and Molecular Medicine*, 2007, **8**, 413-422.

R. Bassel-Duby and E. N. Olson, Signaling Pathways in Skeletal Muscle Remodeling. *Annual Reviews of Biochemistry*, 2006, **75**, 19-37.

C. A. Collins, I. Olsen, P. S. Zammit, L. Heslop, A. Petrie, T. A. Partridge and J. E. Morgan, tem Cell Function, Self-Renewal, and Behavioral Heterogeneity of Cells from the Adult Muscle Satellite Cell Niche. *Cell*, 2005, **122**, 289-.

T. Barberi, M. Bradbury, Z. Dincer, G. Panagiotakos, N. D. Socci and L. Studer, Derivation of engraftable skeletal myoblasts from human embryonic stem cells. *Nature Medicine*, 2007, **13**.

L. Thorrez, J. Shansky, L. Wang, L. Fast, T. VandenDriessche, M. Chuah, D. Mooney and H. Vandenburgh, Growth, differentiation, transplantation and survival of human skeletal myofibers on biodegradable scaffolds. *Biomaterials*, 2008, **29**, 75-84.

K. A. Beningo and Y. L. Wang, Flexible substrata for the detection of cellular traction forces. *Trends in Cell Biology*, 2002, **12**, 79-84.

D. E. Ingber, Mechanical control of tissue growth: function follows form. *Proc Natl Acad Sci U S A*, 2005, **102**, 11571-11572.

C. E. Murry and G. Keller, Differentiation of Embryonic Stem Cells to Clinically Relevant Populations: Lessons from Embryonic Development. *Cell*, 2008, **132**, 661–680.

S. J. Kattman, T. L. Huber and G. M. Keller, Multipotent Flk-1+ Cardiovascular Progenitor Cells Give Rise to the Cardiomyocyte, Endothelial, and Vascular Smooth Muscle Lineages. *Developmental Cell*, 2006, **11**, 723–732.

L. Yang, M. H. Soonpaa, E. D. Adler, T. K. Roepke, S. J. Kattman, M. Kennedy, E. Henckaerts, K. Bonham, G. W. Abbott, R. M. Linden, L. J. Field and G. M. Keller, Human cardiovascular progenitor cells develop from a KDR1 embryonic-stem-cell-derived population. *Nature*, 2008, **453**, 524-U6.

Chapter 5
Coupling microfluidics and topology

The final step of the presented study, and object of a relevant ongoing study, was represented by the efforts in coupling the developed technologies with the aim of creating integrated devices with all the studied components: microfluidic platforms, controlled substrates and topologies.

5.1 Motivations

In the literature, to our knowledge, not many examples of validated systems of this kind exists. Tourovskaia et al. (Tourovskaia et al. 2006) developed a complex system capable of ensuring the long term culture of murine myotubes (obtained by the *in loco* differentiation of spatially organized cells) and their selective treatment via microfluidic delivery of defined factors. Nevertheless, even if this study proved the effectiveness in performing long-term cultures under perfused conditions, didn't comprise an appropriate system for the control of the flow rates of the entering fluids nor presented biologically relevant data on the above mentioned selective treatment. Other interesting case studies can be found (DiCarlo et al. 2006, Kim et al. 2005, Kim et al. 2007), but they tend to lack of simplicity in fabrication and assembly, combined with an ease of use and/or obtainment of significant results on a relevant cell population.

Given the proper choice of the optimal substrates, the advantages deriving from the coupling of microfluidic technologies and micropatterning techniques would open new and interesting perspectives in the field of pharmacological screenings or clinical tests.

The previous chapters have dealt with the arguments separately, and in particular in Chapter 3 we presented and discussed the research based on the development of topological control and in Chapter 4 the results of the development of microfluidic bioreactors and platforms. In this section we will present the obtained results and the ongoing studies aimed at coupling the developed technologies.

5.2 Dynamic culture of bubble-confined cell arrays

The first step towards the development of integrated devices, has been the coupling of a perfusion system to a spatially organized cell culture within a liquid volume of few hundreds of microliters.

In particular, the aim of this study was to design and develop a culture system allowing for an accurate and automated spatio-temporal control of culture conditions. The system prerequisites were: matching highthroughput requirements, interfacing with existing techniques including microfabrication, sample handling and manipulating and allowing for easy and effective results reading and analysis.

Responding to the need of creating an accurate and controlled micro-environment surrounding the cell while meeting the requirements for biological processes or pharmacological screening tests, we were aimed at designing and developing a microscaled culture system suitable for analyzing the synergic effects of extracellular matrix proteins and soluble environments on cell phenotype in a highthroughput fashion. We produced cell arrays deposing micrometer-scale protein islands on hydrogels using a robotic DNA microarrayer, constrained the culture media in a bubble-like volume and developed a suitable perfusion system. The bubble-confined cell arrays were used either with conventional culture methods (batch operating system) or with automated stable and constant perfusion (steady-state operating system). Mathematical modeling assisted the

experimental design and assessed efficient mass transport and proper fluidodynamic regimes.

All details are reported in the manuscript in Appendix H.

The microarray substrate was a polyacrylamide (PA) hydrogel covalently bound to a pre-functionalized glass surface, similarly with what described in Chapter 4 (Cimetta et al. 2008). In particular, the hydrogel substrate was further characterized performing some swelling experiments aimed at identifying its behavior when submerged in different liquid environments.

The protein array was constructed using a Microgrid II (Biorobotics) contact microarrayer, depositing the chosen protein solutions resuspended in the spotting buffer at the final concentration of 50ng/µl.

The experiments were performed using the murine skeletal muscle immortalized cell line C2C12, on which all analyses and culture techniques were developed and optimized.

The perfusion apparatus was composed of 3 main parts: the bioreactor, a gas exchanger unit and a syringe pump. In detail, the bioreactor was composed of two units: a polycarbonate plate as support for the glass slide and a of poly(dimethylsiloxane) (PDMS) chamber to isolate the culture system from the external environment and to allow easy set up of the micro injection and suction apparatus for each bubble. PDMS has been chosen for its oxygen permeability, thermal stability and optical transparency, thus allowing image acquisition of the culture. The gas exchange unit was made using a tubular non-porous permeable membrane (platinum cured silicone tubing); the surface area and the corresponding length were dimensioned to ensure the gas exchange needed for the maintenance of the physiological oxygen and carbon dioxide concentrations and pH value in the culture medium. All connections were made with microbore Tygon and stainless steel tubings.

The bioreactor and the gas exchanger unit were kept in the incubator at standard conditions (37°C, 95% humidity, 5% CO2) while the syringe pump was left at room temperature.

In order to model the developed system, the 3D domain of the bubble was schematized as a semi-ellipsoid with two cylindrical hollows corresponding to the inlet and outlet tubes. The Navier-Stokes equations for incompressible fluids, numerically solved using the finite elements method implemented in Comsol Multiphysics (Burlington, MA), allowed an

estimation of the flow fields and shear stresses that influence the cells. The meshing was optimized to ensure independency of the solution from the spatial discretization. No-slip boundary conditions were used for the hydrogel surface (bottom plane) and the walls of the tubing, sliding/symmetry for the bubble surface, fixed velocity for the inlet and finally zero pressure for the outlet. The results of the mathematical modeling were validated via a particle tracking experiment combined with an image analysis sought at reproducing the velocity profiles and particles trajectories.

5.2.1 Results and discussion

We first proved that the swelling behavior of the hydrogels was insensitive to the media used; this was particularly important as it established that the ECM pattern deposition using a micro-contact arrayer didn't alter the hydrogel elasticity and that the cells would not be influenced by unpredicted mechanical forces induced by deformations.

Examples of spotted geometries are reported in Figure 5.1.

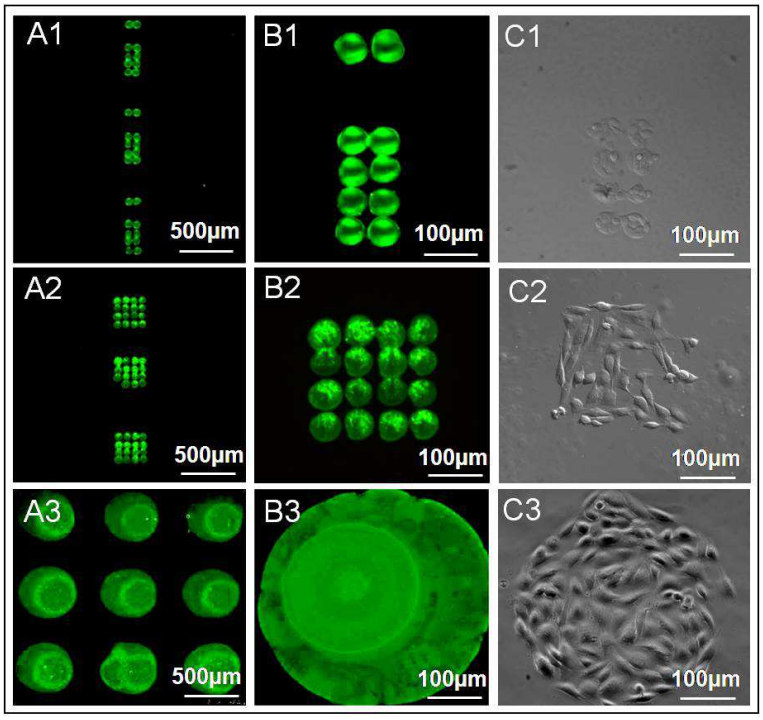

Figure 5.1. *Spotting versatility and materials properties. In columns A and B: fluorescence images of multiple geometries obtained spotting BSA-FITC conjugate with a robotic DNA microarrayer using pins of different diameter. Column C reports the corresponding pictures of living cells selectively adhering to the protein patterned regions due to the hydrogels non-fouling properties.*

The technology employed proved its versatility as we patterned protein arrays characterized by different geometrical arrangements, different spacing between both single and arrays of spots and different diameters of the individual spots themselves, as can be seen in Figure 5.1.

As already seen, the PA hydrogel is a non-fouling material thus preventing cell adhesion to its surface; for this reason, the cells adhered with high selectivity only onto the ECM proteins spotted areas and their migration was hindered, thus allowing a prolonged confinement.

The chosen array geometry for the final experiments was: two separate 4 by 4 (3x3 mm each, 1.5 mm spaced) arrays of individual spotted islands with a 480 µm average diameter located at the center of the circular hydrogel pad.

The results of the fluidodynamic analyses are reported in the following figure.

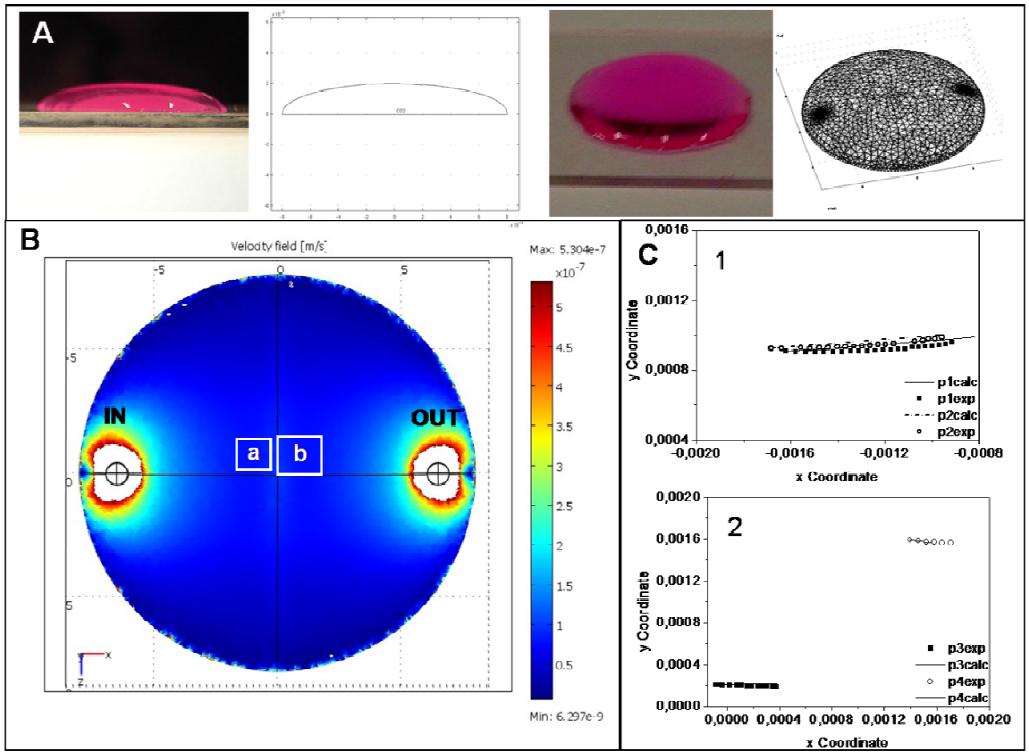

Figure 5.2. *Fluidodynamic analyses and validation. Upper panel (row A) shows the geometry of the bubble of culture medium and the corresponding modeled images and mesh. Lower panel: B report the results of a simulation performed using a 5µL/min flow rate, generating an uniform velocity field. C: experiments with particle tracers (dotted lines) are in accordance with the modeled trajectories (solid lines). The experiments were performed following the movements of particles in the areas represented by a and b in panel B.*

In the upper panel, pictures show the geometry of the bubble of culture medium and the corresponding modeled images, both in 2 and 3 dimensions. In the lower panel, the results (B) of a simulation performed using a 5µL/min flow rate demonstrated the uniformity of the velocity field over the entire surface and thus over the cell arrays, positioned at the center of the bubble. Turbulence was encountered only in the close proximity of the inner and outer conduits (falling out of range in the color coded representation, that was chosen to be able to appreciate the velocity levels in the other areas). In C, the studies performed using devitalized cells as particle tracers (dotted lines) demonstrated accordance with the modeled trajectories (solid lines). The experiments were performed following the movements of particles in the areas represented by a and b in panel B.

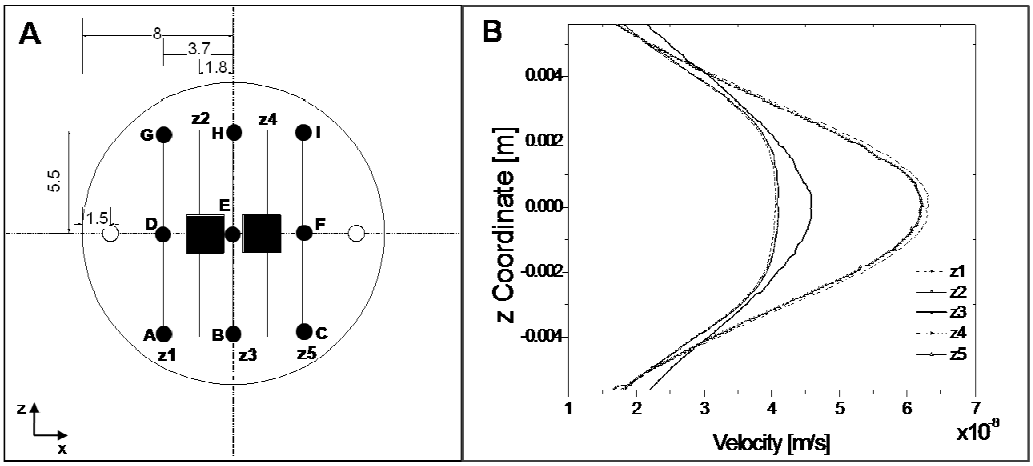

	A	B	C	D	E	F	G	H	I
Velocity [m/s] x10^{-8}	1.72	2.17	1.72	83.2	4.59	82.3	1.75	2.21	1.68
Re x10^{-9}	8.21	10.9	6.88	29.1	15.5	26.6	6.79	12.3	8.07
Shear stress [Pa] x10^{-7}	5.93	8.88	6.56	2.63	19.1	25.9	6.26	9.23	6.34

Figure 5.3. *Modeling validation and measurements. In A: filled squares identify the areas covered by the cell arrays; open circles locate the inner and outer conduits; vertical lines labeled x_i (i=1 to 5) represent the sections were the velocity profiles were calculated and filled circles denoted with capital letters the chosen evaluation points. Represented dimensions are in millimeters. Panel B reports the resulting velocity profiles along xi. The lower table lists the calculated values for velocity, Reynolds number and shear stress on the above mentioned points.*

The modeled velocity profiles reported in panel B are clearly perfectly symmetric with respect to the inner and outer conduit axis. The lower table lists the calculated values for velocity, Reynolds number and shear stress on the above mentioned points; we can observe

how the particular position chosen for the construction of cells array permitted cells to be influenced by the same low shear stresses. This avoided eliciting different cell responses influenced by the position in the array during perfused culture.

Besides the demonstrated feasibility of performing total RNA extraction, the ability of the system to generate consistent biological data has also been verified via morphological evaluations and immunochemistry on the cultured cells, and quantification of the obtained outcomes, as illustrated in Figure 5.4.

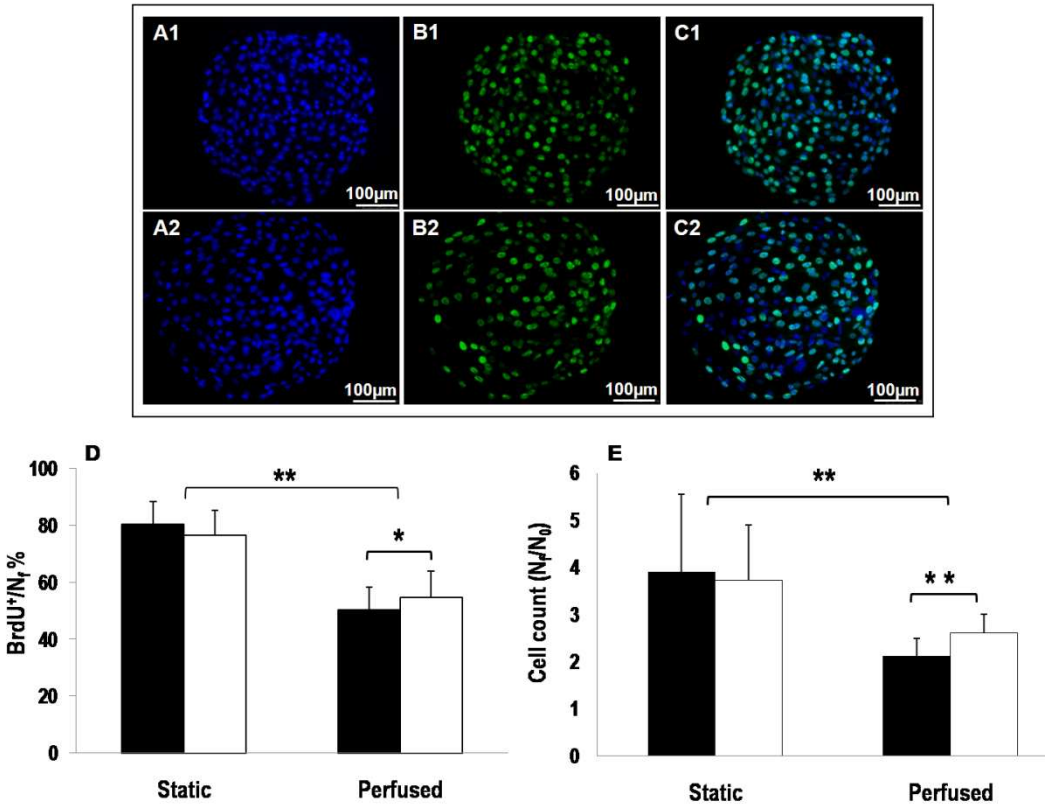

Figure 5.4. *Biological data. Upper panel: immunofluorescence analyses on individual cell islands both after static (A1, B1, C1) and perfused culture (A2, B2, C2). In A nuclei are marked using DAPI, in B BrdU positive cells are stained in green; merged images are reported in column C. Graph D plots the fraction of $BrdU^+$ cells with respect to the total number of cells inside each island for each condition: on fibronectin (■) and laminin (□) and after static and perfused culture. Graph E plots cell counts results (N_f/N_0) in the same conditions. p values were evaluated performing ANOVA tests, (**: $p<0.01$; *: $p<0.05$).*

Upper panel of Figure 5.4 reports images deriving from individual cell islands forming the array, both after static and perfused culture. Graphs D and E were constructed after quantification of the fluorescence images. In D, the fraction of $BrdU^+$ cells with respect to

the total number of cells inside each island (N_f) was evaluated and plotted for each condition: on fibronectin and laminin and after static and perfused culture.

Two statistically significant differences could be noticed: first, static culture resulted in a higher fraction of $BrdU^+$ cells and second, perfused culture allowed us to capture a different behavior on the two proteins used, which were not in evidence in the static culture method. The same trend is observed in E, with a graph plotting the results of the cell counts N_f/N_0 (being N_0 the number of adhering cells counted 2 hours after seeding).

The perfusion of medium and hence the provision of nutrients and oxygen permitted growth and maintenance of the cell array in a more "tissue friendly" condition; however, cell growth was dependent on medium flow rate as this influenced mass transfer, shear stress and hydrostatic pressure which may have a negative impact on cell growth. $BrdU^+$ cells and total number of cells were counted for each spot forming the arrays (number of counted spots >100) from fluorescent images obtained with a double staining for BrdU and DAPI.

In conclusion, cells cultured on arrayed islands (500 µm diameter) maintained the correct phenotype both after static and perfused conditions, confirmed by immunostaining and gene expression analyses through total RNA extraction. The mathematical model, validated using a particle tracking experiment, predicted the constant value of velocities over the cell arrays (less than 10% variation) ensuring the same mass transport regime. BrdU analysis on an average of 96 cell spots for each experimental condition showed uniform expression inside each cell island and low variability in the data (average of 13%). Perfused arrays showed 30% higher doubling times when compared with static cultures. In addition, perfused cultures showed a reduced variability in the collected data, allowing to detect statistically significant differences in cell behavior depending on the spotted ECM protein.

Our technology allowed us to gain increased information-density, resulting in a savings of time and reagents. In addition, the multiple datapoints coming from individual batches possess inherent consistency and higher quality. We thus provided a tool to match existing cell array technologies with the advantage of spatio-temporal controlling the soluble micro-environment for high-throughput biological studies or drug screening tests

Nevertheless, the intrinsic limitations of this work resided in the fact that it didn't comprised a real microfluidic platform and that the liquid bubble surface was free

(sliding/symmetry boundary condition in the simulations) and not confined within sealed culture chambers or similar. Keeping in mind the elevate surface-to-volume ratio, this could increase the relative importance of the less controllable surface effects. In fact, surface tension can exert significant stresses also resulting in free surface deformations and/or bulk liquid motion (Marangoni effect).

The following efforts will thus be aimed at overcoming the above mentioned limitations.

5.3 Microfluidic-cell array coupling

The main aim of this last section of the work, and object of ongoing studies, was the development of a culture system to be coupled with the well established and validated arrayed culture. The cell source has already been presented in Chapter 4, section 4.4, and was the human embryonic stem cells-derived (hESC) cardiomyocytes-enriched population.

In the attempt of exploiting all the advantages of the technologies that we developed so far, this system must comprise:

- polyacrylamide hydrogel substrates;
- controlled cell adhesion via micropatterned surface:
    - highthroughput data-quality via arrayed culture;
- perfused culture:
    - microfluidic platform,
    - controlled and selective delivery of fluids,
    - spatio-temporal pattern of stimulation;
- compatibility with standard analysis techniques.

The feasibility of the arrayed culture of hESC-derived cardiomyocytes onto protein patterned hydrogel surfaces has already been proven (Chapter 4). The crucial point was thus the development of an *ad hoc* system to interface this culture with a perfusion system.

Perfusion would be established using a microfluidic platform, for the previously discussed motivations such the feasibility of a strict control over both the transport regimes and the establishment of defined spatial or spatial-temporal concentration gradients.

It would thus be desirable to study a method for reversibly sealing the microfluidic platform to the supporting material (usually a glass slide), in order to allow for an easy access to the cultured cells and for a more flexible use of the platform itself. To satisfy all these requirements, a multilayered assembled device must be designed and fabricated.

First of all, to ensure reversible sealing we developed a membrane-vacuum system acting as a suction pad. In particular, with the previously described microfabrication techniques, a circular ring was fabricated and then molded with PDMS. Its dimensions were chosen with respect to the geometrical constraints given by the glass coverslip dimensions while its height was 150 μm. Figure 5.5 shows a schematization of the layers composing the bottom part of the platform, with particular attention to the just mentioned vacuum-mediated reversible sealing.

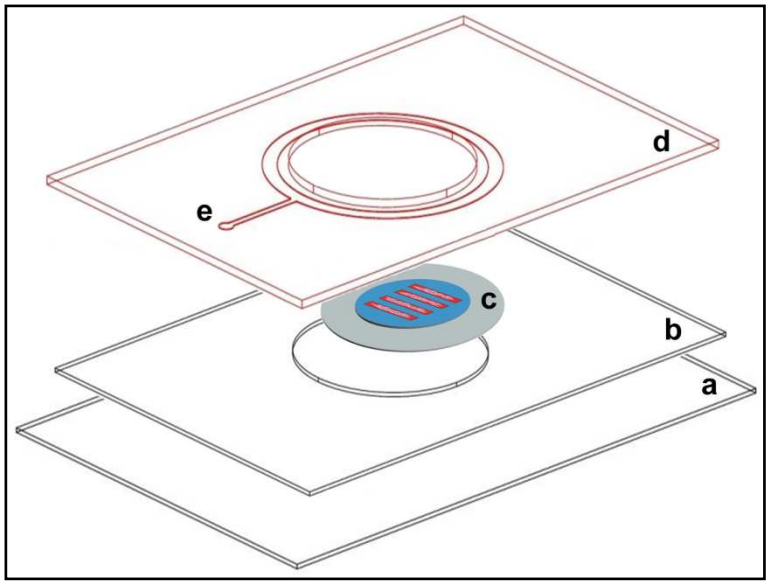

Figure 5.5. *Exploded view of the bottom part of the device with the vacuum system. A thin PDMS membrane (b) was laid over the supporting glass slide (a). The membrane had a circular hole shaped to fit the coverslip onto which the hydrogel is covalently bonded (c). Cells (parallel lanes) are adhering to the hydrogel surface. The final PDMS layer was constituted by the actual vacuum system (d), which was operated by punching a hole through the PDMS in e and inserting a microbore flexible tubing connected to the vacuum pump. The microfluidic platform (non shown in the figure), could be irreversibly sealed to the upper face of this layer.*

More in detail: cells were adhering with a spatially organized topology to the hydrogel substrates (as seen in Chapter 4), which were in turn covalently bonded to a 100 μm thick glass coverslip (c). In order to ensure mechanical stability of the assembled device, a supporting 1 mm glass slide was used beneath the coverslip (a). A thin PDMS membrane (b) laid over the glass slide contributed in avoiding possible movements of the glass coverslip. The final layer (d) was the actual vacuum layer, formed by a circular ring that, once connected to a vacuum line though the appropriate port (e) worked as a suction pad creating a stable but reversible sealing to the underlying layer.

5.3.1 Preliminary results

This system has been validated to ensure that no leaking occurred even at high fluid flow rates. In particular, no leaking nor failures in proper adhesion were detected below a 500 μL/min flow rate, which is more than ten-fold higher than the values commonly employed during microfluidics experiments.

Even thought the final design of the optimal microfluidic platform to be coupled to the arrayed cultures in order to perform selective delivery of factors is still under development phases, some prototypes have been produced and tested.

As an example, in a simple configuration we coupled a microfluidic platform formed by an array of parallel channels (“III” design seen in Chapter 3) to the hydrogel/vacuum system. The microfluidic platform has been irreversibly bonded at the top of the vacuum-layer membrane. The bottom layers were as in Figure 5.5.

Due to the dimensions of the hydrogel, only 4 out of the 5 microfluidic channels had access to the of the squared chamber where the cells culture would be located. With this configuration, to test the capability of the system to perform selective delivery or generate concentration gradients of factors, we flowed fluorescein solutions from one of the inlets. Figure 5.6 shows images of the assembled device.

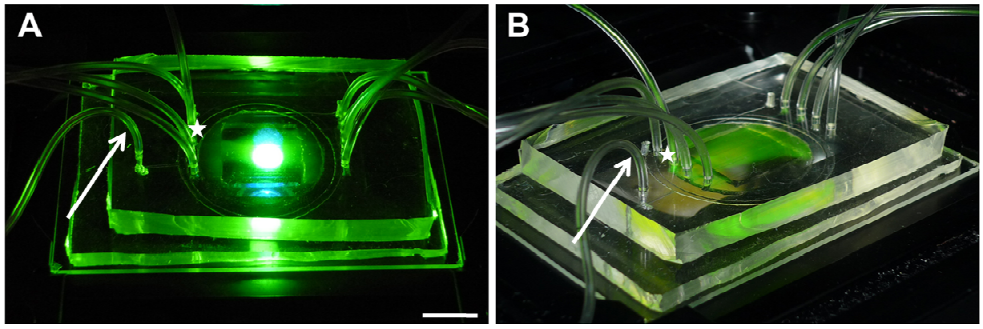

Figure 5.6. *Images of the assembled prototype under fluorescent light in A and in bright field in B. Arrows identify the tubing connected to the vacuum layer and external vacuum line. Asterisk identify the inlet from which the fluorescein solution was injected. Scale bar 10 mm.*

The tubing highlighted by the arrow was connected to the vacuum layer and to the external vacuum system ensuring proper sealing between the two main platform levels. The others, similarly inserted through the PDMS, delivered the fluids to the culture chamber.

The platform was perfectly compatible with microscope imaging, and the experiments were performed assembling the system directly on the microscope stage. The fluorescein distribution within the chamber was thus visualized on line in real time and pictures were taken at defined time points. Fluorescein solution was injected from one of the inlets (see asterisk in Figure 5.6) and the evaluated fluorescence intensity allowed to visualize the concentration profiles developed within the chamber applying different flow rates (Figure5.7).

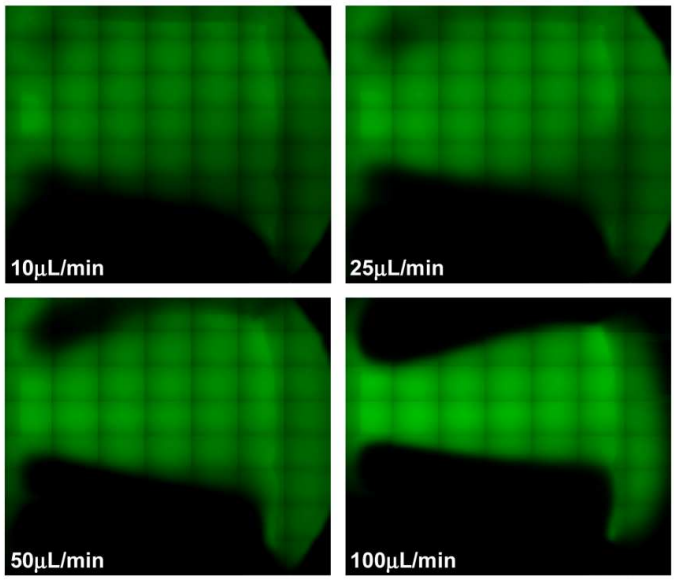

Figure 5.7. *Results of the preliminary experiment performed flowing fluorescein solutions at different flow rates ranging from 10 to 100 µL/min.*

The images shown in Figure 5.7 were obtained by a merging of individual pictures, reconstructing almost the entire chamber.

It was evident how at higher flow rates the concentration profiles were more sharp and well defined if compared with those obtained at lower flow rates. The applied flow rates were relatively high, but if we consider the elevate diffusion coefficient of fluorescein ($D \sim 1 \cdot 10^{-10}$ m^2/s), to obtain similar concentration profiles using different molecules with higher molecular weight, would require lower flow rates.

Those preliminary results are extremely promising in sight of the following applications of the system and its interface with the biological system of interest.

For example, it would be possible to selectively treat neighboring areas of the human-derived cardiomyocytes dots array with different drugs or to simultaneously evaluate the effects of a range of concentrations of a defined substance.

This would prove extremely useful for pharmacological and toxicological studies, as already described.

5.4 References

A. Tourovskaia, X. Figueroa-Masot and A. Folch, Long-term microfluidic cultures of myotube microarrays for high-throughput focal stimulation. *Nature Protocols*, 2006, **1**, 1092-1104.

D. DiCarlo, L. Y. Wu and L. P. Lee, Dynamic single cell culture array. *Lab on a Chip*, 2006, **6**, 1445–1449.

L. Kim, M. D. Vahey, H.-Y. Lee and J. Voldman, Microfluidic arrays for logarithmically perfused embryonic stem cell culture. *Lab on a Chip*, 2005, **6**, 394-406.

M. S. Kim, J. H. Yeon and J. K. Park, A microfluidic platform for 3-dimensional cell culture and cell-based assays. *Biomedical Microdevices*, 2007, **9**, 25-34.

E. Cimetta, S. Pizzato, S. Bollini, E. Serena, P. DeCoppi and N. Elvassore, Production of arrays of cardiac and skeletal muscle myofibers by micropatterning techniques on a soft substrate. *Biomedical Microdevices*, 2008, Epub ahead of print.

Chapter 6
Conclusions

The strong need for improving the processes of drug and therapy development has pushed the scientific community towards the search for innovative and advanced technologies. Standard methodologies are limited in several ways as they tend to lack of highthroughput characteristic, are poorly controllable and force cell cultures within environments that are way distant from the natural *niche* in which they reside *in vivo*.

For these reasons, engineering tools coupled with biotechnological and medical skills, hold the potentialities to propose alternative and relevant solutions to these issues.

We have thus been focused on the design and development of innovative microscale technologies for stem cell cultures to be used as tools in biological screenings. The importance of using living cells as sensing element has been discussed, thus the importance of realizing devices capable of effectively being coupled with human stem cells assumes an even increased value. We have been guided by the so-called “biomimetic approach”, a principle directing the efforts towards a better understanding of the natural environment encountered by cells *in vivo* and its recapitulating within *in vitro* cultures. In this sight, we engineered biological principles and techniques so to artificially recreate both the soluble and structural microenvironment constituting the cell *niche*. We approached these issues at the microscale, so to be on a more relevant biological-level and simultaneously meet the requirements of highthroughput screenings.

To this aim, we performed an extensive phenomenological study based on a mathematical approach, aimed at understanding and thus controlling the main phenomena occurring at the microscale within both conventional and innovative cultures (Chapter 2). We reported our main achievements in terms of control of the mechanical properties of the substrates, the topological control over cell cultures via microscale techniques and the use of microfluidic platforms for the delivery of factors mimicking the soluble microenvironment (Chapter 3 and 4). The final efforts have been directed towards the coupling between the above

described technologies within an integrated platform exploiting all their intrinsic advantages (Chapter 5).

We identified the main factors dictating the behavior of the systems in terms of dominating phenomena and gave practical rules for correctly performing an accurate control over transport phenomena for a broad range of conditions, both geometrical and operative.

We achieved an extremely accurate control over the topology of adhesion and growth of cells using micropatterning techniques and we engineered the substrates so to meet the requirements for the recreation of an *in vivo*-like mechanical microenvironment.

Microfluidic techniques were used to design and realize platforms capable of recreating the soluble microenvironment over cell cultures, both in the form of “simple” provision of the required factors or the recreation of more complex concentrations gradients. Particular attention has always been paid at the length and time scales, together with the respect of the physiological thresholds imposed by the use of living cells as sensing element. The final efforts were spent to accomplish the task of developing an integrated technological platform enclosing all the achieved results and innovations. We proposed two solutions, the most promising of which is currently object of ongoing studies.

The important results that have been obtained on a technology-perspective have been strengthen also on the biological side: in our experimentations, representative cell lines were used for the preliminary studies, while the final validations were performed on extremely relevant systems such as human primary myoblasts derived from diseased patients (Duchenne Muscular Dystrophy) and human-derived cardiomyocytes, or on fundamental studies such as of Wnt signaling pathway.

Taken together, these results exemplify the possible active role of chemical engineering skills on the design, development and realization of new tools and novel technologies to support biological and biomedical research.

Appendix A

Micro-bioreactor arrays for controlling cellular environments: Design principles for human embryonic stem cell applications

Elisa Cimetta[a], Elisa Figallo[a], Christopher Cannizzaro[b], Nicola Elvassore[a,*] Gordana Vunjak-Novakovic[c,*]

[a] Department of Chemical Engineering, University of Padova, Padova, Italy

[b] Department of Biomedical Engineering, Tufts University, Medford, MA, USA

[c] Department of Biomedical Engineering, Columbia University, 622 West 168th Street, VC12-234, New York, NY 10032, USA

[*] Corresponding authors

Methods 47 (2009) 81–89

Keywords: Bioreactor; Human embryonic stem cells; Hydrogel; Microfluidics; Steady-state; Dynamic conditions; Time scale; Transport phenomena

Abstract

We discuss the utilization of microbioreactor arrays for controlling cellular environments in studies of factors that regulate the differentiation of human embryonic stem cells. To this end, we have designed a simple and practical system that couples a microfluidic platform with an array of micro-bioreactors, and has the size of a microscope slide [1] [E. Figallo, C. Cannizzaro, S. Gerecht, J.A. Burdick, R. Langer, N. Elvassore, G. Vunjak-Novakovic, Lab Chip 7 (2007) 710–719]. The system allows quantitative studies of cells cultured in monolayers or encapsulated in three-dimensional hydrogels. We review the operating requirements for studies of human embryonic stem cells (hESCs) under steady-state and dynamic conditions, and the related control of the mass transport and hydrodynamic shear. We describe the design and fabrication of the individual bioreactor components, and the criteria for selecting the bioreactor configuration and operating parameters, based on the analysis of the characteristic times and scales of reaction, convection and diffusion. To illustrate the utility of the bioreactor, we present a “case study” of hESC cultivation with detailed experimental methods and representative biological readouts.

A.1 Introduction

Novel cell culture technologies developed in recent years mimic the *in vivo* cellular microenvironments with an increasing fidelity [2], through improved control and the provision of cascades of multiple regulatory factors. Miniaturization of the culture systems is an important step towards accurate control of the cultured cells and tissues. Some of the most interesting outcomes come from the optimization and accurate use of microfluidic platforms [3, 4]. Small transport distances are key for enabling fast responses to environmental stimuli in studies involving spatial and temporal gradients of factors. Since its first appearance decades ago, microfluidics have been adapted to many different applications; several excellent reviews give insights into the operating principles for system configurations of interest [5-8]. Microscale technologies were designed for applications ranging from studies at a single cell level [9] to the recreation of more complex 3D tissues [10] and the development of diagnostics platforms [11, 12]. High-tech platforms involving integrated microdevices such as micro-valves, injectors, pumps or mixers [13] are also being considered for use in live cell experimentation.

Our laboratory has been interested in developing a micro-bioreactor array that would allow high throughput studies of the most challenging cell source: human embryonic stem cells (hESCs). To this end, we have designed an efficient, multiplexed device that couples a microfluidic platform with an array of micro-bioreactors and allows quantitative studies of hESCs in two-dimensional (2D) and three-dimensional (3D) settings [1]. This system enables quantitative measurement of performance and accurate control over the culture microenvironment with a relative simplicity, not requiring additional integrated devices such as micro- valves, pumps or mixers. In this paper, we first summarize the design requirements for systems of this kind. We review the operating requirements for studies of cultured cells under steady-state and dynamic conditions, and the related control of the mass transport and hydrodynamic shear. The design and fabrication of the individual bioreactor components and the system assembly are described in detail. Then we describe the design specifications for important operating parameters and the principles for their optimization at the microscale level that are based on the analysis of transport rates and characteristic times of the involved phenomena. Finally, we present a "case study" of hESC cultivation, with detailed experimental methods and representative biological readouts.

A.2 Overall Requirements

A.2.1 Biomimetics

Our body is composed of highly organized tissues formed by multiple cell types and sustained through complex structure-function relationships at many hierarchical levels. Short and long range communication between single cells and/or tissues occurs through an enormous cascade of signaling pathways, most of which involve mechanisms, intermediate steps and connections that are not fully understood. Ideally, biological studies should be performed under conditions that are controllable and at the same time capture the complexity of the native environment.

A.2.2 Scale

When it comes to scaling down to the biologically relevant lengths and time scales, the conventional methodologies of the so-called "flat biology" fail. Standard culture methods involving cell culture in Petri dishes cannot be representative of the real state of physiologic systems and therefore often result in unrealistic and uncontrollable biological readouts. The

relatively large volume of medium in contact with cells and the batch-wise operation associated with the periodic medium exchange does not allow for the generation and control of precise patterns of stimulation such as spatio-temporal gradients. Petri dishes are therefore not suitable for use in studies of either steady-state or dynamic system The batch processes have unpredictable timescales, are diffusion-limited and, most important, are intrinsically uncontrollable. Macroscale observations of averaged cell/tissue properties cannot be reliable in defining complex biological systems and must thus be replaced by more precise and realistic microscale observations. In this respect, the microscale culture technologies help overcome most of the above limitations, and to operate at the characteristic time and length scales of biological phenomena.

A.2.3 Time constants

At the microscale - inside the microchannels and culture chambers - the dominating forces change and differ from the most known, macroscale ones. Flow is always laminar (Reynolds numbers are well below the turbulence threshold, and in most cases Re<100) the inertial forces are therefore dominated by viscous forces, and the transport is dominated by molecular diffusion or by convective regime of well-defined hydrodynamic profile. Reducing the characteristic dimensions to a microscale level allows a more rigorous control of the operating parameters involved, due to the very short transport distances, which are in turn associated with very short time constants. As a result, biological responses are not limited anymore by the slow kinetics of physical phenomena.

A.2.4 Multi-parametric analysis

The miniaturization of the system also results in the reduction of the amounts of cells, culture media and supplements and thereby helps reduce the cost and time involved in cell culture, and enables the high throughput quality of the data. The possibility to control multiple factors, molecular and physical, allows multi-parametric analyses, thus again reducing both time and cost of experimentation.

A.2.5 Imaging compatibility

Most micro-bioreactors are optically transparent and fully compatible with conventional imaging techniques. They allow online analyses and real time experimentation such as time-lapse monitoring the state of the system and the time-course of specific phenomena.

A.3 Specific Requirements

A.3.1 Steady state conditions

Perfused systems offers the advantage of working under well-defined and stable steady-state conditions. Standard culture systems, such as Petri dishes, can be compared to batch reactors in which conditions are precisely defined only at time zero, and then continuously vary until next medium exchange. Working at steady-state conditions maintains, by definition, the parameters of interest at their constant levels. Precise perturbations of the system may then be introduced to investigate the dynamic biological responses of the cells.

A.3.2 Fast transients in space and time

It is often necessary to accurately modulate transients in space and time to recreate precise stimulation patterns in the form of concentration gradients, and deliver particular signals. Working with small volumes (order of a few μL) generally leads to fast-response systems. This means that the switch between defined sets of conditions can be fast and still controllable. For example, operating parameters can be changed by a simple variation of the medium flow rate. At the microscale, one can design the system to provide tightly controlled, orderly conditions of flow and mass transport.

A.3.3 Control of mass transport and flow shear

Due to the well-defined geometry, short transport distances, and fast transients, transport phenomena occurring in microdevices can be more easily subjected to theoretical analysis and precise control than those in larger scale systems. Accurate predictions of the velocity gradients and shear stresses are indeed very important because of the profound effects of

flow environment on biological systems. Again, the versatility of microscaled systems, allows decoupling the effects of mass transport phenomena such as the generation of specific concentration patterns from physical phenomena such as the application of mechanical forces.

A.4 Technical description of the micro-bioreactor platform

This section contains the description of the main components of the micro-bioreactor array culture system: the cell culture chamber, the microfluidic platform, the gas-exchange unit, the tubing and connections, and the flow circulation system. The described elements can be visualized in Figure 1, keeping in mind that their application can be extended to different configurations. Briefly, panel A shows a top view of the micro-bioreactor array assembly with its functional units, which will be treated more in detail in the following paragraphs. Panel B presents an image of the culture system set up in the incubator, while the lateral views in panel C clarify the layered structure of the micro-bioreactor array exemplifying the two configurations used.

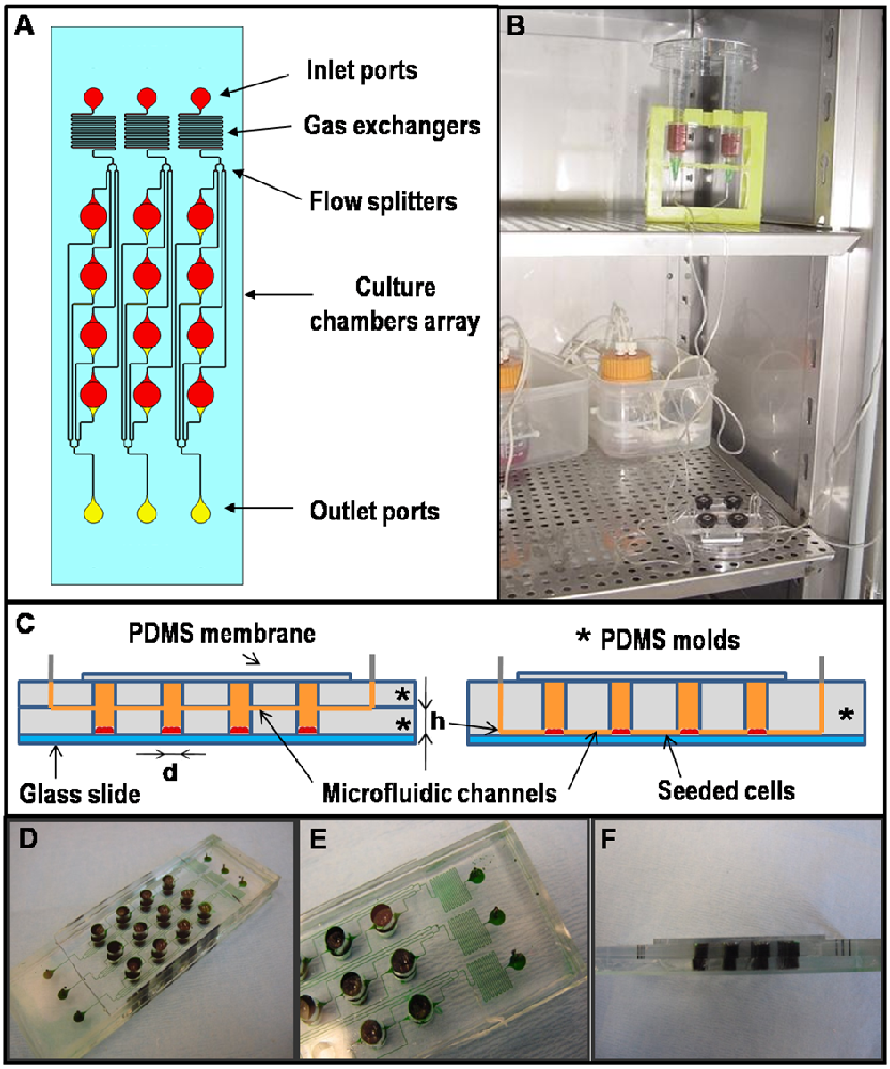

Figure 1. *Micro-bioreactor array. Panel A shows the top view of the micro-bioreactor array assembly with its functional units: the separate inlet ports for each chamber, the serpentine-shaped channels of the gas exchanger, the splitter dividing the flow into 4 equal parts, the array of culture chambers, and the outlet ports. The 12 independent culture chambers (diameter d = 3.5 mm) are arranged in a 4x3 array (8 mm vertical and 7 mm horizontal center-to-center spacing); the microfluidic channels (100 μm wide by 100 μm high) are printed in a PDMS mold attached via plasma treatment to a glass slide or to a punched PDMS slab of thickness h. The inlets, outlets and culture chambers are all punched though the PDMS. Panel B shows the culture system set up, with connections and tubings, inside the incubator. The lateral views in panel C clarify the layered structure of the micro-bioreactor array in the two configurations used. The glass slide supports the cells culture and allows the irreversible sealing of PDMS via an air-plasma surface treatment while the open culture chambers are reversibly sealed by the PDMS membrane on top of them. In the first presented configuration (left), the microfluidic channels are positioned at the height of h = 4 mm above the glass substrate. In another configuration (right), the microfluidic channels are positioned at the level of the glass substrate where the cells are cultured (h = 0). Both configurations support cell culture in 2D setting, and the first also supports the culture of hydrogel-encapsulated cells in a 3D setting. A contrast dye is used in images D-F to show the fluid paths in both axonometric and lateral views.*

A.4.1 Culture chamber – 2D and 3D settings

The cell culture chambers were designed to provide (i) culture of a statistically significant number of cells for biological assays, (ii) easy and rapid access to the chamber for application of standard protocols (i.e. coating, fixing, staining), (iii) the maintenance of versatility in choosing proper characteristic dimensions (chamber height and diameter), and (iv) high throughput characteristics of the system (e.g., a 96-well plate or 384 well plate format), and (v) easy adaptation to 2D and 3D culture configurations.

The chambers must also ensure rapid establishment of the desired medium composition in the surroundings of the cultured cells. The chamber is shaped as a cylindrical well with a 3 mm diameter, with PDMS walls and a glass bottom, by coring the PDMS layer using a stainless steel biopsy punch. The height of the chamber depends on the chosen configuration (2D or 3D), and in either case is determined by the height of the PDMS slab. Fitting the device to a standard microscope slide, an array of 4x3 culture chambers is formed. The open wells are reversibly sealed on the top by using a thin, gas permeable PDMS membrane that is fixed with four thumbscrews within a polycarbonate-aluminum frame. The membrane isolates the cells and medium from the external environment while allowing for gas exchange. The 96-well configuration further enables easy interface of the bioreactor slide with robotic system for fluid manipulation and fast analysis and readout.

A.4.2 Microfluidic platform

The microfluidic platform was designed to flow the culture medium and any supplements in and out the culture chambers. Consideration was given to the time and length scales of diffusion and convective transport inside the microfluidic channels and cell culture chambers. Responding to the need for uniform hydrodynamic conditions inside the culture chambers and over the cultured cells, the fluid flow rates and the geometry of the microfluidic channels need to be accurately determined. Computational modeling of the steady-state momentum balance and time-dependent mass transfer balance within the micro-bioreactors and the channels, provided the quantitative basis for system design. The modeling had crucial role in analyzing the mass transport and in defining the relative contributions of convection and diffusion as a function of the medium flow rate.

The microfluidic platform was fabricated by standard soft lithography. In most cases the channel cross section is 100 µm x 100 µm. These dimensions and aspect ratio (height versus width) enabled the formation of structurally stable channels with great precision. As can be seen in Figure 1, the platform is composed of three independent inlets that deliver the culture medium to a 4x3 array of chambers; consequently, each entering stream must be connected to a set of four chambers. A flow splitter was thus designed to ensure that each well received the same amount of medium with the same flow rate. Each fluid stream traveled the same path-length from the inlet to the outlet of the microfluidic platform, thereby providing equal flow resistance in each of the three channels. The inlets and outlet ports were cored from the PDMS slab using stainless steel biopsy punches.

A.4.3 Gas exchange

The gas exchange unit ensures the maintenance of the correct, physiological levels of gases inside the culture chambers: carbon dioxide to regulate the pH of the culture medium, and oxygen to ensure the correct metabolic activity of cells. The gas exchange depends on the permeability coefficient of each gas through the top membrane, geometry of the system, temperature, composition of the gas atmosphere and the flow rate which determines the residence time of the fluids in the channels.

The only gas-permeable material used is PDMS; the system is maintained at a temperature of 37 °C, 95% humidity and 5% carbon dioxide partial pressure; the cross section of the channels is 100 µm x 100 µm and the height of the PDMS platform is set at 3 mm. The fresh culture media, injected at the inlet of the system, must be perfectly equilibrated at the physiological values before entering the culture chambers, thus the shape and dimensions of the gas exchanger are designed based on the assumption of gas equilibrium. From the performed calculation, using coefficient values from the literature, the length of 20 mm was determined to be sufficient. We chose a serpentine-like shape of the gas exchanger channels to maintain the arrayed configuration of the platform.

A.4.4 Other components

The PDMS layer with the microfluidic channels, the gas exchanger, the punched ports and culture chambers is irreversibly bonded to the glass slide by air-plasma surface treatment.

The assembled unit is connected to the pump by Tygon tubing. A syringe pump is used to control the medium flow rate at a steady level and with extreme accuracy; in particular, the pump served the purpose to control a motor fluid (water) that would transmit the motion to the culture media through a flow transducer. The complete set up, shown in Figure 2, has two advantages: (1) the culture medium could be maintained at a low temperature to prevent denaturation of delicate components such as growth factors, and (2) the syringes containing the culture media are protected from contamination or contact with external components. The assembled micro-bioreactor and the connecting tubing are placed inside an incubator (37°C, 95% humidity, 5% carbon dioxide), the discarded culture medium is collected in reservoirs that are placed 20 cm above the platform plane and connected to the chamber outlets.

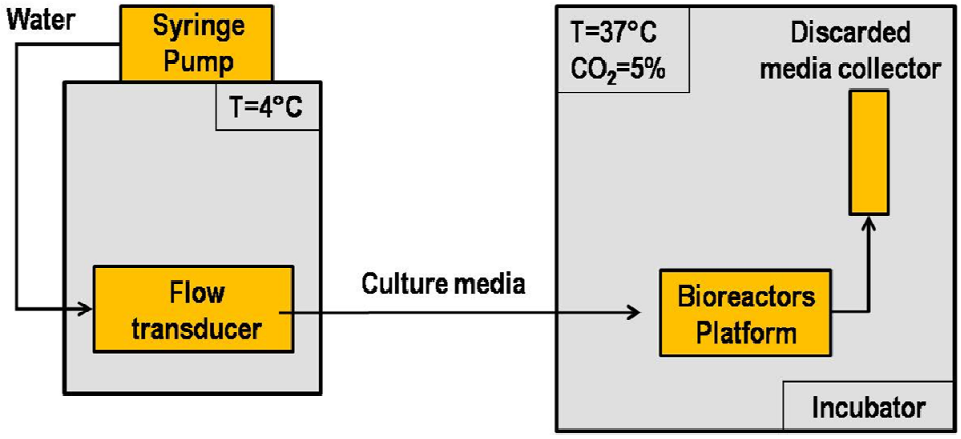

Figure 2. *The micro-bioreactor platform. A syringe pump transmits the motion of the motor-fluid (water) to the culture medium, without direct contact between the two fluids. The culture medium is kept at controlled temperature (4 °C) to prevent the degradation of medium components such as growth factors, and pumped into the inlet ports of the bioreactor residing inside incubator (37 °C, CO_2 5%); the waste medium from the outlet ports is collected in a container.*

It is worth describing in more detail the 2D and 3D configurations that our platform allows. The 2D setting allows for two different configurations; in the first configuration, the cell layer is at the same level as the microfluidic channels, directly adhering to the glass slide; in the second configuration, an additional PDMS layer with the punched chamber-wells is used to set the distance between the cell culture-level (still adhering to the glass slide) and the microfluidic channels, adhering to the PDMS layer. For the 3D culture setting, the second configuration is used and the cells are encapsulated in a volume of hydrogel (e.g., photopolymerized hyaluronate). The assembled micro-bioreactor platform is entirely optically transparent and can be easily interfaced with microscopes for real-time observation and experimentation.

A.5 Operational Parameters

The operational parameters affecting the pool of variables in the cell micro-environment can be divided into two categories: the initial parameters that are normally set before the experiment (such as the characteristic dimensions of the culture chamber, the cell seeding density, the medium composition), and operative parameters that can be controlled during the experiment (such as the medium flow rate). In this section, we discuss the principles guiding the selection of the optimal variables and their values through the analysis of characteristic times of fundamental phenomena such as cellular uptake and release, and diffusional and convective mass transport rates.

The configuration of the culture chamber is mainly determined by the chamber diameter and height. The selection of the chamber diameter is mainly dependent upon the minimum number of cells required for obtaining biological data on a relevant population size. Typical number of 10^3 cells per square millimetre is required to apply most biological assays. The height of the cell culture chamber has great influence on the cell micro-environment; large chamber heights reduce the average velocity for a given flow rate and decrease the rates of mass transport. Also, a deep chamber acts as a reservoir for exogenous factors and causes dilution of endogenous factors, at the rates that depend on the kinetics of cellular processes and the number of cells per unit volume.

The ratio of the time scales of uptake at the bottom of the culture chamber (by cultured cells) τ_{UP}, to species diffusion from the medium, τ_D, can be estimated. For example, assuming a maximum uptake reaction rate expressed by a mass action law for a ligand-receptor association kinetics [14], the above mentioned time scale ratio can be expressed by:

$$\frac{\tau_{UP}}{\tau_D} = \frac{D}{h\rho_C k_{on}[R]} \qquad 1.$$

where D is the diffusion coefficient of the chemical species, h is the height of the culture chamber, k_{on} is the ligand-receptor association rate constant, $[R]$ is the number of receptors on cell surface and ρ_C is the surface cell density. The values for all parameters used are listed in Table 1.

Table 1. *Parameters used. The table reports a list of the parameters and variables used for the performed calculations with their values and ranges. When applicable, references are reported in the last column.*

Variable	Values	Units	Reference
D_{02}	3.30E−09	m^2/s	[1]
D_{Alb}	7.00E-11	m^2/s	[1]
h	$0 < h < 0.004$	m	[1]
ρ_c	$1.0E+7 < \rho_c < 4.0E+10$	cells/m^2	This study
k_{on}	1.00E + 07	I/Ms	[14]
$[R]$	1000	Molecules/cell	[14]
μ	0.0007	Pas	[1]
d	0.004	m	[1]
Q	$0 < Q < 2.3E-10$	m^3/s	This study

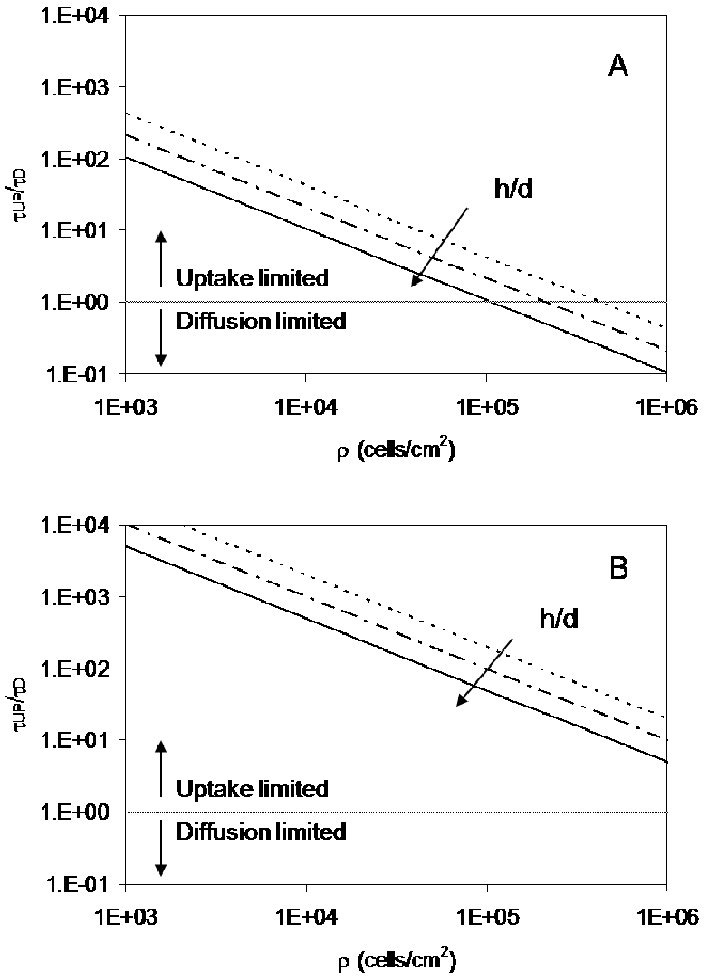

Figure 3. *Diffusion and reaction time constants as a function of cell density and culture chamber geometry. The ratio of characteristic times of the uptake reactions and molecular diffusion, τ_{UP}/τ_D, is shown as a function of the cell density, for three values of the culture chamber height (see Fig. 1): h = 1, 2 and 4 mm; d = 4 mm. Panel A shows data for a small metabolite, such as oxygen while panel B shows data for albumin representative of large growth factors. The values for all the parameters used are listed in Table 1.*

Figure 3 shows the calculated ratio of the time constants at the bottom of the culture chamber between the reaction, τ_{UP}, and diffusion, τ_D, as a function of cell seeding density. The ratio is shown for two representative molecules: oxygen (the most important upon small molecules, panel A) and albumin (a protein representative of larger growth factors, panel B). At low cell densities, the characteristic time scale for reaction is longer than that for diffusion. Therefore, mass transport at low cell densities is dominated by uptake reaction rates. As cell density increases up to its maximum value (i.e. at confluence), the time constant for diffusion becomes comparable with that for reaction. It is interesting to note that the height of the culture chamber only slightly influences the ratio of the two time constants. This semi-quantitative analysis suggests that for higher cell seeding densities, medium perfusion is required to enhance mass transport rates and establish a kinetic-limited operating regime.

In this context, the most important variable that can be precisely controlled is the medium flow rate; selecting the syringes volume, the tubings cross section and using accurate syringe pumps, it is possible to provide precise volumetric flow rates down to 10 nL/min. The flow rate affects the local cellular micro-environment both by inducing the shear stresses and by altering the mass transport rates.

Shear stress results from the tangential forces applied to cell surfaces, and can be mathematically represented by the Newton's law of viscosity. The shear stress depends on the velocity gradient at the surface and for constant flow rate it linearly depends on the height of the culture chamber. The values of shear stress can quickly be estimated assuming that the flow profile in the middle of the culture chamber would be well-approximated by a parallel Poiseuille flow. The maximum amount of shear that can be tolerated by the cells will depend on the cell type since certain cells (e.g., mesenchymal and endothelial) require shear stress to differentiate and develop properly while other cells are affected by shear stress without the change in their phenotype [15]. Most cells tolerate shear stress, $\bar{\tau}_{shear}$ up to 1 dyne/cm, which are generated in the culture chamber and are calculated assuming parabolic flow between parallel plate:

$$\bar{\tau}_{shear} = \frac{6\mu Q}{dh^2} \qquad 2.$$

where μ is the medium viscosity, Q is the flow rate, h and d are the height and the diameter of the chamber, respectively. Again, the values for all parameters used are listed in Table 1.

The analysis of the influence of the medium flow rate on mass transport is carried as follows. The ratio of the time scales of diffusion in the culture chamber, τ_D, to convection, τ_C (residence time of the medium in the culture chamber), can be defined as:

— —— 3.

where D is the diffusion coefficient of the chemical species, h is the height of the culture chamber, Q is the medium flow rate and d is the culture chamber diameter.

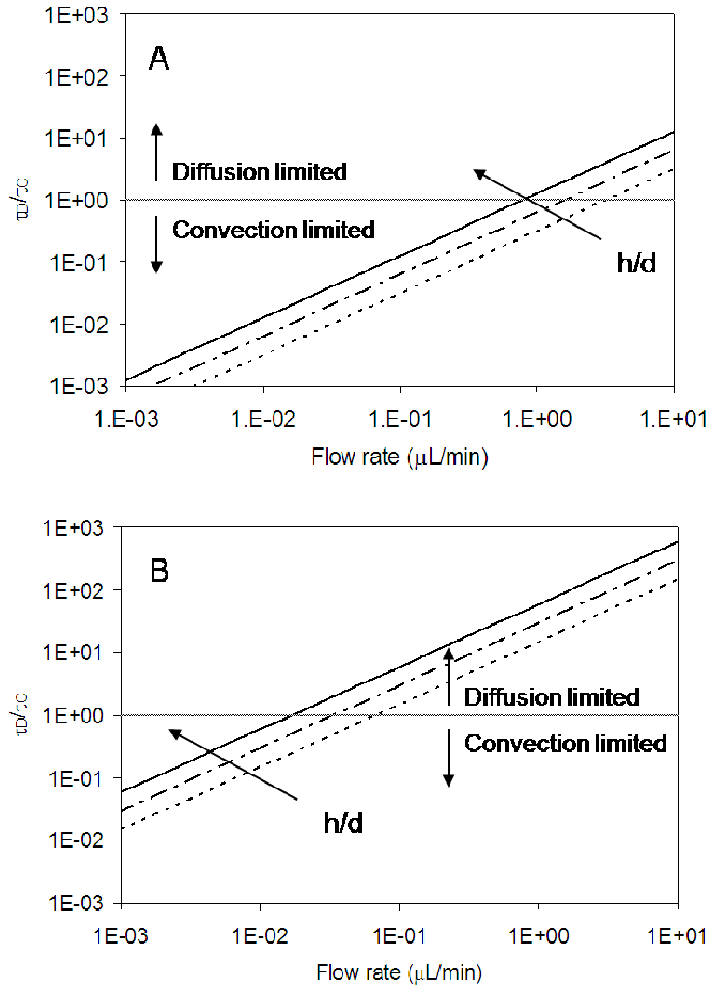

Figure 4. *Diffusion and convection time constants as a function of medium flow rate and culture chamber geometry. The ratio of characteristic times of molecular diffusion and convection, τ_D/τ_C, is shown as a function of medium flow rate, for three values of the culture chamber height. All parameter values are as specified in Fig. 3. Panel A shows data for a small metabolite, such as oxygen while panel B shows data for albumin representative of large growth factors. The values for all the parameters used are listed in Table 1.*

Figure 4 shows the ratio of the time scales of diffusion to convection as a function of medium flow rate, for different heights of the culture chamber. In the presented logarithmic graphs, values greater than 1 represent culture conditions that are reaction controlled, whereas <1 values correspond to the convection-limited regimes, and values of ~1 indicate the competition between the two rates. From these graphs we can conclude that for small metabolites with high diffusion rates in the 4 mm diameter culture chamber, flow rates >1 μL/min are necessary to cross from a diffusion- to a convection-controlled regime. In addition, it is possible to adjust the mass transport phenomena at a given flow rate by changing the height of the culture chamber. The chamber geometry thus provides an additional degree of freedom for setting the proper culture conditions (Table 2).

Table 2. *Parameters involved and their main targets. The main geometrical and operative parameters are summarized in the table, listing also the corresponding symbols and the main targets of their variations.*

Parameter	Symbol	Description	Phenomena
Design	L_g	Channel length	Gas-liquid mass transfer
	h	Chamber height	Cell-liquid mass transfer
	d	Chamber diameter	Total number of cells
	$h \times d$	Chamber cross section	Velocity field; Mass transport
Operation	ρ_c	Seeding density	Total uptake and release rates
	Q	Total flow rate	Velocity field; Shear stress; Mass transfer

Figure 5 shows the distance *z* from the bottom of the culture chamber at which the diffusion and convection time scale are comparable as a function of the flow rate. Introducing the above mentioned variable z, and traducing the flow rate Q in terms of the linear velocity v_z, the following equation for the ratio of τ_D and τ_C was obtained.

$$\frac{\tau_D}{\tau_C} = \frac{(h-z)^2}{D}\frac{v_z}{d} \qquad 4.$$

Assuming that the flow profile would be well-approximated by parallel-plate Poiseuille flow, v_z can be expressed as:

$$v_z = 1.5\langle v\rangle\left(1-\left(\frac{z}{h}\right)^2\right) \qquad 5.$$

where $<v>$ is the mean channel velocity.

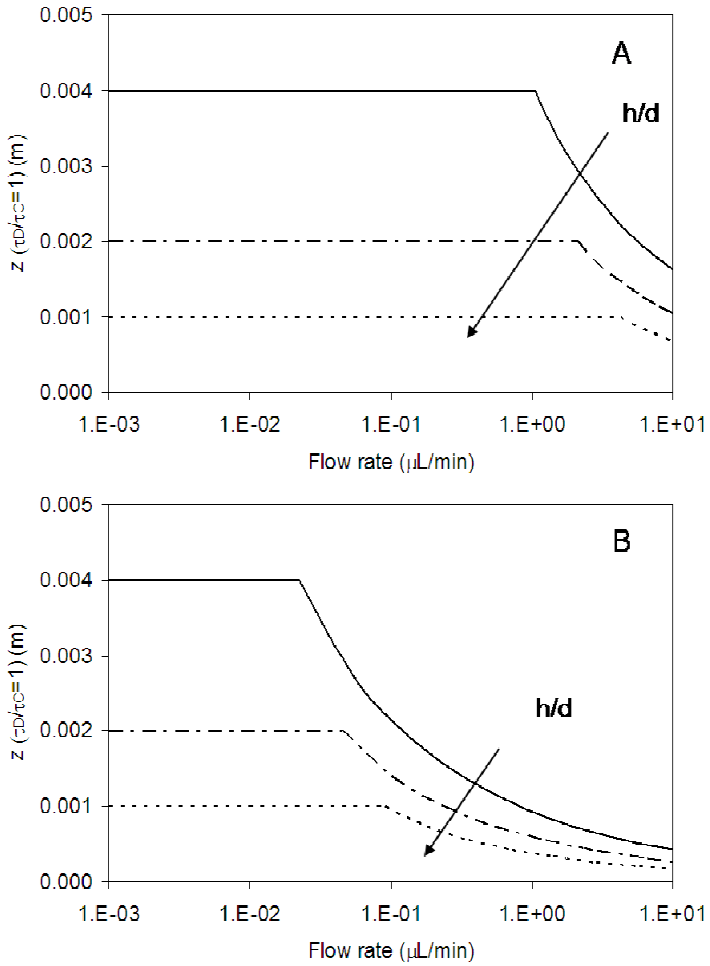

Figure 5. *Characteristic length scale as a function of medium flow rate and culture chamber geometry. The distance from the bottom of the culture chamber at which the ratio of the diffusion and convection time constants is equal to one is shown as a function of the flow rate and culture chamber geometry h = 1, 2 and 4 mm; d = 4 mm. Panel A shows data for a small metabolite, such as oxygen while panel B shows data for albumin representative of large growth factors.*

The data in Figure 5 were obtained by simultaneously solving equations 4 and 5 for $\tau_D/\tau_C = 1$. At low flow rates, the values of *z* correspond to the height of the culture chamber, indicating that diffusion dominates at all levels. By increasing the flow rate, *z* decreases and takes values between the top and bottom of the chamber. In turn, increasing the height of the culture chamber decreases the transport rates at the cell culture surface and thereby decreases the wash-out of endogenous factors. This latter aspect can be relevant to cultures of stem cells, where the preservation and recreation of the natural diffusion-limited cell niche is of fundamental importance.

The above discussion is generally applicable to steady state conditions. Microfluidic bioreactors can also be used in principles to modulate and control transients in environmental conditions to mimic some of the processes to which the cells are exposed *in vivo*. However, it is rather difficult to replicate short and fast episodes of biochemical stimulation. In principle, the residence times of culture media in the microfluidic channels and inside the culture chamber should be shorter than the characteristic times for the phenomena involved in step-wise biochemical stimulation.

A.6 Case study: culture of human embryonic stem cells in a micro-bioreactor at steady-state conditions

This section describes the design and detailed protocols for hESC culture in a micro-bioreactor array. Two different bioreactor configurations have been chosen for this case study, to assess the influence of cell density and mass transport regime on stem cell differentiation [1].

A.6.1 Microfluidic platform

Design criteria for hESC culture. Human embryonic stem cells (hESC) can give rise to any of the cell types in the human body. However, the pluripotency and plasticity of hESC are the reason why these cells are difficult to control in culture. It has been shown that poorly defined combinations of factors in serum and even the differences between different serum lots could be a source of variability and difficulties in reproducing hESC culture outcomes. These problems can be partially overcome by the use of serum-free media and well-defined biochemical stimuli to direct proliferation or induce differentiation [16]. However, defined medium compositions are not sufficient, because they only provide the consistency of average conditions in the culture system, whereas the conditions in the cellular environment are further mediated by the spatio-temporal gradients. The spatial organization of hESC, the local cell density and hESC clustering, the uptake of exogenous factors and release of endogenous factors are all involved in creating the hESC micro-environment that strongly influences cell fate. Recently, a niche-dependent effect on hESC colonies has been

demonstrated, proving that cell density and the agonistic/antagonistic local effects of endogenous/exogenous factors play important roles in determining cell differentiation [17].

Bioreactors can be used for modulating and controlling the hESC niche by controlling the thickness of the diffusional layer (Figure 5) and consequently, the transport and the accumulation of endogenous and exogenous factors. Bioreactors can be continuously perfused with fresh medium, to culture hESC at steady-state conditions without the periodic and dramatic environmental changes associated with the conventional batch-wise culture in Petri dishes. The experimental setup discussed below allows the application of precise hESC cultivation protocols with tight control of mass transport at the cellular level. By medium perfusion at small operating volumes, the system enables rapid establishment of steady-state conditions, at either low shear (diffusion-limited transport) or high shear (convection-limited transport).

A.6.2 Micro-bioreactor assembly

The micro-bioreactor, reported in Figure 1, consists of (1) a microfluidic PDMS platform with culture chambers, (2) an additional PDMS slab with punched holes for an optional increase in the height of the culture chambers, (3) a smooth PDMS membrane, (4) a supporting glass slide, (5) a polycarbonate-aluminum frame with four thumbscrews, (6) a set of Tygon tubing and stainless steel tubing for the connections, (7) a set of plastic syringes, (8) a syringe-based flow transducer, and (9) a syringe pump.

The microfluidic platform is used in conjunction with two micro-bioreactor configurations, with different geometries and transport regimes. In the first configuration, the microfluidic platform is positioned at the height ($z = 0$) of the cell monolayer at the bottom of punched culture chamber:

- z = 0: supporting glass slide with PDMS layer (h = 4 mm) with the microfluidic platform and the punched culture chambers;
- z = 4 mm; PDMS membrane sealing the tops of culture chambers.

In the second configuration, the microfluidic platform is positioned 4 mm above the cultured cells:

- z = 0: supporting glass slide with culture chambers in the h = 4 mm high PDMS slab;

- z = 4 mm: PDMS layer with the microfluidic platform and punched holes aligned with the culture chambers;
- z = 6 mm: PDMS membrane sealing the tops of culture chambers.

For each micro-bioreactor configuration, all layers except for the PDMS top sealing membrane are first irreversibly bonded by plasma treatment, and the functionality of the bioreactor is then verified. The microfluidic platform is tested to exclude the presence of clogging in the channels and/or failures in the hydraulic sealing of the channels and the culture chambers. Ethanol may be used to render the channels more hydrophilic prior to sterilization. The entire assembly, the membrane and all connections and tubings are then sterilized via autoclave treatment. It is helpful to arrange the components in a way that facilitates subsequent operations in a laminar hood.

A.6.3 Cell culture set up and analysis

Once the micro-bioreactor is assembled, tested and sterilized, the cell culture steps include: *(i)* surface coating, *(ii)* cell seeding, *(iii)* setting the medium flow rate, and *(iv)* biological data readout and analysis.

Surface coating and treatment: The glass surface of each culture chamber was treated with a solution of 4% 3-aminopropyltrimethoxysilane in acetone for 15 min. The solution was removed, the chamber rinsed with PBS and coated with 0.05 mg/ml collagen IV for 1 h at room temperature. Particular attention must be taken in keeping the collagen solution at +4°C in ice before dispensing it over the glass surface.

Cell seeding: The excess collagen solution was removed and the cell suspension was applied to the coated substrate to achieve a desired initial density. Bubble formation must be avoided in this phase, as bubbles would affect the subsequent steps.

Medium flow: The microfluidic channels were filled culture medium, and the PDMS membrane was positioned on top of the other PDMS layers and held in place with the polycarbonate-aluminum frame and secured with four thumbscrews. Again, bubble formation inside the culture chambers and the microfluidic channels should be avoided.

Cells were allowed to attach to the coated surface for 24 hours before starting media perfusion. To initiate medium perfusion, the syringes and the tubing were filled with the amount of fresh culture medium necessary for the entire experiment. Any air bubbles inside

the syringes or the tubing were removed. The syringes were kept at +4°C and coupled to the flow transducer; the tubings were connected to the inlet ports of the micro-bioreactors microfluidic channels, and the syringe pump was set to the chosen flow rate.

Biological analysis: The cultured cells were evaluated by on-line bright field imaging and by immunofluorescence for specific markers. Primary staining included Smooth Muscle Actin (SMA; Dako, Troy, Michigan, USA) or Oct4 (R&D Systems, Minneapolis, MN, USA), and DAPI for nuclei (Sigma–Aldrich, St. Louis, MO, USA). Secondary staining included Cy3 or the FITC-conjugated antibodies (Sigma–Aldrich, St. Louis, MO, USA). Automated image analysis via custom-adapted scripts in MATLAB (The MathWorks, Natick, MA, USA) was used to quantify the percentages of differentiated and undifferentiated cells, in form of FACS-like data, as previously reported [1].

A.6.4 Results

The entire set of results obtained using the micro-bioreactor array for hESC cultures was reported in Figallo et al. [1]. In this section, to prove the validity of our methods and procedures, we discuss some of the results to illustrate the application of the above principles for designing micro-bioreactors for hESC culture. We report an example for evaluating the effects of transport regimes for two micro-bioreactor configurations on a specific cell type (hESC).

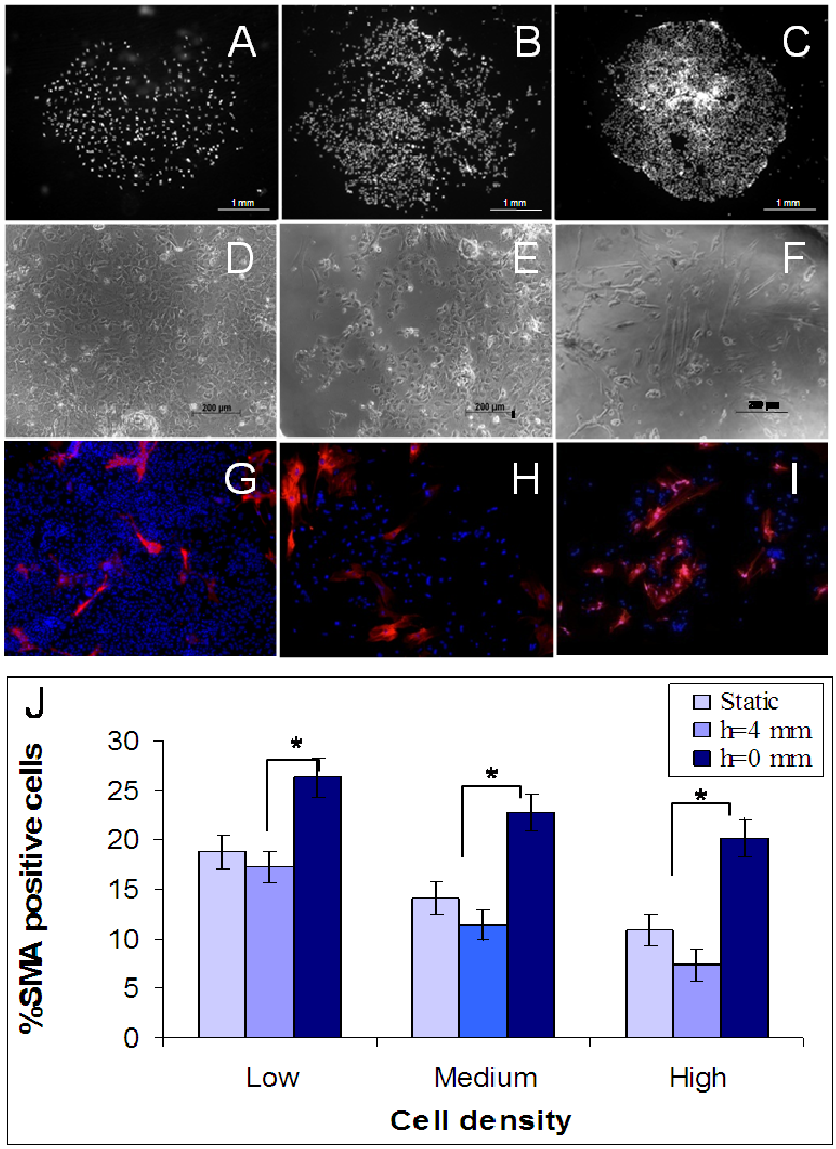

Figure 6. *Effects of cell density and transport regime on cell morphology and differentiation. A-C Bright field images of the culture wells with three different cell densities (increasing from left to right: 60, 160 and 314 cells/well). Cell nuclei are stained with DAPI. The coordinates of each nucleus is individuated by automated system analysis. Phase contrast images (D-F) and fluorescence images (G-I) of a static (non-perfused) bioreactor, a low shear bioreactor (h = 4 mm) and a high shear bioreactor (h = 0). J The fractions of cells expressing smooth muscle actin (SMA), a marker of vascular cell differentiation, as a function of cell density and bioreactor configuration.*

At all cell densities studied, homogeneous surface coating of a given extracellular matrix protein was achieved that resulted in homogeneous distribution of hESC over the entire surface of each culture chamber (Figure 6 A-C).

The two different bioreactor configurations described above, result in two completely different transport regimes at the same flow rate of 0.3 µL/min. Specifically, for the configuration corresponding to h = 0 mm, a convection-dominated mass transport regime was established with relatively high shear stress at the cell surface. In contrast, for the configuration corresponding to h = 4 mm, a diffusion dominated mass transport regime was established with negligible shear stress effects. The same micro-bioreactor arrays were also used without perfusion, to serve as static controls.

The effect of shear stress on hESC cell morphology is shown in Figure 6 D-F, where the shear stress increases from left to right, from statically operated micro-bioreactors, to the low-shear and high-shear perfused configurations. The low-shear condition appeared to have the sole effect of removing poorly adhering cells, and the cell morphology changed only after exposure to high shear stress.

Notably, cell differentiation depends on cell density (Figure 6 G-H), and this is due in part to the changes in the transport vs. reaction limitation of the system. Cell density and the bioreactor configuration each determine the rates of reaction and transport. As a result, the limiting phenomena (transport vs. reaction, Figure 3) can change and influence the biological responses of the cultured cells.

Figures 4 and 5 suggest that the static and low-shear perfused conditions can lead to similar transport regimes. This is consistent with the results of cell differentiation studies (Figure 6 L), where the statically operated and low-shear perfused conditions (both groups in the h = 4 mm configuration) gave statistically indistinguishable results. In contrast, an increase in shear stress that shifts the controlling transport regime from diffusion to convection (in the second configuration h = 0 mm), led to significantly different cell outcomes. The increased vascular differentiation of the cultured hESC cells at higher shear stress could be due to the dilution and depletion of endogenous factors and the constant supply of exogenous factors.

A.7 Conclusion and further developments

Micro-bioreactors are versatile as they allow one to vary the geometrical, configuration-related and operating parameters, and to explore with a high accuracy a broad range of cell cultivation conditions. Even thought the exploration of signaling pathways is leading to constantly increasing levels of understanding of stem cell behavior, the properties of compounds produced or required by living cells are still far from being fully known. Thus, the use of perfused micro-bioreactors designed and operated using rational principles outlined in this paper would be beneficial for gaining more control over culture parameters for answering specific biological questions.

Tight control over transport phenomena allows the modulation of regulatory signals in space and time, and helps mimic *in vitro* the physiological patterns found in living organisms. The integration with high-tech components such as micro pumps or micro valves could further improve the quality and the highthroughput of the data.

A.8 Acknowledgments

We gratefully acknowledge research support of the NIH (P41 EB002520 and R01 HL076485 to GV-N) and the University of Padova and Fondazione CARIPARO (stipend to EC).

A.9 References

[1] Figallo, E., Cannizzaro, C., Gerecht, S., Burdick, J. A., Langer, R., Elvassore, N., and Vunjak-Novakovic, G. (2007) *Lab on a Chip* **7,** 710-19.

[2] Powell, K. (2005) *Nature* **435,** 268-70.

[3] Hung, P. J., Lee, P. J., Sabounchi, P., Aghdam, N., Lin, R., and Lee, L. P. (2005) *Lab on a Chip* **5,** 44–48.

[4] Khademhosseini, A., Langer, R., Borenstein, J., and Vacanti, J. P. (2006) *PNAS* **103,** 2480–87.

[5] Breslauer, D. N., Lee, P. J., and Lee, L. P. (2006) *Mol. BioSyst.* **2,** 97-112.

[6] Haeberle, S., and Zengerle, R. (2007) *Lab on a Chip* **7,** 1094–110.

[7] Sia, S. K., and Whitesides, G. M. (2003) *Electrophoresis* **24,** 3563–76.

[8] Squires, T. M., and Quake, S. R. (2005) *Reviews of Modern Physics* **77,** 977-1016.

[9] DiCarlo, D., Wu, L. Y., and Lee, L. P. (2006) *Lab on a Chip* **6,** 1445–49.

[10] Hui, E. E., and Bhatia, S. N. (2007) *Proc Natl Acad Sci USA* **104,** 5722–26.

[11] Linder, V. (2007) *The Analyst* **132,** 1186–92.

[12] Toner, M., and Irimia, D. (2005) *Annu. Rev. Biomed. Eng.* **7,** 77–103.

[13] Melin, J., and Quake, S. R. (2007) *Annual Review of Biophysics and Biomolecular Structure* **36,** 213–31.

[14] Lauffenburger, D. A., and Linderman, J. (1993) Receptors - Models for binding, trafficking, and signaling, Oxford University Press.

[15] Wang, H., Riha, G. M., Yan, S., Li, M., Chai, H., Yang, H., Yao, Q., and Chen, C. (2005) *Arterioscler Thromb Vasc Biol* **25,** 1817-23.

[16] Kubo, A., Shinozaki, K., Shannon, J. M., Kouskoff, V., Kennedy, M., Woo, S., Fehling, H. J., and Keller, G. (2004) *Development* **131,** 1651–62.

[17] Peerani, R., Rao, B. M., Bauwens, C., Yin, T., Wood, G. A., Nagy, A., Kumacheva, E., and Zandstra, P. W. (2007) *The EMBO Journal* **26,** 4744–55.

Appendix B

Production of arrays of cardiac and skeletal muscle myofibers by micropatterning techniques on a soft substrate

Elisa Cimetta[1], Sara Pizzato[1], Sveva Bollini[2], Elena Serena[1], Paolo De Coppi[2], Nicola Elvassore[1]*

[a] Department of Chemical Engineering, University of Padua, Via Marzolo, 9 Padua, Italy

[a] Department of Pediatrics, University of Padua, Via Giustiniani, 3, Padua, Italy

*Corresponding author

Biomed Microdevices

DOI 10.1007/s10544-008-9245-9

Keywords: micro-patterning, soft substrate, hydrogel, cardiomyocytes, satellite cells, cell array.

Abstract

Micropatterning and microfabrication techniques have been widely used to pattern cells on surfaces and to have a deeper insight into many processes in cell biology such as cell adhesion and interactions with the surrounding environment. The aim of this study was the development of an easy and versatile technique for the *in vitro* production of arrays of functional cardiac and skeletal muscle myofibers using micropatterning techniques on soft substrates. Cardiomyocytes were used for the production of oriented cardiac myofibers whereas mouse muscle satellite cells for that of differentiated parallel myotubes. We performed micro-contact printing of extracellular matrix proteins on soft polyacrylamide-based hydrogels photopolymerized onto functionalized glass slides. Our methods proved to be simple, repeatable and effective in obtaining an extremely selective adhesion of both cardiomyocytes and satellite cells onto patterned soft hydrogel surfaces. Cardiomyocytes resulted in aligned cardiac myofibers able to exhibit a synchronous contractile activity after 2 days of culture. We demonstrated for the first time that murine satellite cells, cultured on a soft hydrogel substrate, fuse and form aligned myotubes after 7 days of culture. Immunofluorescence analyses confirmed correct expression of cell phenotype, differentiation markers and sarcomeric organization. These results were obtained in myotubes derived from satellite cells from both wild type and MDX mice which are research models for the study of muscle dystrophy. These arrays of both cardiac and skeletal muscle myofibers could be used as *in vitro* models for pharmacological screening tests or biological studies at the single fiber level.

B.1 Introduction

The major advantage introduced by high-throughput technology resides in the possibility of simultaneously acquiring vast amounts of information (Kozarova et al. 2006; Chen et al. 2006). Recently, protein microarrays (Brueggemeier et al. 2005), tissue microarrays (Chen et al. 2004) and living cell microarrays (Albrecht et al. 2005) have been developed. Living cell-arrays offer unique advantages when used as the sensing element for biological assays or in drug development and differentiation studies (Flaim et al. 2005). Two-dimensional arrays of single cells or clusters of cells can provide appropriate culture conditions for adherent cells, however, the lack of structural and topological cues may alter cell behavior and phenotype expression. Mammalian cells integrate and respond to a combination of

factors in the micro-scale environment, such as chemical and mechanical properties, shape, organization and cell-cell interactions (Albrecht et al. 2006; Jang et al. 2006; Kaplan et al. 2005; Vunjak-Novakovic et al. 1998). These aspects are particularly important for cell phenotypes such as cardiac, skeletal, and smooth muscular, which are highly dependent on three-dimensional (3D) cell organization (Motlagh et al. 2003). For instance, in the heart, cardiomyocytes are organized in interconnected cardiac myofibers that contract synchronously, whereas skeletal muscle is formed by parallel multinucleate myofibers. In addition, surface mechanical properties are of particular relevance for the functionality of contractile cells (Engler et al. 2004a; Ingber2002; 2005; Khatiwala et al. 2006), and this translates into the coupling to a soft or stiff substrate. In muscle tissue, contractions are transmitted through cell-cell and cell-matrix interactions. and in a recent study, Engler and colleagues proved that myotube differentiation and the development of myosin/actin striations necessary for functional muscle activity occurs preferentially on substrates with tissue-like stiffness (Engler et al. 2004a).

To guide cell adhesion, many patterning techniques have been proposed and widely reviewed over the last few years (Falconnet et al. 2006; Xia et al. 1998). Various lithographic techniques have been used to guide cell adhesion and orientation onto different substrates (Karp et al. 2006; Rohr et al. 1991; Suh et al. 2004) while microfluidics have been employed to pattern cardiomyocites on PDMS or glass substrates (Gopalan et al. 2003; Khademhosseini et al. 2007). Muscle cells have been studied on surfaces comprising nanopatterned gratings, microgrooves and microtextures (Motlagh et al. 2003; Vernon et al. 2005; Yim et al. 2005). Patterns of proteins have been created on glass or polystyrene surfaces via micro-contact printing (μCP) (Ruiz et al. 2007) and laminin lanes have been patterned using the same technique on polimeric films for the subsequent adhesion of cardiomyocytes (McDevitt et al. 2003; McDevitt et al. 2002).

The major limitations of the enumerated techniques are related to the stiffness of the substrates used - gold, silver, metal or metal-oxide, glass and polystyrene - on the one hand and to the difficulties encountered while producing controlled patterning on soft materials on the other.

Among soft substrates, hydrogels have recently captured attention in the field of tissue engineering because of their high water content, biocompatibility and elastic properties, resembling those of native tissues. In recent years many kinds of hydrogels, especially poly(ethylene glycol) (PEG) and derivatives (Britton-Keys et al. 1998; Burdick et al. 2004;

Lin-Gibson et al. 2005), have been widely used for encapsulating living cells or as substrates for cell culture. A wide variety of copolymers, composed of a synthetic backbone and grafted biomolecules (or vice versa) such as fibrinogen (Almany et al. 2005) and hyaluronic acid (Leach et al. 2003; Leach et al. 2005) or short peptides sequences such as RGD (Hern et al. 1998), was proposed and tested to develop substrates with the biological cues required for cell attachment. In addition, the elastic properties can be controlled and modulated by changing the amount of polymer and crosslinker, thus obtaining stiff or soft gels with a different influence on cell behavior at the cytoskeletal level (Engler et al. 2004b; Peyton et al. 2005).

Thus, an advisable approach is the production of arrays of isolated and independent cellular aggregates in a fiber-like fashion in which cells can align, express their phenotype, eventually fuse and differentiate or show contractile activity. In this perspective, an array of fibers able to reproduce these particular features and maintain the functionality of natural tissues can potentially become a good alternative to animal models for high-throughput pharmacological screenings. In addition, fiber arrays with the capacity of mimicking and reproducing the structural cues of native muscular tissue could represent an *in vitro* model resembling more closely the *in vivo* responses than the conventional cell cultures.

To achieve this goal we needed: 1) to spatially organize cells and drive their alignment, 2) to allow cells to differentiate and express their correct phenotype, and 3) to ensure that cells fully develop the functionality peculiar to their native tissue (i.e. contractile activity).

A poly-acrylamide (PA) based hydrogel was used as the substrate for cell culture because of its elastic properties, which are particularly suitable for muscle cell culture (Engler et al. 2004a). Moreover, this hydrogel is easy to produce, inexpensive, biocompatible ,and optically transparent; the latter being an important prerequisite for performing optical image analyses. PA hydrogel can be produced as a thin film and covalently bonded to a functionalized glass slide showing long term stability in culture.

As PA hydrogel is a non-fouling material, an adhesion-protein pattern was micro-contact printed onto the PA surface; this technique was chosen for being a simple and versatile method to pattern adhesion proteins with a resolution of ~1 μm. The immobilization on the surface occurred through physical adsorption and allowed proteins to maintain their activity

without suffering from major denaturation phenomena. In addition, patterning proteins on hydrogel films enabled microscope observations on the same focal plane of the substrate.

We developed arrays of cardiac and skeletal muscle fibers on soft substrates that are potentially able to provide independent responses to different stimuli. The techniques here proposed open new and important perspectives in the field of pharmacological screening and drug testing, in order to achieve accurate biological and physiological *in vitro* studies.

B.2 Material and Methods

B.2.1 Cell isolation and culture

C2C12.

The murine skeletal muscle immortalized cell line C2C12 (ATCC) was grown in Dulbecco's modified Eagle's medium (DMEM, Sigma-Aldrich) supplemented with 10% foetal bovine serum (FBS, Gibco-Invitrogen), 1% penicillin-streptomycin and 1% L-glutamine (all from Invitrogen), on standard 100 mm Petri dishes, in a 95% humidified and 5% CO_2 atmosphere at 37ºC and maintained at low confluence.

Subconfluent plates of C2C12 cells were detached on day 0 using trypsin/EDTA (Sigma-Aldrich), pelleted by centrifugation for 5 min at 1200 rpm and counted.
Cells were resuspended in DMEM and 300 μl, of the cell suspension was deposited on the hydrogel surface at 104 cells/cm^2 and incubated for 2 hours. After that, the culture medium and the cells that had not yet adhered were removed. The hydrogels were then gently rinsed, by first adding and then immediately removing 300 μl of DMEM. Seeded hydrogels were then incubated for one week replacing culture medium once a day.

Cardiomyocytes.

Rat neonatal cardiomyocytes (CM) cultures were obtained by enzymatic digestion of newborn rat hearts. Neonatal (2-3 days-old) Sprague-Dawley rats were provided by the Department of Sperimental Surgery of the University of Padua.

The hearts were washed with ice-cold, sterile HBBS (Hank's Balanced Salt Solution, Worthington Biochemical Corporation), trimmed of auricles and excess connective and

adipose tissue, and minced with sterile scissors. Myocardial tissue was then dissociated to release ventricular CM by an enzymatic isolation procedure first using a trypsin solution (50 µg/ml), incubating overnight at 4°C, and then a collagenase solution (300 units/ml, Worthington Biochemical Corporation) at 37°C for 45 minutes (Pedram et al. 2005; Speicher et al. 1974; Xiao et al. 1997). CM were then collected by centrifugation and non-myocytes cells were removed by preplating on culture dishes.

Enriched CM were seeded on the hydrogels at a density of $1.6 \cdot 10^5$ cells/cm^2 in plating medium (DMEM –Sigma-Aldrich, enriched with 5% FBS, 10% Horse Serum – all from Biochrom Ag., 1% L-Glutamine 1% Penicillin and Streptomicin -all from Gibco, and medium M199 17% -Biochrom Ag.) and cultured in a 95% humidified incubator 5% CO_2 at 37°C.

At day one after seeding, hydrogels were rinsed with culture medium to remove non adhering cells. The culture medium was replaced once a day.

Satellite cells.

Primary myoblasts were obtained from the expansion of satellite cells isolated from single-muscle fibers adjusting the protocol previously described by Rosenblatt (Rosenblatt et al. 1995). For this reason, we refer to our myoblast culture as satellite cells. Briefly, flexor digitorum brevis from C57BL/6J mouse muscles were removed and enzimatically digested with 0,2% collagenase type I (Sigma-Aldrich). The single fibers obtained were selected on an inverted microscope (Olympus IX71) and plated on Petri dishes pre-coated with Matrigel® (BD Bioscience). Myofibers were maintained in a humidified tissue culture incubator. On day three, the plating medium, which consisted of DMEM (Sigma-Aldrich), 20% horse serum (Gibco-Invitrogen), 1% chicken embryo extract (MP-Biomedicals), and 1% penicillin-streptomycin (Gibco-Invitrogen), was added to the Petri dishes. Released and proliferated cells were detached from the plate with trypsin (Gibco-Invitrogen) before fusion into myotubes occurred, and cultured with proliferating medium (DMEM, 20% foetal bovine serum, 10% horse serum, 0.5% chicken embryo extract and 1% penicillin streptomycin).

300 µl of cell suspension in proliferating medium were seeded at a density of $3 \cdot 10^4$ cells/cm^2 on the hydrogel surfaces. After approximately 5 hours, cells that had not adhered to the surface were removed by gently rinsing the hydrogel films with proliferating

medium. Satellite cells were kept in culture for one week, replacing the culture medium every two days.

B.2.2 Glass slide functionalization

Glass slides surfaces were chemically modified creating a hydrophobic layer of methacrylate groups to ensure covalent binding of the hydrogel films. Briefly, slides were washed in ethanol and rinsed with distilled water, dried at 110°C and treated with air-plasma (Plasma Cleaner PDC-002, Harrick Plasma) for 5 minutes at 0,5 mbar. A few drops of 3-(trimethoxysilyl)propyl methacrylate (Sigma-Aldrich) were deposited on the glass slides which were then stacked and after 1 hour dried in oven at 100°C for 10 minutes.

B.2.3 Hydrogel preparation

Hydrogel films.

Hydrogels were prepared optimizing previously developed procedures (Flaim et al. 2005). Briefly, acrylamide/bis-acrylamide 29:1 40% solution (Sigma-Aldrich) was diluted in phosphate-buffered saline (PBS, Sigma-Aldrich) to the final concentrations of 8, 10, 15 and 20%. The photoinitiator (Irgacure 2959; Ciba Specialty Chemicals), was initially dissolved in methanol at 200 mg/ml and then added to the acrylamide/bis-acrylamide solution in order to obtain a final concentration of 20 mg/ml, and mixed thoroughly.

Three individual 20 μl volumes of the prepolymer solution were dropped over the functionalized glass surface and a glass coverslip was floated over each drop. Hydrogel polymerization occurred by exposing the prepolymer solution to UV light for 3 minutes. Irradiation was provided by a high-pressure mercury vapor lamp (Philips HPR 125W) emitting at 365 nm with an incident light intensity of 20 mW/cm^2. Selective photo-polymerization of acrylamide solutions on the glass surface was achieved by interposing a photomask with the desired geometry between the light source and the glass slide. Non-exposed regions were washed using distilled water to remove the non-polymerized solution. Such procedures resulted in homogeneous hydrogel films with an average thickness of 40 μm.

Mechanical test

The hydrogel samples for the compression tests were realized using different acrylamide/bis-acrylamide solutions (29:1) at 5, 10, 15 and 20% (v/v) in PBS. The photoinitiator Irgacure 2959, previously dissolved in methanol (200 mg/ml), was added to the prepolymer solution to achieve the final concentration of 20 mg/ml. Hydrogel samples, shaped as 60 mm diameter disks, were obtained photopolymerizing 20 ml of the prepolymer solution under UV light (λ=365 nm).

Young's modulus of the hydrogel was determined by a uniaxial compression test, performed at room temperature using the Sun 2500 Galdabini testing machine. Hydrogel disks were placed between two parallel plates and compressed at the constant rate of 1 mm/min, until a final deformation of 120% was reached. The Young's modulus for each composition of the PA hydrogel was measured on 5 replicates.

B.2.4 Hydrogel sterilization and cytotoxicity assay

Glass slides with covalently bonded hydrogel films were immersed in ultra-pure distilled water for 48 hours to ensure complete removal of the un-reacted monomeric units or photoinitiator and then soaked in a 70% ethanol solution. After rinsing with ultra-pure distilled water, hydrogels were allowed to dry completely overnight; final sterilization occurred after 20 minutes exposure to UV light under a sterile hood.
Cell viability was assessed with Live/Dead® Viability Cytotoxicity Assay (Invitrogen) based on calcein and etidium homodimer (EthD-1) dyes, following and optimizing the supplied protocol. After mounting on microscope slides, samples were analyzed using a Leica CTR6000 fluorescence microscope.

B.2.5 Array design and realization

The desired array design was realized in digital form with Adobe Illustrator and consisted of 400 lanes 100 μm wide and 1 mm long, horizontally spaced by 100 μm and 300 μm vertically.

This pattern was printed onto an overhead transparency and used as a photomask. A standard photolithographic technique was employed for the fabrication of the master using an SU-8 photoresist (MicroChem Corporation). Briefly, the SU-8 was spun over a silicon

wafer, which was thermally treated, selectively polymerized by interposing the patterned photomask, and exposed to UV light (λ=365 nm) for 50 seconds. It was finally developed with 1-methoxy-2-propanol acetate (Sigma-Aldrich).

The PDMS stamp was obtained via replica molding, curing Sylgard 184 (Dow Corning) on the patterned silicon master.

Laminin lanes (100 μm wide) were printed on smooth hydrogel surfaces via μCP technique using the PDMS stamp just described. Specifically, the stamp was inked in the protein solution (mouse-laminin 100 μg/ml in PBS) for a few seconds, and then the excess solution was removed. Conformal contact between the dry hydrogel surface and the stamp was then achieved by applying a gentle pressure, thus transferring the desired protein micropattern on the substrate.

B.2.6 Immunostaining analyses

Cardiomyocytes-troponin I

After 4 or 7 days of culture, cells on patterned hydrogel were fixed with 2% paraformaldeyde (PFA; Carlo Erba) for 20 minutes at 4°C and permeabilized with a 0.1% Triton X-100 solution (Sigma-Aldrich) at room temperature. CM were then incubated for 25 minutes at 37°C with primary antibodies specific for cardiac troponin I (mouse IgG 1:1000, Chemicon) and diluted in a 1% PBS/BSA solution. Alexa Fluor 594-conjugated goat anti-mouse IgG (Molecular Probes) was diluted 1:150 in a 1% BSA/PBS. Human serum solution (1:100) was used as secondary antibody and incubated for 25 minutes at 37°C. Cell nuclei were then stained for 5 minutes at room temperature with a 1:5000 Hoechst solution (Sigma-Aldrich) in PBS.

After mounting the samples with Elvanol® (DuPont), immunofluorescence analyses were performed using a fluorescence microscope (Leica CTR6000).

C2C12-desmin

After 4 or 7 days of culture, cells on patterned hydrogel were fixed with 2% PFA for 7 minutes at room temperature. After permeabilization with a 0.5% Triton X-100 solution (Sigma-Aldrich) for 8 minutes at room temperature, samples were blocked with a 10% FBS/PBS solution for 45 minutes at room temperature. The samples were treated with primary rabbit polyclonal antibody for desmin (AbCam) diluted 1:100 in a 3% BSA/PBS

solution, and incubated for 1 hour at 37°C; then, incubation with a secondary antibody Cy™3-conjugated anti-rabbit IgG (Jackson) diluted 1:200 in a 3% PBS/BSA for 45 minutes at 37°C followed. Nuclei were counterstained with a 1:5000 Hoechst solution (Sigma-Aldrich) in PBS for 5 minutes at room temperature; the samples were then mounted with Elvanol® and analyzed with a fluorescence microscope.

Satellite cells-desmin, myosin heavy chain and troponin I

Immunofluorescence analyses were performed on patterned cells after 4 or 7 days in order to detect desmin and troponin I. The cells were fixed with 2% PFA for 7 minutes at room temperature and permeabilized with 0.5% Triton X-100 solution (Sigma-Aldrich). Patterned cells were blocked in PBS-2% horse serum (HS) for 45 minutes at room temperature. Desmin primary antibody (AbCam), rabbit polyclonal, was diluted 1:100 in PBS-3% BSA; troponin I primary antibody (Chemicon), mouse monoclonal, was diluted 1:100 in PBS-3% BSA; Myosin Heavy Chain primary antibody, mouse monoclonal, was diluited 1:50 in PBS-3% BSA. Each antigen was individually applied for 1 hour at 37 °C. the secondary antibody Cy™3-conjugated anti-rabbit IgG was diluted 1:200 in PBS-3% BSA and FITC-conjugated anti-mouse IgG (Jackson) was diluted 1:250 in PBS-3% BSA and applied for 45 minutes at 37°C. Finally, cells were incubated in 1:5000 Hoechst solution at room temperature for 10 min. Samples were mounted with Elvanol®, and viewed under a fluorescence microscope.

B.3 Results

With the aim of mimicking as close as possible the *in vivo* muscular microenvironment, the substrate was designed to reproduce the mechanical properties of natural tissue. With this in mind, we produced a polyacrylamide based hydrogel and quantitatively measured its elastic properties through standard compression tests (Galdabini, Sun 2500), determining the bulk Young’s modulus (E).

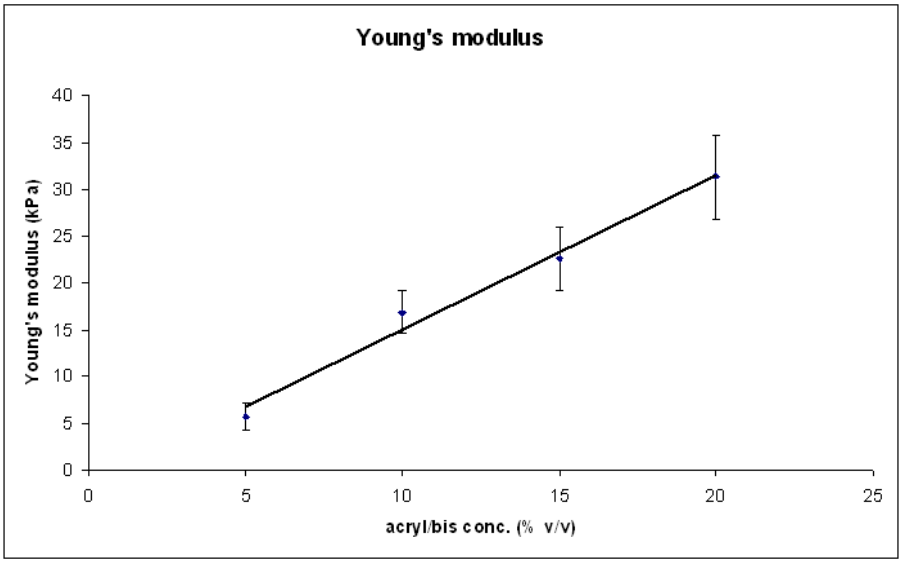

Figure 1. *Young's modulus of PA hydrogel. Elastic moduli were quantitatively measured through standard compression tests for four different hydrogel compositions, i.e. 5-10-15-20% (v/v) acrylamide/bis-acrylamide 29:1 mixture in the prepolymer solution.*

Figure 1 shows the result of mechanical tests performed on hydrogel samples taking in account four different concentrations of polymer (5, 10, 15 and 20% v/v of acrylamide/bis-acrylamide 29:1 mixture) in the prepolymer solution. Young's modulus increases as the acrylamide/bis-acrylamide concentration increases. A linear interpolation of the data was used to determine the optimal hydrogel compositions, which fairly approximate the elastic modulus of mouse muscle (Engler et al. 2004a). For instance, hydrogels with 8.2±2.5% (v/v) acrylamide/bis-acrylamide may reproduce the values of the elastic modulus of normal mice (En=12±4 kPa) whereas hydrogels with 12.0±3.7% reproduce that of dystrofin-deficient mice (Ed=18±6 kPa) (Engler et al. 2004a). It is worth noting that hydrogels with any bulk elastic modulus in the range of 5-30 kPa can be easily fabricated by adjusting the hydrogel composition (5-20 % v/v). If not otherwise indicated, hydrogels derive from a 10% (v/v) acrylamide/bis-acrylamyde 29:1 solution.

PA hydrogels were homogenously photopolymerized and covalently bonded to a functionalized glass slide; with the aim of selectively guiding cell adhesion on the non-fouling hydrogel surfaces, we created protein patterns using a micro-contact printing technique (Figure 2). The protein deposition procedure, involving the pressing of a microstructured PDMS stamp, previously inked in the protein solution, allowed us to reproduce the desired pattern with high spatial resolution, virtually allowing us to create arrays of any geometry on the hydrogel surface.

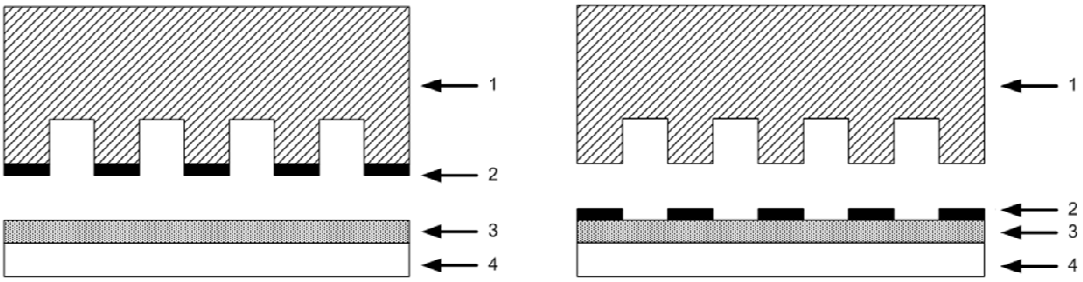

Figure 2. *Schematic representation of the micro-contact printing (μCP) technique. Panel A exemplifies the microstructured PDMS stamp (1) with a monolayer of laminin (2) adsorbed on its surface. A thin film of PA hydrogel (3) is covalently bonded to a glass slide (4). Panel B schematically represents the result of the protein printing: the laminin (2) previously adsorbed on the PDMS stamp surface (1) has been transferred onto the hydrogel surface (3) adhered on the glass slide (4).*

The evaluation of the fluorescence intensities of images obtained patterning different concentrations of BSA-FITC conjugated onto PA hydrogels (data not shown), allowed us to observe how the amount of adsorbed protein can be adjusted by changing its concentration in the solution used for inking the PDMS mold; in addition, it was proven that equal amounts of protein in the inking solution gave repeatable fluorescence signals. Moreover, the unchanged fluorescence signal of the protein, after washing with distilled water and incubation with culture medium at 37°C for two days, demonstrated that the protein was permanently adsorbed on the hydrogel surface.

A Live/Dead® Viability/Cytotoxicity assay performed on cardiomyocytes cultured on hydrogel surfaces clearly demonstrated that PA hydrogel, after the purification treatment previously described, was completely biocompatible and non-cytotoxic and allowed cells to grow and spread without affecting their viability (data not shown).

Figure 3 shows C2C12 cells cultured on laminin micro-patterned hydrogels.

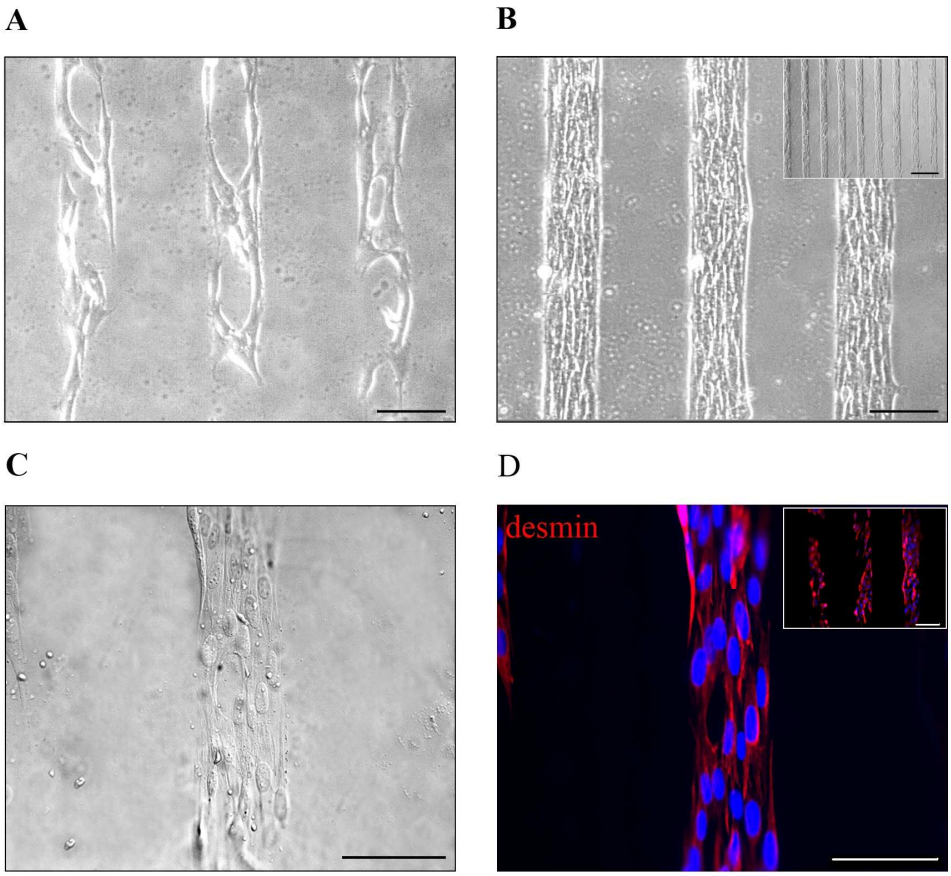

Figure 3. *C2C12 cells cultured on patterned PA hydrogel at three different time points. Laminin lanes were printed on the hydrogel surface using a microstructured PDMS stamp, as described in Fig. 1A-B. The 10x (scale bar=100 μm) magnification pictures (Panels A-B) show the time course of C2C12 cells culture: 4 hours after seeding cells were spreading and attaching to the substrate (A), after 2 days they reached confluence confined inside the laminin lanes (B); the inset picture shows the high selectivity of the cell pattern on the hydrogel surface at 5x magnification (bar=300 μm). Panel C reports the bright field image at 40x magnification of C2C12 cells on which the immunofluorescence analysis to detect desmin was performed (Panel D, 40x). Cell nuclei were counterstained with Hoechst (blue). (scale bar=75 μm).*

Figures 3A and 3B show the time course of adhesion, spreading, and proliferation at 4 hours and 2 days after seeding, respectively. Four hours after seeding, cells were attaching to the patterned regions and after two days reached confluence inside the protein coated lanes. Changes in cell morphology became noticeable a few hours after seeding; both the hydrogel properties and the high affinity towards laminin allowed and induced cells to spread and acquire an elongated shape. After 7 days of culture, the construct appeared perfectly organized with cells aligned and oriented along the main axis of the arrayed protein-patterned lanes (inset of Figure 3B). Optimization of the seeding protocol with the addition of a gentle rinsing 5 hours after deposition of the cell suspension, led to an increased

selectivity because of the removal of unattached cells. An immunostaining for desmin, a typical muscle cell marker, confirmed the correct expression of cell phenotype, which was neither affected by the supporting hydrogel nor by the morphological constraints created by the laminin lanes (interferential image in 3C, fluorescence image in 3D). The inset of Figure 3D shows again that both the nuclei position and the elongated cell shape was oriented in accordance with the underlying protein pattern.

Figure 4 reports extensive studies performed seeding satellite cells onto hydrogels of varying stiffness.

The histogram in panel 4A shows the results of cell counts after three and five days form seeding; it demonstrates how softer hydrogels allow the attachment of a statistically significant ($p<0.005$) higher cell number. No significant differences emerge either comparing 8% and 10% hydrogels or the two time points, this last is due to the fact that the patterned lanes readily reach a confluent state and thus inhibiting proliferation. The polar diagrams in panel B quantify the extent of organized orientation of the cells seeded in uniformly patterned (B1) and micro-patterned (B2) hydrogels; more than 90% of the cells adhering on the micropatterned lanes fall on an angle range between -10 and +10° from the longitudinal direction. Respecting the need for the optimal range of elastic modulus and following from the cell counts-observations, we chose to realize hydrogels with a 10% of acrylamide/bis-acrylamide in the prepolymer solution.

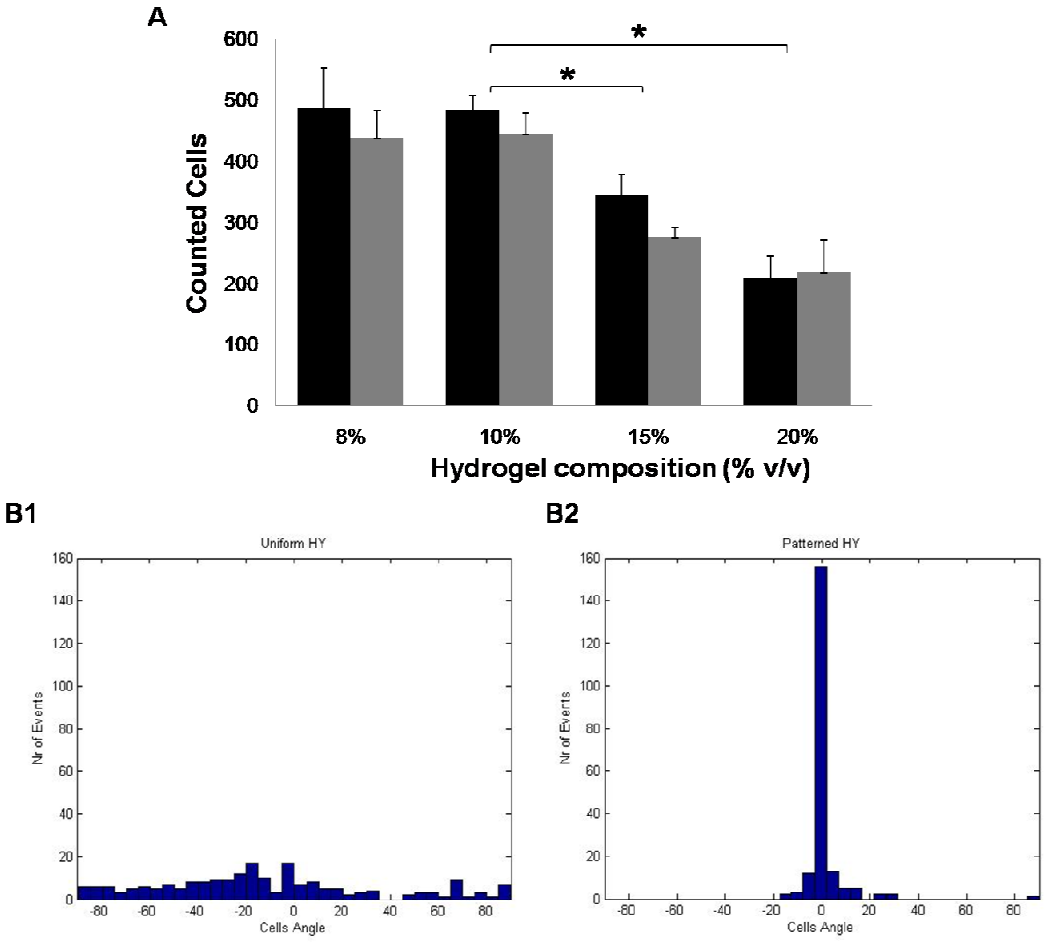

Figure 4. *Satellite cells on hydrogels: counts and orientation. The histogram of panel A represents cell counts at two time points: 3 and 5 days (in black and gray, respectively) after seeding. The number of cells adhered to softer (8 and 10%) hydrogels is significantly higher than that on stiffer (15 and 20%) hydrogles ($p<0.005$). The polar diagrams in panel B quantify the extent of organized orientation of the cells seeded in uniformly patterned (B1) and micro-patterned (B2) 10% composition hydrogels; more than 90% of the cells adhering on the micropatterned lanes fall on an angle range between -10 and +10° from the main direction of the micropatterned lanes.*

Figure 5 shows the results of the micro-patterning of satellite cells.

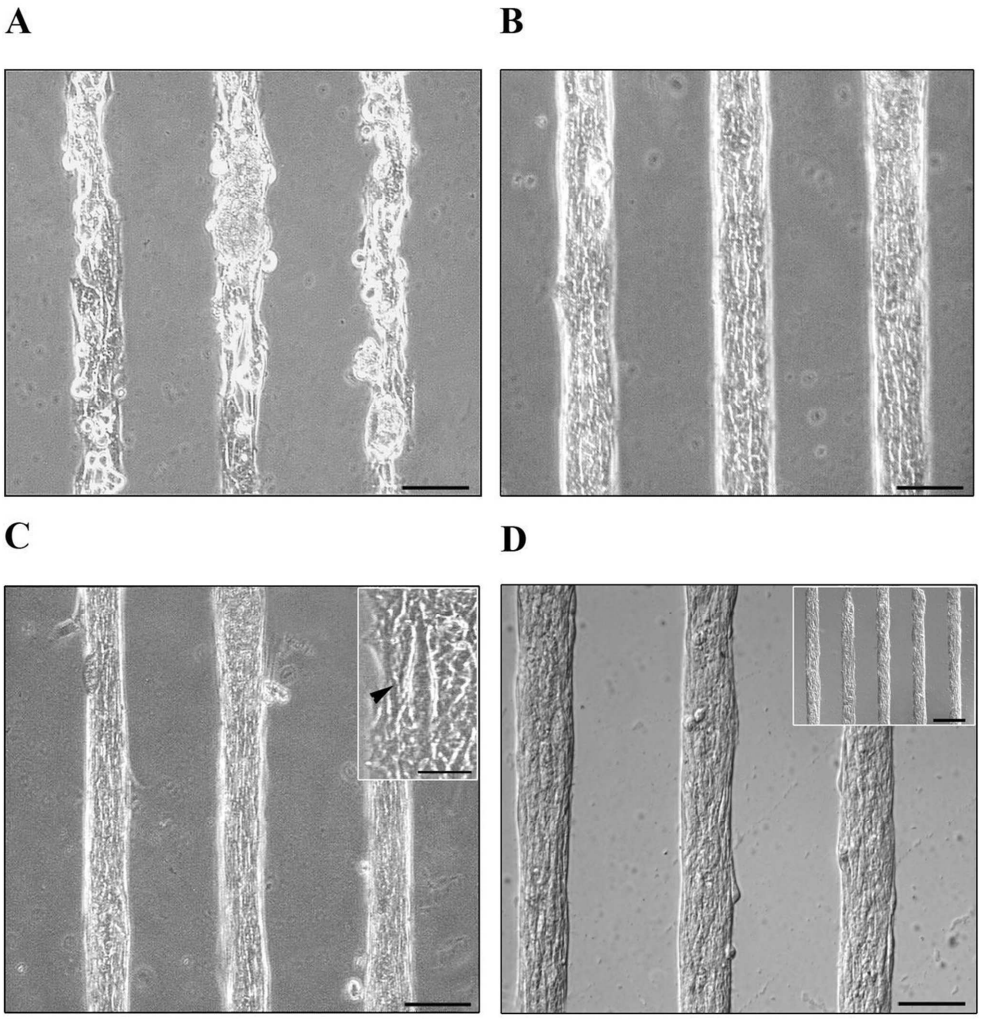

Figure 5. *Satellite cells on hydrogels: counts and orientation. The histogram of panel A Satellite cells cultured on patterned PA hydrogel. Laminin lanes were printed on the hydrogel surface using a microstructured PDMS stamp, as described in Fig. 1. Mouse satellite cells attached in correspondence of the laminin lanes, as shown in A, 5 hours after seeding, and aligned following the underlying protein pattern, as shown in B and C after 3 and 7 days in culture, respectively (scale bar=100 μm). The inset in Panel C shows the occurred fusion into myotubes at 40x magnification (scale bar=37.5 μm). Panel D (10x, scale bar=100 μm) and the inset picture (5x, scale bar=300 μm) report interference microscope images showing aligned satellite cells after 7 days in culture, proving the efficiency of the patterning technique and the durability of the fiber array.*

As the myogenic potential of satellite cells strongly depends on the number of passages of the expansion, we used early passages (first and second) and noticed that the results were similar in both cases in terms of cell adhesion. Figures 5A-C show the temporal evolution of satellite cell cultures on Matrigel 2.5% patterned hydrogels respectively at 5 hours, 4

days and 7 days from seeding. The Matrigel pattern and the early removal of non-adherent cells by rinsing led to a great efficiency in the selective adhesion of satellite cells. After 4 and 7 days of culture, cells proliferated extensively and aligned significantly along the direction of the lanes. Confluence was usually reached after 2 days of culture; after 7 days, satellite cells fused to give myotubes (inset of Figure 5C). Figure 5D demonstrates the high specificity of the patterned substrate and shows the elongated cell morphology within the lanes.

Figures 6A-C show immunofluorescence analyses for three specific myogenic markers, desmin, troponin I and Myosin Heavy Chain (Myhc) on satellite cells after 4 days of culture.

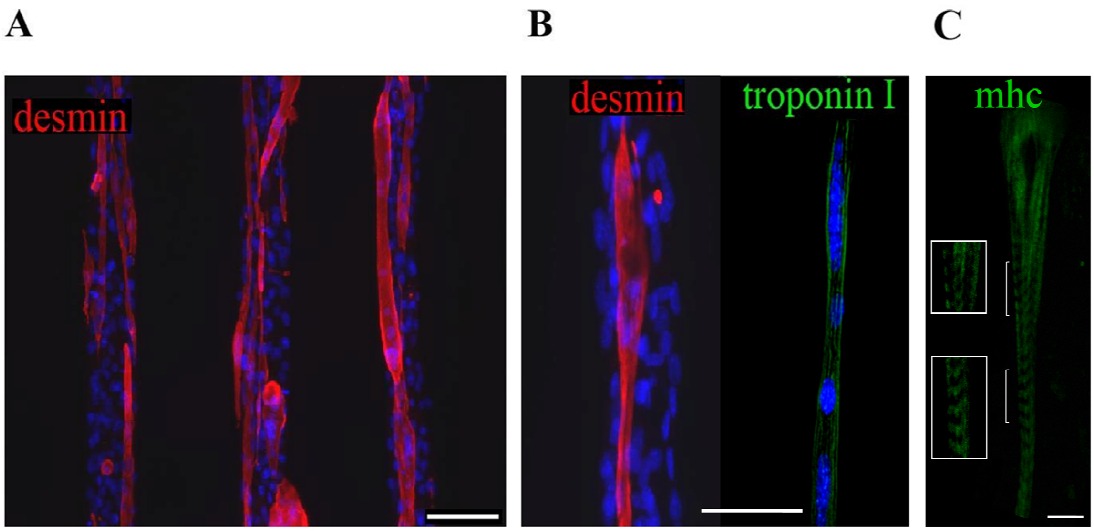

Figure 6. *Satellite cells cultured on patterned PA hydrogel. Immunofluorescence analyses reported in panel A (10x, scale bar=100 μm; inset: 5x, scale bar=300 μm) and B (40x, scale bar=75 μm) assessed the correct phenotype expression in the newly formed myotubes, positively stained for desmin, red, and troponin, green. Cell nuclei were counterstained with Hoechst (blue). Panel 6C demonstrates the correct expression of Myhc and its organization in regular and uniform striations, also highlighted on the two insets (63x, scale bar=25 μm).*

Immunofluorescence analyses for desmin (Figure 6A), clearly demonstrate the presence of newly formed and aligned myotubes. Figure 6B shows detailed images of the immunofluorescence analyses for desmin and troponin I on a single myotube, correctly resulting from the fusion of a large number of satellite cells as can be seen by the presence of many nuclei along each myotube. Figure 6C shows that myotubes cultured on hydrogel express Myhc and, more interestingly, that it is organized in regular and uniform striations.

Satellite cells-derived myotubes exhibited fast spontaneous contraction, quantified and discussed in Figure 8.

Figure 7 shows cardiomyocytes seeded at a density of $1.6 \cdot 10^5$ cells/cm^2 and underlines the extreme selectivity obtained in cell adhesion.

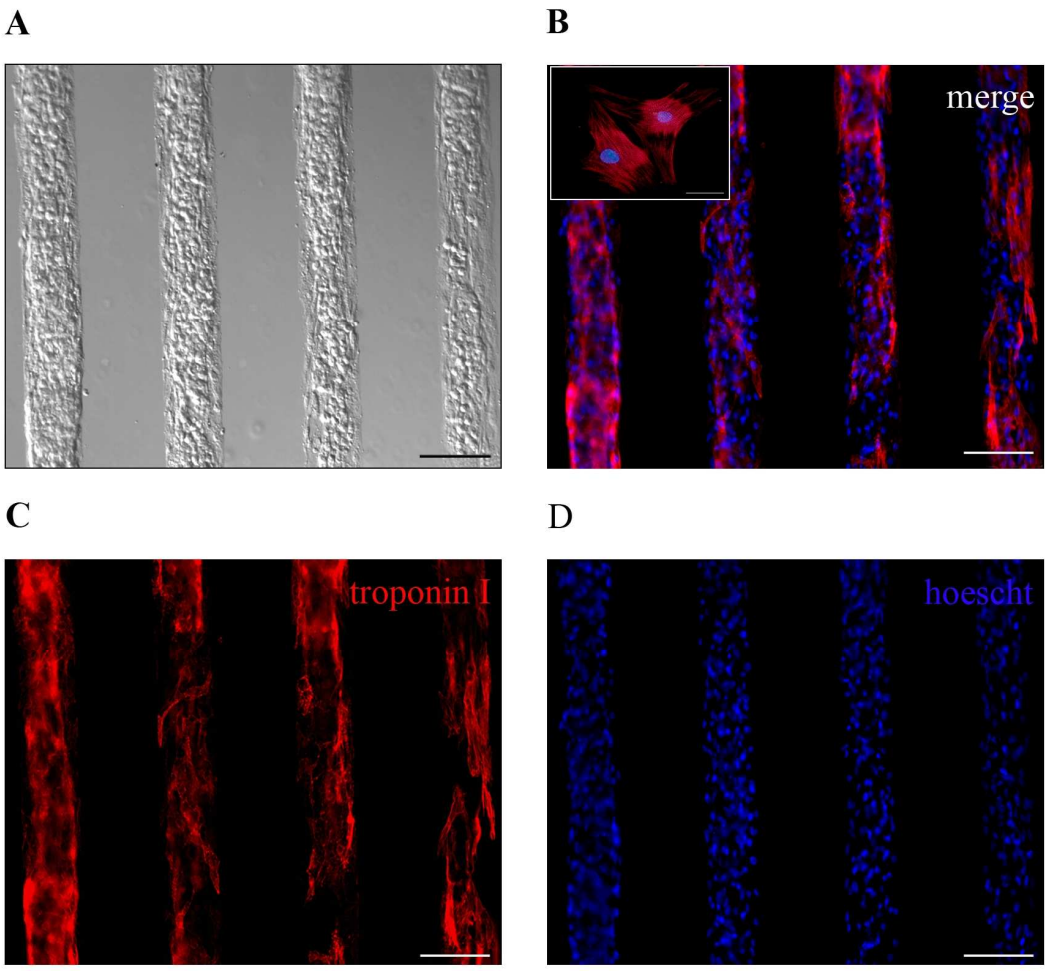

Figure 7. *Cardiomyocytes cultured on patterned PA hydrogel. Images were taken at 10x magnification. (A): bright field image of cardiomyocytes after 4 days in culture; (B): cultured cardiomyocytes express troponin I (red), a typical cardiomyocytes marker; nuclei were counterstained with Hoechst (blue). Unmerged images are reported in panels C and D (bars=100μm). Immunostaining for troponin I represented in the inset of picture B shows at higher magnification (40x) a developed contractile apparatus. (scale bar=75 μm).*

Four days after seeding, cardiomyocytes created aligned and organized cardiac myofibers expressing peculiar functional properties, i.e. synchronous contractile activity; the culture was maintained up to 10 days. Cell cultures (interferential image in Figure 7A) were stained for troponin I (Figure 7B-C) and the nuclei were marked with Hoechst (Figure 7B and 7D):

troponin was uniformly expressed and, as it was noticeable at higher magnification (inset picture of Figure 7B), a contractile apparatus was observable.

Figure 8 reports diagrams quantifying the contractions of the myofibers obtained through image analyses of representative movies. Panel 8A refers to satellite cells-derived fibers while 8B refers to cardio-myofibers. The measured mean extents of contraction and frequency are 1.6 µm, 2 Hz and 7.1 µm, 0.3 Hz respectively.

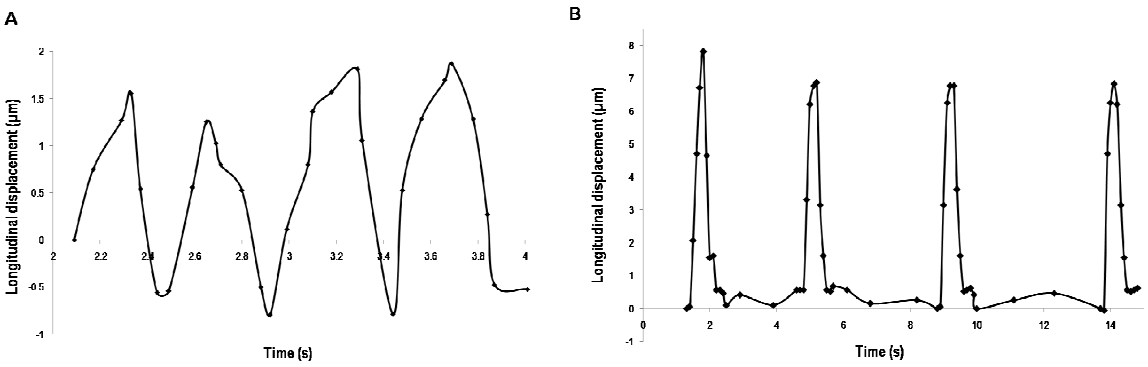

Figure 8. *Fibers contraction. The reported diagrams derive from image analyses of representative movies. Panel 8A refers to satellite cells-derived fibers while 8B refers to cardio-myofibers. The measured mean extents of contraction and frequency are 1.6 µm, 2 Hz and 7.1 µm, 0.3 Hz respectively. The longitudinal displacement is evaluated in the direction of the micropatterned lanes.*

B.4 Discussion

The objective of this study was to fabricate an *in vitro* model for cardiac and skeletal muscle fibers arranged in a high-throughput fashion for biological or physiological studies as well as for pharmacological screening tests. The essential pre-requisites to successfully achieve this goal can be summed up in two major issues: i) the fabrication of muscle substitutes that express correct markers and functional activity; and ii) the replication of this single muscle fiber in a large number of identical samples that can be used for high-throughput analyses.

In order to produce aligned muscle fibers we developed the µCP technique on soft substrates. Among many other possibilities, this technique couples simplicity and rapid realization timings with high accuracy and selectivity. Other techniques, such as micro-transfer molding (Suh et al. 2004) or the direct photo-lithography of hydrogels (Karp et al.

2006), can guide cell alignment through physical barriers and not through a functionalized area where cells can selectively adhere; thus, a potential limitation can be represented by the non-proper control over cell-surface interactions. In addition, microfluidic patterning of hydrogel surfaces proved to be successful for long-term cell adhesion only for collagen, that gelates under particular conditions (Gopalan et al. 2003) and are applicable only on geometries that show interconnected channels.

The μCP technique on soft hydrogel substrates developed here, is an easy, robust, reliable and versatile technique that enables to pattern different proteins on hydrogels with high spatial resolution.

PA hydrogels are biocompatible and non-fouling materials; the latter property allowed us to selectively drive cell adhesion on their surface by means of micro-contact printing technique used to create protein patterns. The realization of the laminin lanes by μCP led to an array of adhesive lanes, with accurate control of shape and size. Subsequent cell seeding all over the hydrogel surface resulted in an extremely selective adhesion of every cell type used, with cells only adhering to and spreading within the patterned regions.

The techniques and procedures proposed here have been demonstrated to be successful in culturing primary cell cultures as cardiomyocytes and satellite cells up to 10 days.

We showed for the first time that mouse satellite cells spread, proliferated and differentiated into aligned myotubes on a micro-patterned soft surface (Figure 5 and 6). The time required for satellite cell to fuse and differentiate into myotubes is 4-5 days, depending on the seeding density, and is completely compatible with the hydrogel structural and physical stability. Satellite cells adhered to laminin lanes, showed an elongated morphology, and a strong alignment, which is significantly different from what is observable in conventional *in vitro* culture (data not shown). After 4 days in culture, the newly formed myotubes show a fully developed sarcomeric structure, as Myhc is organized in the characteristic striations of the A-band of sarcomer. Moreover, they exhibited spontaneous and electrically induced contractions.

Even if newly formed myotubes were uniformly observed over the entire array of lanes, only part of the cell population possessed the potential to differentiate. The low efficiency of myotube formation is strongly related to the extraction and expansion methods of satellite cells, which cause a loss of their myogenic potential. As reported in the literature, rat satellite cells showed a decrease in the differentiation potential from cell isolation to the

third passage (from 46.7% to 12.5%) (Machida et al. 2004). To enhance myotube formation efficiency, we aim to develop and optimize a better isolation and expansion procedure resulting in a satellite cell population with a higher myogenic potential. It is worth emphasizing that the amount of myotubes obtained on our hydrogel substrates was comparable with that obtained on glass or standard Petri dishes (data not shown). Moreover, myotubes obtained on hydrogel were parallel-oriented and spatially separated, whereas those obtained on Petri dishes form a non-oriented and interconnected network. Even more significant, is the stage of differentiation that myotubes can reach on hydrogel substrate; as using a soft substrate as hydrogel enables the spatial organization of Myhc in the physiological structure of the sarcomere, the basic structural and functional contractile unit of muscle. Once again, this result is particularly significant as it opens new perspectives in developing an *in vitro* substitute for biological and pharmacological studies on skeletal muscle.

Cardiomyocytes were cultured on such patterned elastic substrate and guided to form aligned and organized cardiac myofibers (Figure 7). After 3 days of culture, it was demonstrated that cardiomyocytes to express the correct phenotypic markers and, after 4 days, exhibited spontaneous synchronous contractile activity. This result is particularly significant in view of the development of a model for drug testing or other biological studies.

The methodology that has been proposed shows intrinsic advantages over traditional cell arrays, which lack the typical and basic features of complex tissues such as heart and skeletal muscle. Those functional fibers can now be analyzed simultaneously and/or differentially, marking a step further in the study of the actual morphology, structure, behaviour, and responses to determined stimuli.

B.5 Conclusions

In our work, we produced an array of contractile cardiac myofibers and skeletal muscle myotubes starting from primary cells supported on protein patterned soft PA hydrogels. Both cardiac myofibers and skeletal muscle myotubes were part of an array composed of independent, spatially, and dimensionally controlled individual fibers. These array of fibers

can reproduce the particular features and maintain the information related to the functionality and structure of cardiac tissue and skeletal muscle more closely than the traditional *in vitro* cultures or cell array approaches, potentially becoming a useful candidate for accurate biological and physiological studies and opening new perspectives in the field of high-throughput pharmacological screenings.

B.6 Acknowledgments

This work was supported by MIUR, University of Padua, Regione Veneto (Azione biotech II), Città della Speranza.

B.7 References

1. Kozarova, A.; Petrinac, S.; Ali, A.; Hudson, J. W., Array of informatics: applications in modern research. *J Proteome Res* **2006,** 5, (5), 1051-1059.
2. Chen, D. S.; Davis, M. M., Molecular and functional analysis using live cell microarrays. *Curr Opin Chem Biol* **2006,** 10, (1), 28-34.
3. Brueggemeier, S. B.; Wu, D.; Kron, S. J.; Palecek, S. P., Protein-acrylamide copolymer hydrogels for array-based detection of tyrosine kinase activity from cell lysates. *Biomacromol* **2005,** 6, 2765-2775.
4. Chen, D. S.; Soen, Y.; Davis, M. M.; Brown, P. O., Functional and molecular profiling of heterogeneous tumor samples using a novel cellular microarray. *J Clin Oncol* **2004,** 22, 9507.
5. Albrecht, D. R.; Tsang, V. L.; Sah, R. L.; Bathia, S. N., Photo- and electropatterning of hydrogel-encapsulated living cell arrays. *Lab Chip* **2005,** 5, 111-118.
6. Flaim, C. J.; Chien, S.; Bhatia, S. N., An extracellular matrix microarray for probing cellular differentiation. *Nature Methods* **2005,** 2, 119-125.

7. Albrecht, D. R.; Underhill, G. H.; Wassermann, T. B.; Sah, R. L.; Bhatia, S. N., Probing the role of multicellular organization in three-dimensional microenvironments. *Nat Methods* **2006,** 3, (5), 369-375.
8. Jang, J. H.; Schaffer, D. V., Microarraying the cellular microenvironment. *Mol Syst Biol* **2006,** 2, (39).
9. Kaplan, D.; Moon, R. T.; Vunjak-Novakovic, G., It takes a village to grow a tissue. *Nat Biotechnol* **2005,** 23, (10), 1237-1239.
10. Vunjak-Novakovic, G.; Freed, L. E., Culture of organized cell communities. *Adv Drug Deliv Rev* **1998,** 33, (1-2), 15-30.
11. Motlagh, D.; Senyo, S. E.; Desai, T. A.; Russell, B., Microtextured substrata alter gene expression, protein localization and the shape of cardiac myocytes. *Biomaterials* **2003,** 24, (14), 2463 76.
12. Engler, A. J.; Griffin, M. A.; Sen, S.; Bönnemann, C. G.; LeeSweeney, H.; Discher, D. E., Myotubes differentiate optimally on substrates with tissue-like stiffness: pathological implications for soft or stiff microenvironments. *J Cell Biol* **2004a,** 166, 877-887.
13. Ingber, D. E., Mechanical signaling and the cellular response to extracellular matrix in angiogenesis and cardiovascular physiology. *Circ Res* **2002,** 91, (10), 877-887.
14. Ingber, D. E., Mechanical control of tissue growth: function follows form. *Proc Natl Acad Sci U S A* **2005,** 102, (33), 11571-11572.
15. Khatiwala, C. B.; Peyton, S. R.; Putnam, A. J., Intrinsic mechanical properties of the extracellular matrix affect the behavior of pre-osteoblastic MC3T3-E1 cells. *Am J Physiol Cell Physiol* **2006,** 290, (6), C1640-1650.
16. Falconnet, D.; Csucs, G.; Grandin, H. M.; Textor, M., Surface engineering approaches to micropattern surfaces for cell-based assays. *Biomat* **2006,** 27, 3044-3063.
17. Xia, Y.; Whitesides, G. M., Soft lithography. *Angew Chem Int Ed* **1998,** 37, 550-575.
18. Karp, J. M.; Yeo, Y.; Geng, W.; Cannizarro, C.; Yan, K.; Kohane, D. S.; Vunjak-Novakovic, G.; Langer, R. S.; Radisic, M., A photolithographic method to create cellular micropatterns. *Biomat* **2006,** 27, 4755-4764.
19. Rohr, S.; Scholly, D. M.; Kleber, A. G., Patterned growth of neonatal rat heart cells in culture. Morphological and electrophysiological characterization. *Circ Res* **1991,** 68, 114-130.
20. Suh, K. Y.; Seong, J.; Khademhosseini, A.; Laibinis, P. E.; Langer, R., A simple soft lithographic route to fabrication of poly(ethylene glycol) microstructures for protein and cell patterning. *Biomat* **2004,** 25, 557-563.
21. Gopalan, S. M.; Flaim, C.; Bhatia, S. N.; Hoshijima, M.; Knoell, R.; Chien, K. R.; Omens, J. H.; McCulloch, A. D., Anisotropic stretch-induced hypertrophy in neonatal ventricular myocytes micropatterned on deformable elastomers. *Biotechnol Bioeng* **2003,** 81, (5), 578-587.
22. Khademhosseini, A.; Eng, G.; Yeh, J.; Kucharczyk, P. A.; Langer, R.; Vunjak-Novakovic, G.; Radisic, M., Microfluidic patterning for fabrication of contractile cardiac organoids. *Biomed Microdevices* **2007,** 9, 149-157.
23. Vernon, R. B.; Gooden, M. D.; Lara, S. L.; Wight, T. N., Microgrooved fibrillar collagen membranes as scaffolds for cell support and alignment. *Biomat* **2005,** 26, 3131-3140.
24. Yim, E. K. F.; Reano, R. M.; Pang, S. W.; Yee, A. F.; Chen, C. S.; Leon, K. W., Nanopattern-induced changes in morphology and motility of smooth muscle cells. *Biomat* **2005** 26, 5405-5413.
25. Ruiz, S. A.; Chen, C. S., Microcontact printing: A tool to pattern. *Soft Matter* **2007,** 3, 1–11.

26. McDevitt, T. C.; Woodhouse, K. A.; Hauschka, S. D.; Murry, C. E., Spatially organized layers of cardiomyocytes on biodegradable polyurethane films for myocardial repair. *J Biomed Mater Res* **2003,** 66A, 586-595.
27. McDevitt, T. C.; Angello, J. C.; Whitney, M. L.; Reinecke, H.; Hauschka, S. D.; Murry, C. E.; Stayton, P. S., In vitro generation of differentiated cardiac myofibers on micropatterned laminin surfaces. *Journal of biomedical materials research* **2002,** 60, 472-479.
28. Britton-Keys, K.; Andreopoulos, F. M.; Peppas, N., Poly(ethylene glycol) star polymer hydrogels. *Macromolecules* **1998,** 31, 8149-8156.
29. Burdick, J. A.; Khademhosseini, A.; Langer, R., Fabrication of gradient hydrogels using a microfluidics/photopolymerization process. *Langmuir* **2004,** 20, 5153-5156.
30. Lin-Gibson, S.; Jones, R. L.; Washburn, N. R.; Horkay, F., Structure-property relationships of photopolymerizable poly(ethylene glycol) dimethacrylate hydrogels. *Macromolecules* **2005,** 38, 2897-2902.
31. Almany, L.; Seliktar, D., Biosynthetic hydrogel scaffolds made from fibrinogen and polyethylene glycol for 3D cell cultures. *Biomat* **2005,** 26, 2467-2477.
32. Leach, J. B.; Bivens, K. A.; Patrick, C. W.; Schmidt, C. E., Photocrosslinked hyaluronic acid hydrogels: natural, biodegradable tissue engineering scaffolds. *Biotechnol Bioeng* **2003,** 82, 578-5.
33. Leach, J. B.; Schmidt, C. E., Characterization of protein release from photocrosslinkable hyaluronic acid-polyethylene glycol hydrogel tissue engineering scaffolds. *Biomat* **2005,** 26, 125-135.
34. Hern, D.; Hubbell, J. A., Incorporation of adhesion peptides into nonadhesive hydrogels useful for tissue resurfacing. *J Biomed Mater Res* **1998,** 39, 266-276.
35. Engler, A.; Bacakova, L.; Newman, C.; Hategan, A.; Griffin, M.; Discher, D., Substrate compliance versus ligand density in cell on gel responses. *Biophys J* **2004b,** 86, 617-628.
36. Peyton, S. R.; Putnam, A. J., Extracellular matrix rigidity governs smooth muscle cell motility in a biphasic fashion. *J Cell Physiol* **2005,** 204, 198-209.
37. Pedram, A.; Razandi, M.; Aitkenhead, M.; Levin, E. R., Estrogen inhibits cardiomyocyte hypertrophy in vitro. Antagonism of calcineurin-related hypertrophy through induction of MCIP1. *J Biol Chem* **2005,** 280, (28), 26339–26348.
38. Speicher, D. W.; McCarl, R. L., Pancreatic enzyme requirements for the dissociation of rat hearts for culture. *In Vitro* **1974,** 10, 30-41.
39. Xiao, Y. F.; Gomez, A. M.; Morgan, J. P.; Lederer, W. J.; Leaf, A., Suppression of voltage-gated L-type Ca2+ currents by polyunsaturated fatty acids in adult and neonatal rat ventricular myocytes. *Proc Nat Acad Sci U S A* **1997,** 94, (8), 4182–4187.
40. Rosenblatt, J. D.; Lunt, A. I.; Parry, D. J.; Partridge, T. A., Culturing satellite cells from living single muscle fiber explants. *In Vitro Cell Dev Biol Anim* **1995,** 31, 773-779.
41. Machida, S.; Spangenburg, E. E.; Booth, F. W., Primary rat muscle progenitor cells have decreased proliferation and myotube formation during passages. *Cell Prolif* **2004,** 37, 267-277.

Appendix C

Enhancement of viability of muscle precursor cells on 3D scaffold in a perfusion bioreactor

Elisa Cimetta[1], Marina Flaibani[1], Marco Mella[1], Elena Serena[1], Luisa Boldrin[2], Paolo De Coppi[2], Nicola Elvassore[1]*

[a] Department of Chemical Engineering, University of Padua, Via Marzolo, 9 Padua, Italy

[a] Department of Pediatrics, University of Padua, Via Giustiniani, 3, Padua, Italy

*Corresponding author

The International Journal of Artificial Organs

Vol. 30 / no. 5, 2007 / pp. 415-428

Keywords: bioreactor, perfusion, dynamic culture, C2C12, satellite cells, skeletal-muscle precursor cells, three dimensional culture.

Abstract

The aim of this study was to develop a methodology for the *in vitro* expansion of skeletal-muscle precursor cells (SMPC) in a three dimensional (3D) environment in order to fabricate a cellularized artificial graft characterized by high density of viable cells and uniform cell distribution overall the 3D domain. Cell seeding and culture within 3D porous scaffolds by conventional static techniques can lead to a uniform cell distribution only on the scaffold surface, whereas dynamic culture systems have the potential of allowing a uniform growth of SMPCs within the entire scaffold structure.

In this work, we designed and developed a perfusion bioreactor able to ensure long term culture conditions and uniform flow of medium through 3D collagen sponges. A mathematical model to assist the design of the experimental set-up and of the operative conditions was developed. The effects of dynamic vs static culture in terms of cell viability and spatial distribution within 3D collagen scaffolds were evaluated at 1, 4 and 7 days and for different flow rates of 1, 2, 3.5 and 4.5 mL/min using C2C12 muscle cell line and SMPCs derived from satellite cells. C2C12 cells, after 7 days of culture in our bioreactor, perfused applying a 3.5 mL/min flow rate, showed a higher viability resulting in a three-fold increase when compared with the same parameter evaluated for cultures kept under static conditions. In addition, dynamic culture resulted in a more uniform 3D cell distribution. The 3.5 mL/min flow rate in the bioreactor was also applied to satellite cells derived SMPCs cultured on 3D collagen scaffolds. The dynamic culture conditions improved cell viability leading to higher cell density and uniform distribution through the whole 3D collagen sponge for both C2C12 and satellite cells.

C.1 Introduction

The *in vitro* reconstruction of engineered skeletal-muscle grafts holds the potential of becoming a new means for treating muscular diseases such as dystrophy and traumatic injuries (1), by improving muscle regeneration and overcoming the limitations of direct myoblast transplantation (2, 3). For these cell-mediated therapies, the engineered skeletal muscle graft must meet specific requirements such as high cell density and uniform cells distribution (4, 5). These new therapeutic strategies are limited by the lack of automatic, efficient and robust culture systems able to expand small biopsy-derived cells populations up to the large number of cells required for an *in vivo* implantation.

To date, for this expansion procedure, conventional culture systems such as Petri dishes and tissue culture flasks, are usually employed. Even if many studies on two-dimensional (2D) culture systems helped improving general knowledge on culture techniques and cells behaviour, 2D cultures show a poor efficiency and expensive implementation of cell expansion process at clinical level. In addition, 2D cultures cannot fully replicate the natural *in vivo* microenvironment affecting the viability, proliferation and functional differentiation of most types of cells (6). On the other hand, 3D cell culture methods using scaffolds as supporting materials can generate a micro-environment better resembling the *in vivo* conditions, improve cell survival and proliferation (7) and offer a means for potentially obtaining high cell density constructs. Scaffolds must respond to many specific requirements such as biocompatibility, adequate mechanical, physical and chemical properties and proper conformational structure. However, static 3D cultures face problems such as the inadequate mass transfer of nutrients and the limited gas species diffusion which, *in vivo*, are overcome by the functionality of the capillary net, the means by which gases and nutrients are exchanged, wastes removed and biochemical signals transported (8, 9). Thus, the supply of oxygen and nutritive elements to the *in vitro* growing grafts can be a strong limitation in their functionality and size (10). In order to overcome such limitations, new scaffold materials and geometries, combined with dynamic perfusion culture methods in different types of bioreactors have been developed (11-13).

Bioreactors have the purpose of granting the culture of cells in sterile, physiological and controlled conditions while ensuring, through the dynamic regime, a more efficient mass transfer of nutrient and gases between the cellularized scaffold and the culture medium and removal of debris. These specific features co-operate to obtain a more uniform cell distribution through the entire 3D structure of the supporting material (14, 15). Bioreactors have already proved useful in improving the quality of *in vitro* skin and cartilage, the main commercially available 3D tissue-engineered products (16, 17). In addition, the study of dynamic culture systems lead to the development of many different devices including: rotating vessels (18, 19), spinner flasks (20) and perfusion bioreactors (21, 22). Bioreactor designs can differ depending on the cell source and the aim of the study; and indeed many works have dealt with the optimization of the dynamic culture for cartilage, bone, cardiac and vascular tissues and liver (23). Only a limited number of studies involved the 3D culture of muscle cells in a bioreactor. Some of these works, for example, are focused on cell differentiation under mechanical stimuli using myoblasts seeded on microcarrier beads (24), on the improvement of the architecture of engineered cardiac tissues (25) or on smooth

muscle cells cultured on stretched scaffolds (26). All these works do not deal nor overcome the limitations related to the expansion of muscle precursor cells and the realization of an uniform density of undifferentiated cells in a 3D structure and aimed to be used for cell-mediated therapy. In none of these studies, to our knowledge, have muscle precursor satellite cells been used. Satellite cells are a pluripotent population of muscle progenitor cells located, in their quiescent phase, beneath the basement membrane of myofibers. Upon activation due to muscle damage and fibre injury, satellite cells begin to proliferate and can both differentiate into newly formed multinucleated myotubes and fuse with pre-existing damaged fibers repairing them (27-30). For these reasons, the satellite-derived muscle cells are good candidates for being used as a source for cell-mediated therapy (31).

The aim of this work was to design and develop a perfusion bioreactor studied to maintain high viability and proliferation of skeletal muscle precursor cells (SMPCs) seeded on three-dimensional scaffolds in sight of their employment in clinical cell therapies. We compared static and dynamically perfused cultures and, in optimizing operating conditions for our bioreactor, we evaluated the effects of different medium flow rates and culture time points on both cells viability and cells spatial distribution inside the scaffold. Preliminary investigations sought use of the C2C12 skeletal muscle immortalized cell line; and subsequently, the entire culture procedure has then been tested on satellite cells. In particular, being oxygen a strong limiting factor in the development of a 3D cellularized construct and in particular for muscular cells (32), we employed the use of a mathematical model to assist in the design and development of our bioreactor. In particular, this mathematical model describes the oxygen concentration at the outlet of the culture chamber as a function of the cell density and medium flow rates. The model simulations aided the choice of the optimal operating parameters and assessed the maintenance of the proper physiological condition, in terms of minimum concentration of oxygen in the culture chamber, during the entire culture time.

In this study, we have demonstrated how our bioreactor has succeeded in maintaining sterile culture conditions, efficient nutrients and gases transfer, a more uniform 3D cell distribution and a higher cell density when compared with static cultures. These results open a new perspective for the development of robust and automatic systems capable of expanding the small population of SMPCs harvested from a biopsy up to the suitable number of cells required for any biomedical use.

C.2 Material and Methods

C.2.1 Cell isolation and culture

C2C12.

The murine skeletal muscle immortalized cell line C2C12 (ATCC, USA) was grown in Dulbecco's modified Eagle's medium (DMEM, Sigma-Aldrich, Milano, Italy) supplemented with 10% foetal bovine serum (FBS, Gibco-Invitrogen, Milano, Italy), 1% penicillin-streptomycin solution (1000U/mL) and 1% L-glutamine (all from Invitrogen), on standard 100 mm Petri dishes, in a 95% humidified and 5% CO2 atmosphere at 37ºC and maintained at low confluence. The medium was regularly changed every three days.

Satellite cells.

Pure satellite cells cultures were obtained following the protocol previously described by Rosenblatt et al. in 1995, and performed in Stem Cell Processing Laboratory, Department of Pediatrics, University of Padua.

Briefly, *flexor digitorum brevis* mouse muscles were removed and enzymatically digested with 0.2% Collagenase Type I (Sigma-Aldrich). The single fibers were selected on an inverted microscope (Olympus IX71, Japan) and plated on Matrigel coated (BD Bioscience, California, USA) Petri dishes. Myofibers were maintained in a humidified tissue culture incubator. On day three, plating medium consisting of DMEM, 10% horse serum (Gibco-Invitrogen), 1% chicken embryo extract (MP-Biomedicals, Verona, Italy), 1% penicillin-streptomycin solution (1000U/mL), was added to the Petri dishes. After 72 more hours, culture medium was switched to proliferating, consisting of DMEM, 20% foetal bovine serum, 10% horse serum, 1% chicken embryo extract and 1% penicillin-streptomycin solution (1000U/mL). Cells were kept in culture with proliferating medium and detached from the plates with Trypsin (Gibco-Invitrogen) before fusion in myotubes occurred. Cells were then re-plated and expanded.

C.2.2 Scaffold characterization

The morphology of collagen sponges (Avitene® UltrafoamTM Collagen Hemostat. Davol inc., Cranston, USA) was analyzed using an Environmental Scanning Electron Microscope (ESEM, model XL30, Philips). Briefly, dried collagen sponges were gold sputtered under

high vacuum (0.05 mTorr) and photographs were taken at different magnifications ranging from 300x to 10,000x. The mean pore diameter R of 75 μm was estimated using a imaging software (Image Tool 3.0).

In order to evaluate the hydrodynamic conditions within the 3D collagen sponge, measurements of the scaffold void fraction and head loss through the scaffold were performed. The void fraction was roughly evaluated by gravimetrical measurements; the weight difference between a wetted and dry scaffold giving the amount of water filling the scaffold porosity.

Pressure drops through the scaffold were measured as a function of the medium flow rate ranging from 0.5 to 4.5 mL/min using a differential manometer. It is worth noting, that in this range of flow rates the collagen scaffold integrity and morphology were not altered. The experimental data were correlated by the following equation:

$$\Delta P = K \cdot Q \tag{1}$$

where ΔP is the pressure drop (Pa), Q the flow rate (mL/min) and K is a constant evaluated to be 7.4 (Pa min/mL).

Using this data, the scaffold permeability coefficient, k_s, was calculated from the Darcy's law for Newtonian fluid in a laminar flow regime through a porous media (33):

$$k_s = \frac{L_{sc} \cdot \mu}{A_{sc} \cdot K} = 30.54\ \mu m^2 \tag{2}$$

where μ = *0.80 cP* (34, 35) is the medium dynamic viscosity and $L_{sc} = 3\,mm$ and $A_{sc} = 177\,mm^2$ are length and cross section area of scaffold, respectively.

Assuming that the collagen sponge can be represented as a package of tangled micro-channels, the mean-velocity can be approximately considered uniform through the entire scaffold cross-section (33). Under these hypothesis and approximating our scaffold to a package of micro-channels with a radius corresponding to the mean pore radius $R = 75\ \mu m$ the maximum value of shear stress (τ_w) acting on the surface of a cell attached on the collagen tube wall can be estimated using the following empirical correlation (36):

$$\tau_w = \left(\frac{4\mu}{\pi}\right) \cdot \frac{Q_{ch}}{R^3} \quad (3)$$

where Q_{ch} is the volumetric flow rate in a single micro-channel.

C.2.3 Cell seeding

As the scaffold wettability can affect cell adhesion, the dry scaffolds (16 mm diameter and 3mm height cylinders) were pre-treated with 500 μl of culture medium inside standard 35 mm Petri dishes and incubated for 12 hours. Before cell seeding, the exceeding medium was removed by absorption with a sterile gauze.

Subconfluent plates of C2C12 and satellite cells were detached on day 0 using trypsin/EDTA, pelletted by centrifugation for 5 min at 1200 rpm and counted. In the experiments performed for the viability analyses 10^5 cells were suspended in 150 μl of culture medium and deposed over the scaffolds upper surfaces and incubated for 2 hours. In the experiments performed for the histological analyses, 10^6 C2C12 and $5 \cdot 10^5$ satellite cells were seeded following the same procedure. After the first incubation phase, 200 μl of medium were added at aliquots of 50 μl per hour. 2 mL of medium were finally added to the seeded scaffolds before the final incubation of 12 hours.

Considering the screening experiments done using the C2C12 cell line, we performed a total of 27 static cultures distributed in the different time points as follows: 4 at 1 day, 11 at 4 days and 12 at 7 days; the effect of different flow rates applied during dynamic culture (see Results) was evaluated on at least 2 replicas of the same experimental conditions at a 7 days time point. Finally, using the optimized flow rate, 14 dynamic runs were distributed in the different time points as: 4 at 1 day, 6 at 4 days and 4 at 7 days. Concerning satellite cells we ran 5 dynamic cultures and 4 static controls, all at a 7 day time point.

C.2.4 Bioreactor

The main requisites of the bioreactor can be summed as follows: i) homogeneous culture condition within the 3D domain; ii) a high cell density; iii) steady-state long-term cell culture. To achieve these objectives we needed to design a system in which the metabolites are evenly distributed within the entire 3D domain, the cells' uptake rate of metabolites are not limited by transport phenomena, and, in particular, the metabolite concentration must not change with time due to the increasing number of cells.

For these reasons, the design and development of the bioreactor was assisted by a mathematical modelling describing the time evolution of the oxygen concentration at the inlet and outlet of the culture chamber unit. Oxygen was chosen as it represents the most important metabolite for skeletal muscle precursor cells.

Experimental set up

Our dynamic culture system (Figure 1a) was composed of four units: a cell culture chamber, a gas-exchange unit, a medium reservoir and a peristaltic pump. The culture chamber was assembled with four Teflon (PTFE) parts and EPDM O-rings were used to prevent medium leaking as shown in Figure 1b. The seeded scaffold was positioned inside the cylindrical chamber between two 70 μm mesh stainless steel nettings. In order to have a simple and easily cleanable set up, the gas-exchange unit was made of a tubular non-porous permeable membrane (platinum cured silicone tubing, Vetrotecnica, Padova, Italy) wrapped around a custom made INOX-Teflon support. The medium reservoir was composed by a 200 mL Pyrex® glass laboratory bottle whose stopper was modified with the insertion of a PTFE block hosting the connections with the bioreactor and the gas exchanger and ensuring aseptical sealing. We used a Watson-Marlow peristaltic pump (314D model) to ensure stable and controllable flow of medium through the entire apparatus. The culture medium hold up of the system was approximately of 80 mL.

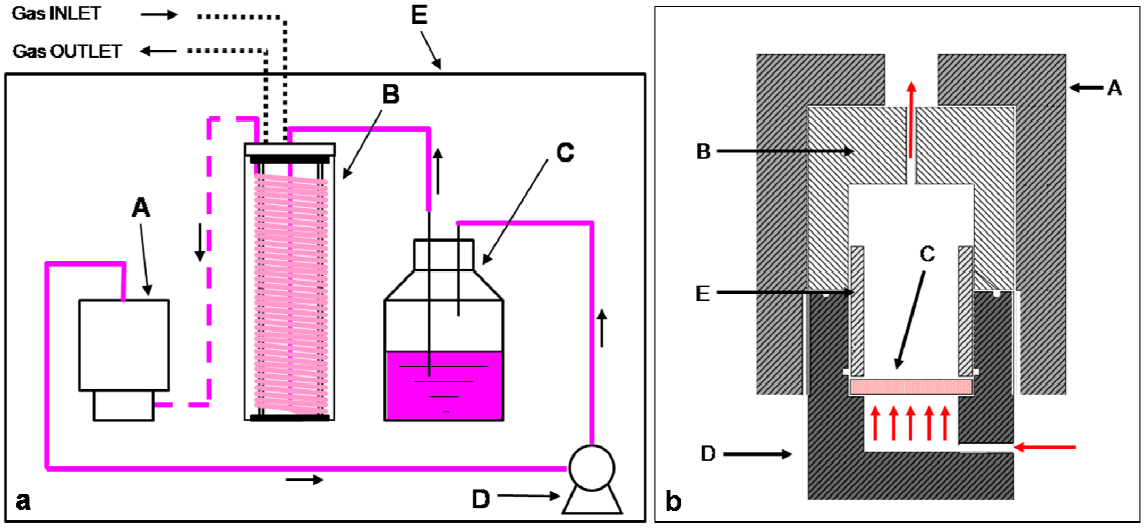

Figure 1. *Schemes of the experimental set up. Figure 1a shows culture apparatus scheme: A) culture chamber; B) Gas exchange unit; C) medium reservoir; D) peristaltic pump; E) air thermostatic bath. ▪▪▪) air tubing; - - -) tubing for oxygenated medium; ——) tubing from the bioreactor. The culture medium was withdrawn from the reservoir, fed into the gas exchange unit and, successively, into the culture chamber by a peristaltic pump.*

Figure 1b shows the detailed scheme of the culture chamber: A) screw cap; B) upper flange; C) collagen sponge between the two metallic net; D) lower flange; E) scaffold holder. Two O-rings (not drawn) were used: the first sealed the upper and the lower flange, the second avoided fluid leaking between the collagen scaffold and the culture chamber body. This experimental configuration ensured medium perfusion through the scaffold from the bottom to the top without external channelling. All connections were made with 1/8" INOX 316 junctions and silicone tubing.

All connections were made by 1/8" INOX 316 junctions and platinum-cured silicone tubing with an internal diameter of 3.2 mm and 1.6 mm wall thickness (Vetrotecnica, Padova, Italy).

The materials used ensured biocompatibility, non-reactivity and allowed the use of repeated autoclave sterilization cycles.

C.2.5 Model assisted design

As previously underlined, for muscular cells and skeletal muscle precursor cells in particular, oxygen is one of the most critical metabolites and has thus been chosen as the reference metabolite for the development of the mathematical model.

The bioreactor model framework can be reduced to a closed loop, shown in Figure 2, composed of two units: the cell-culture chamber and the membrane gas-exchanger. Inside

the culture chamber, the oxygen level decreases as a function of both the increasing number of cells and the decreasing medium flow rate, whereas it rises in the membrane gas-exchange units as function of the flow rate.

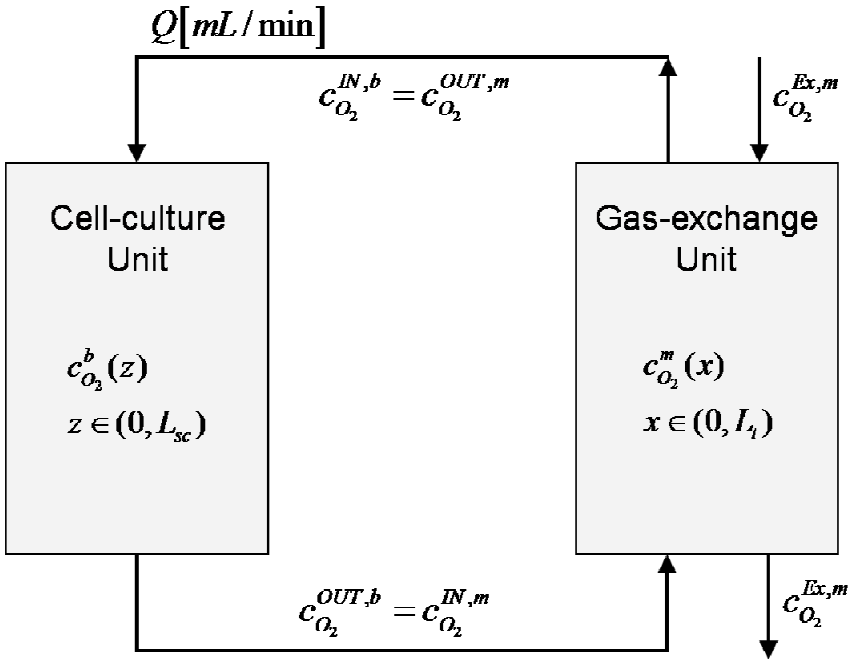

Figure 2. *Bioreactor model framework. The bioreactor apparatus, for modelling purposes, was reduced to a closed loop composed of two units: the cell-culture chamber and the membrane gas-exchanger. The variables and their dependences are explicitly listed.* $c_{O_2}^{b}(z)$ *and* $c_{O_2}^{m}(x)$ *are the oxygen concentration at a given axial coordinate z and x within the scaffold and the gas exchange unit, respectively.* L_{sc} *and* L_t *are the high of the scaffold and the length of the tubing of the membrane exchange unit, respectively. The superscripts OUT and IN refer to the and inlet section of both units.* $P_{O_2}^{Ex,m}$ *is the oxygen partial pressure in the atmosphere on the external side of the gas-exchange unit. Q is the flow rate of the recirculated medium.*

The mathematical model was obtained by simultaneously solving the steady-state mass balance equations governing the oxygen uptake rate in the cell culture chamber and the oxygen transfer rate in the membrane gas-exchange units. The results of the simulation gave the oxygen concentration at the outlet of the culture chamber as a function of the medium flow rate and the cell density.

The cell culture chamber.

The model considered a homogeneous oxygen uptake within the perfused 3D scaffold. We assumed the collagen scaffold to be a cylinder with a geometry which didn't change nor

degrade during the experiments. The oxygen consumption rate was assumed to follow a zero-order kinetic as oxygen profiles obtained using higher-order kinetics doesn't differ significantly (37). In particular, the oxygen uptake rate of a single cell in a resting muscular tissue is: $R_{O_2,tissue} = 4 \cdot 10^{-4}\ cm^3_{O_2} \big/ cm^3_{tissue} \cdot s$ (38). This uptake rate can be approximated to $R_{O_2,cell} = 0.21 \cdot 10^{-9}\ \mu L/s$ (µL at 298K and 0.1 MPa) or $R_{O_2,cell} = 8.59 \cdot 10^{-18}\ mol/s$ per cell, considering a cellular density of 1.06 gr/cm^3 (39) and an average cell diameter of 10 µm. In order to over-dimension our system, we referred our calculations to a maximum oxygen uptake rate of $R_{O_2} = 5 \cdot 10^{-9}\ \mu L/s$ or equivalently $R_{O_2} = 2.04 \cdot 10^{-16}\ mol/s$ per cell.

The culture medium was considered as an incompressible Newtonian fluid and its flow was oriented along the reactor length (z-direction) from the bottom to the top. The hydrodynamic regime was laminar and the calculated Reynolds number was *Re=5.9* for the flow rate of 3.5 mL/min. We have also evaluated (basing our calculations on formulations cited by Fournier (36)) that the hydrodynamic flow was fully developed in a laminar profile at any axial position before permeating the scaffold for any of the flow rates tested (data not shown).

Under the considerations listed above, the steady-state mass balance for the oxygen within the scaffold is:

$$-Q\frac{\partial c^b_{O_2}(z)}{\partial z} - R_{O_2}\rho_{cell}A_{sc} = 0 \qquad (4)$$

where $c^b_{O_2}(z)$ is the oxygen concentration at the generic cross section of the scaffold along the *z* coordinate, R_{O_2} is the oxygen uptake rate, ρ_{cell} the cell density, A_{sc} the scaffold cross section area and *Q* the medium flow rate.

Eq. (4) can be integrated from the inlet (z=0) to the outlet (z= L_{sc}) sections yielding to:

$$c^{OUT,b}_{O_2} = c^{IN,b}_{O_2} - R_{O_2}\rho_{cell}A_{sc}L_{sc}/Q = c^{IN,b}_{O_2} - A_2 \qquad (5)$$

where superscripts OUT and IN refer to the corresponding bioreactor sections, L_{sc} is the scaffold length and A_2 is a non-dimensional constant equal to $R_{O_2}\rho_{cell}A_{sc}L_{sc}/Q$.

Membrane gas-exchange unit.

The gas exchanger is a 10 m long silicone platinum cured tubing. The steady state mass balance of oxygen species, hypothesizing the concentration profile to be uniform in the radial direction and to vary along the tubing length is:

$$-Q\frac{\partial c_{O_2}^m(x)}{\partial x}+N_{O_2}(x)=0 \tag{6}$$

where $c_{O_2}^m(x)$ is the oxygen concentration along the tubing length coordinate x, varying from 0 to L_t, and Q is again the medium flow rate. The oxygen flux per unit length, N_{O_2}, can be expressed as:

$$N_{O_2}=K_0 2\pi R^{\text{int}}\left[P_{O_2}^{Ex,m}-Hc_{O_2}^m(x)\right] \tag{7}$$

Where K_0 is the global exchange coefficient, $R^{\text{int}}=1.6\cdot10^{-3}m$ is the tubing internal radius, $p_{O_2}^{Ex,m}=20.22kPa$ is the oxygen partial pressure in the atmosphere and H the Henry's constant for oxygen in the medium ($H=9,457\cdot10^4\ Pa\cdot m^3/mol$ (40)). Oxygen exchange can be seen as a three-step process: diffusion through the gas-phase, through the tubing walls and through the liquid phase. Assuming no-resistance in the gas phase, the global exchange coefficient, K_0, is expressed as follows:

$$\frac{1}{K_0}=\frac{H}{K_L}+\frac{1}{K_M} \tag{8}$$

Where $K_M=P_m/\delta$ (40) and K_L are the mass transfer coefficient in the membrane and in the liquid phase, respectively; $\delta=1.6\cdot10^{-3}\,m$ is the tubing wall thickness and P_m is the oxygen permeability ($P_m=2,84\cdot10^{-13}\,mol\cdot m/m^2\cdot s\cdot Pa$ (41)). K_L is evaluated considering that, for fluids under a laminar flow regime inside a cylindrical duct of length L and internal diameter, d_{ti}, we have (42):

$$K_L=\frac{D_{O_2}}{d_{ti}}1,62\left(\frac{d_{ti}^2\cdot\nu}{L_t\cdot D_{O_2}}\right)^{1/3} \tag{9}$$

where $D_{O_2} = 3.29 \cdot 10^{-9}\ m^2/s$ (43) is the oxygen diffusion coefficient in the culture medium and $\nu = 8.6 \cdot 10^{-7}\ m^2/s$ is the cinematic viscosity of culture medium (44).

Being that $c_{O_2}^{IN,b} = c_{O_2}^{OUT,m}$ and $c_{O_2}^{OUT,b} = c_{O_2}^{IN,m}$, substitution of Eq. 7 in Eq. 6 and integration of Eq.6 yields:

$$\frac{c_{O_2}^{IN,b} - P_{O_2}^{Ex,m}/H}{c_{O_2}^{OUT,b} - P_{O_2}^{Ex,m}/H} = \exp(-A_1) \tag{10}$$

Where A_1 is a non-dimensional constant equal to $K_0 2\pi R^{\text{int}} HL/Q$.

Rearranging Eq. (5) in Eq. (10) we obtain:

$$c_{O_2}^{IN,b} = \frac{P_{O_2}^{Ex,m}/H - \left(A_2 + P_{O_2}^{Ex,m}/H\right)}{1 - \exp(-A_1)} \tag{11}$$

$$c_{O_2}^{OUT,b} = c_{O_2}^{IN,b} - A_2 \tag{12}$$

Using Eq. 11-12 we evaluated oxygen concentration values at the inlet and outlet section of the cell culture chamber for the different flow rates of 0.01, 0.1, 1 and 10 cm3/min and different cell densities of 10^5, 10^6 and 10^7 per cm^3. We calculated the ratios of the variation of oxygen concentration between the two sections and the initial concentration at the inlet section.

C.2.6 Dynamic culture protocol

The start up operations of the dynamic culture system were the following: under a sterile hood the medium reservoir was filled with culture medium and sealed, the bioreactor chamber was opened and the first netting allowed in place using sterile tweezers. Twelve hours after seeding, the collagen scaffold was moved from the Petri dish and placed above the supporting netting with the seeded surface upside down; the second netting was then placed upon the collagen sponge. The culture chamber was then sealed and the entire apparatus moved to the thermostatic air bath where the gas exchange unit was connected to the gas cylinder supplying air-5% CO_2 and the tubing ducting the culture medium was

connected to the peristaltic pump. Finally, the pump was allowed to operate at a voltage corresponding to the desired flow rate.

For each scaffold kept under dynamic culture, at least one static control culture was performed following the same seeding procedure and incubated at 37°C, 95% humidity and 5% CO_2. Culture medium was changed every other day.

The culture time points for both dynamic and static controls have been 1, 4 and 7 days; the samples were then carefully removed from the bioreactor culture chambers or Petri dishes and processed for histological and viability assessment.

C.2.7 Cell viability

Cellular viability was measured with the MTT test (Sigma-Aldrich, St.Louis, USA): 300 µL of the dye solution containing 5 mg/mL of the tetrazolium salt MTT in PBS was diluted to a final volume of 3 mL with fresh PBS and added to the samples; 3 hours incubation at 37°C followed. After the removal of the dye solution, 3 mL of a solubilization solution made with 10% DMSO and 90% Isopropanol was added to lyse the cells and dissolve the formazan crystals. The samples were then placed inside the incubator at 37°C for a time allowing the complete dissolution and then centrifuged at 1200 rpm for 5 minutes to precipitate wastes. Clear solutions were processed for absorbance readings at 580 nm with an UV500 spectrophotometer, Spectronic Unicam (Cambridge, UK). In our range of absorbance, the recorded optical density (OD) was directly proportional to the number of viable cells.

C.2.8 Histological analysis

The samples were fixed in 4% PFA for 1 hour, rinsed thrice with PBS for 10 min and kept at +4°C covered by a thin layer of PBS. Before sectioning, fixed tissue specimens were dehydrated and embedded in paraffin. Sectioning was performed with a microtome and 7 µm thick sections of the cultured collagen matrices were analyzed both by Hematoxylin-Eosin (H-E) staining and Masson's trichrome staining using phosphomolybdic acid. Cell density and distribution within the scaffold were then assessed by microscope observations (inverted microscope Olympus IX51 Tokjo, Japan); images were captured and acquired using a JVC KY-F30 3-CC camera supported by Pinnacle, DVTools – Capture & Playback Application software.

C.2.9 Statistical analysis

Data are presented as histogram when only three replicates were available, whereas box plots are used in case of higher number of data. Briefly, box plots are statistical graphs in which the lower and upper lines of each box stand for the 1st and 3rd percentiles of the represented sample. The distance between the top and bottom of the box is the interquartile range. The middle line is the sample median, which is the 50th percentile of a given sample. The median is a robust estimate of the centre of a sample of data since it is affected very little by outlying points. A median not centred in the box is an index of skewness for the data. The vertical lines extending above and below the boxes show the distribution of the data falling outside the ranges cited above. Assuming no outliers, the maximum of the sample is the top of the upper whisker while the minimum is the bottom of the lower one. Values exceeding 1.5 times the interquartile range are represented with plus signs (+) and can be considered as outlier data.

One-way ANOVA test was used and $p<0.01$ was considered statically significant.

C.3 Results

A representative image of 3D collagen scaffold is reported in Figure 3, showing its high porosity; mean pore diameter estimated at 150±10μm, and void fraction evaluated by gravimetric analysis at approximately ε=97%. These properties ensured the availability of a high specific surface for cell adhesion within the 3D scaffold and consequently, the potential for obtaining a high cell density. However, as transport phenomena can be strongly limited by slow diffusion processes, we needed to develop dynamic culture conditions contributing to recreating a suitable microenvironment for cell adhesion, spreading and proliferation within the entire 3D domain of the scaffold.

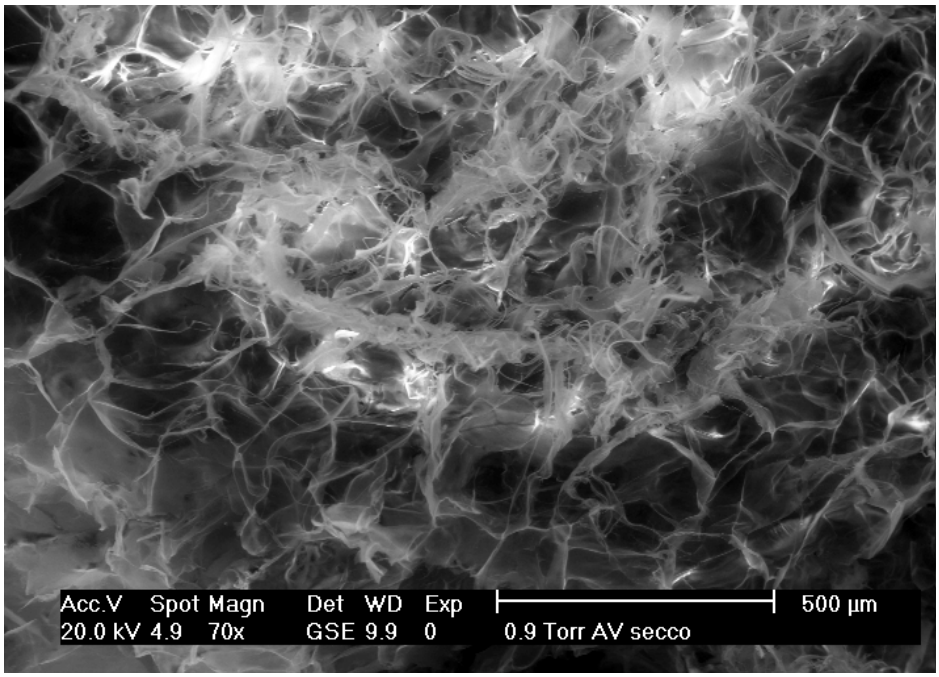

Figure 3. *ESEM micrograph of dry collagen scaffold at 70x magnification.*

The seeding procedure was optimized in order to achieve high cell adhesion on 3D collagen sponges for both C2C12 and satellite stem cells. The pre-treatment of the collagen scaffolds with culture medium helped in creating a more suitable environment for cells adhesion, such that the pre-wetted sponge was able to uniformly adsorb the 150 µL cell suspension used for seeding without showing preferential sites of adhesion. This seeding protocol valuably succeeded in granting cell adhesion without Matrigel coating, as its use, similarly of other chemically undefined reagents, may represent a limit for clinical applications.

For an *a priori* choice of medium flow rate we evaluated the oxygen concentrations at the inlet and outlet sections of the bioreactor culture chamber for the different flow rates of 0.01, 0.1, 1 and 10 cm3/min at the different cell densities of 10^5, 10^6 and 10^7 cell/cm^3. Figure 4 shows the fractional variation of oxygen concentration which is calculated as the oxygen concentration difference between the inlet and outlet sections normalized by the initial inlet concentration.

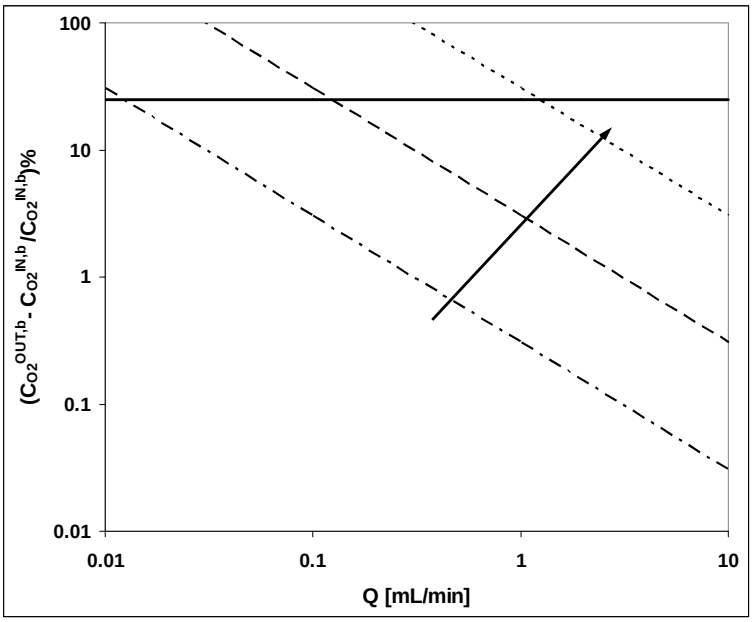

Figure 4. *Profiles of the variation of oxygen concentration from the inlet to the outlet section of the culture chamber normalized with respect to the inlet concentration, as a function of the medium flow rate calculated from Eq (11) and (12). Profiles are parametric in the cell density (cell/cm^3): ▪—▪) 10^5; — —) 10^6; ▪▪▪) 10^7. Upper horizontal line represents the threshold level of oxygen concentration that ensures a physiological value throughout the scaffold This value corresponds to the 40 mmHg partial pressure of oxygen in the interstial fluid, thus being the 26% of the initial saturation value. The parameters characterizing the graph region above such threshold assess proper physiological conditions for cells cultures during the perfusion experiments. Arrow indicates the direction of increasing cell density.*

Figure 4 shows that: 1) increasing the flow rate at constant cell density leads to a decrease in the percent variation of the oxygen concentration between the inlet and the outlet sections of the culture chamber; 2) increasing the cell density (see arrow) the curve shifts up, so that at the same flow rate, a higher cell density corresponds to higher variation of oxygen level between the inlet and the outlet sections.

The diagram shown in Figure 4 can prove very useful in verifying whether the operative variables in the culture chamber ensured viable cell culture conditions within the entire 3D domain of the scaffolds. For instance, the medium flow rate with a given cell density should yield to oxygen concentration at the outlet section higher than the physiological limit at any moment. The horizontal line, shown in Figure 4, represents the threshold of the physiological oxygen level (the partial pressure level of oxygen in the interstitial fluid of a resting tissue(36)) which is cautiously set to 5.33 KPa representing the 26% of the oxygen concentration value at the inlet section of the culture chamber. This latter value was verified to fairly approximate to the partial pressure of oxygen in the atmosphere.

Figure 5 shows a comparison between viabilities of C2C12 cells seeded on collagen sponges and cultured for 7 days in dynamic conditions at different medium flow rates ranging from 1 mL/min to 4.5 mL/min. A control is represented by C2C12 cells seeded onto identical collagen scaffolds at the same density and statically cultured changing media every other day.

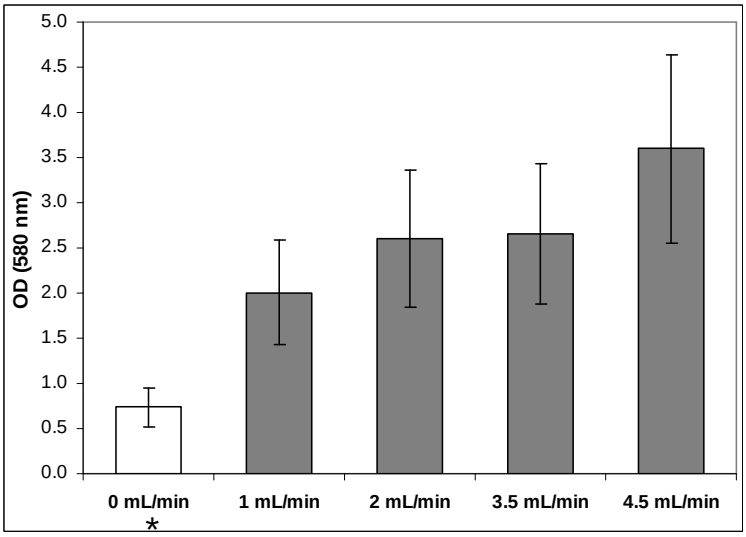

Figure 5. *Influence of medium flow rate ranging between 1mL/min and 4.5mL/min on C2C12 viability measured after 7 days of continuous culture in the bioreactor. (*) The column labelled "0mL/min" is an internal control which shows the viability of C2C12 cell statically cultured in 3D collagen sponges in standard Petri dishes.*

Figure 5 shows the significant differences between static and dynamic culture conditions, however there aren't noticeable differences between the various flow rates tested. Error bars are reported as 29% of mean values and represent an average of the measured errors on all the independent tests.

Considering the non-significant influence of the flow rate value, we chose to use 3.5mL/min in all following experiments. For this flow rate we calculated the mean perfusion velocity of medium through the scaffold being $330\ \mu m/\text{sec}$ and the shear stress being $0.14\ dyne/cm^2$. Literature reports *in vivo* shear stress values ranging between 1 and 100 $dyne/cm^2$ and a threshold of 10 $dyne/cm^2$ for the *in vitro* loosening of intercellular interactions (45).

Comparison between static and dynamic culture of C2C12 cells (Figure 6) showed how, at the earlier time points of 1 and 4 days, there were no significant differences in mean culture viabilities. Evaluating the 7th day results, we noticed how static culture viabilities were

comparable with those measured at 4 days, while dynamic conditions gave rise to a three-fold increment ($p = 4.3 \cdot 10^{-4}$). Moreover, viabilities of dynamic cultures measured at day 7 were significantly higher than the static ones at the same time point ($p = 8.3 \cdot 10^{-6}$).

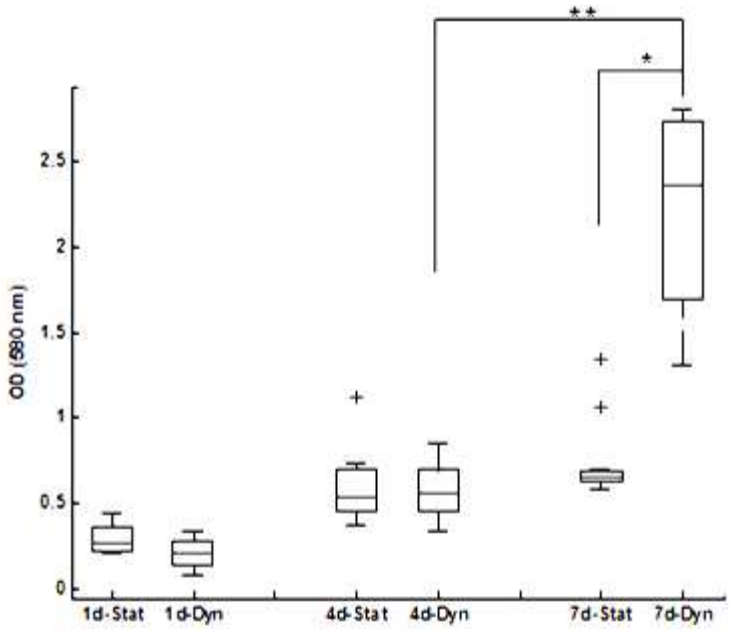

Figure 6. *Box plot graph shows the comparison between C2C12 cell viabilities cultured in static (Stat) and dynamic (Dyn) conditions after 1, 4 and 7 days. Values exceeding 1.5 times the interquartile range are represented with plus signs (+) and can be considered as outlier data. * $p = 8.3 \cdot 10^{-6}$; ** $p = 4.3 \cdot 10^{-4}$.*

The MTT semi-quantitative assay demonstrated a significant increment in cells viability after 7 days of dynamic culture but it was histological analysis which revealed the most interesting effect of the application of a perfusion bioreactor (Figure 7).

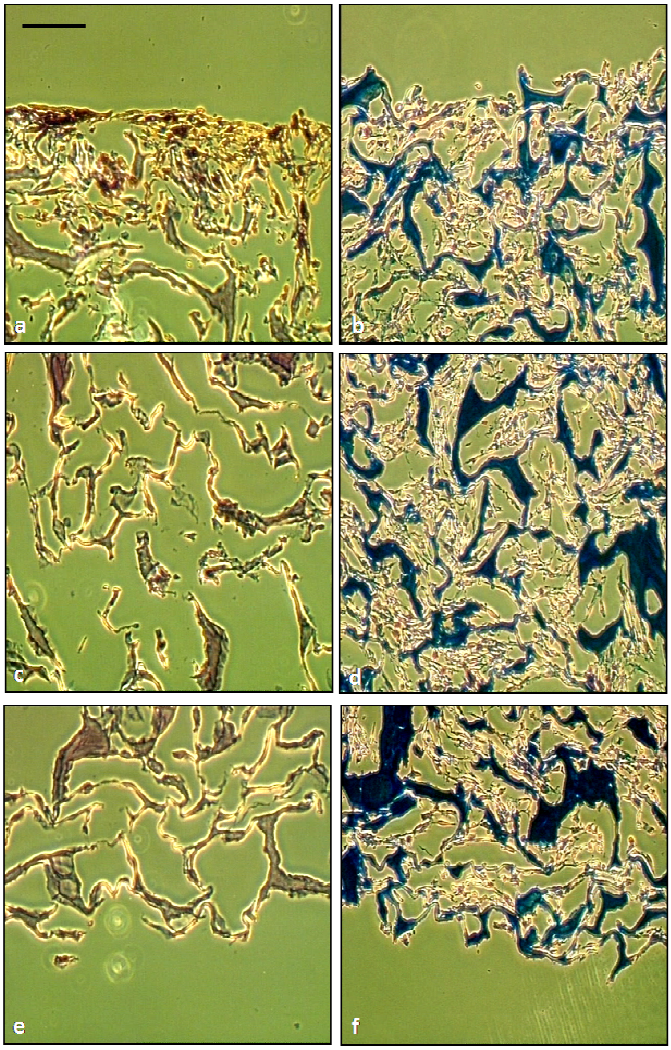

Figure 7. *Histology on 7µm thick cross sections of collagen sponges cultured with C2C12 cells stained with Masson's trichrome. The collagen matrix is stained blue, the nuclei are stained black and the cytoplasm is stained red. Left column (a; c; e) refers to a static control culture while right column (b; d; f) refers to a 7 days dynamic culture at a flow rate of 3.5mL/min. Picture a and b represent the seeded surface; c and d the central volume of the sponge; e and f the surface opposite to initial seeding. Magnification x100. Scale bar 200 µm.*

Statically cultured scaffolds resulted in a thick, high density layer of cells on the seeded surface (7a) while few or no cells at all could be seen in the core and bottom sections of the collagen sponge (7c and 7e respectively); on the contrary, histologies related to dynamic culture showed an uniform, high density cells distribution in the sequence of pictures covering the entire three-dimensional structure of the scaffold. Last, microscope observation of the culture medium performed after scaffold removal, proved that no cells detached during perfusion.

Our experiments on C2C12 cells allowed individuation of the optimal operating conditions in terms of seeding protocol, imposed medium flow rate and culture time points; with these data we undertook a preliminary study on satellite cells.

Figure 8 represents box plots showing the comparison between viabilities of satellite cells cultured in static and dynamic conditions using a medium flow rate of 3.5mL/min evaluated after 7 days of culture.

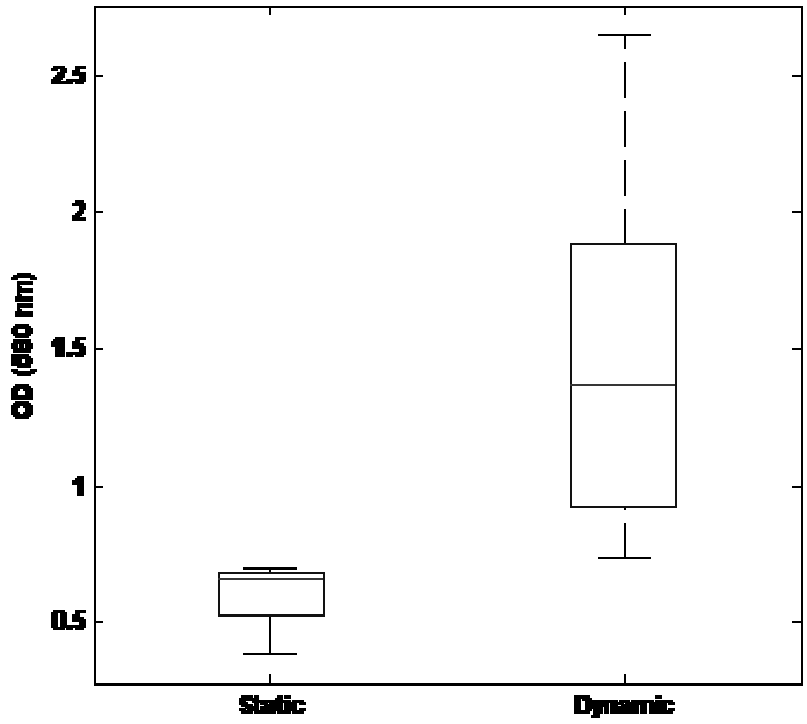

Figure 8. *Box plot graph shows the comparison between viabilities of satellite stem cell cultured in static and dynamic conditions (flow rate of 3.5mL/min) after 7 days ($p<0.06$).*

When cultured in our bioreactor, satellite cells expressed a 2.4 fold increase in their metabolic activity. Dynamic culture resulted again in a 3D construct with improved characteristics in terms of uniformity of cellular density (Figure 9).

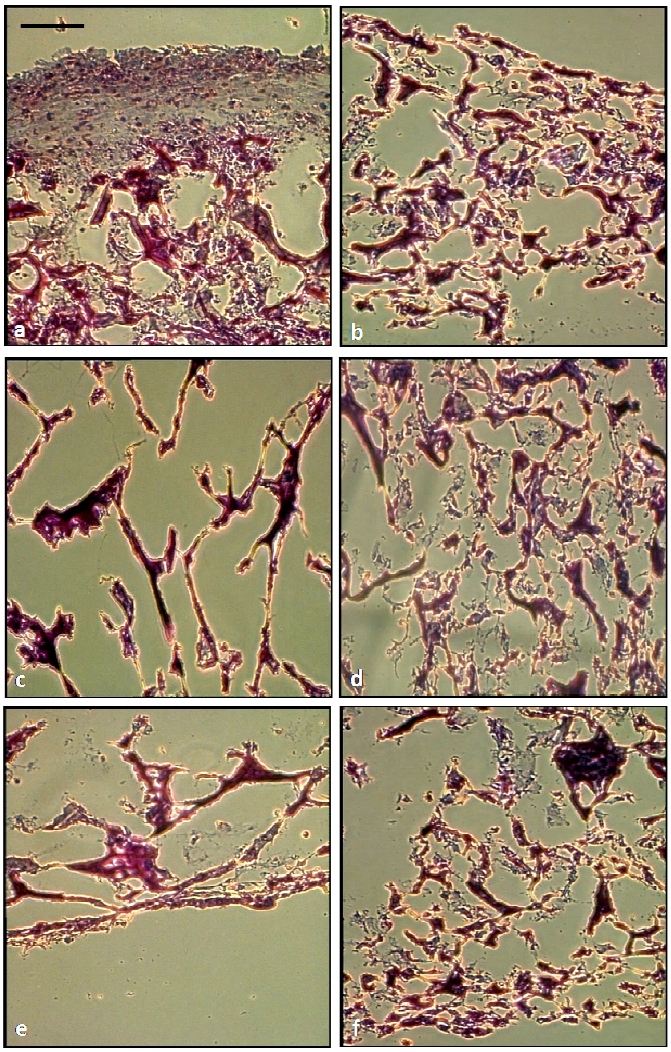

Figure 9. *Histology on 7µm thick transversal sections of collagen sponges cultured with satellite stem cells in static (a; c; e) and dynamic (b; d; f) conditions stained with Hematoxylin-Eosin. Nuclei are stained "blue" with hematoxylin. Cytoplasm, connective, and all other tissues are counterstained "red" with eosin. Pictures a and b represents the seeded surface; c and d the central volume of the sponge; e and f the surface opposite to initial seeding. Magnification x100. Scale bar 200 µm.*

C.4 Discussion

The development of a 3D cellular construct engineered starting from stem cell cultures becomes necessary in sight of possible future clinical application. The homogeneity of a 3D construct, in terms of cell density and cell phenotype, is fundamental to improve the success of skeletal muscle grafts. Focused on that aim, we recognize the importance of properly choosing all the materials involved in cell culture, of optimizing the seeding protocols and,

last but not least, finding and pointing the optimal values of the operating variable conditions at which the culture should be lead.

In this study we tested the properties of collagen scaffold: a natural and biocompatible material, relatively simple to process and with a high potential in sight of an *in vivo* utilization. Collagen scaffolds were confirmed to be appropriate for supporting 3D cultures because of its their diameter, high porosity and permeability(46).

Collagen proved to be a good support for cell growth also in granting a solid structure not suffering from the prolonged permanence under total perfusion culture conditions. The high material porosity did not hinder the flow of nutrients and gases and promoted cell diffusion thus resulting in a complete cellularization of the 3D sponge when cultured in dynamic conditions.

The cell seeding protocol has been optimized, in terms of timing and volume of medium, which yields an initially uniform cell distribution over the entire scaffold surface and reduces cell losses during all the operations up to the bioreactor start up.

We showed that all of the materials used to fabricate the bioreactor apparatus responded to our needs of biocompatibility, reliability, resistance to repeated high thermal stress due to autoclave sterilizations (thus avoiding employment of potentially toxic chemicals for sterilization) and prolonged usage.

Profiles of oxygen concentration variation from the inlet to the outlet sections of the bioreactor, normalized over the inlet concentration were calculated from Eq (11) and (12) (Figure 4). This graph confirms that the flow rates used in this study ensured physiological oxygen concentration in the outlet scaffold section for cell densities up to an approximated value of 108cell/cm3. Considering this finding and the low value of shear stress evaluated with equation (3), results reported in Figure 5 are not surprising. The flow rates tested are in a range that does not allow observation of significative differences in viability.

A relevant increase in viability of dynamically cultured cells compared with static control is noticeable after 7 days of culture while at earlier time points medium perfusion does not seem to have the same effect. This result can evidence of an initial “adaptative phase” which could be needed for cells cultured under dynamic conditions to adhere on the scaffold and start to proliferate.

We have demonstrated that dynamic conditions resulted in improved characteristics of the final cellularized construct not only in terms of cellular viability, but also of density and spatial distribution through the whole 3D scaffold. Histological analyses (Figure 7) proved

that perfusion can promote cell diffusion through the scaffold layers thus allowing a complete coverage of the sponge volume. Static culture, on the contrary, resulted in the formation of a thick layer of cells located on the seeding surface which constitutes a barrier hindering the further migration of proliferating cells inside the 3D construct. In addition, diffusion alone can not fulfil nutrient demands of the growing cells without cooperation of the convective flow deriving from medium perfusion. We thus unequivocally demonstrated how dynamic culture assured a more efficient mass transfer leading to cellular constructs with improved properties. In our previous work (47), we have shown through a mathematical modelling of 3D cell cultures in perfusion bioreactors the fundamental role of metabolite mass transport on cell growth and proliferation.

Finally, preliminary experiments demonstrated how our culture system proved to be reliable in granting suitable conditions for the survival and proliferation even of a primary cell culture such as that of satellite cells. Nevertheless, in underlining the increased variability of the resulting data we note that operative conditions tested with the C2C12 cell line does not necessarily correspond to an optimum for satellite cells. Consequently, a further step will be a deeper insight in monitoring satellite cells' behaviour under dynamic culture conditions and their response in terms of viability following variations in culture parameters such as medium flow rate and culture time point. Our 3D collagen scaffolds recreated a microenvironment which was suitable for satellite cells, promoting adhesion, maintaining viability and proliferation. Dynamic culture served the purpose of increasing viability and giving rise to a uniformly and densely cellularized 3D construct. A recent work confirms how transplantation of muscle precursor cells seeded on a scaffold improves muscle regeneration more than direct cell injection (48). In addition, the efficacy of other cell therapy approaches employing different cell sources and interacting factors(49, 50) could be improved and increased by the usage of 3D scaffolds and the dynamic perfusion conditions developed in bioreactors. Interesting future directions would involve the use of oriented scaffolds in sight of the obtainment of an aligned structure and a network of microchannels mimicking the vascular network existing *in vivo*, an essential feature for a capillary delivery of metabolites and for a more efficient waste removal. Combining all these fundamental issues highlights how the employment of dynamically cultured 3D scaffolds for *in vivo* transplantation seeded with muscle precursor cells could highly increase and help natural host tissue repair and regeneration.

C.5 Acknowledgement

We would like to thank Dr. G. Abatangelo and Dr. B. Zavan for their collaboration in histological analyses and MIUR, University of Padova and Fondazione Città della Speranza for financial support.

C.6 References

1 Bach AD, Beier JP, Stern-Staeter J and Horch RE. Skeletal muscle tissue engineering. Journal of Cell. Mol. Med 2004; 8(4):413-422

2 Partridge TA. Invited review: myoblast transfer: a possible therapy for inherited myopathies? Muscle Nerve 1991; 14(3):197-212

3 Huard J LY, Fu F. H. Muscle Injuries and Repair: Current Trends in Research. J. Bone Joint Surg. Am. 2002; 84(822-832

4 Carrier RL, Papadaki M, Rupnick M, Schoen FJ, Bursac N, Langer R, et al. Cardiac tissue engineering: Cell seeding, cultivation parameters, and tissue construct characterization. Biotechnology and Bioengineering 1999; 64(5):580-589

5 Okano T and Matsuda T. Muscular tissue engineering: capillary-incorporated hybrid muscular tissues in vivo tissue culture. Cell Transplantation 1998; 7(5):435-442

6 Freed LE and Vunjak-Novakovic G. Culture of organized cell communities. Advanced Drug Delivery Reviews 1998; 33(1-2):15-30

7 Hill E, Boontheekul T and Mooney D. Designing Scaffolds to Enhance Transplanted Myoblast Survival and Migration. Tissue Engineering 2006; 12(5):1295-1304

8 De Coppi P, Delo D, Farrugia L, Udompanyanan K, Yoo JJ, Nomi M, et al. Angiogenic Gene-Modified Muscle Cells for Enhancement of Tissue Formation. Tissue Engineering 2005; 11(7-8):1034-1044

9 Nomi M, Atala A, De Coppi P and Soker S. Principals of neovascularization for tissue engineering. Molecular Aspects of Medicine 2002; 23(6):463-483

10 Lewis MC, MacArthur BD, Malda J, Pettet G and Please CP. Heterogeneous proliferation within engineered cartilaginous tissue: the role of oxygen tension. Biotechnology and Bioengineering 2005; 91(5):607-615

11 Figallo E, Flaibani M, Zavan B, Abatangelo G and Elvassore N. Micropatterned Biopolymer 3D Scaffold for Static and Dynamic Culture of Human Fibroblasts. Biotechnol Prog 2007; 23(1):210-6

12 Cha JM, Park S-N, Park G-O, Kim JK and Suh H. Construction of Functional Soft Tissues From Premodulated Smooth Muscle Cells Using a Bioreactor System. Artificial Organs 2006; 30(9):704-707

13 Marolt D, Augst A, Freed LE, Vepari C, Fajardo R, Patel N, et al. Bone and cartilage tissue constructs grown using human bone marrow stromal cells, silk scaffolds and rotating bioreactors. Biomaterials 2006; 27(36):6138-6149

14 Papadaki M, Bursac N, Langer R, Merok J, Vunjak-Novakovic G and Freed LE. Tissue engineering of functional cardiac muscle: molecular, structural, and electrophysiological studies. Am J Physiol Heart Circ Physiol 2001; 280(1):H168-178

15 Radisic M, Park H, Shing H, Consil T, Schoen FJ, Langer R, et al. Functional assembly of engineered myocardium by electrical stimulation of cardiac myocytes cultured on scaffolds. Proc Natl Acad Sci U S A 2004; 101(52):18129-34

16 Kuo CK, Li W-J, Mauck RL and Tuan RS. Cartilage tissue engineering: its potential and uses. Current Opinion in Rheumatology 2006; 18(1):64-73

17 Mansbridge J. Commercial considerations in tissue engineering. Journal of Anatomy 2006; 209(4):527-532

18 Freed LE, Hollander AP, Martin I, Barry JR, Langer R and Vunjak-Novakovic G. Chondrogenesis in a Cell-Polymer-Bioreactor System. Experimental Cell Research 1998; 240(1):58-65

19 Gooch KJ, Blunk T, Courter DL, Sieminski AL, Bursac PM, Vunjak-Novakovic G, et al. IGF-I and Mechanical Environment Interact to Modulate Engineered Cartilage Development. Biochemical and Biophysical Research Communications 2001; 286(5):909-915

20 Vunjak-Novakovic G, Obradovic B, Martin I, Bursac PM, Langer R and Freed LE. Dynamic Cell Seeding of Polymer Scaffolds for Cartilage Tissue Engineering. Biotechnol. Prog. 1998; 14(2):193-202

21 Bancroft GN, Sikavitsas VI and Mikos AG. Technical Note: Design of a Flow Perfusion Bioreactor System for Bone Tissue-Engineering Applications. Tissue Engineering 2003; 9(3):549-554

22 Cartmell SH, Porter BD, Garcia AJ and Guldberg RE. Effects of Medium Perfusion Rate on Cell-Seeded Three-Dimensional Bone Constructs in Vitro. Tissue Engineering 2003; 9(6):1197-1203

23 Bilodeau K and Mantovani D. Bioreactors for Tissue Engineering: Focus on Mechanical Constraints. A Comparative Review. Tissue Engineering 2006; 12(8):2367-2383

24 Torgan C, Burge S, Collinsworth A, Truskey G and Kraus W. Differentiation of mammalian skeletal muscle cells cultured on microcarrier beads in a rotating cell culture system. Med Biol Eng Comput 2000; 38(5):583-590

25 Carrier R, Rupnick M, Langer R, Schoen F, Freed L and Vunjak-Novakovic G. Perfusion Improves Tissue Architecture of Engineered Cardiac Muscle. Tissue Engineering 2002; 8(2):175-188

26 Cha J, Park S-N, Park G-O, Kim J and Suh H. Construction of Functional Soft Tissues From Premodulated Smooth Muscle Cells Using a Bioreactor System. Artificial Organs 2006; 30(9):704-707

27 Asakura A, Komaki M and Rudnicki M. Muscle satellite cells are multipotential stem cells that exhibit myogenic, osteogenic, and adipogenic differentiation. Differentiation 2001; 68(4-5):245-253

28 Conconi MT, Coppi PD, Bellini S, Zara G, Sabatti M, Marzaro M, et al. Homologous muscle acellular matrix seeded with autologous myoblasts as a tissue-engineering approach to abdominal wall-defect repair. Biomaterials 2005; 26(15):2567-2574

29 De Coppi P, Bellini S, Conconi MT, Sabatti M, Simonato E, Gamba PG, et al. Myoblast-Acellular Skeletal Muscle Matrix Constructs Guarantee a Long-Term Repair of Experimental Full-Thickness Abdominal Wall Defects. Tissue Engineering 2006; 12(7):1929-1936

30 Partridge TA. Cells that participate in regeneration of skeletal muscle. Gene Therapy 2002; 9(11):752-753

31 Boldrin L, Elvassore N, Malerba A, Flaibani M, Cimetta E, Piccoli M, et al. Satellite Cells Delivered by Micro-Patterned Scaffolds: A New Strategy for Cell Transplantation in Muscle Diseases. Tissue Eng 2006;

32 Portner R, Nagel-Heyer S, Goepfert C, Adamietz P and Meenen N. Bioreactor Design for Tissue Engineering. Journal of Bioscience and Bioengineering 2005; 100(3):235-245

33 Bird RB, Stewart WE and Lightfoot EN. Transport Phenomena. Second John Wiley & Sons, inc.; 2002

34 Bacabac RG, Smit T-H, Cowin SC, Loon JJWAV, Nieuwstadt FTM, Heethaar R, et al. Dynamic shear stress in parallel-plate flow chambers. Journal of Biomechanics 2005; 38(159-167

35 Gosgnach W, Messika-Zeitoun D, Gonzalez W, Philipe M and Michel J-B. Shear stress induces iNOS expression in cultured smooth muscle cells: role of oxidative stress. Am J Physiol Cell Physiol 2000; 279(6):C1880-1888

36 Fournier RL. Basic Transport Phenomena in Biomedical Engineering. Lillington, NC: Edwaed Brothers; 1998

37 Chow DC, Wenning LA, Miller WM and Papoutsakis ET. Modeling pO(2) distributions in the bone marrow hematopoietic compartment. II. Modified Kroghian models. Biophys J. 2001; 81(2):685-96

38 Salathe EP and Gorman AD. Modelling oxygen concentration in skeletal muscle. Mathematical computing modelling 1997; 26(4

39 Richardson RS. Oxygen transport and utilization: an integration of the muscle system. Advances in physiology education 2003; 27(4):183-191

40 Perry RH and Green DW. Perry's chemical engineers' handbook. Seventh Mc Graw-Hill International; 1998

41 Brandrup J, Immergat EH and Grulke EA. Polymer handbook. IV Wiley Interscience publication; 1999

42 Cussler EL. Diffusion: Mass Transfer in Fluid System. Second Cambridge University Press; 1997

43 Zhao F, Pathi P, Grayson W, Xing Q, Locke BR and Ma T. Effects of Oxygen Transport on 3-D Human Mesenchymal Stem Cell Metabolic Activity in Perfusion and

Static Cultures: Experiments and Mathematical Model. Biotechnol. Prog. 2005; 21(4):1269-1280

44 Sen A, Kallos MS and Behie LA. Expansion of mammalian neural stem cells in bioreactors: effect of power input and medium viscosity. Developmental Brain Research 2002; 134(103-113

45 Reutelingsperger CPM, Van Gool RGJ, Heijnen V, Frederik P and T. L. The rotating disc as a device to study the adhesive properties of endothelial cells under differential shear stresses. J. Matr Sci.: Mater. In Medicine 1993; 5(6-7):361-367

46 Desai TA. Micro- and nanoscale structures for tissue engineering constructs. Medical Engineering & Physics 2000; 22(9):595-606

47 Coletti F, Macchietto S and Elvassore N. Mathematical modeling of three-dimensional cell cultures in perfusion bioreactors. Industrial & Engineering Chemistry Research 2006; 45(24):8158-8169

48 Hill E, Boontheekul T and Mooney D. Regulating activation of transplanted cells controls tissue regeneration. Proc Natl Acad Sci U S A 2006; 103(8):2494-2499

49 Deasy B M LYaHJ. Tissue engineering with muscle-derived stem cells. Current Opinion in Biotechnology 2004; 15(419–423

50 Urish K KY, Huard J. Initial failure in myoblast transplantation therapy has led the way toward the isolation of muscle stem cells: potential for tissue regeneration. Current Topics in Developmental Biology 2005; 68(263-280

Appendix D

Muscle differentiation and myotubes alignment is influenced by micro-patterned surfaces and exogenous electrical stimulation

Marina Flaibani[*1], Luisa Boldrin[*2], Elisa Cimetta[1], Martina Piccoli[2], Paolo De Coppi[2,3], Nicola Elvassore[1^]

[1]Department of Chemical Engineering, University of Padova, via Marzolo 9, 35100, Padova, Italy

[2]Stem Cell Processing Laboratory and Division of Paediatric Surgery, Department of Paediatrics, University of Padova, via Giustiniani 3, 35128, Padova, Italy

[3]Surgery Unit, UCL Institute of Child Health and Great Ormond Street Hospital, 30 Guilford Street, London WC1N 1EH, UK

[*] These authors contributed equally to this work

^ Corresponding authors

Tissue Engineering in press

Abstract

An in vitro muscle-like structure with parallel-oriented contractile myotubes is needed as a model of muscle tissue regeneration. For this purpose it is necessary to reproduce a controllable microscale environment mimicking the *in vivo* cues.
In this work we focused on the application of topological and electrical stimuli on muscle precursor cell (MPC) culture in order to influence MPC orientation and induce myotube alignment. The two stimulations were tested both independently and together. A structural and topological template was achieved by using micro-patterned PLA membranes. Electrical stimulation, consisting of square pulses of 70mV/cm amplitude each 30s, was applied to the MPC culture. The effect of different pulse durations on cultured was evaluated by galvanotaxis analysis. The highest cell displacement rate towards the cathode was observed for 3ms pulse stimulation, which was then applied in combination with topological stimuli. Topological and electrical stimuli had an additive effect in enhancing differentiation of cultured MPC, shown by high Troponin I protein production and, in parallel, Myogenin and Desmin genes respectively down and up-regulation.

D.1 Introduction

The ability of adult skeletal muscle to regenerate, even after total disruption (1), is mainly due to the principal muscle stem cells, called satellite cells for their distinct localization, in the quiescent state, between the sarcolemma and the basal lamina of each myofibre (2-4). In response to growth or tissue regeneration stimuli, satellite cells efficiently activate to proliferate and differentiate in muscle precursor cells (MPCs), in order to repair muscle tissue. Because of their self-renewal, high proliferative and multi-potent capability, satellite cells can be a suitable cell source for muscle cell therapy, tissue engineering and drug screening (5-8).

The single myofibre technique allows the *in vitro* activation of satellite cells and MPC proliferation and expansion. In this way, MPC growth can be controlled, by means of a micro-scale environment: a complex system defined by means of biochemical and mechanical cues, as well as morphological and electrical signals produced by cultured cells, which function as physical anchor and generate many extrinsic factors (9).

Recent reports highlight an increasing knowledge about satellite cell behaviour, in particular with respect to both *in vivo* and *in vitro* biochemical signal effects (10-12). However, few studies have so far investigated the effect of physical stimulations on MPCs. In particular it has been reported the influence of mechanical stimuli on myotube alignment obtained from myoblasts seeded on elastic membranes or between artificial tendons (13, 14) and appropriate scaffold micro-patterns were found to influence myotubes orientation, allowing parallel alignment of C2C12-derived myotubes (15, 16). *In vitro* mechanical stretch can also influence muscle differentiation triggering an intracellular signalling cascade which results in HGF release and satellite cell activation (17), in analogy with what happens *in vivo* when a muscle is passively stretched (18).

These findings highlight that it is possible to reproduce *in vitro* a muscle-like environment, where adult stem cells integrate and respond to structural and topological organization of micro-scale environment surrounding the cells (19).

Furthermore, electrical stimuli were also recently been applied to different cell types proving their large effect on cell behaviour (20). *In vitro* 2D studies showed that chronic electrical stimulation, mimicking neuronal activity, promoted the maturation of primary muscle cultures in terms of the expression of adult myosin heavy chain (MHC) slow isoform (21, 22). On the other hand, in 3D culture an increment in cell proliferation (23) and a reduced expression of myogenic genes (MyoD, Myogenin and AChR-□) have been observed following electrical stimulation (24). So far, electrical stimuli have been applied *in vitro* to primary cultures on standard plate (21, 22) or non-organized 3D-scaffold (23, 24).

All reported works about the influence of biochemical, mechanical and electrical stimuli on muscle cell culture are mainly focused on describing the effect of one type of stimulus at a time; however, it is well known that response to a particular stimulus can be different depending not only on cell type but also on cell-cell interactions and the surrounding multiplicity of micro-environment cues, *in vitro* as *in vivo* (25). In addition, these stimuli need to be coupled with an adequate extracellular structural template to give rise to functional tissue with directed force production (26).

In this work, we suggest that the application of electrophysiological stimuli can play an important role in skeletal muscle cell differentiation as previously demonstrated in both cardiac (27, 28) and neuronal environments (20). We thus designed the exogenous electric

field specifically to mimic the electrophysiological neuronal activity *in vivo* and combined it to the application of a micro-patterned support in order to reproduce a muscle-like morphology domain. The micro-patterned scaffold coupled to the electrical stimulation proved to be an efficient tool to induce MPC orientation and differentiation.

D.2 Materials and Methods

D.2.1 Single fibre isolation and culture

Single myofibers were isolated from Flexor Digitorum Brevis (FDB) muscles of Wistar rats (Charles River, USA) (n=8). As previously described (29), removed muscles were rinsed in PBS (GIBCO, Invitrogen LifeTecnologies, UK) and digested for 3 hours at 37° C with collagenase type I 0.2% (w/v) (Sigma-Aldrich, USA). Following digestion, muscles were transferred into plating medium, consisting of DMEM supplemented with 10 % (v/v) horse serum (HS) (GIBCO) and 1 % (v/v) chicken embryo extract (CEE) (MP Biomedicals, Irvine, CA, USA). Muscles were triturated with a wide-bore pipette to release single myofibers which were then individually selected under an inverted microscope (Olympus IX51, Tokjo, Japan), placed on dishes pre-coated with 1 mg/ml Matrigel (Falcon, BD Biosciences, San Jose, CA, USA) and cultured at 37.5°C, 5% CO2. Two days after seeding, the plating medium was replaced with proliferating medium, consisting of DMEM containing 20% of foetal bovine serum (FBS) (GIBCO), 10 % of HS and of 0.5% of CEE. Medium was changed every 2-3 days.

D.2.2 Cytofluorimetric analysis

Immunofluorescence analyses were performed on expanded rat muscle precursors cells (rMPC) before cell fusion. One million rMPC were detached using citrate buffer solution (Sigma-Aldrich), washed in PBS and stained for 10 minutes at 4°C with FITC or PE conjugated antibodies against CD29, CD31, CD44, CD73, CD90 (BD Pharmingen, Italy), CD45 (Immunotech, Coulter company, France). Staining with antibodies against CD54 (BD Pharmingen) and MHCII (Immunotech) were performed at room temperature for 1 hour and, after washing in PBS, secondary antibodies FITC or PE conjugated (Invitrogen) were added for 30 minutes at room temperature. Analyses were performed on three replicates of

two different MPC preparations with a Coulter EPICS-XL (Beckman Coulter, Marseille, France) using EXPOTM 32 ADC Software.

D.2.3 Micro-patterned membrane fabrication

Micro-patterned (MP) membranes were fabricated using poly-(L-lactic acid) (PLA, Resomer L206, Molecular weight 102kDa, Boehringer Ingelheim Pharma, Germany) by a soft-lithography technique (19, 30) adapting a procedure previously described by Kane (31). Briefly, silicon wafers (500µm thick by Wacko, Germany) surface was oxidized by nitric acid solution for 24h and thermally treated at 180°C for 12h. Thin films of photoresist (EPON SU-8 100 from Microchem Corp., Newton, MA) were uniformly deposed on silicon wafers using a Delta 10 spin-coater (BLE, Germany). The micro-patterned was design with Adobe Illustrator 10.0 and printed on a transparency film photomask; the geometry was composed of parallel lanes of 200x50µm rectangles spaced of 30µm and 60µm between short and long sides respectively (Fig.1A). The 30µm spaces were necessary to give structural consistency to the final polymeric membrane and their dimension was the smaller one allowed by technical limitation. Photoresist-coated silicon wafers were thermally pre-treated, exposed to UV light (UV Philips lamp HPR 125W) through the photomask for the proper time and thermally treated to prevent photoresist mechanical stresses. The photo-resist was developed with 1-methoxy-2-propanol acetate (MPA) at 25°C. PDMS moulds were fabricated by pouring over the photo-resist master a 10:1 w/w solution of base and curing agent (PDMS Sylgard 184 distributed by Dow Corning, USA) (30). The PDMS mould was used to produce 2-dimensional membranes by deposing and spreading 10%w/w PLA/dichloromethane solution on the micro-patterned mould surface, scraping the exceeding polymer solution and finally peeling the polymerized membrane. Non micro-patterned PLA membranes were obtained by simply pouring and spreading the pre-polymer solution onto standard microscope glass slides, without employing any shaped mould.

Micro-patterned membrane were made with 10x10mm dimensions and with an average thickness of 60µm. These membranes were adhered on glass slides to ensure their stability during cell culture and stimulation.

The negative control was fabricated depositing on 10x10mm area of a glass slide a 60µm thickness PLA membrane with a non micro-patterned surface.

D.2.4 Culture conditions

rMPC were detached from plate using trypsin (Invitrogen) 6 days after single fiber plating in order to avoid fusion and myotube formation in the culture dish. $1.4 \cdot 10^6$ cells were seeded on PLA membranes obtaining the density of $1.4 \cdot 10^6$ cells/cm2. 24 hours after cell seeding, electrical stimulation was applied to both non micro-patterned and micro-patterned scaffolds. Seeded scaffolds were kept on culture in Petri dishes for 11 days; 3ml of culture medium were stored daily and replaced with fresh myogenic medium in each plate for NO_2^- release analysis. The experimental plan was designed using two parameters (topological and electrical stimuli) on two levels. Muscular differentiation was quantified at three different time points (4, 7, 10 days of culture).

D.2.5 Micro-patterned membrane fabrication

Micro-patterned (MP) membranes were fabricated using poly-(L-lactic acid) (PLA, Resomer L206, Molecular weight 102kDa, Boehringer Ingelheim Pharma, Germany) by a soft-lithography technique (19, 30) adapting a procedure previously described by Kane (31). Briefly, silicon wafers (500µm thick by Wacko, Germany) surface was oxidized by nitric acid solution for 24h and thermally treated at 180°C for 12h. Thin films of photoresist (EPON SU-8 100 from Microchem Corp., Newton, MA) were uniformly deposed on silicon wafers using a Delta 10 spin-coater (BLE, Germany). The micro-patterned was design with Adobe Illustrator 10.0 and printed on a transparency film photomask; the geometry was composed of parallel lanes of 200x50µm rectangles spaced of 30µm and 60µm between short and long sides respectively (Fig.1A). The 30µm spaces were necessary to give structural consistency to the final polymeric membrane and their dimension was the smaller one allowed by technical limitation. Photoresist-coated silicon wafers were thermally pre-treated, exposed to UV light (UV Philips lamp HPR 125W) through the photomask for the proper time and thermally treated to prevent photoresist mechanical stresses. The photo-resist was developed with 1-methoxy-2-propanol acetate (MPA) at 25°C. PDMS moulds were fabricated by pouring over the photo-resist master a 10:1 w/w solution of base and curing agent (PDMS Sylgard 184 distributed by Dow Corning, USA) (30). The PDMS mould was used to produce 2-dimensional membranes by deposing and spreading 10%w/w PLA/dichloromethane solution on the micro-patterned mould surface, scraping the exceeding polymer solution and finally peeling the polymerized membrane. Non micro-

patterned PLA membranes were obtained by simply pouring and spreading the pre-polymer solution onto standard microscope glass slides, without employing any shaped mould.

Micro-patterned membrane were made with 10x10mm dimensions and with an average thickness of 60µm. These membranes were adhered on glass slides to ensure their stability during cell culture and stimulation.

The negative control was fabricated depositing on 10x10mm area of a glass slide a 60µm thickness PLA membrane with a non micro-patterned surface.

D.2.6 Culture conditions

rMPC were detached from plate using trypsin (Invitrogen) 6 days after single fiber plating in order to avoid fusion and myotube formation in the culture dish. $1.4 \cdot 10^6$ cells were seeded on PLA membranes obtaining the density of $1.4 \cdot 10^6$ cells/cm^2. 24 hours after cell seeding, electrical stimulation was applied to both non micro-patterned and micro-patterned scaffolds. Seeded scaffolds were kept on culture in Petri dishes for 11 days; 3ml of culture medium were stored daily and replaced with fresh myogenic medium in each plate for NO_2^- release analysis. The experimental plan was designed using two parameters (topological and electrical stimuli) on two levels. Muscular differentiation was quantified at three different time points (4, 7, 10 days of culture).

D.2.7 Electrical-stimuli

Cell culture electrical stimulation.

The apparatus for cell culture electrical stimulation is schematized in figure 1D and 1E. Two platinum electrodes of 0.3mm diameter and 20mm length were placed at 10mm distance at the scaffolds extremes. A rectangular PTFE holder was appropriately designed to keep the platinum wires in a position perpendicular to the scaffold micro-patterned lanes and immersed in the culture medium during the culture. The central holder hole of 20x30mm allowed constant culture monitoring. The electrodes were connected to a wave generator (AMEL model 568. Milan, Italy) programmed to produce a square wave with a 0V baseline. For differentiation process analyses, impulses of 70mV for 3ms with

frequency of 33mHz (Fig.1F) were applied. The amount of current flowing between the electrodes was measured (Fig.1G) by monitoring the potential drop across a 50Ω resistor placed in series with the culture chamber. The electrical stimuli were started 48 hours after the seeding on polymeric membranes.

Galvanotaxis (Cell motility).

Electrical stimuli influence on cell motility was investigated by continuously monitoring rMPCs in culture and tracking their motile activity. A see-through incubation chamber was custom built on the microscope plate to ensure maintenance of the Petri Dish at 37°C in a controlled atmosphere with 5% CO_2 and 95% of humidity. The cells were electrically stimulated with pulses of 100-1000mV in amplitude, 3ms-3s duration and 33-167mHz frequency. Pictures were taken at fixed intervals for a maximum total time of 4 hours. An image analysis Matlab program was applied to identify the major and the minor axis lengths and mass-centre position of each individual cell in every picture at different frame points. Using the data obtained from the sequence of pictures we estimated the cell displacement rate of the cell centre; a migration towards the positive electrode was considered positive.

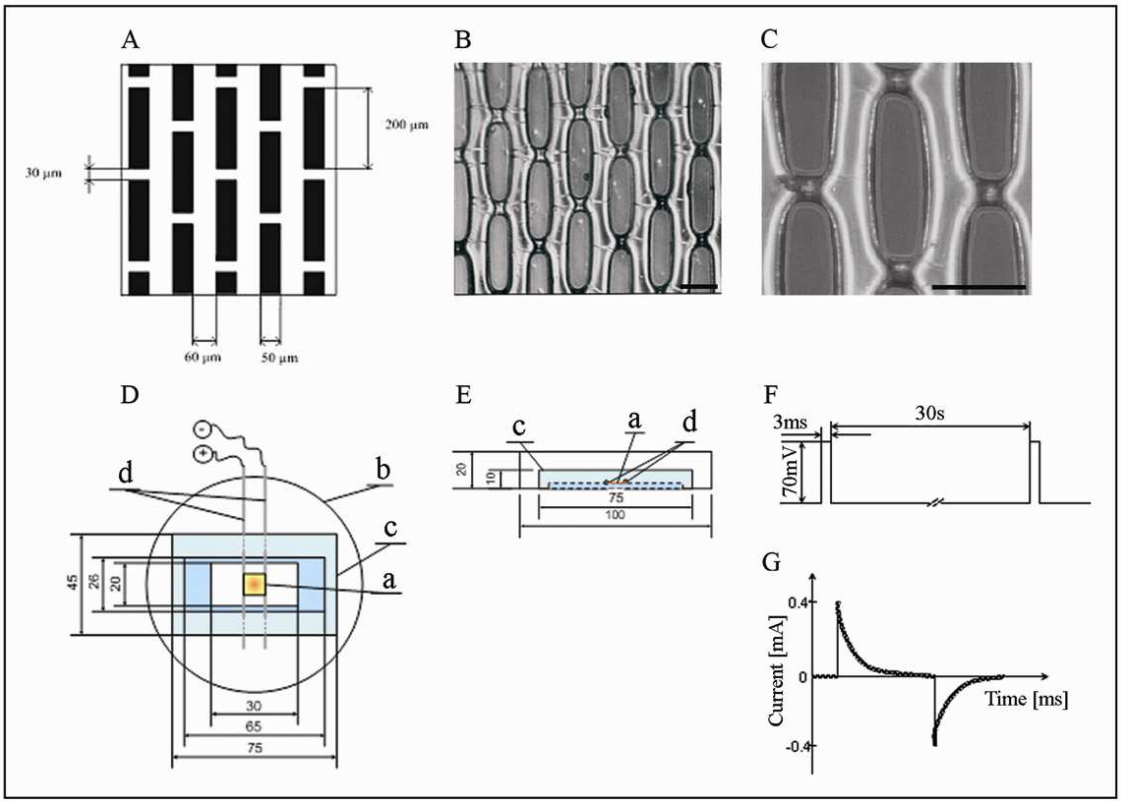

Figure 1. *External stimuli: micro-patterned membrane and electrical stimuli. (A) Schematic view of the photomask designed for the soft-lithography process. (B) 10x magnification micrograph of a micro-patterned PLA membrane. (C) 20x magnification showing the connecting lateral bridges. Scale bar=100 µm. (D) and (E) up and lateral schematic view of electrical stimulation apparatus: microscope slide (26x65mm) with the attached polymer (a – yellow/orange) was placed in a 100mm Petri dish (b); the PTFE frame (c –45x75mm area) holding the Pt wire electrodes (d) at 10mm distance, was added in the Petri dish and placed on the microscope slide. The PTFE frame has a central 30x20mm hole allowing microscope observation. The electrodes were connected with the pulse generator. (F) and (G) imposed potential difference square waves and current during charging/discharging phenomenon measured using a 50Ω resistance.*

D.2.8 Data analysis

Microscope imaging.

The cell cultures were monitored daily using an optical microscope Olympus IX51 (Tokyo, Japan) and pictures were taken periodically with a JVC KY-F30 3-CC camera supported by a Pinnacle, DVTools-Capture & Playback Application software.

Immunostaining.

Seeded polymers were stained with anti-Troponin I antibody (Chemicon International, Inc., USA) diluted in PBS 2% BSA. Primary antibody binding was visualized with fluorochrome-conjugated secondary antibody (Invitrogen). Cells nuclei were counterstained with DAPI and stained cultures were finally mounted in aqueous fluorescent mounting media (DakoCytomation, Glostrup, Denmark).

Images of Troponin I immunostaining after 10 days of culture where graphically analyzed in order to evaluate the angles formed between each myofiber axis and electric field direction.

The polar graphs report myotube frequency, defined the ratio between myotubes falling into the same class of orientation angle and total number of myotubes, as a function of orientation angle. In the case of culture on micro-patterned membrane the pictures were taken aligning the main rectangle axis with the horizontal direction.

NO_2^- analysis.

Conditioned medium was assayed for NOx, which were measured as nitrite ( ) accumulation using Griess' reagent (Fluka-Aldrich, Milan, Italy). Briefly, 1.5ml of medium extracted from cells cultures were added with 0.5ml of Griess' Reagent. After allowing the reaction to go to completion in 10 minutes, the solution was analyzed with a spectrophotometer (UV 500 Spectronic Unicam, Cambridge, UK). The absorbance was measured at 524nm using non-conditioned medium as baseline. NO_2^- concentration was determined using a standard calibration curve obtained from known concentration of sodium nitrite in non-conditioned culture medium. The total amount of nitrite released in the medium during the culture was then evaluated and the release speeds were calculated.

RNA extraction and quantitative real time PCR determinations.

Total RNA was extracted from the whole seeded polymers using RNAzol reagent (Tel-Test Inc., Friendswood, Texas, USA) as well as from mouse skeletal muscle and liver. One μg of total RNA was then purified with the DNAse Treatment & Removal Reagents (Ambion Inc., Texas, USA) and reverse-transcribed with Superscript II reverse transcriptase (Invitrogen). Quantitative Real Time PCR (LigthCycler, Roche Diagnostic GmbH, Germany) analysis was performed in differentiated cells. Standard curves with Syber green detection system were set up by using serial dilutions of control cDNA which had been retro-transcripted from the RNA extracted from cultured MPCs in plates. The target primers were specific for Myogenin (forward: 5'-GCA ATG CAC TGG AGT TTG GT-3', reverse: 5'-CAC GAT GGA CGT AAG GGA GT-3'; size 95bp) and Desmin (forward: 5'-GTG AAG ATG GCC TTG GAT GT-3', reverse: 5'-GCT GGT TTC TCG GAA GTT GA-3'; size 117bp). The housekeeping gene considered was β-Actin (forward: 5'-ATG CAG AAG GAG ATT ACT GCC CTG-3', reverse: 5'-ATA GAG CCA CCA ATC CAC ACA GAG -3'; size 98 bp).

Statistical analysis.

One-way ANOVA test was used and $p<0.05$ and $p<0.01$ were considered significant and reported.

D.3 Results

D.3.1 Method validation

In this section the results of preliminary tests, aimed to validate the cell isolation method, the micro-patterned membrane fabrication technique and the electrical stimulation equipment, are presented.

Cell isolation and characterization.

Single muscle fibers were successfully isolated from rat FDB muscles and plated on matrigel-coated dishes. Satellite cells, present in the quiescent state on isolated single fibres (Fig.2A), entered the cell cycle following *in vitro* activation and started to proliferate as

rMPCs 24 to 48 hours after plating (Fig.2B and 2C). When the cells became confluent, they were able to form a network of myotubes (Fig.2D) that expressed spontaneous contractile activities. Flow cytometric analyses were performed to rule out the presence of contaminant cells. In particular, rMPCs did not present CD31 (endothelial), CD45 (hematopoietic marker) and MHCII markers, while they expressed marker of mesenchymal pattern proper of cultured and expanded myogenic cells: CD29, CD44, CD90,and the majority of the cells expressed CD54 and CD73 (Fig.2E).

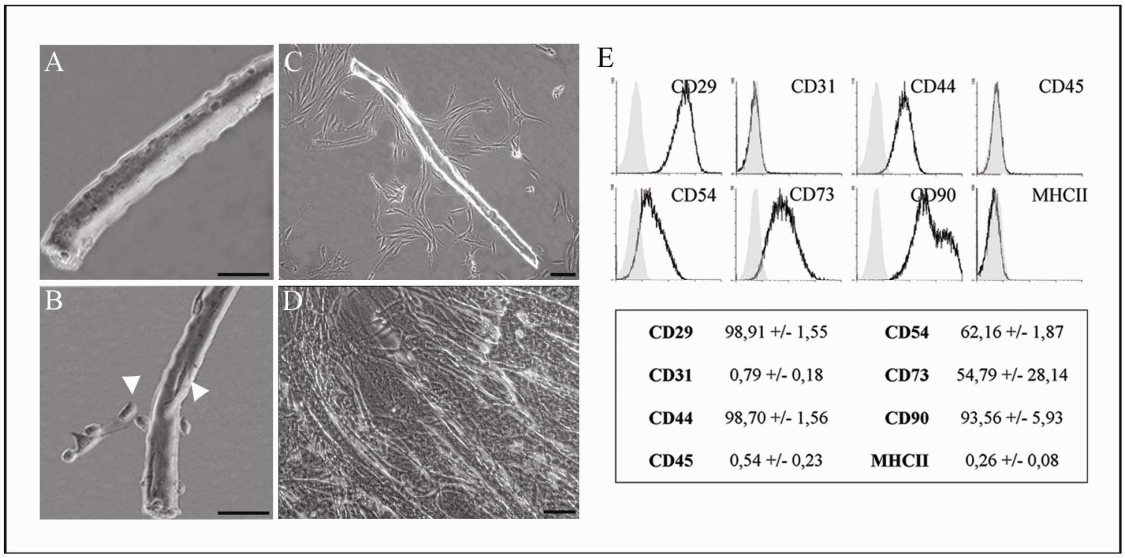

Figure 2. *Characterization of rMPCs. (A) Single isolated and plated fibre, carrying quiescent satellite cells. (B) Following activation, satellite cells activated to proliferate in culture, on the single fibre before (arrow head) and then around the fibre (arrow head). (C) Activated satellite cells migrated around the single fiber adopting a spindle form. (D) rMPCs maintained in culture fused to form multi-nucleated sincitia. Scale bar=50 µm. (E) Cytofluorimetric analyses of rMPCs before seeding on scaffolds.*

Micro-patterned membrane fabrication.

The replica-moulding and soft-lithographic techniques ensured an accurate control over the micro-pattern of the PLA membranes; the photo-mask geometry was reproduced with high accuracy and repeatability on the entire membrane area (Fig.1A-C). PLA is characterized by a very slow degradation rate, and only the small polymeric spaces between the short sides of two rectangles degraded before the end of the culture.

By seeding and culturing rMPCs onto polymeric membranes scaffolds, we verified that the polymer processing and membrane fabrication method did not affect cell viability. Cell

fusion and differentiation in myotubes was experimentally observed on both non-micro-patterned and micro-patterned membranes. It is worthwhile to note that the polymeric membrane did not inhibit the functional differentiation of rMPCs: spontaneous myotube formation and contractions were observed after 3-4 days of cell culture.

Electrical stimulation equipment.

The presence of non-reversible faradaic reactions at the electrodes, which can lead to release of soluble toxic reaction products, was evaluated by measuring the amount of current flowing in the culture media during the charging/discharging transient of the electrochemical double layer. When only reversible phenomena occur, the amount of current is exactly the same for both charging and discharging regimes. Performing those measurements with our experimental apparatus with electrical stimuli of 70mV amplitude and 3ms duration we proved the reversibility of the electrochemical phenomena. Considering the short duration of our electric pulses, the risk of toxic effects of reversible reaction products was negligible. These tests and consideration ensured the absence of toxic electrolytic reactions, electrode oxidation and, in general, of harmful temporal changes of culture conditions due to the imposed electrical potential.

After the assessment of the temporal-stability and biocompatibility of our electric stimulation experimental method, we examined if and how the imposed electric field influences the cell behaviour. The galvanotaxis analyses were performed to easily verify that rMPCs answer to electrical stimuli by continuous monitoring and tacking of cell shape and displacement.

MPCs were seeded on non patterned surface and after 48 hours electrical stimulation was started.

Our experimental observations revealed that rMPCs subjected to voltage pulses change their cell shape, elongating and producing lamellipodia extension, and they migrate towards the positive electrode (Fig.3A). The displacement rate of the mass cell centre was estimated for a statistically significant number of cells for different types of stimuli (two levels full factorial design). A negative control represented by non-stimulated cells shows negligible displacement rate (0.011±0.005µm/s) while short stimuli of 3ms duration, mimicking electrophysiological condition, increased cell displacement rate to 0.70±0.1µm/s. Longer pulses of 3ms induced a lower rate of 0.50±0.16µm/s (Fig.3B).

In our experiments, the actual electric potential difference in the media between two points nearby the electrodes drops from 70mV to 30mV after 3ms of stimulation due to the electrode polarization. This result indicated that the electric field is substantially reduced by 60% during the 3ms pulse stimulation.

These galvanotaxis experiments confirm the effectiveness of the electro-chemical cell signal transduction of the exogenous electrical stimulation and suggest 70mV amplitude, 3ms duration and 0.03Hz as the best type of electrical wave to apply in the following experiments on rMPCs.

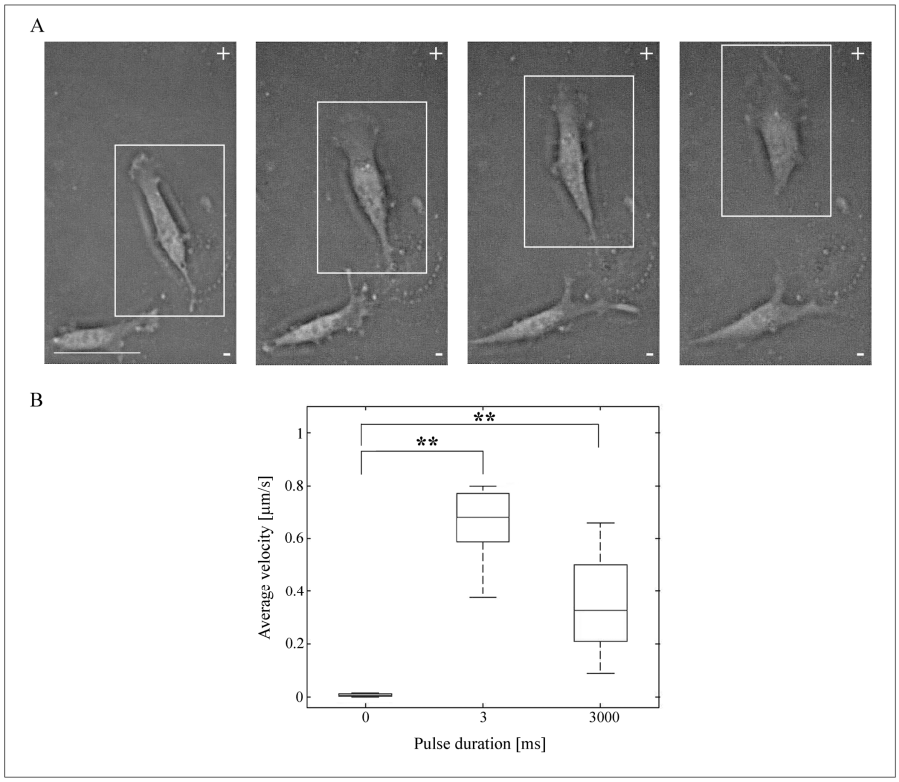

Figure 3. *rMPC galvanotaxis under exogenous electric field application. (A) Bright field images at 20x magnification of rMPCs collected at 20 minutes intervals since the beginning of the electrical stimulation (square pulses of 1 V/cm amplitude, 3ms duration and 0.03 Hz); (+) and (-) signs display the electric field (EF) orientation. Cells oriented according to the EF direction show higher initial displacement rate (cell marked with white frame). Box plots (B) show the comparison between the calculated velocities of the centre of mass of the cells in the absence of electrical stimulation (0ms) and with electrical stimulation for two different pulse duration (3ms and $3 \cdot 10^3$ms). The lower and upper lines of each box stands for the 1st and 3rd percentiles of the represented sample; the distance between the top and bottom of the box is the interquartile range and the middle line is the sample median. There are no outlier points, exceeding the range delimited by the boxes, so the upper and lower whiskers represent the actual maximum and minimum value of our data set. A standard one-way ANOVA was performed between data of each group, pairs labelled with ** resulted in $p<0.01$.*

D.3.2 Myotube alignment

Myotubes resulting from MPCs cultures on non-patterned PLA membranes showed the formation of a network lacking of a preferential orientation (Fig.4A). Immunostainings for Troponin I performed after 4 and 10 days of culture on non-patterned membranes (Fig.4B-D) confirmed that myotubes were randomly oriented and the corresponding polar graph reports tangent values in the range [-0.9, +0.9] with an uniform occurrence frequency (Fig.4E). On the contrary, MPCs seeded on micro-patterned PLA membranes were strongly influenced in their alignment by the surface template. The PLA micro-patterned membranes allowed cells adhesion and influenced their orientation guiding cell fusion in parallel myotubes to the longitudinal axis of the micro-patterned rectangles. Structural and topological constraint of micro-patterned scaffold guided myotubes to an ordered assembly (Fig.4F-L). At earlier time points, i.e. of 4 days, even thought fewer myotubes could be detected, the influence of topological stimulation could already be observed (Fig.4G). The shape of the polar graphs representing myotubes orientations on micro-patterned PLA films (Fig.4L) resembles a symmetric Gaussian distribution centered in 0 value with a narrow distribution (0.3). The combination of electrical and topological stimulation with micro-patterned PLA membrane resulted in a similar myotube alignment pattern (Fig.4M-P) and in comparable polar graphs: narrow Gaussian distributions centred on 0 (Fig.4Q).

As immediate consequence, we observed spontaneous contractions only in one direction: parallel to the main rectangle axis.

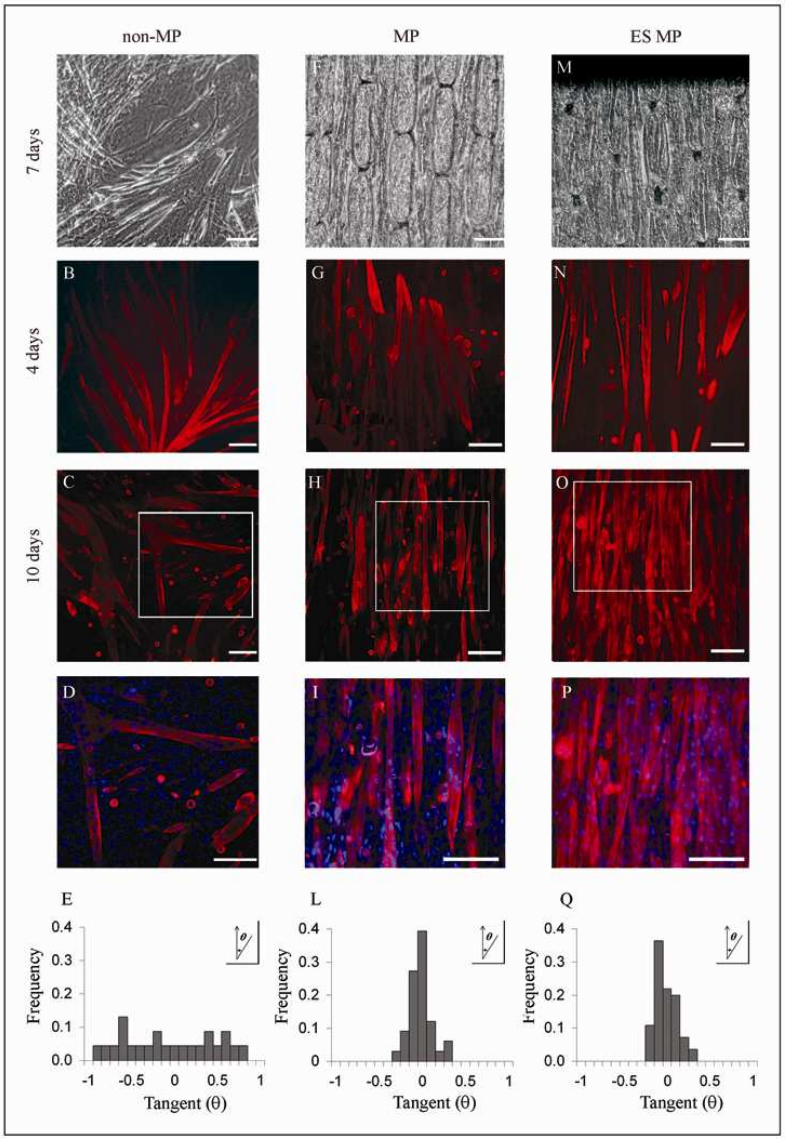

Figure 4. *Cell alignment and Troponin I expression of rMPCs cultured on non-micropatterned (non-MP) (A-D), micropatterned (MP) (F-I) and electrically stimulated micropatterned (ES MP) scaffolds (M-P). Brigthfield images of rMPCs on non-MP membranes show myotubes randomly oriented after 7 days of culture (A) as proved by immunostaining for Troponin I after 4 (B) and 10 (C) days of culture. rMPCs cultured on MP scaffolds fused into myotubes uniformly oriented with the pattern, as visible in brightfield after 7 days of culture (F) and by immunostaining after 4 (G) and 10 (H) days. More myotubes uniformly oriented with the pattern were visible in brightfield (M, the black line visible in the top part of the image is the platinum electrode) and highlighted by immunostaining for Troponin I at 4 (N) and 10 (O) of culture. Magnification of stroked area in C, H, O are respectively reported in D, I, P, where nuclei are counterstained with DAPI. Scale bars=50µm.*

Graphics in E, L and Q report myotubes frequency as a function of tanθ after 10 days of culture. θ is the angle between the myotubes direction and the vertical axis of the picture (E) or with the micro-pattern main direction (L and Q). The frequency is the ratio between myotubes falling into the same tanθ class orientation and total number of myotubes.

D.3.3 Cell differentiation

Immunostaining for Troponin I performed after 10 days of culture showed that following application of an electrical field, the number of myotubes was increased while the number of mononucleated cells was decreased (Fig.4Q-P). Moreover, the application of electrical pulses induced an increased rate of production of nitrites in all the experiments. Figure 5A shows an example of a total nitrites production profile; the data were normalized over the maximum cumulative value of nitrites released, measured at the end of the culture. In particular, nitrite production released in the medium by rMPCs was significantly increased right after the application of the electrical stimuli (48h after seeding) to a cultured micropattered scaffold. After 3 days of stimulation, the nitrite profile reached a plateau that was not observed in absence of exogenous electric field. The box plot graph in Figure 5B shows an average of production rates evaluated on a set of 6 experiments; in the case of electrical stimulation on micro-patterned membranes (ES MP) the slope was calculated considering the data from the first 3 time points since the beginning of the stimulation. ES MP median value reveals a 30% increment of release rate if compared with non-stimulated samples on both micro-patterned membrane (MP) and non-micro-patterned ones (non-MP).

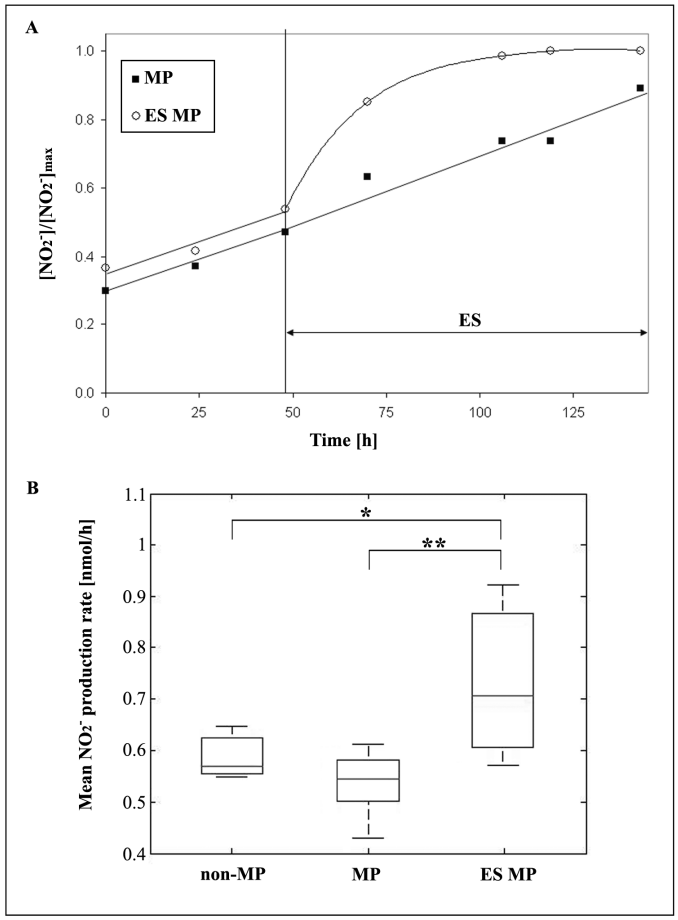

Figure 5. *Analysis of NO_2^- release profiles from rMPC cultures on PLA membranes. (A) shows the comparison between the profiles of NO_2^- released in the culture media by rMPCs under two different conditions: open circles (○) report the values obtained from a sample cultured in the absence of exogenous electrical stimulation for the first 48 hours and subsequently exposed to square pulses of 1 V/cm amplitude, 3ms duration and 0.03 Hz; filled squares (▪) report values obtained from a sample cultured in the absence of exogenous electrical stimulation for the entire duration of the experiment. Data were normalized to the maximum value obtained at the end of the experiment (i.e. last value of the series with electrical stimuli). Box plots in (B) represent nitrite production rates measured in rMPCs cultures on: non micro-patterned polymeric membranes in the absence of exogenous electric field (non-MP), micro-patterned polymeric membranes in the absence of exogenous electric field (MP) and electrically stimulated micro-patterned polymeric membranes (ES MP). A standard one-way ANOVA was performed between data of each group: * $p<0.05$; ** $p<0.01$.*

Finally, from semi-quantitative real time PCR analyses, differences in Myogenin and Desmin gene expression were observed. As attended, Myogenin gene was down-regulated, while Desmin gene was progressively up-regulated during the time in all seeded scaffolds (Fig.6). This pattern was enhanced when both electrical and topological stimulations were

applied. In particular, after 4 days, Myogenin expression reached the maximum expression level when electrical stimulation was added to topological one, and more significant difference was detected between ES MP and not electrically stimulated scaffolds (Fig.6). After 10 days Desmin was more highly expressed in ES MP membranes compared to non-MP ones which showed a significant lower expression also in comparison to MP scaffolds (Fig.6B).

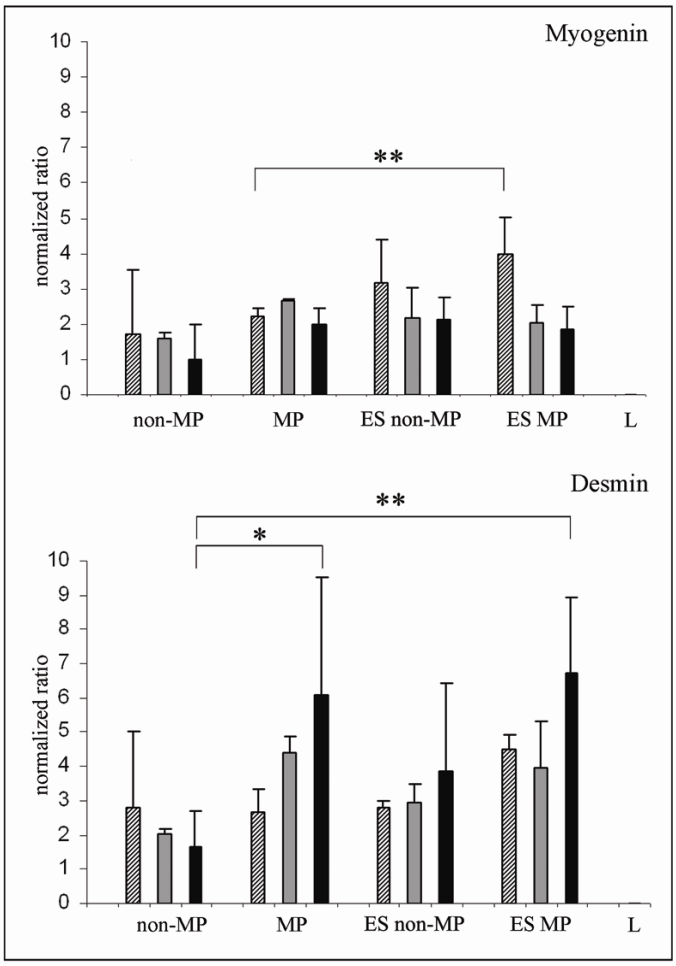

Figure 6. *Real time PCR analysis for Myogenin and Desmin. Quantifications of Myogenin and Desmin gene expressions by semi-quantitative real time PCR analysis were performed in non-patterned polymeric membranes (non-MP), in micro-patterned (MP), electrically stimulated non-micro-patterned (ES non-MP) and micro-patterned (ES MP) at different time points of: 4 (hatched bars), 7 (grey bars) and 10 days (black bars). Liver (L) was used as negative control. A standard one-way ANOVA gave * $p<0.05$ and ** $p<0.01$.*

D.4 Discussion

Satellite cells are considered a promising source of myogenic cells for skeletal muscle regeneration because of their self-renewal ability and high proliferate capacity (4, 7, 32). Previous studies confirmed the possibility of culturing satellite cells, preserving their capability of muscle differentiation and fusion into contractile myotubes (29) showing asynchronous and multi-directional contractions (33). In sight of an application in tissue engineer, skeletal muscle cells need to fuse in parallel oriented myotubes showing synchronous contractions in order to ensure directed force production (16). Only *in vitro* replication of the spatio-temporal micro-environmental cues controlling MPC behaviour would allow their application as therapeutic tool.

It's well known that cell behaviour can be highly influenced by external stimuli such as structural logistic and topological template (34), or exogenous electrical field (20).

Different scaffold materials and topologies have already been tested with C2C12 skeletal muscle cells and these studies confirmed the possibility to recreate *in vitro* a structure with aligned myofibers (15, 16) but, to our knowledge, no studies deal on the orientation of primary myogenic cells derived from a pure rMPC population.

We applied soft-lithography and replicate-moulding techniques to realize micro-patterned membranes in PLA, a FDA approved polymer for clinical use which has also been used as substrate for cultures of skeletal muscle cells (35). This technique was previously applied in our laboratory for fabrication of membranes in Poly(lactic-co-glycolic acid) and in a Hyaluronic acid ester with a resolution of 20µm (36, 37). The scaffold micro-structure geometry of 60µm spaced parallel lines of 200x50µm rectangles with 30µm distance was chosen by considering desired myotubes disposition, cell dimensions and resolution of our fabrication method. The 30µm polymeric spaces between the short sides of the rectangles were drown to give structural property to the membrane and their dimension was kept as small as possible to allow a quick degradation during cell culture. After 7 days of culture many of these polymeric spaces were broken (Fig.4F,M) allowing the progressive modification of the scaffold geometry in a series of parallel lanes. In this way, the scaffold micro-structure could not only influence the initial cell disposition, but also prolong its effect in time inducing the formation of parallel myotubes. The polar graphs highlighted that the direction of myotubes cultured on micro-patterned scaffold without and with electrical stimulation (Fig.4E and 4Q) followed a narrow Gaussian-like distribution centred

in 0. This distribution underlined the presence of a high percentage of parallel myotubes to the longitudinal axis of micro-patterned rectangles, while all the other myofibers had tangent values ranging in ±0.3.

On the contrary, rMPCs cultured on non micro-patterned PLA membrane couldn't give rise to an organized structure and resulted in a myotubes network with random directions, reproducing the same cell behaviour on plate where no topological stimuli are applied, as showed in the polar graph reporting the uniform distribution of the tangent angles (Fig.4E).

In this study we applied electrical stimulation to cultures on micro-patterned scaffold with the main aim of resulting in an electric potential drop across the cell membrane whose value overtake the threshold allowing electro-chemical signal transduction activity and thus regulation of cell behaviour. Electrical stimuli have previously been applied on non-organized 2D- and 3D-cultures of MPCs with varying effects (21, 23, 38). However topological and electrical stimulation have never been applied together in order to enhance the formation of contractile alignment myotubes.

Platinum electrodes have been chosen for their low reactivity and their resistance to corrosion that make them biocompatible. An electric potential difference between electrodes submerged in the culture media (which contains a high number of small and large electrolytes: ions, small peptides, proteins, etc.) can produce a transient electric field at the cell level thought three mechanisms: (i) non-faradaic charging/discharging of the electrochemical double layer, (ii) reversible faradaic reactions, and (iii) non-reversible faradaic reactions (27). These mechanisms are responsible for the spatial-temporal shape of the electric field on cell culture. The last two phenomena are related with reactions occurring at the electrode surfaces and they can lead to the production and release of soluble toxic reaction products. We assessed the temporal-stability and biocompatibility of our electric stimulation experimental method and then, we examined if and how the imposed electric field could influence the cell behaviour by galvanotaxis analysis, a simple, non-invasive and non-destructive technique. Previous studies on cardiomyocytes showed that cells need at least 24 hours to recover from detachment after being seeded again. Starting stimulation too early had negative effects (28), thus we waited a lag period of 48h before start electrical stimulation. The galvanotaxis analysis not only confirmed that rMPCs are responsive to electrical stimulation but also showed that the cells with the main axe parallel

to electric field lines displayed the highest velocities because they felt a higher voltage difference through their cell body. rMPCs mean velocity was not influenced by pulse frequency or amplitude but it does depend on pulse duration: stimuli of 3ms induced a 40% higher velocity than 3s pulses (Fig.3B). We underline how the most efficient pattern of electrical stimulation is the one which better reproduce the timing of action potential propagation through muscle membranes.

3ms square pulses of 70mV/cm amplitude each 30s have then been chosen for investigating their effects on myotubes alignment and cell differentiation in combination with topological stimuli. In these cases the 48h lag period before electrical stimulation allowed cell adhesion to the micro-patterned surface and cell parallel orientation. The micro-pattern induced cells to displace with the main axis in the same direction of the electric field. As observed during galvanotaxis analysis, the cells characterized by this displacement felt the highest potential drop across their body and had the strongest reaction to electrical field.

While image analyses on phase contrast and fluorescent images were performed to evaluate myotube alignment, three different types of analysis were carried out to investigate cell differentiation and each of them contributed in proving an effect of topological and electrical stimuli in enhancing MPC differentiation toward functional myotubes.

Immunostaining for Troponin I revealed a higher myotube density in electrically stimulated culture (Fig.4O-P). Moreover, application of exogenous electric field was proved to induce a 30% increment in NO_2^- release rate, in analogy to what observed by our group in a 3D non micro-structured scaffold (38). NO_2^- is known to be a signalling molecule involved in many cellular pathways and Anderson's research group demonstrated an additional role for nitric oxide in mediating muscle regeneration (39). There are evidences that nitric oxide helps to regulate activation and quiescence of satellite cells (40, 41), myoblast fusion and myotube growth (42). An increase of nitrite release rate is an additional evidence of the enhancement in cell differentiation due to electrical stimuli.

Semi-quantitative real time PCR of Myogenin and Desmin showed that not only electrical but also topological stimuli can influence MPC gene expression. Desmin up-regulation seemed to be influenced to a major extent by polymeric surface topology while Myogenin down-regulation was enhanced mainly by electrophysiological pulses. Electrical stimuli had

the highest effect on Myogenin expression when applied on micro-patterned membrane, i.e. on parallel oriented MPCs.

Mimicking the *in vivo* cues is fundamental to improve results of *in vitro* cultures (9, 43) for tissue engineering application. The combination of micro-patterned membranes and exogenous electrical stimuli allowed a better control of the multiplicity of culture micro-environment cues for MPCs. This improvement led to a highly organized muscle-like structure capable of mono-directional contractions.

Biocompatible and biodegradable micro-patterned polymers have already been used *in vivo* to improve cell delivery in muscle therapy (36). Here we showed that the application of electrophysiological stimuli to cultured MPCs can give rise to new tools with great potentiality both for tissue engineering and as an *in vitro* model of muscle differentiation.

D.5 Acknowledgments

The authors are grateful to Citta della Speranza, University of Padova and MIUR.

D.6 References

1. Carlson, B.M. Regeneration of entire skeletal muscles. Fed. Proc. 45, 1456, 1986.

2. Mauro, A. Satellite cell of skeletal muscle fibers. J. Biophys. Biochem. Cytol. 9, 493, 1961.

3. Boldrin, L., and Morgan, J.E. Activating muscle stem cells: therapeutic potential in muscle diseases. Curr Opin Neurol 20, 577, 2007.

4. Anderson, J.E. The satellite cell as a companion in skeletal muscle plasticity: currency, conveyance, clue, connector and colander. J. Exp. Biol. 209, 2276, 2006.

5. Bach, A.D., Beier, J.P., Stern-Staeter, J., and Horch, R.E. Skeletal muscle tissue engineering. J. Cell. Mol. Med. 8, 413, 2004.

6. De Coppi, P., Delo, D., Farrugia, L., Udompanyanan, K., Yoo, J., Nomi, M., Atala, A., and Soker, S. Angiogenic gene-modified muscle cells for enhancement of tissue formation. Tissue Eng 11, 1034, 2005.

7. Collins, C.A., Olsen, I., Zammit, P.S., Heslop, L., Petrie, A., Partridge, T.A., and Morgan, J.E. Stem cell function, self-renewal, and behavioral heterogeneity of cells from the adult muscle satellite cell niche. Cell 122, 289, 2005.

8. Deasy, B.M., Gharaibeh, B.M., Pollett, J.B., Jones, M.M., Lucas, M.A., Kanda, Y., and Huard, J. Long-Term Self-Renewal of Postnatal Muscle-derived Stem Cells. Molecular Biology of the Cell 16, 3323, 2005.

9. Powell, K. Stem-cell niches: it's the ecology, stupid! Nature 435, 268, 2005.

10. Bassel-Duby, R., and Olson, E.N. Signaling pathways in skeletal muscle remodeling. Annual Review of Biochem 75, 19, 2006.

11. Péault, B., Rudnicki, M., Torrente, Y., Cossu, G., Tremblay, J.P., Partridge, T., Gussoni, E., Kunkel, L.M., and Huard, J. Stem and Progenitor Cells in Skeletal Muscle Development, Maintenance, and Therapy. Mol Ther 15, 867, 2007.

12. Kuang, S., Kuroda, K., Le Grand, F., and Rudnicki, M. Asymmetric self-renewal and commitment of satellite stem cells in muscle. Cell 129, 999, 2007.

13. Dennis, R.G., and Kosnik, P.E. Excitability and isometric contractile properties of mammalian skeletal muscle constructs engineered in vitro. In Vitro Cell Dev Biol Anim 36, 327, 2000.

14. Vandenburgh, H.H., Swasdison, S., and Karlisch, P. Computer-aided mechanogenesis of skeletal muscle organs from single cells in vitro. FASEB J. 5, 2860, 1991.

15. Neumann, T., Hauschka, S.D., and Sanders, J.E. Tissue engineering of skeletal muscle using polymer fiber arrays. Tissue Engineering 9, 995, 2003.

16. Shen, J.Y., Chan-Park, M.B., Feng, Z.Q., Chan, V., and Feng, Z.W. UV-embossed microchannel in biocompatible polymeric film: application to control of cell shape and orientation of muscle cells. J. Biomed. Mater. Res. B Appl. Biomater. 77, 423, 2006.

17. Tatsumi, R., Hattori, A., Ikeuchi, Y., Anderson, J.E., and Allen, R.E. Release of hepatocyte growth factor from mechanically stretched skeletal muscle satellite cells and role of pH and nitric oxide. Mol. Biol. Cell. 13, 2909, 2002.

18. Tatsumi, R., Liu, X., Pulido, A., Morales, M., Sakata, T., Dial, S., Hattori, A., Ikeuchi, Y., and Allen, R.E. Satellite cell activation in stretched skeletal muscle and the role of nitric oxide and hepatocyte growth factor. Am J Physiol Cell Physiol 290, C1487, 2006.

19. Desaj, T.A. Micro- and nanoscale structures for tissue engineering constructs. Medical Engineering & Physics 22, 595, 2000.

20. McCaig, C.D., Rajnicek, A.M., Song, B., and Zhao, M. Controlling cell behavior electrically: current views and future potential. Physiol Rev 85, 943, 2005.

21. Naumann, K., and Pette, D. Effects of chronic stimulation with different impulse patterns on the expression of myosin isoforms in rat myotube cultures. Differentiation 55, 203, 1994.

22. Wehrle, U., Dusterhoft, S., and Pette, D. Effects of chronic electrical stimulation on myosin heavy chain expression in satellite cell cultures derived from rat muscles of different fiber-type composition. Differentiation 58, 37, 1994.

23. Pedrotty, D.M., Koh, J., Davis, B.H., Taylor, D.A., Wolf, P., and Niklason, L.E. Engineering skeletal myoblasts: roles of three-dimensional culture and electrical stimulation. Am. J. Physiol Heart Circ. Physiol 288, H1620, 2005.

24. Stern-Straeter, J., Bach, A.D., Stangenberg, L., Foerster, V.T., Horch, R.E., Stark, G.B., and Beier, J.P. Impact of electrical stimulation on three-dimensional myoblast cultures - a real-time RT-PCR study. J. Cell Mol. Med. 9, 883, 2005.

25. Kalhovde, J.M., Jerkovic, R., Sefland, I., Cordonnier, C., Calabria, E., Schiaffino, S., and Lomo, T. "Fast" and "slow" muscle fibres in hindlimb muscles of adult rats regenerate from intrinsically different satellite cells. J. Physiol 562, 847, 2005.

26. Okano, T., and Matsuda, T. Tissue engineered skeletal muscle: preparation of highly dense, highly oriented hybrid muscular tissues. Cell Transplantation 7, 71, 1998.

27. Cannizzaro, C., Tandon, N., Figallo, E., Park, H., Gerecht, S., Radisic, M., Elvassore, N., and Vunjak-Novakovic, G. Practical aspects of cardiac tissue engineering with electrical stimulation. Methods in molecular medicine: Tissue engineering, 2007.

28. Radisic, M., Park, H., Shing, H., Consi, T., Schoen, F.J., Langer, R., Freed, L.E., and Vunjak-Novakovic, G. Functional assembly of engineered myocardium by electrical stimulation of cardiac myocytes cultured on scaffolds. Proc. Natl. Acad. Sci. U. S. A. 101, 18129, 2004.

29. Rosenblatt, J.D., Lunt, A.I., Parry, D.J., and Partridge, T.A. Culturing satellite cells from living single muscle fiber explants. In Vitro Cell Dev Biol Anim 31, 773, 1995.

30. Vozzi, G., Flaim, C., Ahluwalia, A., and Bhatia, S. Fabrication of PLGA scaffolds using soft lithography and microsyringe deposition. Biomaterials 24, 2533, 2003.

31. Kane, R.S., Takayama, S., Ostuni, E., Ingber, D.E., and Whitesides, G.M. Patterning proteins and cells using soft lithography. Biomaterials 20, 2363, 1999.

32. Hill, E., Boontheekul, T., and Mooney, D.J. Regulating activation of transplanted cells controls tissue regeneration. PNAS 103, 2494, 2006.

33. De Coppi, P., Bellini, S., Conconi, M.T., Sabatti, M., Simonato, E., Gamba, P.G., Nussdorfer, G.G., and Parnigotto, P.P. Myoblast-acellular skeletal muscle matrix constructs guarantee a long-term repair of experimental full-thickness abdominal wall defects. Tissue Eng 12, 1929, 2006.

34. Khademhosseini, A., Langer, R., Borenstein, J., and Vacanti, J.P. Microscale technologies for tissue engineering and biology. PNAS 103, 2480, 2006.

35. Cronin, E.M., Thurmond, F.A., Bassel-Duby, R., Williams, R.S., Wright, W.E., Nelson, K.D., and Garner, H.R. Protein-coated poly(L-lactic acid) fibers provide a substrate for differentiation of human skeletal muscle cells. J. Biomed. Mater. Res. A 69, 373, 2004.

36. Boldrin, L., Elvassore, N., Malerba, A., Flaibani, M., Cimetta, E., Piccoli, M., Baroni, M.D., Gazzola, M.V., Messina, C., Gamba, P., Vitello, L., and Coppi, P.D. Satellite cells deliveres by micro-patterned scaffolds: a new strategy for cell trasplantation in muscle diseases. Tissue Engineering 13, 253, 2007.

37. Figallo, E., Flaibani, M., Zavan, B., Abatangelo, G., and Elvassore, N. Micro-patterned biopolymer 3D scaffold for static and dynamic culture of human fibroblasts. Biotech Prog 23, 210, 2007.

38. Serena, E., Flaibani, M., Carnio, S., Boldrin, L., Vitiello, L., Coppi, P.D., and Elvassore, N. Electrophysiologic stimulation improves myogenic potential of muscle precursor cells grown in a 3D collagen scaffold. Neurological Research 30, 207, 2007.

39. Anderson, J.E. A role for nitric oxide in muscle repair: nitric oxide-mediated activation of muscle satellite cells. Mol. Biol. Cell 11, 1859, 2000.

40. Wozniak, A.C., and Anderson, J.E. Single-fiber isolation and maintenance of satellite cell quiescence. Biochem. Cell Biol. 83, 674, 2005.

41. Wozniak, A.C., Kong, J., Bock, E., Pilipowicz, O., and Anderson, J.E. Signaling satellite-cell activation in skeletal muscle: markers, models, stretch, and potential alternate pathways. Muscle Nerve 31, 283, 2005.

42. Pisconti, A., Brunelli, S., Di, P.M., De, P.C., Deponti, D., Baesso, S., Sartorelli, V., Cossu, G., and Clementi, E. Follistatin induction by nitric oxide through cyclic GMP: a tightly regulated signaling pathway that controls myoblast fusion. J. Cell Biol. 172, 233, 2006.

43. Scadden, D.T. The stem-cell niche as an entity of action. Nature 441, 1075, 2006.

Appendix E

Satellite Cells Delivered by Micro-Patterned Scaffolds: A New Strategy for Cell Transplantation in Muscle Diseases

L BOLDRIN, M.Sc.,[1] N ELVASSORE, Ph.D.,[3] A MALERBA, Ph.D.,4 M FLAIBANI, M.Sc.,[3] E CIMETTA, M.Sc.,[3] M PICCOLI, M.Sc.,[1] M D BARONI, Ph.D.,[4] M V GAZZOLA, M.Sc.,[1] C MESSINA, M.D.,[1] P GAMBA, M.D.,[5] L VITELLO, Ph.D.,[5] AND P DE COPPI, M.D., Ph.D.[1,2]

[1] Stem Cell Processing Laboratory, Department of Pediatrics, [2]Department of Chemical Engineering, [3]Gene Transfer Laboratory, Department of Biology, [4]Cell Cycle Laboratory, Department of Biology, [5]Pediatric Surgery, Department of Pediatrics, University of Padova, Padova, Italy.

[*] Corresponding author

TISSUE ENGINEERING

Volume 13, Number 2, 2007

Abstract

Myoblast transplantation is a potentially useful therapeutic tool in muscle diseases, but the lack of an efficient delivery system has hampered its application. Here we have combined cell biology and polymer processing to create an appropriate microenvironment for *in vivo* transplantation of murine satellite cells (mSCs). Cells were prepared from single muscle fibers derived from C57BL/6-Tgn enhanced green fluorescent protein (GFP) transgenic mice. mSCs were expanded and seeded within micro-patterned polyglycolic acid 3-dimensional scaffolds fabricated using soft lithography and thermal membrane lamination. Myogenicity was then evaluated *in vitro* using immunostaining, flow cytometry, and reverse transcription polymerase chain reaction analyses. Scaffolds containing mSCs were implanted in pre-damaged tibialis anterior muscles of GFP-negative syngenic mice. Cells detached from culture dishes were directly injected into contra-lateral limbs as controls. In both cases, delivered cells participated in muscle regeneration, although scaffold-implanted muscles showed a much higher number of GFP-positive fibers in CD57 mice. These findings suggest that implantation of cellularized scaffolds is better than direct injection for delivering myogenic cells into regenerating skeletal muscle.

E.1 Introduction

Post-natal skeletal muscle maintains a lifelong ability to grow and self-repair in response to damage. This capability relies on satellite cells—quiescent myogenic cells located adjacent to the plasma membrane of myofibers beneath the basal lamina.[1] Once activated by damage, they start to proliferate and then fuse together to form myotubes, which then mature into myofibers, or fuse with the pre-existing damaged fibers. Cell transplantation has long been explored as a potential therapeutic approach for muscle disorders such as Duchenne Muscular Dystrophy (DMD).[2] Despite encouraging results obtained in small animals, gene delivery has superseded cell based therapy,[3] mostly because of the low survival rate of the injected cells. At present, in addition to the obvious need to modulate the immunological, inflammatory response, two major concerns need to be addressed: what are the best muscle progenitors and what is the most efficient way of delivering them? Different cell sources have been tested to find the optimal cell type that would proliferate and integrate in the

regenerating muscle or replenish the satellite reservoir. In the case of DMD, transplantation of normal myoblasts into dystrophic muscles could lead to dystrophin restoration.[4,5] Early results suggested that direct intramuscular injection of normal myoblasts could lead to dystrophin expression in dystrophic mdx mice [6,7] and in humans.[8–10] However, the majority of transplanted cells die quickly after intramuscular injection,[11–13] likely because of inflammatory, immune response.[14,15] Collins and colleagues, on the other hand, recently showed that transplantation of single, intactmyofiberswith their attached satellite cells led to high levels of cell integration and proliferation.[16] Systemic delivery of muscle stem cells has also led to good results,[17,18] but characterization and large-scale isolation of the optimal cell type(s) from non-embryonic tissue still need to be determined.

Tissue engineering, a field that combines engineering and cell biology, has recently been explored as a means of creating functional skeletal[19–21] or cardiac[22] muscle. Here we describe for the first time a novel tissue-engineering protocol that can improve the efficacy of cell delivery into a model of skeletal muscle regeneration. In particular, our approach led to a great increase in the grafting efficiency of single fiber-derived satellite cells into regenerating muscle.

E.2 Materials and Methods

E.2.1 Animals

For this study, we used 4- to 6-month-old C57BL/6 wildtype mice, C57BL/6-Tg(actin, beta–enhanced green fluorescent protein (EGFP)1Osb/J transgenic mice (Jackson Laboratories, Bar Harbor, ME). In transgenic animals, the GFP transgene was under the control of the cytoplasmic beta actin promoter.

The animals had been housed and operated on at the Animal Colony of the ‘‘Centro Interdipartimentale Vallisneri,’’ University of Padova, under the conditions specified in the "D.L. 27-1-92, numero 116, circolare applicativa del Ministero della Sanita` numero 8 del 22-4-94".

E.2.2 Single fiber cultures from adult mouse

Murine satellite cells were obtained from the *flexor digitorum brevis* muscles of the hind feet of animals killed using cervical dislocation. Cells were prepared from isolated myofibers as described previously.[23] Briefly, single fibers obtained using enzymatic dissociation were plated onto Matrigel-coated (BD Biosciences, Milano, Italy) dishes and left undisturbed for 5 days so that satellite cells couldmove to the plate and proliferate. After this time, cells were trypsinized and kept in culture for 2 to 3 more passages in proliferating medium (Dulbecco's modified Eagle medium (DMEM), 20% fetal bovine serum, 10% horse serum, and 0.5% chicken embryo extract) before being seeded onto the scaffold or injected into muscles (see below). All cell culture reagents were from Gibco-Invitrogen, Milano, Italy.

E.2.3 Characterization of satellite cells using flow cytometry

Cytofluorimetric analysis was performed at passages 2 to 3 in culture. One million murine cells were detached from the plates and stained with fluorescein isothiocyanate– or phycoerythrin-labeled antibodies against CD34, CD44, CD45, CD90 (Thy-1.1), CD117 (c-kit), fetal liver kinase (Flk)-1, major histocompatibility complex (MHC)-I and -II (all from BD Pharmingen, Milano, Italy). Analysis was performed using a Beckman Coulter cytometer (COULTER Epics XL-MCL, Milano, Italy) using EXPOTM 32 ADC Software (BECKMAN COULTER, Milano, Italy).

E.2.4 Scaffolds

Biodegradable/biocompatible 3-dimensional (3D) scaffolds were prepared by overlapping polymeric micro-patterned membranes produced using the soft-lithography technique.[24] Even depositions of 50 μm thick, photo-resist films (SU-8, Microchem, Rapperswil, Switzerland) on silicon wafers (Wacko, Neuss, Germany) were prepared using a spin-coater (Delta 10 spin-coater, BLE, Singen, Germany). Photo-resist was cross-linked using thermal treatment, followed by ultraviolet light exposition through a positive mask (shown in Fig. 3A). Photo-resist was eventually developed by raising the SU-8 master with 1-methoxy-2-propanol acetate (Sigma-Aldrich, Taufkirchen, Germany). A poly(dimethylsiloxane)

(PDMS) mold was prepared by filling the SU-8 master (Sylgard 184, Dow Corning, Midland, MI) as reported in the literature.[25] The PDMS mold was used to produce the polymeric micropatterned membrane using solvent casting: a 15% w/w solution of poly(lactic-co-glycolic acid) (PLGA50/50DL2.5A, Mw 26kDa, Medisorb, Alkermes Inc., Cincinnati, OH) in acetone was dropped on the PDMS mold, and after solvent evaporation, a 30 μm thick polymeric membrane was peeled out of the mould. The scaffolds used in the experiments were made by stacking eight 5x5mm membranes, achieving a thickness of 150 to 200 μm.

E.2.5 RT-PCR analyses

Total ribonucleic acid (RNA) was extracted using RNAzol reagent (Tel-Test Inc., Friendswood, TX) from satellite cell cultures and from mouse skeletal muscle and liver. One μg of total RNA was then purified using the DNAse Treatment and Removal Reagents (Ambion Inc., St. Austin, TX) and reversetranscribed using Superscript II reverse transcriptase (Invitrogen). RT-PCR was performed with the following primers: Pax7(F:5'-GAGTTCGATTAGCCGAGTGC-3';R:5'-CGGGTTCTGATTCCACATCT-3');Myf5(F:5'-CTGTCTGGTCCCGAAAGAAC-3';R:5'-GAGAGGGAAGCTGTGTCCTG-3');MyoD(F:5'-TACCCAAGGTGGAGATCCTG-3';R:5'-CATCATGCCATCAGAGCAGT-3');Myogenin(F:5'-CAGTGAATGCAACTCCCACA-3';R:50-GGCGTCTGTAGGGTCAGC-3');Desmin(F:5'-ACTTGACTCAGGCAGCCAAT-3';R:5'-ATCCTCCAGCTCCCTCATCT-3');beta-actin(F:5'-CTAAGGCCAACCGTGAAAAG-3'; R:5'-GG AGAGCATAGCCCTCGTAG-3').

E.2.6 *In vivo* cell delivery

At passage 3, satellite cells were detached from the plates using citrate buffer solution, and 10^6 cells were seeded onto one 5x5mm scaffold that had been previously coated with Matrigel (1/10 vol/vol in DMEM). After cell adhesion, seeded scaffolds were kept in proliferating medium for 24 h. For control muscles, 10^6 cells from the same batch and passage were also detached using citrate buffer solution and directly injected with a 30G insulin syringe. Each scaffold was inserted in a *tibialis anterior* muscle, in a pocket created by removing a volume of tissue comparable to that of the matrix itself; the insertion points were then closed with non-absorbable sutures. Similar pockets were also created in the

counter-lateral (control) muscles, which, after suturing, were injected with the dish-cultured cells and suspended in 50 μl of 1/10 ice-cold Matrigel in DMEM. Particular care was put into avoiding leakage of the cell suspension. Satellite cells from GFP-positive mice were implanted in C57BL/6 wild-type mice.

E.2.7 Immunocytochemistry and histochemistry analyses

For immunocytochemistry, the antibodies were anti-MyoD (Santa Cruz, Heidelberg, Germany) and anti-troponin I (Chemicon,Chandlers Ford,Hampshire,UK). After treatment with fluorescent secondary antibodies, cells were counterstained using 4',6-diamidino-2-phenylindole and mounted in fluorescent mounting medium (DakoCytomation, Milano, Italy). Percentages of MyoD-positive cells were determined by counting 2x5 independent fields in two 2 cm^2 wells. Immuno-histochemical analyses were performed on 10 mm cryo-sections at the indicated time points after cell transplantation. Sections were taken at different levels, spanning the whole muscle length. In C57BL/6mice, GFP was detected using an anti-GFP antibody (Molecular Probes-Invitrogen, Milano, Italy). Percentages of GFP-positive fibers were determined on the best section in each condition, counting all the fibers from low-magnification images.

E.2.8 Western blot analyses

Thirty muscle sections were dissolved in 100 μl of lysis buffer (Tris-phosphate 25mM, ethylenediaminetetraacetic acid 2mM, dithiothreitol 2 mM, Triton X100 1%, glycine 10%). Approximately 11 mg of proteins were loaded in each lane in a pre-cast 4% to 12% gradient poly-acrylamide gel (Invitrogen) that was then run for 2.5 h before being blotted onto nitrocellulose membrane. Filters were then treated using an anti-GFP monoclonal antibody (Roche, Milano, Italy), followed by goat anti-mouse immunoglobulin G horseradish peroxidase–conjugated (Dako-Cytomation, Milano, Italy). Chemi-luminescence was induced with an enhanced chemiluminescence reagents kit (Sigma-Aldrich), and light emission was recorded using a Kodak Image Station 440 CF (Kodak- Celbio,Milano, Italy).Membranes were then stripped and reprobed using an antibody against cytoplasmic actin (Roche).

E.2.9 Microscope and imaging system

Phase-contrast images were acquired using an inverted microscope (Olympus IX71, Tokyo, Japan). Immunofluorescence images were acquired using a fluorescence microscope (Leica DMR, San Francisco, CA) fitted with a CCD photocamera (Leica DFC 480). Measurements of the area of cell migration were taken using the AnalySIS Image Processing software (Microscopy, MA, Olympus, Tokyo, Japan), marking the virtual perimeter identified by the most peripheral satellite cells and positive myofibers.

E.3 Results

E.3.1 Murine satellite cells isolation and characterization

Single muscle fibers were successfully isolated from GFP-positive mice. Once seeded on matrigel-coated dishes, the quiescent satellite cells present on the fibers started to proliferate and originated a myogenic population, which we termed murine satellite cells (mSCs) (Fig. 1A). mSCs usually migrated from the original fibers and started to proliferate 24 to 48 h after plating. In each experiment, myogenicity of the isolated cells was the first parameter we controlled. When the cells were allowed to reach full confluence, they formed a wide network of myotubes (Fig. 1B) that showed spontaneous contractile properties. Immunostaining analyses revealed that murine cells expressed MyoD and, once fused into myotubes, troponin I (Fig. 1C). Flow cytometric analysis showed that isolated cells were rather homogeneous; in particular, the majority of mSCs expressed CD44 and low levels of CD34 and of the stem cell marker CD117. Also, mSCs were negative for CD45, CD90, Flk-1, MHC-I, and MHC-II (Fig. 1D). The expression patterns did not change between the first and third passages. Immunofluorescence further confirmed this latter finding, because the percentage of MyoD-positive cells was more than 95% at passages 1 and 3 (data not shown).

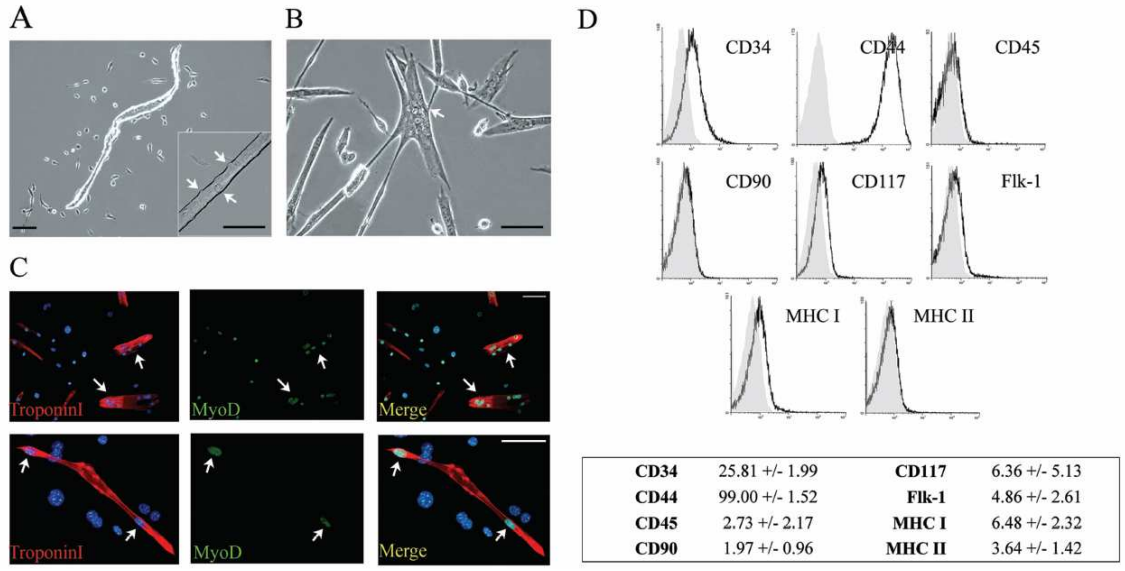

CD34	25.81 +/- 1.99	**CD117**	6.36 +/- 5.13
CD44	99.00 +/- 1.52	**Flk-1**	4.86 +/- 2.61
CD45	2.73 +/- 2.17	**MHC I**	6.48 +/- 2.32
CD90	1.97 +/- 0.96	**MHC II**	3.64 +/- 1.42

Figure 1. *Characterization of murine satellite cells (mSCs). (A) Proliferation of mSCs around a single, isolated muscle fiber. Nonproliferating cells could be seen on the fiber's surface (arrows). (B) Satellite cells maintained in culture fused to form multi-nucleated syncytia (arrows). Scale bar 100 μm. (C) Immunostaining revealed the expression of the myogenic factor MyoD and sarcomeric protein troponin I. Scale bar 30 μm. (D) Cytofluorimetric analyses of mSC.*

E.3.2 Preparation of bio-compatible scaffolds

The geometry of the polymer's grid (Fig. 2A) was chosen to mimic the topology of the muscle's fibers *in vivo* and to promote the alignment of the seeded cells. The micropattern of the PLGA membrane, shown in Figure 2B, consisted of 50 μm wide polymeric stripes connected by 10 μm lateral bridges that provided the mechanical integrity of the membrane. The 3D scaffold (Fig. 2C) was produced using thermal lamination, a process that preserved the biocompatibility of the final product as well as its micropattern. The 3D scaffold had a porosity of 40%, and its interconnected internal cavities allowed the diffusion of oxygen and metabolites, as well as cell migration. PLGA was chosen to prevent the scaffold biodegradation during the first month of implantation while providing complete degradability in 6 months.[26]

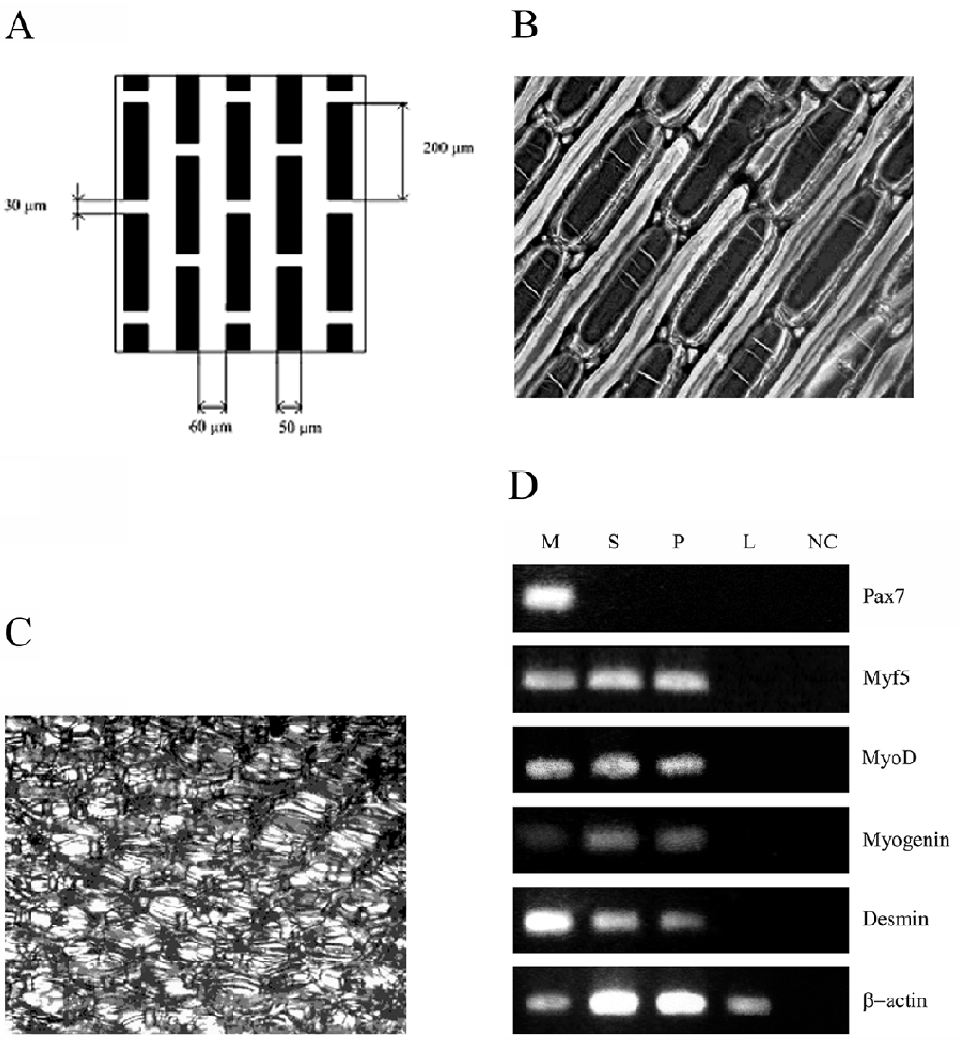

Figure 2. *(A) Graphic representation of the structure of a single layer of the polymer. (B) Actual image of a single poly(lactic co-glycolic acid) layer. (C) Image of nine overlapping layers, ready to be seeded with cells. (D) Reverse transcriptase polymerase chain reaction (RT-PCR) analyses of several muscle-specific transcripts from muscle tissue (M), polymer-seeded cells (S), and cells kept on Matrigel-coated plates (P). Total ribonucleic acid from liver (L) and RT-PCR mix alone (NC) were used as negative controls.*

E.3.3 Culture of satellite cells within micro-patterned scaffold

In this initial set of experiments, we compared the phenotype of satellite cells grown on the scaffold with that of cells kept on plastic. First, we assessed the efficiency of our seeding procedure by counting the number of cells that did not attached to the matrix (i.e., that were still in suspension or had adhered to the plate).

These measurements showed that after 24 h, approximately 90% of mSCs had attached to the scaffold. We then checked whether mSCs could maintain their myogenic characteristics once seeded onto the scaffolds. Using RT-PCR, we observed that the expression of the myogenic transcription factors Myf5, MyoD, and myogenin was virtually identical between satellite cells cultured on dishes and those cultured on the polymer for 24 h (Fig. 2D).

E.3.4 *In vivo* delivery of satellite cells

Equal amounts of mSCs derived from transgenic C57BL/ 6-TgnEGFP animals were seeded on scaffolds and implanted in the tibialis anterior muscles of syngenic, GFPnegative mice or directly injected into the contralateral limbs. In each animal, injected and scaffold-delivered cells were obtained from the same preparation. In addition, the number of matrix-implanted cells was approximately 10% lower than the number of injected cells. For experiments with GFP-positive cells, the immunohistochemical analysis of recipient muscles was carried out 1, 2, and 4 weeks after implantation. Our results indicated that transplanted cells progressively migrated from the polymer into the surrounding muscle and eventually integrated into the regenerating myofibers. In particular, at 1 and 2 weeks after implantation, many cells were still present in the polymer, and only a few satellite cells were fused with the regenerating myofibers (Fig. 3A, B). After 4 weeks, the number of GFP-positive myofibers had increased (Fig. 3E). These were either pre-existing myofibers (with peripheral nuclei) into which the GFP-positive cells had fused or newly formed myofibers (with central nuclei). At this time point, most of implanted cells had fused into myofibers (also at a certain distance from the implantation site), and only a few of them were still present in the scaffolds (Fig. 3C). Furthermore, in some of the samples, we could observe the presence of green fluorescent myotubes within the implanted matrices (Fig. 3D).

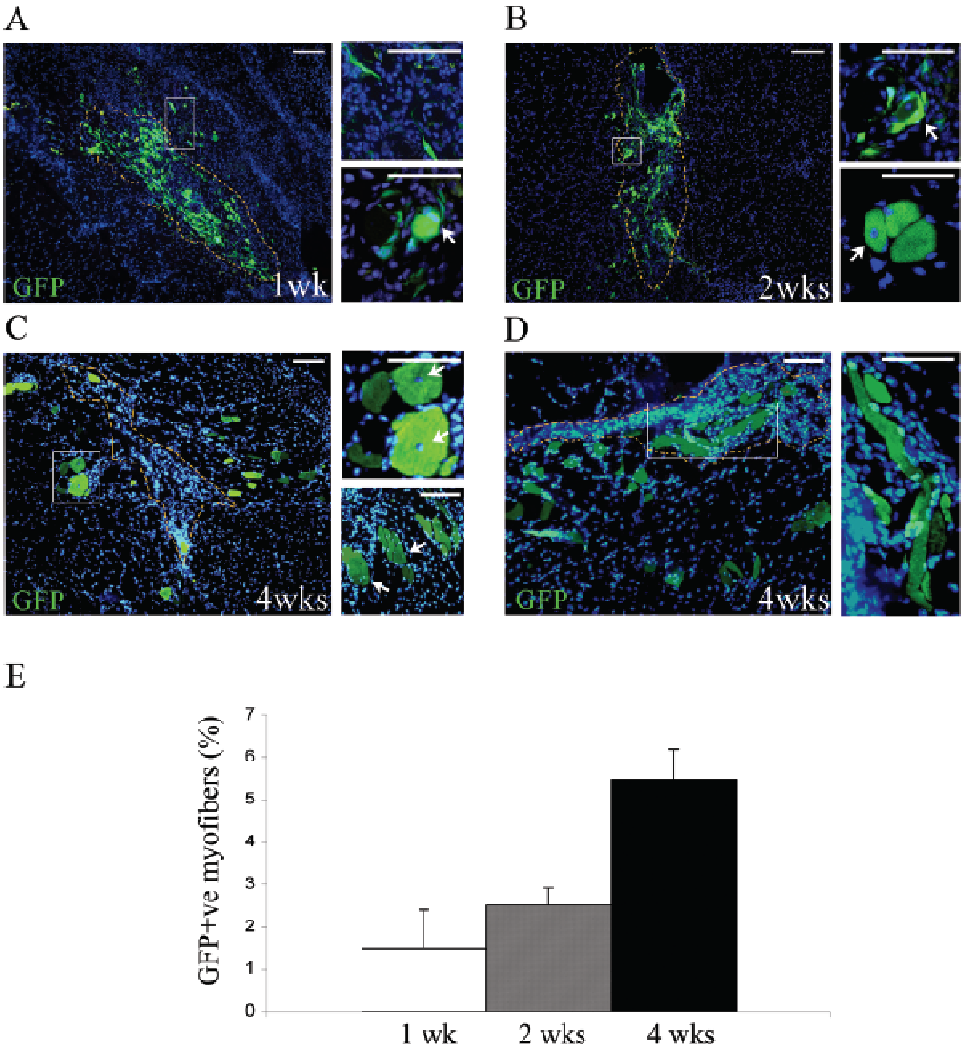

Figure 3. *(A) Graphic Migration of murine satellite cells (mSCs) from the scaffold into regenerating muscle. (A) One week after implantation, mSCs were mostly found within the polymer. Only sporadic GFP-positive fibers could be seen outside the polymer. (B) Two weeks after implantation, mSCs were still present in the polymer, but some more GFP-positive fibers could be found in the muscle mass. (C) Four weeks after implantation, scaffold-delivered mSCs were mostly integrated into the regenerating muscle and were detectable as green positive fibers. (D) At 4 weeks, GFP-positive myotubes could also be found inside the implanted polymer. Small arrows in insets indicate the position of the nuclei inside the fibers. Boundaries of the scaffold visualized in phase contrast were reported. (E) Maximum number of GFP-positive fibers found at the different time points; 4 weeks after implantation, approximately 5% of fibers had incorporated the mSCs. Scale bar=100 μm.*

Despite the fact that the number of scaffold-delivered cells was lower than the number of injected cells, we found that 4 weeks post-transplantation, the number of GFPpositive fibers was significantly higher in muscles that had received the seeded polymers than in those into

which satellite cells had been injected directly (5.5% vs 2.5%, p< 0.001) (Fig. 4A, B). This finding was further confirmed using western blot analysis, which showed that the amount of GFP produced in the muscles that had received the seeded polymers was approximately 3 times as high as that found in contralateral limbs (Fig. 4C, D). We then decided to quantify the capacity of the cells to migrate from the site of implantation/injection.We measured the area of distribution of GFP-positive fibers in serial sections, as described in Materials and Methods, from muscles harvested at the 4-week time point. The analyses indicated that the distribution areas appeared to be wider in muscles that had received the scaffolds (Fig. 5). The fact that statistical significance was not reached was likely due to the high variability found between the different animals (n=6).

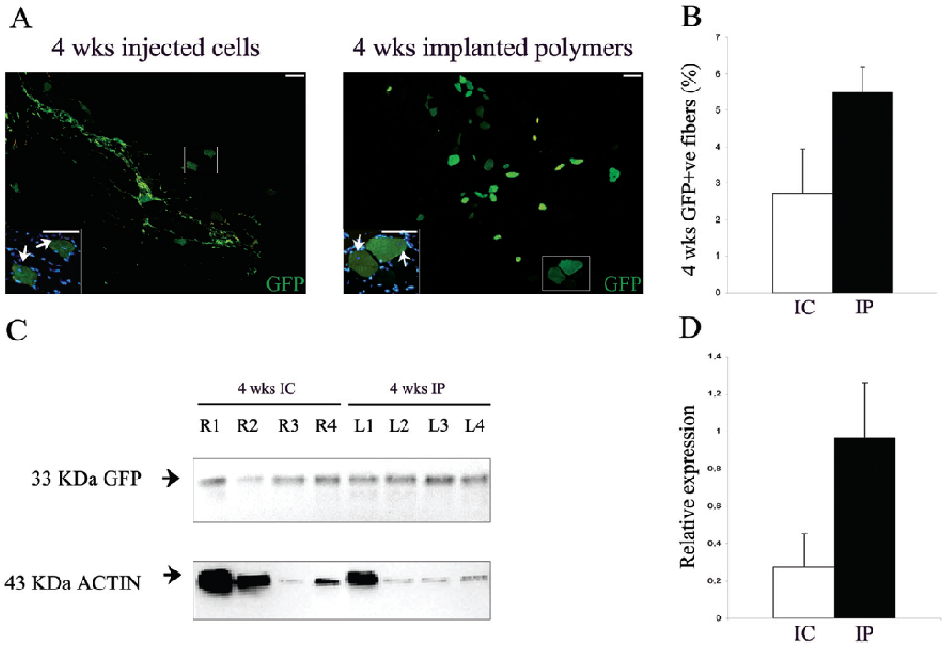

Figure 4. *Scaffold delivery of murine satellite cells (mSCs) is more efficient than direct injection. (A) Muscles that received injected (IC, injected cells) and scaffold-seeded (IP, implanted polymers) mSCs were immunostained for green fluorescent protein (GFP) 4 weeks after surgery. Small arrows in insets indicate the position of the nuclei inside the fibers. Scale bar=100 μm. (B) Maximum percentage of GFP-positive fibers found after mSC injection and polymer implantation. (C) Analysis by western blot of the GFP total content in 8 tibialis anterior muscles, 4 weeks earlier, after receiving injected cells (in the right leg, R), or the seeded scaffold (in the left leg, L). Cytoplasmic actin was used as internal loading control. (D) Normalized amount of relative GFP content in the 2 groups.*

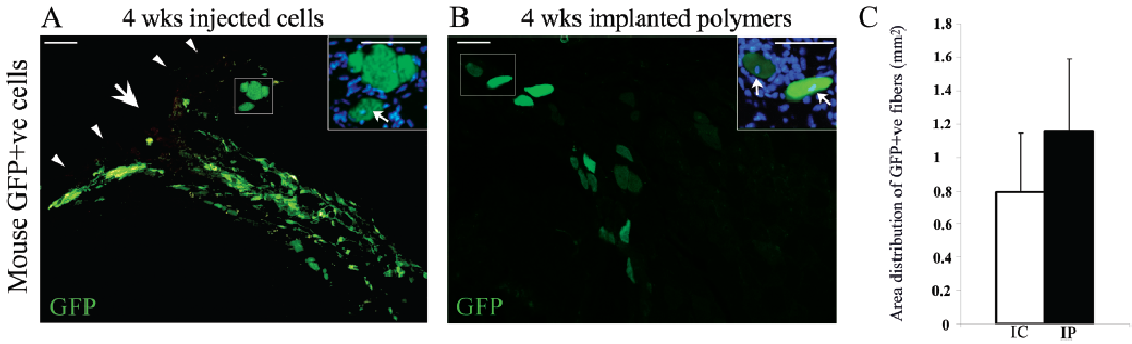

Figure 5. *Distribution area of the transplanted cells 4 weeks after implants. GFP-positive myofibers were observed in serial sections of recipient muscles after cell injection and polymer implantation. (A) Most of the cells remained localized in the injection site and some green myofibers could be seen close to the main pool of green fluorescent protein (GFP)-positive cells. Arrowheads indicate the contour of muscle section; the bigger arrow indicates the injection point. Small arrows in insets indicate the position of the nuclei inside the fibers. (B) GFP-positive murine satellite cells (mSCs) migrated from the polymers and formed positive myofibers far from the site of implant, which was outside the area shown in the photo. Scale bar¼100 mm. (C) Distribution of GFP-positive fibers formed by injected (IC, injected cells) or transplanted by scaffold (IP, implanted polymers) mSCs.*

E.4 Discussion

In most myopathies, clinical outcome is ultimately due to a failure of satellite cells to maintain muscle regeneration after continuous degeneration–regeneration cycles.[27–29] A possible therapeutic option would therefore be the transplantation of progenitor cells into the damaged muscles with the aim of maintaining the regenerative capacity of the muscle itself. There have been several reported strategies, with cells derived from muscles[30,31] and other sources, such as bone marrow and peripheral blood,[32,33] although results have been somewhat discordant; in particular, although administration of circulating hematopoietic cells led to a phenotype improvement in mdx mice, data obtained from a patient with DMD who had received a bone marrow transplant suggested that this might not be the case in humans.[34] Skeletal myoblasts, which can regenerate myofibers without needing other sources of myogenic cells,[35] have also been considered and could be one of the most manageable types of donor cells for muscle cell therapy.[36] However, there are significant limitations described in terms of cell viability with systemic delivery and direct muscle injection.

In this study, we explored the regenerative potential of mSCs delivered into damaged muscle using a biodegradable matrix. As previously described, single fiber isolation is a suitable technique to obtain a pure population of satellite cells, and it has been extensively used in rodents.[37–39] Once they had moved away from the fibers and started to divide, mSCs displayed a homogeneous morphology, and their myogenic characteristics were confirmed using immunostaining analyses with several muscle-specific markers. RT-PCR also showed that cells grown on scaffold and on plastic shared the same expression pattern for myogenic markers.

We also explored the expression of the paired box transcription factor Pax7, a well-established marker of quiescent satellite cells that is also expressed in cultured myoblasts.[40] No Pax7 signal was found in mSCs using RTPCR (Fig. 3D) or immunofluorescence (not shown). We believe that the absence of Pax7 expression suggests that the mSCs were in a later differentiation stage at the time of the analyses.

The phenotype of satellite-derived cells was also investigated using flow cytometry. mSCs maintained in culture a low expression of CD34, normally expressed by quiescent and activated satellite cells.[41] Cultured cells did not appear to be hematopoietic in origin, because they were negative for CD45 and CD117.[42] The presence of endothelial and mesenchymal cells was ruled out because no Flk1 or CD90 was found in mSCs.

Even after several days of culture, absence of MHC-II was demonstrated on mSCs using flow cytometry. Recent studies indicate that mesenchymal stem cells lacking MHCII avoid allogenic reaction.[43] Should this hold true for our satellite-derived cells, it would greatly enhance their therapeutic potential.

More studies will be needed to confirm this hypothesis. Once seeded onto the polymers, mSCs maintained their myogenic characteristics and expressed markers associated with the activated, proliferative state, namely Myf5, Mrf4, and MyoD.44,45 Once implanted in the recipient muscles, the cells began to migrate from the polymer into the area of regeneration, but the process was slow. After 1 week, most of the cells were still inside the polymers, whereas after 2 and 4 weeks, we observed that cells had fused with regenerating, pre-existing fibers and had formed new fibers within the polymers.

To compare the efficiency of our delivery method with direct injection of myoblasts, in each experiment, we injected the same number of cells, derived from the same batch, into the sham-operated, contralateral leg of the same animal. Our data indicated that, even

though the number of cells delivered by the polymer was at best 90% of that delivered using intramuscular injection, the number of GFP-positive fibers obtained with the scaffolds was more than double that obtained using direct injection. Furthermore, western blot analyses showed that, 4 weeks after surgery, the total amount of GFP in scaffold-receiving muscles was almost 3 times as high as in the controls, indicating the presence of more GFP-expressing nuclei. Limited mobility of injected myoblasts has been reported to be one of the main factors hampering such an approach. In our study, using the seeded polymers, we could also appreciate a wider distribution of the GFP-positive myofibers than of controls.

Intra-muscular injection is the only described procedure to introduce large amounts of exogenous myoblasts into an injured muscle. Systemic delivery (i.e. intravenous or intraarterial), has been unsuccessful because satellite cells do not have the ability to pass through the endothelial barrier. In our experiments, part of the muscle mass was removed to create the physical space for the implantation and, at the same time, induce regenerative processes. The amount of damage was not exactly quantified, because our purpose was not to repair the lesion but to create an environment in which implanted cells were stimulated to proliferate and participate in regeneration. Our next step will be to implant the seeded scaffolds in a physiological model of muscle regeneration, the mdx mouse. We believe that this approach for cell delivery would be even more efficient in a dystrophic context, in which the whole muscle is constantly in a degeneration–-regeneration loop.

Polymer-based delivery could be used to treat the diaphragm, arguably the primary target of any treatment in dystrophic patients. In muscular dystrophies, the diaphragm is a target of paramount importance, yet no positive results have been reported with any cell-therapy approach. We believe that seeded scaffolds could prove useful in this regard, by being applied to its surface as laminar patches. Recent results reported for myoblast delivery in the ischemic heart through polymer implantations support the feasibility of this approach. In addition, scaffold-mediated delivery would fit well in a protocol of autologous myoblast transplantation associated with ex vivo genetic manipulation.

Finally, growth factors could also be employed and absorbed in the polymer before cell seeding. They could be released *in vivo*, with time-promoting proliferation, integration, and differentiation of the transplanted myoblasts .

In conclusion, our study shows for the first time the possibility of delivering mouse myoblasts into the skeletal muscle using a fully biodegradable engineered polymer. We

believe that this approach could offer a new therapeutic tool for muscle-related diseases in the near future.

E.5 Acknowledgement

The financial support of the ‘‘Fondazione Citta` della Speranza’’ ONLUS (grant to CM) and of the Association Francaise contre les Myophaties (grant to PGG) is gratefully acknowledged. We are grateful to Premal A. Patel and Roberta Destro for helpful discussion.

E.6 References

1. Mauro, A. Satellite cell of skeletal muscle fibers. J Biophys Biochem Cytol 9, 493, 1961.

2. Skuk, D. and Tremblay, J.P. Progress in myoblast transplantation: a potential treatment of dystrophies. Microsc Res Tech 48, 213, 2000.

3. Skuk, D. and Tremblay, J.P. Myoblast transplantation: the current status of a potential therapeutic tool for myopathies. J Muscle Res Cell Motil 24, 285, 2003.

4. Partridge, T.A. Invited review: myoblast transfer: a possible therapy for inherited myopathies? Muscle Nerve 14, 197, 1991.

5. Huard, J., Bouchard, J.P., Roy, R., Labrecque, C., Dansereau, G., Lemieux, B., and Tremblay, J.P. Myoblast transplantation produced dystrophin-positive muscle fibres in a 16-year-old patient with Duchenne muscular dystrophy. Clin Sci (Lond) 81, 287, 1991.

6. Brussee, V., Merly, F., Tardif, F., and Tremblay, J.P. Normal myoblast implantation in MDX mice prevents muscle damage by exercise. Biochem Biophys Res Commun 250, 321, 1998.

7. Grounds, M.D. Commentary on the present state of knowledge for myoblast transfer therapy. Cell Transplant 5, 431, 1996.

8. Tremblay, J.P., Malouin, F., Roy, R., Huard, J., Bouchard, J.P., Satoh, A., and Richards, C.L. Results of a triple blind clinical study of myoblast transplantations without immunosuppressive treatment in young boys with Duchenne muscular dystrophy. Cell Transplant 2, 99, 1993.

9. Gussoni, E., Pavlath, G.K., Lanctot, A.M., Sharma, K.R., Miller, R.G., Steinman, L., and Blau, H.M. Normal dystrophin transcripts detected in Duchenne muscular dystrophy patients after myoblast transplantation. Nature 356, 435, 1992.

10. Skuk, D., Roy, B., Goulet, M., Chapdelaine, P., Bouchard, J.P., Roy, R., Dugre, F.J., Lachance, J.G., Deschenes, L., Helene, S., Sylvain, M., and Tremblay, J.P. Dystrophin expression in myofibers of Duchenne muscular dystrophy patients following intramuscular injections of normal myogenic cells. Mol Ther 9, 475, 2004.

11. Beauchamp, J.R., Morgan, J.E., Pagel, C.N., and Partridge, T.A. Dynamics of myoblast transplantation reveal a discrete minority of precursors with stem cell-like properties as the myogenic source. J Cell Biol 144, 1113, 1999.

12. Hodgetts, S.I., Beilharz, M.W., Scalzo, A.A., and Grounds, M.D. Why do cultured transplanted myoblasts die in vivo? DNA quantification shows enhanced survival of donor male myoblasts in host mice depleted of CD4þand CD8þcells or Nk1.1þcells. Cell Transplant 9, 489, 2000.

13. Qu, Z., Balkir, L., van Deutekom, J.C., Robbins, P.D., Pruchnic, R., and Huard, J. Development of approaches to improve cell survival in myoblast transfer therapy. J Cell Biol 142, 1257, 1998.

14. Smythe, G.M., Hodgetts, S.I., and Grounds, M.D. Problems and solutions in myoblast transfer therapy. J Cell Mol Med 5, 33, 2001.

15. Skuk, D., Caron, N., Goulet, M., Roy, B., Espinosa, F., and Tremblay, J.P. Dynamics of the early immune cellular reactions after myogenic cell transplantation. Cell Transplant 11, 671, 2002.

16. Collins, C.A., Olsen, I., Zammit, P.S., Heslop, L., Petrie, A., Partridge, T.A., and Morgan, J.E. Stem cell function, selfrenewal, and behavioral heterogeneity of cells from the adult muscle satellite cell niche. Cell 122, 289, 2005.

17. Sampaolesi, M., Torrente, Y., Innocenzi, A., Tonlorenzi, R., D'Antona, G., Pellegrino, M.A., Barresi, R., Bresolin, N., De Angelis, M.G., Campbell, K.P., Bottinelli, R., and Cossu, G. Cell therapy of alpha-sarcoglycan null dystrophic mice through intra-arterial delivery of mesoangioblasts. Science 301, 487, 2003.

18. Torrente, Y., Camirand, G., Pisati, F., Belicchi, M., Rossi, B., Colombo, F., El, F.M., Caron, N.J., Issekutz, A.C., Constantin, G., Tremblay, J.P., and Bresolin, N. Identification of a putative pathway for the muscle homing of stem cells in a muscular dystrophy model. J Cell Biol 162, 511, 2003.

19. Marzaro, M., Conconi, M.T., Perin, L., Giuliani, S., Gamba, P., De Coppi, P., Perrino, G.P., Parnigotto, P.P., and Nussdorfer, G.G. Autologous satellite cell seeding improves in vivo biocompatibility of homologous muscle acellular matrix implants. Int J Mol Med 10, 177, 2002.

20. Conconi, M.T., De Coppi, P., Bellini, S., Zara, G., Sabatti, M., Marzaro, M., Zanon, G.F., Gamba, P.G., Parnigotto, P.P., and Nussdorfer, G.G. Homologous muscle acellular matrix seeded with autologous myoblasts as a tissue-engineering approach to abdominal wall-defect repair. Biomaterials 26, 2567, 2005.

21. De Coppi, P., Delo, D., Farrugia, L., Udompanyanan, K., Yoo, J.J., Nomi, M., Atala, A., and Soker, S. Angiogenic gene-modified muscle cells for enhancement of tissue formation. Tissue Eng 11, 1034, 2005.

22. Christman, K.L., Fok, H.H., Sievers, R.E., Fang, Q., and Lee, R.J. Fibrin glue alone and skeletal myoblasts in a fibrin scaffold preserve cardiac function after myocardial infarction. Tissue Eng 10, 403, 2004.

23. Rosenblatt, J.D., Lunt, A.I., Parry, D.J., and Partridge, T.A. Culturing satellite cells from living single muscle fiber explants. In Vitro Cell Dev Biol Anim 31, 773, 1995.

24. Kane, R.S., Takayama, S., Ostuni, E., Ingber, D.E., and Whitesides, G.M. Patterning proteins and cells using soft lithography. Biomaterials 20, 2363, 1999.

25. Vozzi, G., Flaim, C., Ahluwalia, A., and Bhatia, S. Fabrication of PLGA scaffolds using soft lithography and microsyringe deposition. Biomaterials 24, 2533, 2003.

26. Grayson, A.C., Voskerician, G., Lynn, A., Anderson, J.M., Cima, M.J., and Langer, R. Differential degradation rates in vivo and in vitro of biocompatible poly(lactic acid) and poly(glycolic acid) homo- and co-polymers for a polymeric drug-delivery microchip. J Biomater Sci Polym Ed 15, 1281, 2004.

27. Burghes, A.H., Logan, C., Hu, X., Belfall, B., Worton, R.G., and Ray, P.N. A cDNA clone from the Duchenne/Becker muscular dystrophy gene. Nature 328, 434, 1987.

28. Cossu, G. and Mavilio, F. Myogenic stem cells for the therapy of primary myopathies: wishful thinking or therapeutic perspective? J Clin Invest 105, 1669, 2000.

29. Engel, A.G., Yamamoto, M., and Fischbeck, K.H. Comprehensive description of the clinical and laboratory features and therapy for polymyositis, dermamyositis and inclusion body myositis. 1130, 1994.

30. Asakura, A., Seale, P., Girgis-Gabardo, A., and Rudnicki, M.A. Myogenic specification of side population cells in skeletal muscle. J Cell Biol 159, 123, 2002.

31. Cao, B. and Huard, J. Muscle-derived stem cells. Cell Cycle 3, 104, 2004.

32. Lee, J.H., Kosinski, P.A., and Kemp, D.M. Contribution of human bone marrow stem cells to individual skeletal myotubes followed by myogenic gene activation. Exp Cell Res 307, 174, 2005.

33. Torrente, Y., Belicchi, M., Sampaolesi, M., Pisati, F., Meregalli, M., D'Antona, G., Tonlorenzi, R., Porretti, L., Gavina, M., Mamchaoui, K., Pellegrino, M.A., Furling, D., Mouly, V., Butler-Browne, G.S., Bottinelli, R., Cossu, G., and Bresolin, N. Human circulating AC133(þ) stem cells restore dystrophin expression and ameliorate function in dystrophic skeletal muscle. J Clin Invest 114, 182, 2004.

34. Gussoni, E., Bennett, R.R., Muskiewicz, K.R., Meyerrose, T., Nolta, J.A., Gilgoff, I., Stein, J., Chan, Y.M., Lidov, H.G., Bonnemann, C.G., Von, M.A., Morris, G.E., Den Dunnen, J.T., Chamberlain, J.S., Kunkel, L.M., and Weinberg, K. Long-term persistence of donor nuclei in a Duchenne muscular dystrophy patient receiving bone marrow transplantation. J Clin Invest 110, 807, 2002.

35. Zammit, P.S., Heslop, L., Hudon, V., Rosenblatt, J.D., Tajbakhsh, S., Buckingham, M.E., Beauchamp, J.R., and Partridge, T.A. Kinetics of myoblast proliferation show that resident satellite cells are competent to fully regenerate skeletal muscle fibers. Exp Cell Res 281, 39, 2002.

36. Skuk, D. and Tremblay, J.P. Cell therapies for inherited myopathies. Curr Opin Rheumatol 15, 723, 2003. 37. Hashimoto, N.,Murase, T., Kondo, S., Okuda, A., and Inagawa- Ogashiwa, M. Muscle reconstitution by muscle satellite cell descendants with stem cell-like properties. Development 131, 5481, 2004.

38. Wozniak, A.C., Pilipowicz, O., Yablonka-Reuveni, Z., Greenway, S., Craven, S., Scott, E., and Anderson, J.E. C-Met expression and mechanical activation of satellite cells on cultured muscle fibers. J Histochem Cytochem 51, 1437, 2003.

39. Anderson, J. and Pilipowicz, O. Activation of muscle satellite cells in single-fiber cultures. Nitric Oxide 7, 36, 2002.

40. Seale, P., Sabourin, L.A., Girgis-Gabardo, A., Mansouri, A., Gruss, P., and Rudnicki, M.A. Pax7 is required for the specification of myogenic satellite cells. Cell 102, 777, 2000.

41. Beauchamp, J.R., Heslop, L., Yu, D.S., Tajbakhsh, S., Kelly, R.G., Wernig, A., Buckingham, M.E., Partridge, T.A., and Zammit, P.S. Expression of CD34 and Myf5 defines the majority of quiescent adult skeletal muscle satellite cells. J Cell Biol 151, 1221, 2000.

42. Kinney-Freeman, S.L., Majka, S.M., Jackson, K.A., Norwood, K., Hirschi, K.K., and Goodell, M.A. Altered phenotype and reduced function of muscle-derived hematopoietic stem cells. Exp Hematol 31, 806, 2003.

43. Ryan, J.M., Barry, F.P., Murphy, J.M., and Mahon, B.P. Mesenchymal stem cells avoid allogeneic rejection. J Inflamm (Lond) 2, 8, 2005.

44. Cornelison, D.D. and Wold, B.J. Single-cell analysis of regulatory gene expression in quiescent and activated mouse skeletal muscle satellite cells. Dev Biol 191, 270, 1997.

45. Cooper, R.N., Tajbakhsh, S., Mouly, V., Cossu, G., Buckingham, M., and Butler-Browne, G.S. In vivo satellite cell activation via Myf5 and MyoD in regenerating mouse skeletal muscle. J Cell Sci 112 (Pt 17), 2895, 1999.

Appendix F

Efficient Delivery of Human Single Fiber-Derived Muscle Precursor Cells Via Biocompatible Scaffold

Luisa Boldrin,*¶1,2 Alberto Malerba,*¶1 Libero Vitiello,† Elisa Cimetta,‡ Martina Piccoli,* Chiara Messina,* Pier Giorgio Gamba,§ Nicola Elvassore,‡ and Paolo De Coppi*¶

*Stem Cell Processing Laboratory, Department of Paediatrics, University of Padova, Padova, Italy
†Gene Transfer Laboratory, Department of Biology, University of Padova, Padova, Italy
‡Department of Chemical Engineering, University of Padova, Padova, Italy
§Paediatric Surgery, Department of Paediatrics, University of Padova, Padova, Italy
¶Surgery Unit, Institute of Child Health, University College of London, London, UK

Cell Transplantation

Vol. 17, pp. 577–584, 2008

Key words: Human single fibers; Muscle precursor cells; Biocompatible scaffold; Muscle regeneration

Abstract

The success of cell therapy for skeletal muscle disorders depends upon two main factors: the cell source and the method of delivery. In this work we have explored the therapeutic potential of human muscle precursor cells (hMPCs), obtained from single human muscle fibers, implanted in vivo via micropatterned scaffolds. hMPCs were initially expanded and characterized in vitro by immunostaining and flow cytometric analysis. For in vivo studies, hMPCs were seeded onto micropatterned poly-lactic-glycolic acid 3D-scaffolds fabricated using soft-lithography and thermal membrane lamination. Seeded scaffolds were then implanted in predamaged tibialis anterior muscles of CD1 nude mice; hMPCs were also directly injected in contralateral limbs as controls. Similarly to what we previously described with mouse precursors cells, we found that hMPCs were able to participate in muscle regeneration and scaffold-implanted muscles contained a greater number of human nuclei, as revealed by immunostaining and Western blot analyses. These results indicate that hMPCs derived from single fibers could be a good and reliable cell source for the design of therapeutic protocols and that implantation of cellularized scaffolds is superior to direct injection for the delivery of myogenic cells into regenerating skeletal muscle.

F.1 Introduction

Skeletal muscle has a remarkable regenerative capacity thanks to its resident stem cells. Among these, different populations have been described, depending on techniques of isolation, phenotype expression, and culture characteristics. Muscle-derived stem cells (MDSCs) (14, 32) have been isolated using different preplating techniques and have shown myogenic potential both in vitro and in vivo. Skeletal muscle also contains a population of stem cells, similar to the one isolated from bone marrow (BM), called side population (SP) (16). SP cells are able, if delivered intravenously, to provide a complete reconstitution of the hematopoietic compartment of lethally irradiated recipients, as well as to partially restore dystrophin expression in the muscles of mdx mice (16). Finally, myogenic precursors cells (MPCs) derived from satellite cells (29) have also been described. According to recent studies (10), MPCs represent the main source for progenitors enrolled in the regenerative processes of the skeletal muscle (6). Upon withdrawing from the

quiescent state, adopted in the niche between the sarcolemma and the basal lamina, MPCs enter into the proliferative state, becoming able to differentiate into myotubes and eventually restore skeletal muscle architecture. Many studies have been carried out in these cells, using different animal models (17,20,22,31) and different techniques (3,7,9,33,34).

A recent approach, based on the transplant of entire fibers as a method to conserve the stem character of satellite cells avoiding in vitro manipulation, has opened a new way for cell therapy (10). In this perspective, hMPCs, derived from intact single fibers and expanded in vitro, could show better potential for muscle regeneration than other myogenic progenitors previously described. Transplantation of these precursors could hence be a potential therapeutic approach for genetic and acquired myopathies, as well as for traumatic injuries.

In the past few years we have focused our interest on MPCs derived from single fibers for muscle cell transplantation, showing that these cells are a good tool for tissue engineering applications in rodents (11,12,25). In parallel, we have recently reported that human satellite cells can also be isolated and expanded from single muscle fibers (13). In this work we tested the capacity of hMPCs to contribute to in vivo muscle regeneration and compared two different ways of delivery—direct injection and cellularized scaffolds—as previously described with mouse MPCs (8).

F.2 Materials and Methods

F.2.1 Single Fiber Cultures From Human Skeletal Muscle

hMPCs were prepared from two biopsies of the rectus-abdominis muscle, harvested from healthy individuals who underwent elective surgery. This part of the study was approved by the Ethical Committee of the Azienda Ospedaliera Padova.

hMPCs were prepared from isolated myofibers as a modification of the protocol previously described (28). Single fibers were obtained after 3 h by enzymatic dissociation with collagenase (Sigma-Aldrich, Germany). After being carefully selected under an inverted microscope (Olympus IX71 Japan), isolated fibers were plated onto MatrigelTM (BD Biosciences, Italy) coated dishes and left undisturbed for 3 days so that satellite cells could move to the plate and proliferate. After that, plating medium was added (DMEM, 10% horse serum, and 1% chicken embryo extract). Subsequently, cells were trypsinized and

kept in culture for 2-3 more passages in proliferating medium (DMEM, 20% fetal bovine serum, 10% horse serum, and 0.5% chicken embryo extract) before being seeded onto the scaffold or injected in muscles. All cell culture reagents were from Gibco-Invitrogen, Italy.

F.2.2 Characterization of hMPCs by Flow Cytometry

Flow cytometry was performed with a Beckman Coulter cytometer (COULTER Epics XL-MCL) using EXPOTM 32 ADC Software, at passages 2–3 in culture. hMPCs were detached from the plates and stained with FITC- or PE-labeled antibodies against CD3, CD4, CD8, CD31, CD34, CD44, CD45, CD51, CD54, CD56, CD61, CD90 (Thy-1), CD106, CD117, CD133, HLA-ABC, HLA-DR (Immunotech, Coulter company, France), and CD73 (SH2) (BD Pharmingen).

F.2.3 Scaffolds

The 3D scaffolds used for the in vivo implantation were fabricated using poly(lactic-co-glycolic acid) (PLGA), an FDA-approved biodegradable and biocompatible polymeric material. Scaffolds were composed of overlapped individual, micropatterned membranes obtained using a soft-lithography technique (23). Briefly, an SU-8 mold with the desired geometry was created by spin coating (Delta 10, BLE, Germany) a uniform layer of photoresistant resin (SU-8, Microchem, USA) onto silicon wafers (Wacko, Germany) (Fig. 3A, I, II). After thermal treatment, the resin was selectively cross-linked by exposing the wafer to UV light through a patterned mask (Fig. 3A, III). After exposure, a treatment with the developer 1-methoxy-2-propanol acetate (Sigma-Aldrich) allowed to obtain the final mold (Fig. 3A, IV). Subsequently, a PDMS (Sylgard 184, Dow Corning, Michigan, USA) mold was prepared by pouring and curing the liquid precursor onto the patterned SU-8 as reported in the literature (Fig. 3A, V) (35). Finally, a solvent casting/replica molding technique was used to produce the PLGA membranes: a 15% w/w solution of poly-lactic-co-glycolide (PLGA50/50DL2.5A, Mw 26 kDa; Medisorb, Alkermes Inc., OH, USA) in acetone was dropped and spread over the PDMS mold (Fig. 3A, VI) and, after solvent evaporation, the polymeric micropatterned film was gently peeled from the mold (Fig. 3A, VII). The scaffolds used for the experiments were formed overlapping eight individual 30-μm-thick, 5 × 5-mm squared membranes, allowing a final thickness of 150–200 μm.

F.2.4 Animals

For this study we used six adult (6–8 weeks old) CD1-Foxn1nu nude mice (Charles River, Italy). Animals were housed and operated at the Animal Colony of the "Centro Interdipartimentale Vallisneri," University of Padova, under the conditions specified in the relevant bylaws of the Italian Ministry of Health.

F.2.5 In Vivo Cell Delivery

At passage 3, MPCs were detached from the plates using citrate buffer solution and 106 cells were seeded on one 5 × 5-mm scaffold, previously coated with Matrigel (1:10 v/v in DMEM). Equal amounts of hMPCs were either seeded on scaffolds and implanted in the tibialis anterior muscles of nude mice or directly injected in the contralateral limbs. For each animal, injected and scaffold-delivered cells were obtained from the same preparation. It should be noted that, due to losses during the seeding procedure, the actual number of cells present within the matrix was approximately 10% lower than the number of injected cells.

After cell adhesion, seeded scaffolds were kept in proliferating medium for 24 h. For control muscles, 106 cells from the same batch and passage were also detached with citrate buffer solution and directly injected with a 30-gauge insulin syringe.

Each scaffold was inserted in a *tibialis anterior* muscle, in a pocket created by removing a volume of tissue comparable to that of the matrix itself; the insertion points were then closed with nonabsorbable sutures. Similar pockets were also created in the contralateral (control) muscles, that, after suturing, were injected with the cells cultured on plate, suspended in 50 μl of 1:10 ice-cold Matrigel in DMEM. Particular care was taken to avoid leakage of the cell suspension.

F.2.6 Immunocytochemical and Histochemical Analyses

For immunocytochemistry the antibodies were as follows: anti-MyoD (Santa Cruz, Germany); anti-Pax7 (Developmental Studies Hybridoma Bank, Iowa, Usa); anti-desmin (MP Biomedicals, Belgium); and anti- TroponinI (Chemicon, Italy). After treatment with fluorescent secondary antibodies, cells were counterstained with DAPI and mounted in

fluorescent mounting medium (DakoCytomation, Italy). Immunohistochemical analyses were performed on 10-μm cryosections 1 and 4 weeks after cell transplantation. Sections were taken at different levels, spanning the whole muscle length. hMPCs were detected using a monoclonal antibody against the Human Nuclear Antigen (HNA) (Chemicon, UK).

Immunofluorescence images were acquired using a fluorescence microscope (LEICA DMR, California, USA) equipped with a CCD photocamera (LEICA DFC 480).

F.2.7 Western Blot Analyses

Thirty muscle sections were dissolved in 100 μl of lysis buffer (Tris-phosphate 25 mM, EDTA 2 mM, DTT 2 mM, Triton X-100 1%, glycin 10%). Approximately 40 μg of protein per lane was loaded in a 12% polyacrylamide gel that was then run for 2.5 h before being blotted onto nitrocellulose membrane. Filters were then treated with the anti-HNA monoclonal antibody, followed by goat anti-mouse IGg HRP-conjugated (Dako-Cytomation). Chemiluminescence was induced with the “enhanced chemiluminescence reagents” kit (Amersham, Milano, Italy) and light emission was recorded onto X-ray films (Amersham). Densitometric analysis was performed using a Kodak Image Station 440 CF. Membranes were then stripped and reprobed using an antibody against cytoplasmic actin (Santa Cruz).
Results were expressed as means ± SEM. Statistical significance was evaluated by the unpaired Student t-test, with $p < 0.05$ considered significant.

F.2.8 Western blot analyses

Thirty muscle sections were dissolved in 100 μl of lysis buffer (Tris-phosphate 25mM, ethylenediaminetetraacetic acid 2mM, dithiothreitol 2 mM, Triton X100 1%, glycine 10%). Approximately 11 mg of proteins were loaded in each lane in a pre-cast 4% to 12% gradient poly-acrylamide gel (Invitrogen) that was then run for 2.5 h before being blotted onto nitrocellulose membrane. Filters were then treated using an anti-GFP monoclonal antibody (Roche, Milano, Italy), followed by goat anti-mouse immunoglobulin G horseradish peroxidase–conjugated (Dako-Cytomation, Milano, Italy). Chemi-luminescence was induced with an enhanced chemiluminescence reagents kit (Sigma-Aldrich), and light emission was recorded using a Kodak Image Station 440 CF (Kodak- Celbio,Milano,

Italy).Membranes were then stripped and reprobed using an antibody against cytoplasmic actin (Roche).

F.3 Results

F.3.1 hMPC Isolation and Characterization

Single muscle fibers were successfully isolated from human muscle biopsies. Once seeded on Matrigel-coated dishes, the quiescent satellite cells present on the fibers started to proliferate and originated a cell population, defined as hMPCs (Fig. 1A). hMPCs usually started to proliferate and migrated from the original fibers 72 h after plating. hMPCs were highly fusogenic, in that they tended to form myotubes as soon as they touched each other (Fig. 1B), and expressed MyoD, Pax7, desmin, and, in myotubes, TroponinI (Fig. 1C). Analysis by flow cytometry showed that hMPCs were rather homogeneous. In particular, most of them expressed CD44, CD56, CD73, and HLA-ABC, and a lower level of CD51, CD54, and CD90. On the other hand, they were negative for CD3, CD4, CD8, CD31, CD34, CD45, CD61, CD106, CD117, CD133, and HLA-DR (Fig. 2). Importantly, such expression patterns did not change between the first and the third passage (data not shown).

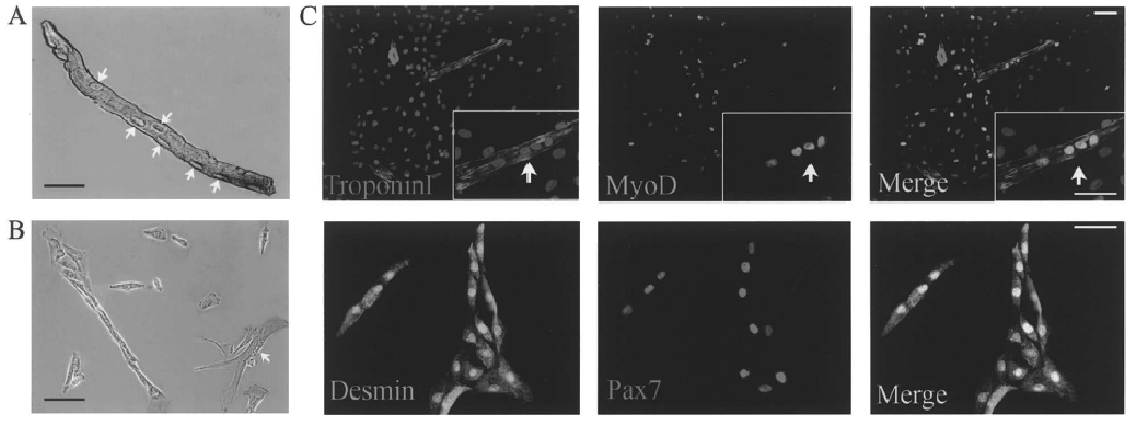

Figure 1. *hMPC characterization. (A) Single fiber derived from human biopsy, with its adhering satellite cells (arrows). (B) Once released, hMPCs proliferated and tended to align and fuse into myotubes (arrow). Scale bar: 100 μm. (C) hMPCs were immunostained for MyoD and TroponinI. Aligned hMPCs were also desmin positive and some of them were Pax7 positive as well. Scale bar: 30 μm.*

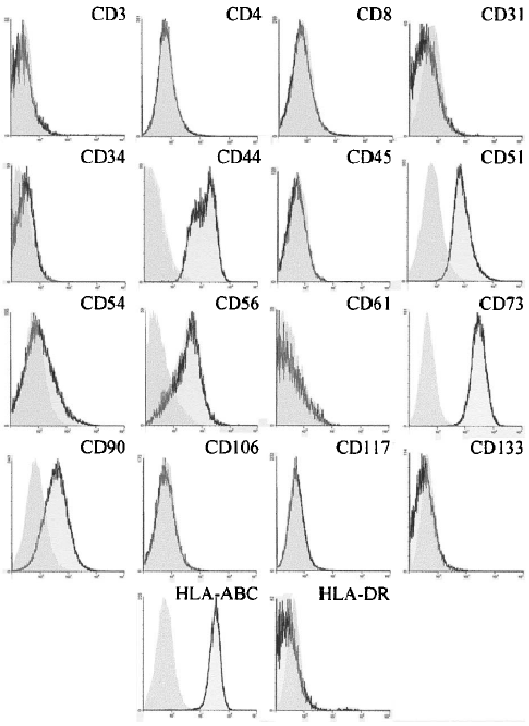

CD3	0.54±0.12
CD4	0.53±0.18
CD8	1.55±0.90
CD31	0.25±0.21
CD34	0.32±0.50
CD44	99.59±0.52
CD45	0.25±0.35
CD51	33.42±1.32
CD54	18.95±26.61
CD56	81.97±1.08
CD61	1.44±0.06
CD73	94.18±5.64
CD90	29.65±9.63
CD106	0.74±0.48
CD117	1.72±2.64
CD133	0.12±0.13
HLA-ABC	99.53±0.25
HLA-DR	0.11±0.13

Figure 2. *Flow cytometric analyses of hMPCs.*

F.3.2 Preparation of bio-compatible scaffolds

The geometry of the micropatterned membranes was specifically designed to mimic the in vivo topology of the 3D assembly of muscle fibers (Fig. 3A). Preliminary in vitro tests showed that the 10 μm lateral bridges, designed for providing the initial mechanical integrity of the membrane, had a faster degradation rate (not shown). After such degradation, the 3D scaffold produced by overlapping individual micropatterned membranes results in a cluster of parallel-oriented biodegradable and biocompatible polymeric stripes (Fig. 3B).

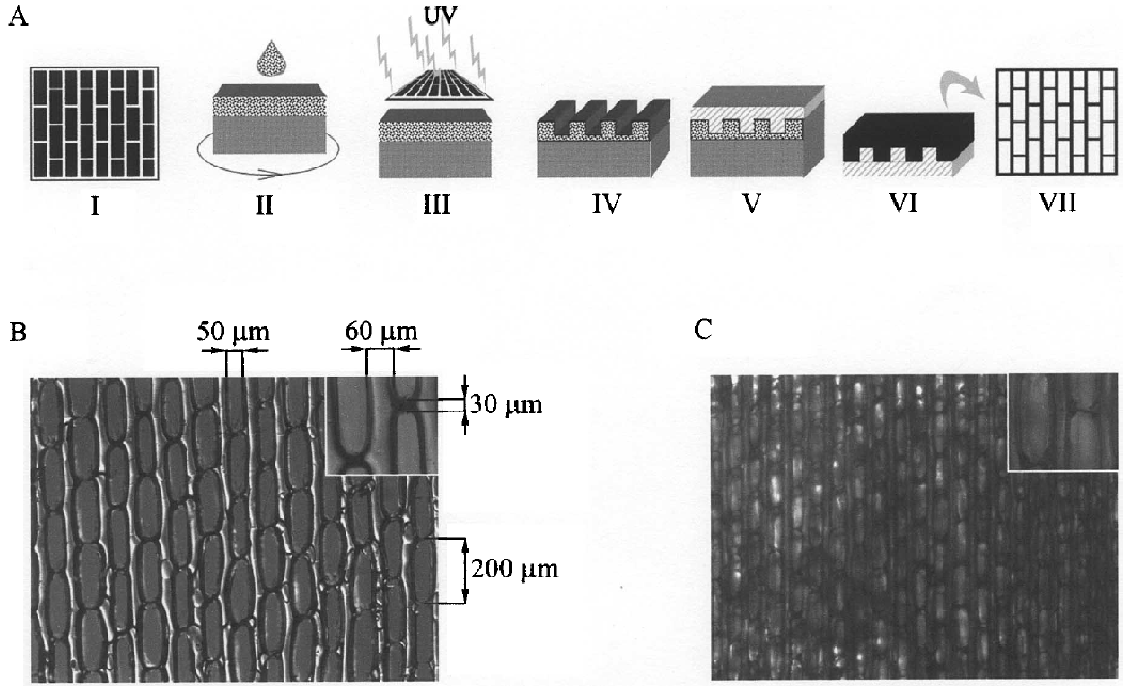

Figure 3. *(A) Schematic representation of scaffold preparation. Details are described in Materials and Methods. (B) Image obtained at the optical microscope of a single layer of the polymer. The regular scaffold structure can be appreciated in the inset. (C) Multilayer scaffold ready to be seeded.*

F.3.3 In Vivo Delivery of hMPCs

H&E staining allowed us to identify the areas of muscle regeneration into which we had delivered the hMPC (Fig. 4). One week after delivery, the damaged area in injected muscles was populated by mononuclear cells (Fig. 4A). On the other hand, in the case of polymer implantation, regenerating myofibers were also present in the area adjacent to the scaffold (Fig. 4B, right). The histological differences were even more evident at the 4-week time point, when a substantial amount of connective tissue had formed in case of cell injection (Fig. 4C), whereas in the case of polymer implantation the PLGA scaffold had been progressively degraded and the damaged area had been largely substituted by centrally nucleated regenerating myofibers (Fig. 4D).

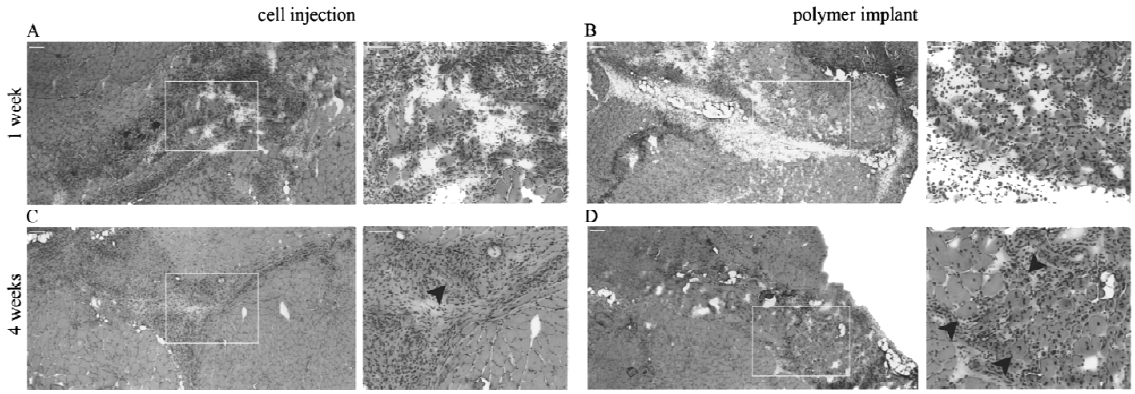

Figure 4. *Histological analysis revealed different patterns of regeneration. After 1 week, many mononucleated cells were mainly localized in the injection area (Fig. 4A) or inside and near the implanted scaffold (Fig. 4B). At this time point many regenerating fibers were present in the damaged area (magnification of A and B). After 4 weeks the damage was repaired in both cases. However, in case of cell injection H&E staining revealed that many mononucleated cells were still present, with only a few regenerating fibers (C and magnification). On the contrary, where scaffold had been implanted, many regenerating fibers repopulated the damaged area (D and magnification with centrally nucleated fibers indicated by arrowheads) and polymer was no longer recognizable. Scale bar: 100 μm.*

The presence of implanted cells was detected using an antibody specific for the human nuclear antigen, HNA. Double staining with HNA and laminin allowed us to confirm that the delivered cells were indeed participating in the muscle regeneration process (Fig. 5A–D).

After 1 week, comparable amounts of human nuclei were found in injected and implanted muscles, with a similar distribution (Fig. 5A, C). On the other hand, after 4 weeks, injected hMPCs appeared to be present in much lower number, and to be localized in a smaller area, compared to implanted limbs (Fig. 5B, D).

Western blot analyses confirmed that the number of hMPCs present 1 week after delivery was indeed similar between the injected and implanted muscles, whereas after 4 weeks the number of hMPCs present in implanted muscles was much higher that that found in the injected controls (Fig. 5E, F).

In particular, the HNA signal found in the muscles that had received the seeded polymers was approximately threefold higher than that found in contralateral limbs (Fig. 5E, F).

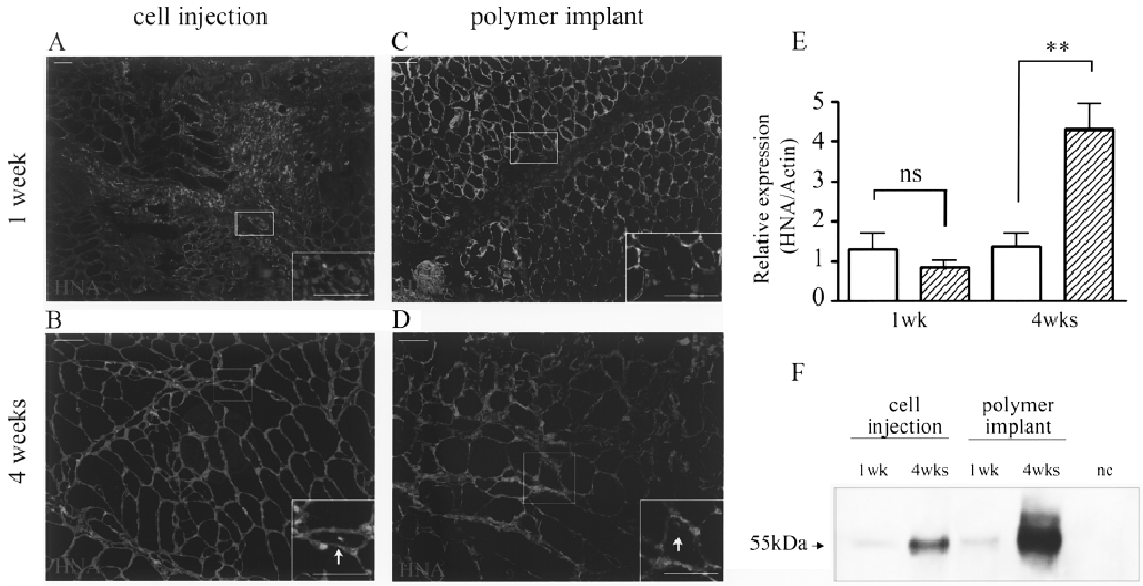

Figure 5. *Immunostaining for human nuclear antigen (HNA, in red) and laminin protein (labeled in green) revealed the presence of hMPCs in the muscle tissue (in the insets, nuclei were also counterstained with DAPI). After 1 week hMPCs were localized, in similar amounts in both cases, in injection or implant site (A and C). Some of the HNA-positive cells contributed to muscle regeneration as central nucleated cells (insets in A and C). After 4 weeks, several HNA-positive nuclei were found inside myofibers with a different distribution in the two cases (B and D). Expression of HNA was investigated by Western blot, as shown by the graph in (E) **$p < 0.01$; (F) shows an example of HNA signal in one of the animals sacrificed at 4 weeks. Scale bar: 70 μm.*

F.4 Discussion

In this study we showed for the first time that MPCs isolated from single human muscle fibers maintain the potential to participate in muscle regeneration. Moreover, our findings confirmed that, similarly to what we had previously described for murine MPCs (8), polymer implantation is more efficient than direct injection of the cells.

Although several reports have recently tested the potential of rodents muscle stem cells in muscle regeneration, fewer studies have explored the behavior of human muscle stem cells (1). One group isolated MPCs from human muscle (9), but no one investigated the application of human MPCs isolated from single myofibers for in vivo muscle regeneration. We have recently showed that human satellite cells can be expanded in vitro, originating hMPCs that can differentiate towards different mesenchymal lineages when induced with specific culture conditions (13). Fibers derived from human skeletal muscle are more fragile

and more difficult to maintain alive during the digestion and seeding processes than their murine counterparts. Furthermore, only few human muscles (i.e., intercostals, abdominal, and rectus-femoris) contain in fact relatively short fibers that can be easily selected and maintained in culture and are therefore suitable for this technique.

Once they moved away from the fibers and started to divide, hMPCs displayed a homogeneous morphology and their myogenic characteristics were confirmed by immunostaining analyses with several muscle-specific markers. The expression of the paired box transcription factor Pax7, a well-established marker of quiescent satellite cells, is also expressed in cultured myoblasts (30). hMPCs isolated from single fibers coexpressed desmin and Pax7.

The identity of our satellite-derived cells was also investigated by flow cytometry. hMPCs expressed CD54 (4), CD56 (normally identified in human regenerating muscle and satellite cells) (21), and CD73, while they were CD34 negative. Importantly, hMPCs did not appear to be hematopoietic in origin, as they were negative for CD45 and CD117 (24), as well as for the human markers CD133, CD3, CD4, and CD8. The presence of endothelial and mesenchymal cells was ruled out as no CD61 and CD106 were found in hMPCs (27).

Consequent to hMPC characterization, our set of experiments was aimed at determining if polymer-based delivery was better than direct intramuscular injection when using hMPCs, as previously demonstrated for mouse muscle precursor cells (8).

As expected, histological analyses performed after 1 week showed signs of acute inflammation as well as muscle regeneration. The presence of substantial numbers of mononucleated cells was found in the case of cell injection while fewer mononucleated cells seemed to be present in the case of scaffold-implanted muscles. Furthermore, 1 week after surgery the latter contained many more small, newly formed myofibers. This finding could be related to the fact that, as reported by previous studies (18), transplantation of cells by scaffold seeding could maintain the viability of the transplanted cells by partially protecting them from the inflamed environment (19). After 4 weeks this phenomenon was even more evident. In case of polymer implantation, scaffolds were mostly degraded and presented many center-nucleated fibers inside that extended in a larger zone of muscle-regenerating tissue than in the case of cell injections.

As we have previously reported for rodents (8), immunofluorescence and Western blot analyses showed that muscles receiving cellularized scaffolds yielded higher HNA+ve

signal than contralateral controls. In both the injected and scaffold-implanted muscles, HNA+ve signal after 4 weeks was higher than that revealed at 1 week. It has been reported that murine myoblasts transplanted into muscles of recipient mice mostly die and only a minor stem cell-like subpopulation survives, rapidly proliferates, and participates in muscle regeneration (5). MPCs represent a more homogenous population, seemingly with a higher regeneration potential, but in any case scaffold-mediated delivery appears to improve survival and/or proliferation of hMPCs.

In order to explore the specific role of the delivered cells into the damaged muscle we also stained sections by a double immunostaining against laminin protein and human nuclear antigen, to identify human cells both inside and outside the fibers. Based on the position of some human nuclei, we cannot exclude that hMPCs had also become satellite cells as reported for murine MPCs (26), but further experiments will be needed to address this question.

Our findings are in contrast with previous studies reporting that transplantation of the same number of cells on the scaffolds led to no detectable changes in muscle regeneration compared with cell injection (19). We believe that this different result could be related to the use of a pure population of hMPCs, which have neither been used before in an in vivo approach nor delivered by scaffolds.

In conclusion, our study shows for the first time the possibility of using a pure population of human muscle precursor cells in the skeletal muscle by means of a fully biodegradable, engineered polymer. The laminar structure of the scaffolds we used would be particularly suitable for application as “patches” in sites of high clinical relevance, such as heart and diaphragm, as previously reported with different kinds of matrices (2,15).

F.5 Acknowledgement

The financial support of the “Fondazione Città della Speranza” ONLUS (grant to C.M.) and of the Association Francaise contre les Myophaties (grant to P.G.G.) is gratefully acknowledged. We thank Dr. Jennifer E. Morgan for the careful reading of the manuscript and for her critical comments.

F.6 References

1. Alessandri G.; Pagano S.; Bez A.; Benetti A.; Pozzi S.; Iannolo G.; Baronio M.; Invernici G.; Caruso A.; Muneretto C.; Bisleri G.; Parati E. Isolation and culture of human muscle-derived stem cells able to differentiate into myogenic and neurogenic cell lineages. Lancet 364:1872–1883; 2004.
2. Badylak S. F.; Kochupura P. V.; Cohen I. S.; Doronin S. V.; Saltman A. E.; Gilbert T. W.; Kelly D. J.; Ignotz R. A.; Gaudette G. R. The use of extracellular matrix as an inductive scaffold for the partial replacement of functional myocardium. Cell Transplant. 15(Suppl. 1):S29–S40; 2006.
3. Baj A.; Bettaccini A. A.; Casalone R.; Sala A.; Cherubino P.; Toniolo A. Q. Culture of skeletal myoblasts from human donors aged over 40 years: Dynamics of cell growth and expression of differentiation markers. J. Transl. Med. 3:21–30; 2005.
4. Beauchamp J. R.; Abraham D. J.; Bou-Gharios G.; Partridge T. A.; Olsen I. Expression and function of heterotypic adhesion molecules during differentiation of human skeletal muscle in culture. Am. J. Pathol. 140:387–401; 1992.
5. Beauchamp J. R.; Morgan J. E.; Pagel C. N.; Partridge T. A. Dynamics of myoblast transplantation reveal a discrete minority of precursors with stem cell-like properties as the myogenic source. J. Cell Biol. 144:1113–1122; 1999.
6. Bischoff R. The satellite cell and muscle regeneration. In: Engel, A. G.; Franzini-Amstrong, C., eds. Myology. New York: McGraw-Hill; 1994:97–118.
7. Blau H. M.; Webster C.; Pavlath G. K. Defective myoblasts identified in Duchenne muscular dystrophy. Proc. Natl. Acad. Sci. USA 80:4856–4860; 1983.
8. Boldrin L.; Elvassore N.; Malerba A.; Flaibani M.; Cimetta E.; Piccoli M.; Baroni M. D.; Gazzola M. V.; Messina C.; Gamba P.; Vitiello L.; Coppi P. D. Satellite cells delivered by micro-patterned scaffolds: A new strategy for cell transplantation in muscle diseases. Tissue Eng. 13:253–262; 2007.
9. Bonavaud S.; Agbulut O.; D'Honneur G.; Nizard R.; Mouly V.; Butler-Browne G. Preparation of isolated human muscle fibers: A technical report. In Vitro Cell Dev. Biol. Anim. 38:66–72; 2002.
10. Collins C. A.; Olsen I.; Zammit P. S.; Heslop L.; Petrie A.; Partridge T. A.; Morgan J. E. Stem cell function, self-renewal, and behavioral heterogeneity of cells from the adult muscle satellite cell niche. Cell 122:289–301; 2005.
11. Conconi M. T.; De Coppi P.; Bellini S.; Zara G.; Sabatti M.; Marzaro M.; Zanon G. F.; Gamba P. G.; Parnigotto P. P.; Nussdorfer G. G. Homologous muscle acellular matrix seeded with autologous myoblasts as a tissue-engineering approach to abdominal wall-defect repair. Biomaterials 26:2567–2574; 2005.
12. De Coppi P.; Delo D.; Farrugia L.; Udompanyanan K.; Yoo J. J.; Nomi M.; Atala A.; Soker S. Angiogenic gene-modified muscle cells for enhancement of tissue formation. Tissue Eng. 11:1034–1044; 2005.
13. De Coppi P.; Milan G.; Scarda A.; Boldrin L.; Centobene C.; Piccoli M.; Pozzobon M.; Pilon C.; Pagano C.; Gamba P.; Vettor R. Rosiglitazone modifies the adipogenic potential of human muscle satellite cells. Diabetologia 49:1962–1973; 2006.
14. Deasy B. M.; Jankowski R. J.; Huard J. Muscle-derived stem cells: Characterization and potential for cell-mediated therapy. Blood Cells Mol. Dis. 27:924–933; 2001.
15. Fuchs J. R.; Kaviani A.; Oh J. T.; LaVan D.; Udagawa T.; Jennings R. W.; Wilson J. M.; Fauza D. O. Diaphragmatic reconstruction with autologous tendon engineered from mesenchymal amniocytes. J. Pediatr. Surg. 39:834–838; 2004.

16. Gussoni E.; Soneoka Y.; Strickland C. D.; Buzney E. A.; Khan M. K.; Flint A. F.; Kunkel L. M.; Mulligan R. C. Dystrophin expression in the mdx mouse restored by stem cell transplantation. Nature 401:390–394; 1999.
17. Hathaway M. R.; Hembree J. R.; Pampusch M. S.; Dayton W. R. Effect of transforming growth factor beta-1 on ovine satellite cell proliferation and fusion. J. Cell Physiol. 146:435–441; 1991.
18. Hill E.; Boontheekul T.; Mooney D. J. Designing scaffolds to enhance transplanted myoblast survival and migration. Tissue Eng. 12:1295–1304; 2006.
19. Hill E.; Boontheekul T.; Mooney D. J. Regulating activation of transplanted cells controls tissue regeneration. Proc. Natl. Acad. Sci. USA 103:2494–2499; 2006.
20. Horackova M.; Arora R.; Chen R.; Armour J. A.; Cattini P. A.; Livingston R.; Byczko Z. Cell transplantation for treatment of acute myocardial infarction: Unique capacity for repair by skeletal muscle satellite cells. Am. J. Physiol. Heart Circ. Physiol. 287:H1599–H1608; 2004.
21. Illa I.; Leon-Monzon M.; Dalakas M. C. Regenerating and denervated human muscle fibers and satellite cells express neural cell adhesion molecule recognized by monoclonal antibodies to natural killer cells. Ann. Neurol. 31:46–52; 1992.
22. Jejurikar S. S.; Henkelman E. A.; Cederna P. S.; Marcelo C. L.; Urbanchek M. G.; Kuzon, Jr. W. M. Aging increases the susceptibility of skeletal muscle derived satellite cells to apoptosis. Exp. Gerontol. 41:828–836; 2006.
23. Kane R. S.; Takayama S.; Ostuni E.; Ingber D. E.; Whitesides G. M. Patterning proteins and cells using soft lithography. Biomaterials 20:2363–2376; 1999.
24. Kinney-Freeman S. L.; Majka S. M.; Jackson K. A.; Norwood K.; Hirschi K. K.; Goodell M. A. Altered phenotype and reduced function of muscle-derived hematopoietic stem cells. Exp. Hematol. 31:806–814; 2003.
25. Marzaro M.; Conconi M. T.; Perin L.; Giuliani S.; Gamba P.; De Coppi P.; Perrino G. P.; Parnigotto P. P.; Nussdorfer G. G. Autologous satellite cell seeding improves in vivo biocompatibility of homologous muscle acellular matrix implants. Int. J. Mol. Med. 10:177–182; 2002.
26. Montarras D.; Morgan J.; Collins C.; Relaix F.; Zaffran S.; Cumano A.; Partridge T.; Buckingham M. Direct isolation of satellite cells for skeletal muscle regeneration. Science 309:2064–2067; 2005.
27. Pittenger M. F.; Mackay A. M.; Beck S. C.; Jaiswal R. K.; Douglas R.; Mosca J. D.; Moorman M. A.; Simonetti D. W.; Craig S.; Marshak D. R. Multilineage potential of adult human mesenchymal stem cells. Science 284:143–147; 1999.
28. Rosenblatt J. D.; Lunt A. I.; Parry D. J.; Partridge T. A. Culturing satellite cells from living single muscle fiber explants. In Vitro Cell Dev. Biol. Anim. 31:773–779; 1995.
29. Seale P.; Rudnicki M. A. A new look at the origin, function, and “stem-cell” status of muscle satellite cells. Dev. Biol. 218:115–124; 2000.
30. Seale P.; Sabourin L. A.; Girgis-Gabardo A.; Mansouri A.; Gruss P.; Rudnicki M. A. Pax7 is required for the specification of myogenic satellite cells. Cell 102:777–786; 2000.
31. Shinin V.; Gayraud-Morel B.; Gomes D.; Tajbakhsh S. Asymmetric division and cosegregation of template DNA strands in adult muscle satellite cells. Nat. Cell Biol. 8:677–687; 2006.
32. Torrente Y.; Tremblay J. P.; Pisati F.; Belicchi M.; Rossi B.; Sironi M.; Fortunato F.; El F. M.; D'Angelo M. G.; Caron N. J.; Constantin G.; Paulin D.; Scarlato G.; Bresolin N. Intraarterial injection of muscle-derived CD34(+)Sca-1(+) stem cells restores dystrophin in mdx mice. J. Cell Biol. 152:335–348; 2001.
33. Vazquez M. E.; Cabarcos M. R.; Roman T. D.; Stein A. J.; Garcia N. D.; Nazar B. A.; Dopico M. J.; Nunez C. A.; Garcia F. J. Cellular cardiomyoplasty: development of a

technique to culture human myoblasts for clinical transplantation. Cell Tissue Bank. 6:117–124; 2005.
34. Vilquin J. T. Myoblast transplantation: Clinical trials and perspectives. Acta Myol. 24:119–127; 2005.
35. Vozzi G.; Flaim C.; Ahluwalia A.; Bhatia S. Fabrication of PLGA scaffolds using soft lithography and microsyringe deposition. Biomaterials 24:2533–2540; 2003.

Appendix G

Microfluidics-generated Wnt3a gradients induce a proportionate response in β-catenin signaling pathway

Elisa Cimetta[1,2], Christopher Cannizzaro[3], Richard James[4], Travis Biechele[4], Randall T. Moon[4], Nicola Elvassore[1] *and Gordana Vunjak-Novakovic[2] *

[1] Department of Chemical Engineering, University of Padua, Via Marzolo, 9 Padua, Italy

[2] Columbia University, Department of Biomedical Engineering, Vanderbilt Clinic, 12th floor, 12-234, 622 West 168th Street, New York, NY

[3] Massachusetts Institute of Technology Harvard-MIT Division for Health Sciences and Technology Cambridge, MA

[4] 4University of Washington School of Medicine, HHMI and Dept. of Pharmacology Seattle, WA

[*] Corresponding author

To be submitted to Langmuir

Keywords: Wnt-3a; gradient; microfluidic; β-catenin signaling.

Abstract

The highly conserved Wnt-activated β-catenin pathway plays a major role in embryonic development, stem cell proliferation and differentiation. In developing tissues, Wnt proteins present themselves in form of concentration gradients, and the spatial position of Wnt signals can determine the polarity of the sensing cells. Wnt-3a stimulates the activity of β-catenin pathway, leading to translocation of β-catenin to the nucleus where it activates a series of target genes. To mimic these conditions in vitro, we cultured HEK 293T cells stably expressing a Wnt/b-catenin reporter driving the expression of Venus, pBARVS, inside a microfluidic device that was designed to generate controlled Wnt3a gradients under cell-protective conditions of low hydrodynamic shear. The cells were exposed to a gradient of Wnt-3a that was formed in a culture space between two parallel laminar flow streams, consisting of culture medium with two different concentrations of Wnt3a. The exact algorithm for establishing concentration gradients was established with the aid of mathematical modeling of flow and transport in the microfluidic device. The extent to which the β-catenin pathway was activated in response to a gradient of Wnt3a was assessed in real time over a period of 48 hrs, using the BARVS reporter gene. We observed that β-catenin signaling on a single cell level was proportionate to the concentration gradient of Wnt3a. We propose that the modulation of Wnt-3a gradients in real time can provides new insights into the dynamics of β-catenin pathway, under conditions that replicate some aspects of the actual cell-tissue milieu.

G.1 Introduction

Wnt proteins are a family of powerful macromolecules involved in a multitude of biological phenomena ranging from early-stage cell fate specification, to embryo development, cell proliferation, differentiation and tumorigenesis.(Clevers 2006, Logan and Nusse 2004, Moon 2005, Moon et al. 2002, Moon et al. 2004) Numerous studies have explored the role of Wnt in cell signaling.(Otto et al. 2007, Ueno et al. 2007, Maretto et al. 2003, Green et al. 2008, Witze et al. 2008) Of particular interest is the pattern by which the Wnt signals are presented to the cells, though concentration gradients on a short and long range.(Bartscherer and Boutros 2008, Aulehla et al. 2008) However, surprisingly little is known about the effects of Wnt gradients on cell populations and the quantitative data have not been reported.

Microfluidic devices offer the possibility of generating complex and well defined patterns of stimulation, via tight control of fluid dynamics on a micrometer scale.(Keenan and Folch 2007) Recent literature reflects increased interest in interfacing microfluidic devices with biological systems. (Keenan and Folch 2007) (Amarie et al. 2007, Jeon et al. 2000, Kang et al. 2008) (Whitesides 2006) (Beebe et al. 2002, Squires and Quake 2005, Kim et al. 2007, Sia and Whitesides 2003) Examples include studies of chemotaxis in cell culture systems utilizing hydrogels of differential compositions, (Burdick et al. 2004) short-term perfusion of graded concentrations of regulatory factors over seeded cells, (Saadi et al. 2006) and the assembly of membrane-based diffusion chips. (Diao et al. 2006)

Because of the laminar regime that is inherent to fluid flow in micro-channels, the geometry of the micro-device and the flow rates can be tuned to establish desired patterns of flow and molecular transport. The utilization of flow rates that are in the range of few μL/min enables generation of well-defined, diffusion-independent concentration profiles. However, the use of such microfluidic gradient generators is generally associated with hydrodynamic shear stresses exerted on cultured cells, that arise from the small characteristic dimensions of microfluidic channels.(Chisti 2001) For studies of most cells, control of hydrodynamic shear is vital for the maintenance of the cell well-being during cultivation.(Cimetta et al. 2009)

In this study we focus on β-catenin signaling in response to a concentration gradient of Wnt-3a, using HEK 293T cells stably expressing pBARVS (Biechele and Moon 2008) cells as a model system.

Activation of the BARVS reporter gene was monitored through the expression of Venus signal.

A microbioreactor was designed to enable generation of stable and well defined gradients of Wnt-3a under the conditions of relatively low hydrodynamic shear that allow prolonged culture of cells necessary to cover the time span required for gene activation.

G.2 Experimental section

G.2.1 Culture of HEK293T cells stably expressing pBARVS and generation of Wnt3a conditioned medium

pBARVS contains 12 TCF/LEF DNA binding elements upstream of a minimal promoter, minP, and drives the Wnt/b-catenin-dependent expression of Venus.(Rekas et al. 2002) It also contains a PGK promoter that drives the constitutive expression of a puromycin resistance cassette for stable selection. These elements are located being the LTRs of a third generation lentiviral expression system.(Dull et al. 1998) Lentivirus containing pBARVS was generated and used to infect. Three days post infection cells were cultured in culture media containing 2μg/mL puromycin. A stable heterogeneous line was then cultured with an EC50 dose of Wnt3a conditioned media. 24 hours following stimulation, cells were sorted by FACS and a narrow gate of high Venus expressing cells were collected. Sorted cells were cultured for 4 days in culture media without Wnt3a conditioned media, allowing Venus expression to return to a low basal level. Cells were then sorted by FACS for a narrow gate of the cells expressing the lowest levels of Venus. These cells were collected as a single cell per well in two 96-well plates. The resulting monoclonal lines where then retested with Wnt3a conditioned media and the lines with the greatest dynamic range were selected. Cells were then expanded in standard culture flasks in culture media without Wnt3a (DMEM supplemented with 10% foetal bovine serum (FBS), 1% penicillin-streptomycin) and passaged every 2 days.

Wnt3a conditioned media was prepared as described in Willert et. Al.(Willert et al. 2003) In order to avoid batch-to-batch variability in the gradient experiments, the obtained Wnt3a conditioned medium was tested and “calibrated”. To this aim, cells were seeded in standard 96 well plates (n = 5 per group and time point) and cultured in conditioned medium at a

broad range of dilutions (relative Wnt3a concentration from 100 to 5%). At defined time points, the fluorescence deriving from the activation of the β-catenin pathway was quantified and related to the conditioned media dilution. This served as a basis for the choice of the proper conditioned media dilution in the microfluidic-gradient experiments.

G.2.2 Microfluidic bioreactor design, fabrication and assembly

The shear stresses that STV-293 HEK293 cells can tolerate in long term experiments was empirically determined at <1 dyne/cm^2 (data not shown. Briefly, cells cultured in single microfluidic channels experienced medium flow at different rates; evaluating the fraction of detaching cells at defined time points, the shear stress thresholds were determined when the 50% of detaching cells was reached). The microfluidic bioreactor was designed to generate stable concentration gradients in long term culture, while exposing the cultured cells to low shear stresses.

The device consists of three 500 µm wide channels aligned in parallel, where the middle channel serves as the cell culture space (**Figure 1**). The three channels are connected by an array of smaller channels (25 µm wide x 50 µm deep, spaced at 50 µm) that are perpendicular to the three larger channels, and enable diffusion of molecular species without significant convective flux. This configuration allowed us to obtain sharp and stable concentration gradients inside the middle channel, by the diffusion of species between the two outer large channels.

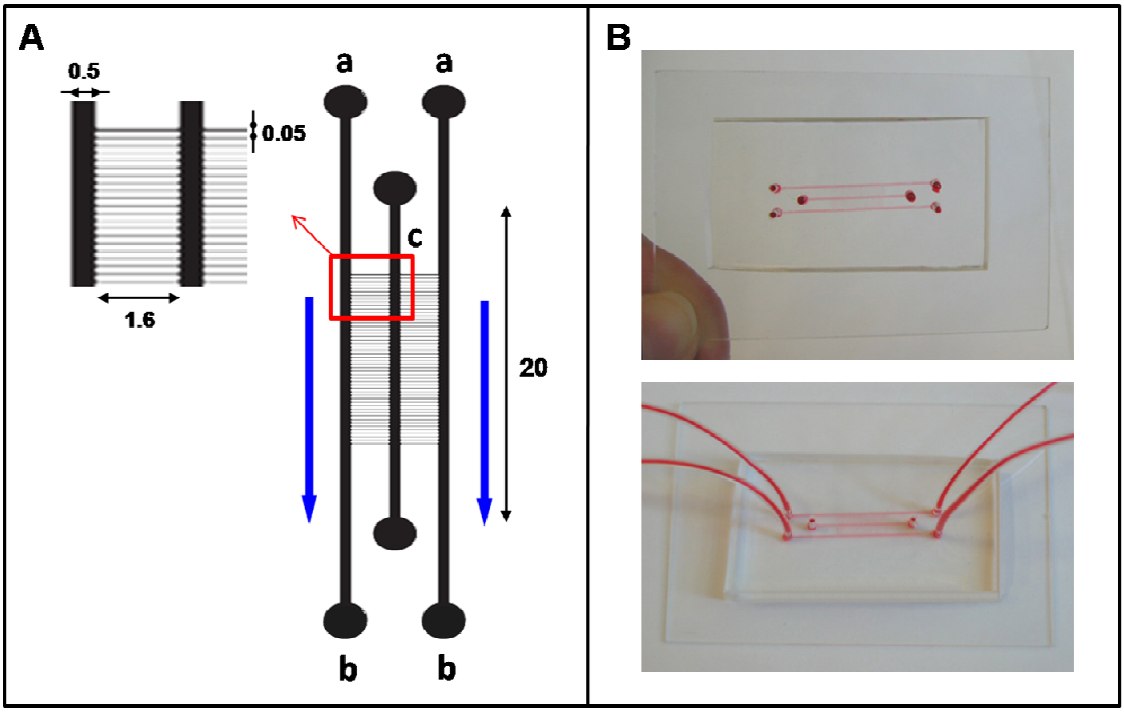

Figure 1. *Microfluidic device. The microfluidic bioreactor (panel A) was composed of two flow channels with inlets in a and outlets in b, that flank the culture channel c. Lateral arrows identify the main flow direction. The reported dimensions are in mm. The height of the microbioreactor is 50 μm. Images in panel B are top views of the microbioreactor in which the fluidic channels are filled with a colour tracer; the inlet and outlet tubing connecting the assembled device to the syringe pump is shown in the lower image.*

The single-layer microfluidic bioreactor was replica-molded in poly(dimethylsiloxane) (PDMS) (Xia and Whitesides 1998) from a SU-8 mold fabricated through standard lithographic techniques (Tourovskaia et al. 2006) and irreversibly bonded to a 75 x 50 mm microscope slide via an air plasma treatment after punching the inlet and outlets ports. Sterilization of the assembled microbioreactor and of tubing and connections for the perfusion apparatus was performed with autoclave treatment.

G.2.3 Cell seeding and microfluidic culture

The culture channel (total volume 0.5 mm^3) was coated with 100 µg/mL Fibronectin for 20 minutes prior to cell seeding. After removing the Fibronectin solution, the entire microfluidic device was filled with culture medium. Confluent flasks of transfected HEK cells were enzimatically detached using trypsin/EDTA, pelleted by centrifugation for 3 minutes at 1100 rpm and counted. A single cell suspension at a density of 10^6 cells/mL in standard culture medium was then prepared for seeding. A maximum of 2 µL of cell

suspension (summing the dead volumes of the inlet and outlet holes and the volume of the culture channel) was loaded into the culture channel. Particular attention must be paid at avoiding extensive invasion of the small lateral channels. Cells were allowed to adhere for 24 hours before starting medium perfusion. After 24 hrs, the two inlet ports of the side flow channels of each microbioreactor were connected via Tygon tubing (0.8 mm ID, 2.4 mm OD, Cole Palmer) to syringes containing standard and conditioned (Wnt3a-containing) medium. The flow rate, controlled by a digital syringe pump (PHD, Harvard Apparatus), was set at 1 µL/min per channel. The flow direction was the same for both channels of an individual microbioreactor and a maximum of 5 microbioreactor were operated in parallel. Perfusion was maintained for 24 hours, after which the cultured cells were analyzed to evaluate their fluorescence levels.

Two sets of static controls were performed for each experiment: the first filling the entire microbioreactor with control media, and the second with Wnt3a conditioned media at the same dilution used for the perfusion experiments.

G.2.4 Mathematical modeling and validation

In order to predict the flow regimes and the concentration profiles within the microbioreactor culture channel, we performed a mathematical modeling with a two-dimensional (2D) geometry of our microbioreactor (top view of the microfluidic channels). The Navier-Stokes equations for incompressible flow, modified for taking into account a surface forces-related component, and the convection-diffusion equation were numerically solved using a finite element analysis solver (Comsol Multiphysics). The values of the parameters used are summarized in **Table 1**; the calculated diffusion coefficients are consistent with literature values (Braga et al. 2004). Several simulations were performed and the most significant covered the different combinations of diffusion coefficients and flow rates listed in **Table 1**.

***Table 1**. Parameters and variables used. The table reports a list of the parameters and variables used for the performed calculations with their values. When applicable, references are reported in the last column.*

Variable	Values	Units	Reference
$\mathbf{D_{Wnt3a}}$	6.00E-11	$m^2\ s^{-1}$	Calculated
$\mathbf{D_{10KDa}}$	4.00E-11	$m^2\ s^{-1}$	Calculated and [27]
$\mathbf{D_{40KDa}}$	6.00E-11	$m^2\ s^{-1}$	Calculated and [27]
$\mathbf{D_{70KDa}}$	5.00E-10	$m^2\ s^{-1}$	Calculated and [27]
μ	0.0007	Pa·s	[26]
ρ	990	$Kg\ m^{-3}$	[1]
Q	0.17E-11 0.17E-10 0.83E-10	$m^3\ s^{-1}$	This study

To validate the model predictions, the resulting Wnt3a concentration profiles were compared with experimentally measured profiles of fluorescently labeled dextrans: Cascade Blue-conjugate 10 KDa, fluorescein-conjugate 40 KDa, tetramethylrhodamine-conjugate 70 KDa (all from Molecular Probes). Again, the calculated diffusion coefficients for each molecule are reported in **Table 1**. It is worth to highlight how the Wnt3a molecule can be represented with good approximation by the 40 KDa dextran. Solutions of each dextran in culture medium were prepared at the final concentration of 1 mg/mL and used for one of the two flow channels. Standard culture medium with no dissolved fluorescent tracers was used for the second channel. Briefly, the microbioreactor was normally assembled, the syringes loaded with the fluids (standard culture medium and culture medium with dissolved fluorescent dextrans), the tubings connected to the proper inlets, and finally the system operated at the mentioned flow rates. The microbioreactor assembly was kept under the microscope (Leica CTR6000) in a controlled chamber (temperature 37°C, 5% CO_2), and fluorescence images were taken at different time points to assess the stability of the formed gradient (data not shown) and at different sections of the culture channel to verify its shape. This experimental validation was performed operating the microbioreactor at all flow rates listed in **Table 1** and using the 3 solutions of different dextrans for one of the two flow channels in order to allow detailed comparison with the modeled profiles.

G.2.5 Quantitative fluorescent imaging of Venus expression in cultured cells

The evaluation of the cell response to Wnt3a concentration gradients was performed on live cell cultures by measuring the presence and the distribution of the fluorescent signal resulting from the activation of the targeted Venus-tagged reporter gene. The quantification of fluorescence images was performed in two ways: (i) by evaluating the mean grey value (MGV) of the image, thus measuring the averaged fluorescence intensity; (ii) by evaluating the fraction of cells expressing Venus signal, determined as the ratio between the area of cells expressing Venus signal and the total area covered by cells. The developed script containing the chosen operations was run with Matlab.

G.3 Results

G.3.1 Establishment of concentration gradients: effects of flow velocity and diffusion coefficient

The capability of the microbioreactor to generate predictable concentration gradients of large soluble molecules was tested for a range of fluid flow rates (0.1, 1, and 5 µL/min, corresponding to linear velocities inside the flow channels of $6.67 \cdot 10^{1}$, $6.67 \cdot 10^{2}$, and $3.33 \cdot 10^{3}$ µm/s, respectively), and diffusion coefficients ($4 \cdot 10^{-11}$, $6 \cdot 10^{-11}$, and $5 \cdot 10^{-10}$ m^2/s, corresponding to the molecular weights of chemical species of 10, 40, and 70 KDa respectively). Experimental data for concentration gradients were obtained using fluorescent dextrans as molecular-weight tracers for proteins of interest in cell culture studies, and compared with the corresponding gradients predicted by a rigorous mathematical model of momentum and mass transport. **Figure 2** reports exemplifying results of both the mathematical modeling (upper panel) and the experimental validation (bottom panel); for an easier understanding, only the mid culture channel is represented.

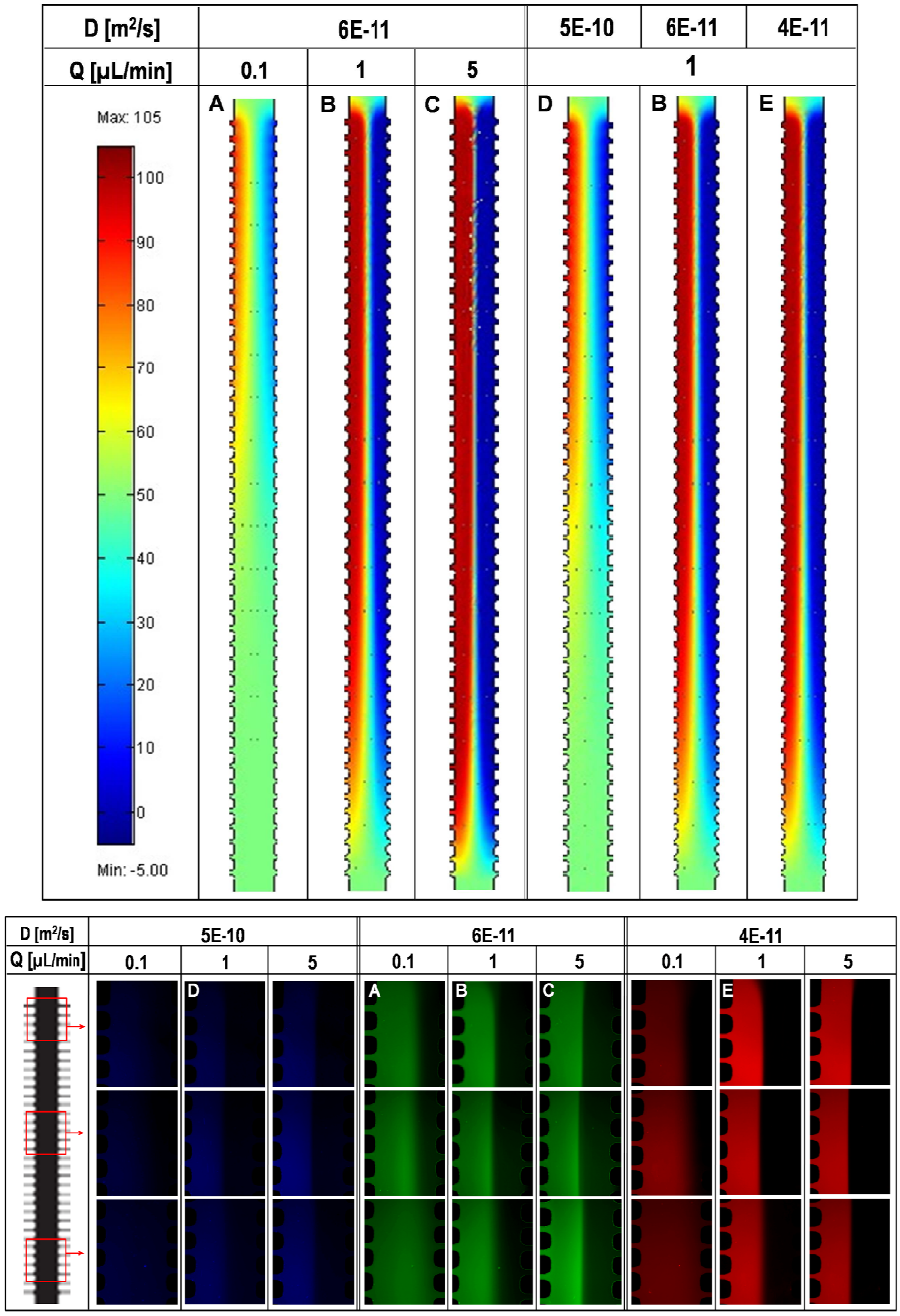

Figure 2. *Microfluidic device validation. Upper panel reports the results of the simulated Wnt3a gradient; mathematical modeling allowed the visualization of the generated gradient and of the spatial distribution of Wnt3a in the culture media (as indicated by the color-coded scale on the left). Three different diffusion coefficients and three flow rates were used as indicated. On the lower panel: the gradients predicted by mathematical modeling were experimentally validated using tracer molecules (fluorescent dextrans with defined molecular weight) with known diffusion coefficients. The same flow rates used for the simulations were experimentally replicated for all nine combinations of the diffusion coefficient and the flow rates. Corresponding conditions are indicated by the capital letters.*

Through the model predictions, on the upper panel of **Figure 2**, the effects of flow rate were analyzed at the diffusion coefficient of $6 \cdot 10^{-11}$ m^2/s, that corresponds to the molecular size of Wnt3a. The color coded bar on the left translates the colors in concentration values, on a percent scale, for the molecule of interest inside the culture channel. The model predicts molecular diffusion as the dominating transport mode at the lower flow rate of 0.1 µL/min (corresponding to linear velocities of $6.67 \cdot 10^{1}$ and $2.59 \cdot 10^{1}$ µm/s in the lateral and culture channel respectively), leading to fast dissipation of the concentration gradient along the length of the microfluidic channel (**Figure 2A**). An increase in flow rate to 1 µL/min (linear velocity of $6.67 \cdot 10^{2}$ and $2.59 \cdot 10^{2}$ µm/s in the lateral and culture channel respectively) and 5 µL/min (linear velocity of $6.67 \cdot 10^{2}$ and $2.59 \cdot 10^{2}$ µm/s in the lateral and culture channel respectively) resulted in a more step-wise concentration gradients that has been maintained along the channel length (**Figure 2B** and **C**).

The effects of molecular size of diffusing chemical species were analyzed at the flow rate of 1 µL/min. For small, fast-diffusing molecules ($D = 5 \cdot 10^{-10}$ m^2/s, corresponding to a 10 KDa molecular size), there was a dissipation of the gradient along the length of the microfluidic channel, such that a relatively uniform concentration was established in the downstream section of the channel (**Figure 2D**). With an increase in molecular size to 40 KDa and 70 KDa (i.e., decrease in the diffusion coefficient to $6 \cdot 10^{-11}$ m^2/s and $4 \cdot 10^{-11}$ m^2/s respectively), a stable concentration gradient was maintained along the channel length, as was the case for relatively high flow rates (**Figure 2B** and **E**).

To validate the model predictions, concentration gradients developed in the culture channel of the microfluidic bioreactor were experimentally measured for the same values of flow velocity and diffusion coefficient, by using solutions of fluorescently labeled dextrans as described in the Experimental section. Representative examples are reported on the bottom panel of **Figure 2**, where corresponding conditions between model and experimental results are denoted with capital letters. Fluorescence images were taken at the sections indicated by the squares in the culture channel schematics reported on the left; fluorescence intensity qualitatively gives a concentration-proportional signal. Therefore, both the experimental and model-predicted concentration profiles showed that at low flow rates and for low molecular weight chemical species (i.e., higher diffusion coefficients) molecular diffusion becomes the dominating transport regime, and that these conditions lead to dissipation of the concentration gradient. On the contrary, flow rates as low as 1 µL/min and species with

approximate sizes of 40 KDa and higher, are sufficient for obtaining a sharp and stable concentration gradient along the entire culture channel length.

G.3.2 Experimental conditions analysis

Considering the above discussed results, and the fact that the value of $6 \cdot 10^{-11}$ m^2/s can be used as Wnt3a diffusion coefficient, the appropriate culture conditions were set choosing a flow rate of 1 µL/min. The choice of the proper Wnt3a conditioned medium dilution strictly depended on the results of the calibration experiments performed for esch medium batch. **Figure 3** shows mathematical analysis of (*i*) concentration gradients, (*ii*) velocity profiles, and (*iii*) hydrodynamic shear stress for the microfluidic device operating with Wnt3a as the diffusing molecule at a flow rate of 1 µL/min.

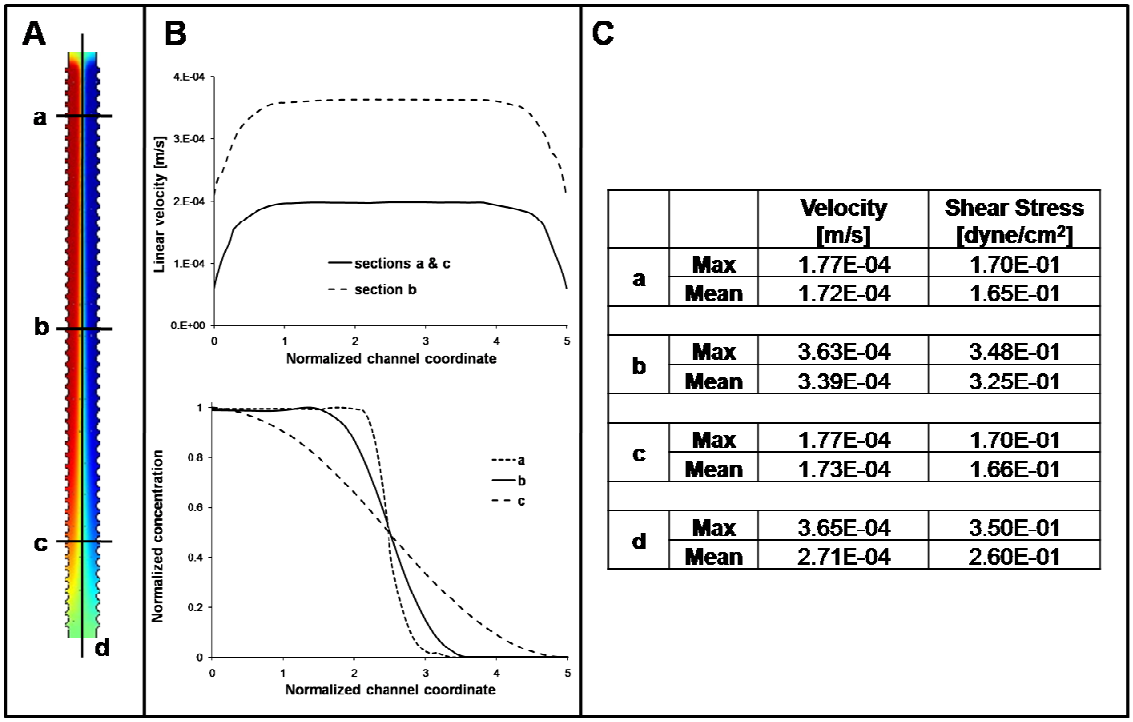

		Velocity [m/s]	Shear Stress [dyne/cm²]
a	Max	1.77E-04	1.70E-01
	Mean	1.72E-04	1.65E-01
b	Max	3.63E-04	3.48E-01
	Mean	3.39E-04	3.25E-01
c	Max	1.77E-04	1.70E-01
	Mean	1.73E-04	1.66E-01
d	Max	3.65E-04	3.50E-01
	Mean	2.71E-04	2.60E-01

Figure 3. *Experimental conditions: concentration, velocity, and shear stress. Using the Wnt3a diffusion coefficient of $6e^{-11}$ m^2/s and the flow rate of 1 µL/min, we evaluated the flow characteristics of 4 sections of the culture channel highlighted in A. Panel B shows the plug-like velocity profiles in the chosen cross sections (upper graph) and the curves representing the concentration profiles on the same sections (bottom graph).The table in panel C summarizes the maximum and minimum values for the velocity and shear stress in the 4 sections of the culture channel.*

Panel **A** shows again the color-coded representation of the Wnt3a concentration gradient inside the culture channel, where a-d letters mark the sections in which further analyses

were carried. Panel **B**, upper graph, shows the modeled plug-like velocity profiles in the chosen cross sections while the curves representing the normalized values of Wnt3a concentration on the same sections are reported in the bottom graph. Finally, the table in panel **C** summarizes the calculated maximum and minimum values for the velocity and shear stress in the 4 sections of the culture channel.

We can conclude that the system was able to generate predictable and stable concentration gradients with flat and uniform velocity profiles within the culture channel, thus exposing the adhering cells to very low values of both velocity and shear stress (which averaged values were $2.63 \cdot 10^{-4} \pm 8.74 \cdot 10^{-5}$ m/s and $2.53 \cdot 10^{-1} \pm 8.39 \cdot 10^{-2}$ dyne/cm^2 respectively).

G.3.3 Activation of the canonical β-catenin pathway in response to constant levels of Wnt3a

To investigate the activation of the β–catenin pathway in response to a range Wnt3a concentrations, HEK293T BARVS cells were cultured in static monolayers at different concentrations of Wnt3a in culture medium, obtained by diluting conditioned medium. β–catenin pathway activation in cultured cells was proportionate to the concentration of Wnt3a in culture medium, as evidenced by the intensity of Venus fluorescence. The Venus signal was detected starting a few hours after Wnt3a addition, and increased with time of culture (**Figure 4A**). The extent of the Venus-related pathway activation was evaluated by the quantification of fluorescence images as described above. The fraction of cells expressing Venus signal, determined as the ratio between the area of cells expressing Venus signal and the total area covered by cells, showed a statistically significant increase with Wnt3a concentration (**Figure 4B**). Similarly, the averaged fluorescence intensity of the whole image (mean grey value, MGV), also increased with Wnt3a concentration in a statistically significant manner (**Figure 4C**). Based on these and similar results, the dilutions of the Wnt3a conditioned medium to be used in the microfluidics experiments were decided. In most cases, the conditioned medium was used as received or diluted at 75% of its initial composition.

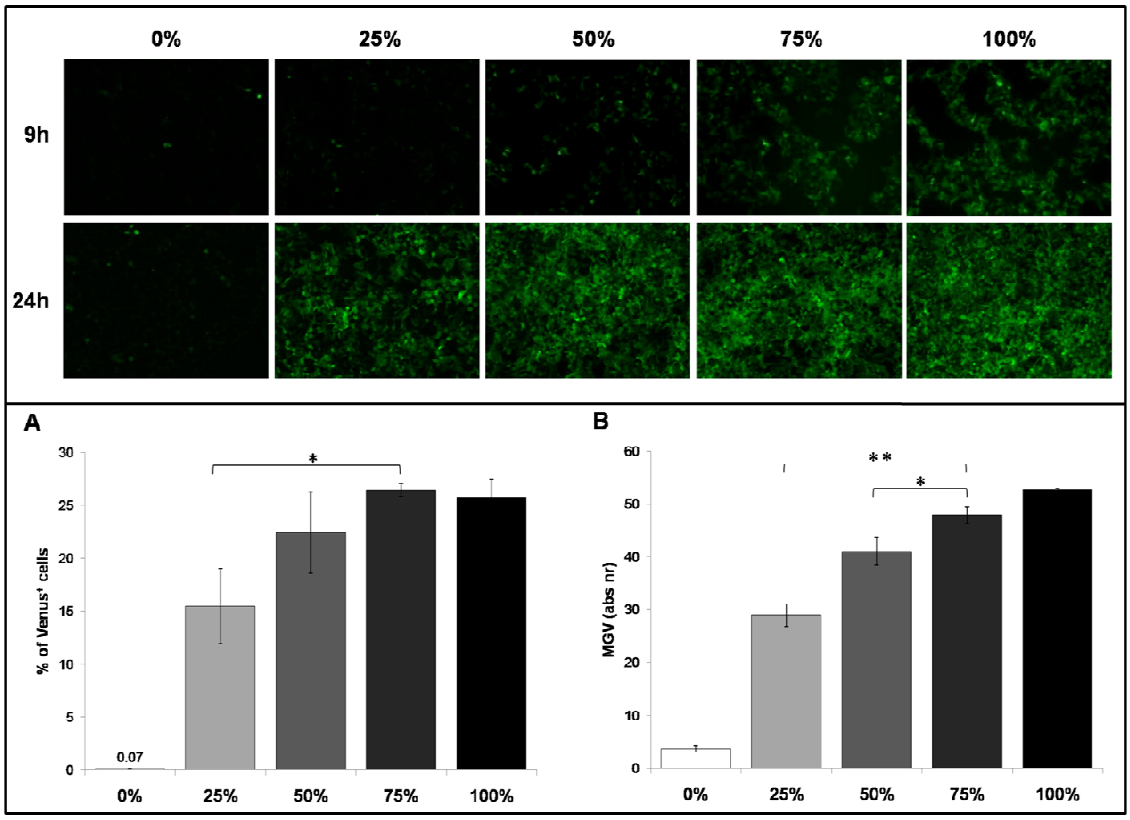

Figure 4. *Differential activation of the canonical Wnt3a/β-catenin pathway: static experiments. Confluent populations of HEK293 cells were cultured in 96 wells plates and exposed to the different levels of the Wnt3a conditioned medium as indicated. Upper panel reports live images of cells expressing different extents of Venus signal, increasing with time and with Wnt3a concentration in culture medium. The lower panel reports the quantification of the above reported results. Two different evaluation approaches were used; both measurements were obtained by analysis of the fluorescence images of Venus expressing cells. In A, the quantification was performed evaluating the fraction of cells expressing Venus signal, determined as the ratio between the area of cells expressing Venus signal and the total area covered by cells, while in B evaluating the mean grey value (MGV) of the image, thus measuring the averaged fluorescence intensity. The control is represented by a cell culture treated with control medium with no Wnt3a. * p<0.05. **p<0.001.*

G.3.4 Differential activation of the canonical β-catenin pathway in response to a gradient of Wnt3a

Cells were successfully cultured inside the microbioreactor for up to 3 days total (static and perfused culture). **Figure 5** reports representative bright field and fluorescence images (first and second row respectively) of cells cultured inside the microbioreactor both in static (left) and perfused conditions (right). The reported static control experiment was performed filling the microbioreactor with Wnt3a conditioned medium at the dilution chosen for the

perfused experiments. In the case of perfused microbioreactors, the Wnt3a conditioned medium was injected from the right inlet port.

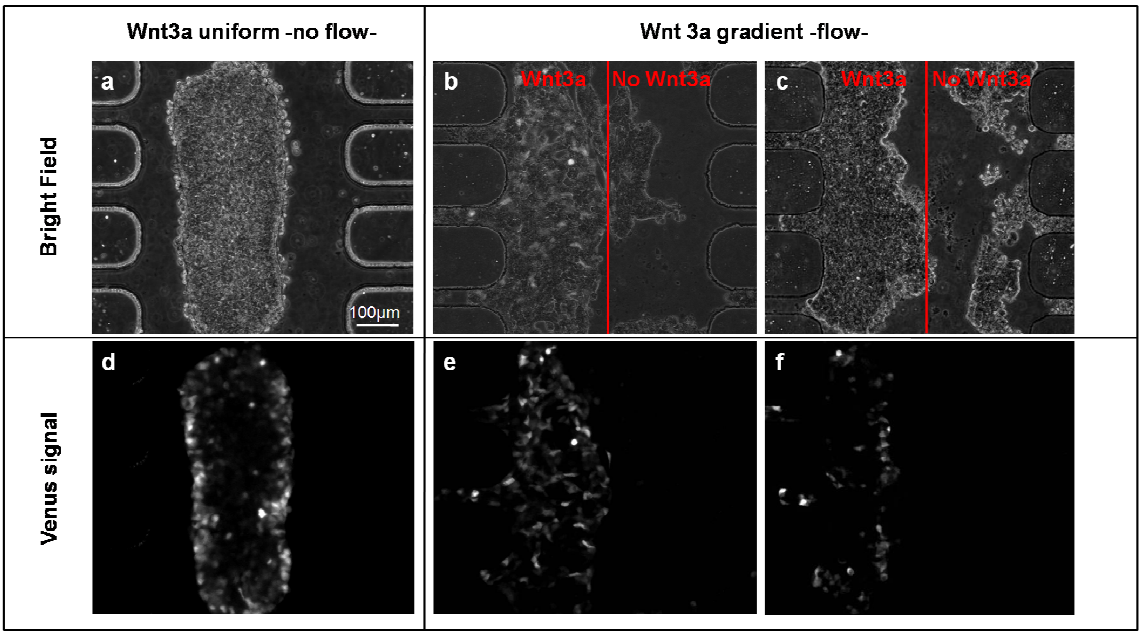

Figure 5. *Differential activation of the canonical Wnt3a/β-catenin pathway: perfused experiments. Cells cultured inside the microbioreactor were exposed for 24 h to a microfluidic-generated Wnt3a gradient. Upper part of panel shows bright field images (a-c), while the lower one shows the fluorescent Venus signal (d-f). The control, performed statically operating a microbioreactor filled with Wnt3a conditioned medium, results in a random activation of cells (panels a and d); while cells cultured under a Wnt3a gradient show a differential activation, in accordance with the imposed concentration gradient. The vertical line in the images divides the channel in two halves, helping the visualization approximately identifying the areas in which the Wnt3a ligand is present.*

During perfusion, a Wnt3a concentration gradient was soon established, thus exposing the cells adhering on the right side of the channel to a defined ligand concentration. The vertical line in the images divides the channel in two halves, helping the visualization approximately identifying the areas in which the Wnt3a ligand is present. As can be noticed from the fluorescent images reported in the second row of **Figure 5**, the Venus expression was detectable only on the cell population fraction that was exposed to the Wnt3a conditioned media. Cells of the control experiments showed a more uniform expression on the entire population.

The quantification of the obtained images was performed as described above, on an average of 20 images per condition, and led to the results reported in **Figure 6**.

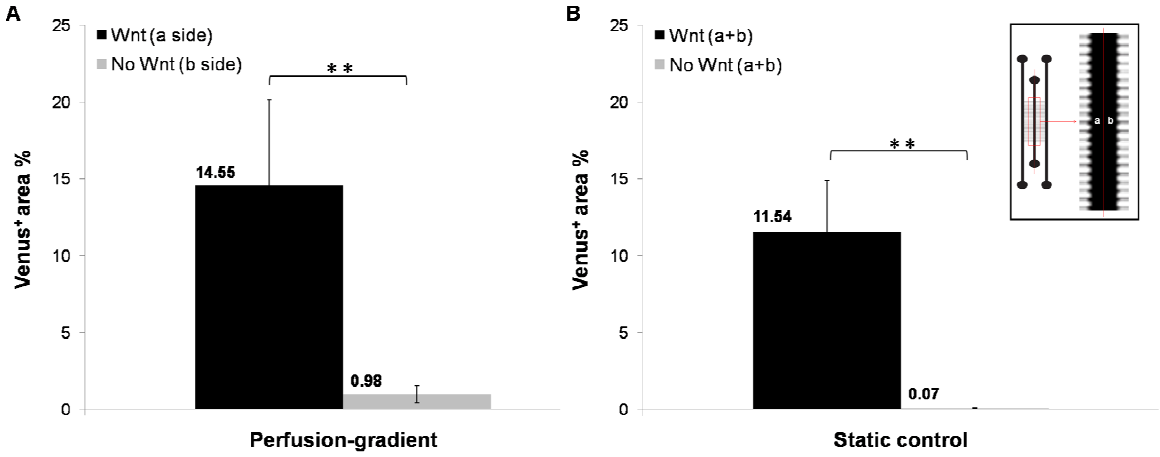

Figure 6. *Differential activation of the canonical Wnt3a/β-catenin pathway: data evaluation for perfused experiments. To more clearly highlight the cell population behaviour, the analysis was performed dividing the culture channel in two halves; the inset in Panel B clarifies the notations used. Quantification was performed on both halves evaluating the fraction of cells expressing Venus signal, determined as the ratio between the area of cells expressing Venus signal and the total area covered by cells. Panel A reports results of the perfused experiments, where the culture channel could be divided in the above mentioned two areas: a, exposed to Wnt3a conditioned medium and b, exposed to control medium (no Wnt3a). Panel B summarizes the outcomes of the static experiments, performed evaluating the images of the entire channel section (a+b). Results are reported for two sets of control experiments where cells were exposed to a defined and uniform Wnt3a concentration or exposed to control medium with no Wnt3a. **p<0.001.*

Panel **A** shows the results of the perfused experiments. In order to more clearly highlight the cell population behavior, the analysis was performed dividing the culture channel in two halves, as described above and clarified by the figure inset. The microfluidics-generated Wnt3a gradient dictated its presence in the right side of the channel (b side), thus eliciting a proportionate response in the exposed cells in terms of Venus signal; the left side of the channel (a side) had no Wnt3a. The fraction of cells expressing Venus signal evaluated on the cell populations adhering on the right side of the channel was 15 fold higher than that on cells on the left side. Panel **B** summarizes the outcomes of the static experiments, performed evaluating the images of the entire channel section (identified in the graph by the notation "(a+b)"). As described above, two sets of control experiments were performed and results are reported for both groups: one where cells were exposed to control medium with no Wnt3a and the other where cells were uniformly exposed to a defined and uniform Wnt3a

concentration. A 11 fold increase in the fraction of GPF positive cells was encountered in cells exposed to Wnt3a when compared with those with no Wnt3a.

These results prove the effective and statistically significant differential activation of the cell population fraction exposed to the microfluidic-generated Wnt3a gradient.

G.4 Conclusions and discussion

In this paper, a microfluidic microbioreactor capable of generating well characterized concentration gradients under low shear stress conditions was designed, developed and validated. The capability of effectively proving the spatio-temporal stability of the imposed gradient is of paramount importance, and in the microfluidic device presented in this work, extremely predictable behaviors in accordance with the results of the mathematical modeling could be developed. In fact, confirmed also by experimental validation, the mathematical modeling allowed to precisely predict the spatio-temporal evolution of the shape of the concentration profiles as a function of the microfluidic configuration, the flow rate and the diffusion coefficient of the dissolved species. In this sight, the natural tendency of a concentration gradient to dissipate can be easily described; for instance, a homogeneous gradient shape can be obtained along the longitudinal coordinate only if the characteristic dissipation time ($\tau_D = w^2/D$; where w is the cell culture channel width and D is the diffusion coefficient) is comparable with the fluid culture-chamber permanence time ($\tau_P = V/Q$; where V and Q are the volume and the flow rate within the cell culture channel, respectively) of the within the.

In addition, as reported in Figure 2, in the proposed system, an increase in flow rate resulted in a more steep gradient. Consequently, it is possible to determine and properly tune the shape of the concentration gradient by simply adjusting the applied flow rates according to the species' diffusion coefficients.

However, even if the microfluidic configuration proposed here lowers the shear stresses within the culture chamber of orders of magnitude if compared with existing devices,(Amarie et al. 2007, Jeon et al. 2000) it is important to underline how we always observed, both experimentally and via computational simulation, the presence of a small velocity filed along the longitudinal coordinate of the culture channel. Being the velocity gradients what determines the shear stresses, the proper design of the microfluidic

configuration and the operational parameters needs to taken into account in order to avoid negative shear stress effect on cell culture.

The system allowed prolonged culture of cells both under static and perfused conditions and proved its efficacy in generating and maintaining stable Wnt3a concentration gradients. In addition, from the quantification of the static multiwell experiments we could observe how the Wnt reporter expression followed more of a threshold-like behavior rather than a graded response.

This observation was confirmed in the the perfused experiments, where Venus expression levels at several points along the axial coordinate of the gradient were evaluated. The Venus expression along the axial coordinate show a steep sigmoid-like shape. This singular effect could be explained as the synergic contributions of the threshold-like response of Venus expression to the Wnt3a stimulation and the sigmoid-like shape of the Wnt3a concentration profiles within the culture channel.

These results, specifically applied to the extremely relevant family of Wnt3a molecules, are promising in sight of further applications aimed at exploring the role of concentration gradients on cell populations.

G.5 Acknowledgement

We gratefully acknowledge research support of the University of Padova and Fondazione CARIPARO (stipend to EC).

G.6 References

H. Clevers, Wnt/β-Catenin Signaling in Development and Disease. *Cell*, 2006, **127**, 469-480.
C. Y. Logan and R. Nusse, The Wnt signaling pathway in development and disease. *Annu. Rev. Cell Dev. Biol.*, 2004, **20**, 781–810.
R. T. Moon, Wnt/ß-Catenin Pathway. *Science Signaling*, 2005, **2005**.
R. T. Moon, B. Bowerman, M. Boutros and N. Perrimon, The Promise and Perils of Wnt Signaling Through b-Catenin. *Science*, 2002, **296**, 1644-1646.
R. T. Moon, A. D. Kohn, G. V. DeFerrari and A. Kaykas, Wnt and b-cat signalling diseases and therapies. *Nature Reviews Genetics*, 2004, **5**, 689-699.
A. Otto, C. Schmidt, G. Luke, S. Allen, P. Valase, F. Muntoni, D. Lawrence-Watt and K. Patel, Canonical Wnt signalling induces satellite-cell proliferation during adult skeletal muscle regeneration. *PNAS*, 2007, **104**, 9685–9690.
S. Ueno, G. Weidinger, T. Osugi, A. D. Kohn, J. L. Golob, L. Pabon, H. Reinecke, R. T. Moon and C. E. Murry, Biphasic role for Wnt/b-catenin signaling in cardiac specification in zebrafish and embryonic stem cells. *PNAS*, 2007, **104**, 9685–9690.
S. Maretto, M. Cordenonsi, S. Dupont, P. Braghetta, V. Broccoli, B. Hassan, D. Volpin, G. M. Bressan and S. Piccolo, Mapping Wnt/beta -catenin signaling during mouse development and in colorectal tumors. *PNAS*, 2003, **100**, 3299-3304.
J. L. Green, T. Inoue and P. W. Sternberg, Opposing Wnt Pathways Orient Cell Polarity during Organogenesis. *Cell*, 2008, **134**, 646–656.
E. S. Witze, E. S. Litman, G. M. Argast, R. T. Moon and N. G. Ahn, Wnt5a Control of Cell Polarity and Directional Movement by Polarized Redistribution of Adhesion Receptors. *Science*, 2008, **320**, 365-369.
K. Bartscherer and M. Boutros, Regulation of Wnt protein secretion and its role in gradient formation. *European Molecular Biology Organization*, 2008, **9**, 977-982.
A. Aulehla, W. Wiegraebe, V. Baubet, M. B. Wahl, C. Deng, M. Taketo, M. Lewandoski and O. Pourquié, A β-catenin gradient links the clock and wavefront systems in mouse embryo segmentation. *Nature Cell Biology*, 2008, **10**, 186-193.
T. M. Keenan and A. Folch, Biomolecular gradients in cell culture systems. *Lab on a Chip*, 2007, **8**, 34–57.
D. Amarie, J. A. Glazier and S. C. Jacobson, Compact Microfluidic Structures for Generating Spatial and Temporal Gradients. *Analytical Chemistry*, 2007.
N. L. Jeon, S. K. W. Dertinger, D. T. Chiu, I. S. Choi, A. D. Stroock and G. M. Whitesides, Generation of Solution and Surface Gradients Using Microfluidic Systems. *Langmuir*, 2000, **16**, 8311-8316.
T. Kang, J. Han and K. S. Lee, Concentration gradient generator using a convective–diffusive balance. *Lab on a Chip*, 2008, **8**, 1220–1222.
G. M. Whitesides, The origins and the future of microfluidics. *Nature*, 2006, **442**, 368-373.
D. J. Beebe, G. A. Mensing and G. MWalker, Physics and applications of microfluidics in biology. *Annu. Rev. Biomed. Eng.*, 2002, **4**, 261–86.
T. M. Squires and S. R. Quake, Microfluidics: Fluid physics at the nanoliter scale. *Reviews of Modern Physics*, 2005, **77**, 977-1016.
L. Kim, Y.-C. Toh, J. Voldman and H. Yu, A practical guide to microfluidic perfusion culture of adherent mammalian cells. *Lab on a Chip*, 2007, **7**, 681–694.
S. K. Sia and G. M. Whitesides, Microfluidic devices fabricated in poly(dimethylsiloxane) for biological studies. *Electrophoresis*, 2003, **24**, 3563–3576.
J. A. Burdick, A. Khademhosseini and R. Langer, Fabrication of Gradient Hydrogels Using a Microfluidics/Photopolymerization Process. *Langmuir*, 2004, **20**, 5153-5156.

W. Saadi, S. J. Wang, F. Lin and N. L. Jeon, A parallel-gradient microfluidic chamber for quantitative analysis of breast cancer cell chemotaxis. *Biomed Microdevices*, 2006, **8**, 109–118.

J. Diao, L. Young, S. Kim, E. A. Fogarty, S. M. Heilman, P. Zhou, M. L. Shuler, M. Wu and M. P. DeLisa, A three-channel microfluidic device for generating static linear gradients and its application to the quantitative analysis of bacterial chemotaxis. *Lab on a Chip*, 2006, **6**, 381–388.

Y. Chisti, Hydrodynamic Damage to Animal Cells. *Critical Reviews in Biotechnology*, 2001, **21**, 67-110.

E. Cimetta, E. Figallo, C. Cannizzaro, N. Elvassore and G. Vunjak-Novakovic, Micro-bioreactor arrays for controlling cellular environments: Design principles for human embryonic stem cell applications. *Tissue Engineering: Methods* 2009, **47**, 81–89.

T. L. Biechele and R. T. Moon, Assaying beta-catenin/TCF transcription with beta-catenin/TCF transcription-based reporter constructs. *Methods in molecular biology*, 2008, **468**, 99 -110.

A. Rekas, J. R. Alattia, T. Nagai, A. Miyawaki and M. Ikura, Crystal structure of venus, a yellow fluorescent protein with improved maturation and reduced environmental sensitivity. *Journal of Biological Chemistry*, 2002, **277**, 50573-8.

T. Dull, R. Zufferey, M. Kelly, R. J. Mandel, M. Nguyen, D. Trono and L. Naldini, A third-generation lentivirus vector with a conditional packaging system. *The Journal of Virology*, 1998, **72**, 8463-71.

K. Willert, J. D. Brown, E. Danenberg, A. W. Duncan, I. L. Weissman, T. Reya, J. R. Yates and R. Nusse, Wnt proteins are lipid-modified and can act as stem cell growth factors. *Nature*, 2003, **423**, 448-52.

Y. Xia and G. M. Whitesides, Soft Lithography. *Annual Review of Materials Science*, 1998, **28**, 153–84.

A. Tourovskaia, X. Figueroa-Masot and A. Folch, Long-term microfluidic cultures of myotube microarrays for high-throughput focal stimulation. *Nature Protocols*, 2006, **1**, 1092-1104.

J. Braga, J. M. P. Desterro and M. Carmo-Fonseca, Intracellular Macromolecular Mobility Measured by Fluorescence Recovery after Photobleaching with Confocal Laser Scanning Microscopes. *Molecular Biology of the Cell*, 2004, **15**, 4749–4760.

Appendix H

Dynamic culture of bubble-confined cell arrays

Elisa Cimetta[1§], Stefano Cagnin[2§], Annamaria Volpatti[1], Gerolamo Lanfranchi[2], Nicola Elvassore[1*]

[1] Department of Chemical Engineering, University of Padua, Via Marzolo, 9 Padua, Italy

[2] CRIBI, Biotechnology Center and Department of Biology, University of Padova, Via U. Bassi, 58/B Padua, Italy

[*] Corresponding author

[§] Equally contributing authors

Submitted to Biotechnology Progress

Keywords: cell array, perfusion, C2C12, hydrogel, ECM.

Abstract

Responding to the need of creating an accurate and controlled micro-environment surrounding the cell while meeting the requirements for biological processes or pharmacological screening tests, we were aimed at designing and developing a microscaled culture system suitable for analyzing the synergic effects of extracellular matrix proteins and soluble environments on cell phenotype in a highthroughput fashion. We produced cell arrays deposing micrometer-scale protein islands on hydrogels using a robotic DNA microarrayer, constrained the culture media in a bubble-like volume and developed a suitable perfusion system. The bubble-confined cell arrays were used either with conventional culture methods (batch operating system) or with automated stable and constant perfusion (steady-state operating system). Mathematical modeling assisted the experimental design and assessed efficient mass transport and proper fluidodynamic regimes. Cells cultured on arrayed islands (500µm diameter) maintained the correct phenotype both after static and perfused conditions, confirmed by immunostaining and gene expression analyses through total RNA extraction. The mathematical model, validated using a particle tracking experiment, predicted the constant value of velocities over the cell arrays (less than 10% variation) ensuring the same mass transport regime. BrdU analysis on an average of 96 cell spots for each experimental condition showed uniform expression inside each cell island and low variability in the data (average of 13%). Perfused arrays showed 30% higher doubling times when compared with static cultures. In addition, perfused cultures showed a reduced variability in the collected data, allowing to detect statistically significant differences in cell behavior depending on the spotted ECM protein.

H.1 Introduction

In the past few years, the need for more accurate and relevant biological data has led to the development of new microscaled and high throughput technologies. The important role and advantages of adopting cell-based testing have been extensively reported (Peterbauer et al. 2006) and its coupling to multi-parametric and multiplexed array technologies (Beske and Goldbard 2002) have allowed an increase in the efficiency and outcome of cell behavior evaluations (Chen et al. 1998, Nelson et al. 2005), drug discovery processes (Bhadriraju and Chen 2002) and gene expression analyses (King et al. 2007, Lee et al. 2006). Moreover, the scientific community acknowledges that the complex extracellular means in natural tissues are capable of providing biochemical, biomechanical and physiological stimuli to the cells constituting the tissues themselves. It is thus of primary importance to accurately engineer the characteristics of the microenvironment surrounding the cultures *in vitro* in order to mimic the natural niche encountered by cells *in vivo* (Powell 2005). For this reason, hydrogels have been widely used as supporting materials for cell cultures (Burnham et al. 2006) and many other satellite applications such as drug delivery (Burdick et al. 2005) and protein microarrays (Angenendt et al. 2003). Hydrogels can be derived from photo-polymerization of prepolymer solutions, are biocompatible, chemically stable and extremely hydrophilic while being relatively non-adhesive towards cells. In addition, the mechanical properties of hydrogels have been recently highlighted, demonstrating how the substrate stiffness can greatly influence and guide cell proliferation and differentiation (Discher et al. 2005, Engler et al. 2004, Georges and Janmey 2005). At the same time, to guide cell adhesion and study positional-geometrical cues, many patterning techniques have been proposed and widely reviewed over the last few years (Falconnet et al. 2006). Even thought micro-contact printing is assuming a pivotal role (Ruizab and Chen 2007), other automated and operator-independent techniques such as robotic protein printing (Revzin et al. 2004) can be employed. The major advantages of this method are versatility, extreme repeatability and spatial resolution. Among others, the work of Flaim et al. (Flaim et al. 2005), contributed to sum up all the cited requirements and made use of a robotic DNA spotter to match highthroughput and repeatability requirements. Finally, the additional application of dynamic culture conditions can intervene in order to obtain better control over culture conditions at the microscale level (Kim et al. 2007). The constant, steady state provision of nutrients and the removal of wastes from cell cultures leads to undeniable advantages and adds other sources of versatility due to the modulation of the operative parameters such as

the composition of the culture media, the flow rates and, consequently, the flow and mass transport regimes.

The aim of this study was to design and develop a culture system allowing for an accurate and automated spatio-temporal control of culture conditions. The system prerequisites are: matching highthroughput requirements, interfacing with existing techniques including microfabrication, sample handling and manipulating and allowing for easy and effective results reading and analysis. We organized our cell cultures in arrays of circular islands inside a liquid bubble of culture media and designed and developed a system ensuring continuous perfusion of medium for such bubble-confined cell arrays. We optimized the techniques and methodologies which involved materials, protein deposition, standard and dynamic culture so to obtain a reliable and repeatable tool for further studies and future applications. We assessed a highly selective adhesion of cells onto polyacrylamide hydrogels conditioned by reproducible deposition of extracellular matrix (ECM) protein islands using a robotic DNA microarrayer and studied such cultures under perfused conditions in a controlled flow regime not resulting in high shear stress levels for the cell arrays. We observed, by immunostaining and molecular analysis, the proliferation and differentiation of cultured cells in response to changed stimuli. This demonstrated that the developed system is an effective solution in terms of feasible control over culture conditions, both concerning static and perfused cultures.

H.2 Material and Methods

H.2.1 Microarray support

The microarray substrate was a polyacrylamide hydrogel covalently bound to a pre-functionalized glass surface. Methacrylation of glass slides resulted in an extremely hydrophobic surface. Slides were washed with ethanol and distilled water, dried in an oven at 110°C and plasma treated (Plasma Cleaner PDC-002, Harrick Plasma) for 5 minutes at 50Pa. After that, approximately 50μL of 3-(trimethoxysilyl)propyl methacrylate (Sigma-Aldrich) was deposited and uniformly distributed onto each slide. All slides were stocked for 1 hour, in order to complete the reaction, and then dried at 100°C for 10 minutes.

Hydrogels were obtained from a prepolymer solution consisting of an acrylamide/bis-acrylamide 29:1 40% (w/v) mixture (Sigma-Aldrich) diluted in phosphate buffered saline

(PBS) to a final concentration of 10%, and the photoinitiator Irgacure 2959 (Ciba Specialty Chemicals), initially dissolved in methanol at 200mg/mL, at a final concentration of 20mg/mL.

A thin hydrogel pad was created by dropping 20µL of the prepolymer solution over the functionalized glass surface and then floating an untreated glass coverslip over it. The crosslinking reaction occurred after exposure to UV light for 3 minutes. Irradiation was provided by a high-pressure mercury vapor lamp (Philips HPR 125W) emitting at 365nm with an incident light intensity of 20mW/cm2. A selective polymerization of the polyacrylamide solution was achieved by interposing a photomask between the light source and the glass slide; this enabled us to obtain three circular hydrogel films with a diameter of 16 mm for each slide.

After carefully removing the coverslip, the glass slides were washed with distilled water to remove the un-polymerized solution and then soaked in ultra pure distilled water for 48h to completely eliminate the un-reacted photoinitiator or monomeric units. Finally, hydrogels were air-dried for 3h and exposed to UV light under a sterile hood for 20 minutes to complete the sterilization.

H.2.2 Hydrogel characterization: swelling experiments

Swelling tests were carried out using hydrogel samples prepared by polymerizing 0.3mL or 1.0mL of polyacrylamide solution inside 18mm diameter wells; following polymerization, the hydrogel discs were pulled out of the wells and immediately weighed. Afterwards, the samples were completely dehydrated by high vacuum treatment for 48h at room temperature. The dry mass of the samples was determined before the rehydration procedure; rehydration was carried out at 25°C with different swelling media: PBS, supplemented and non-supplemented Dulbecco's Modified Eagle Medium (DMEM), culture medium and ultra pure distilled water. Samples with an initial volume of 1.0mL were used to study the effect of different swelling media whereas disks with initial volume of both 0.3mL and 1.0mL were employed to characterize the swelling kinetic. For each swelling experiment three different samples were tested. All samples were allowed to swell in the chosen media at room temperature for 74 hours and were periodically weighed. The percentage mass swelling ratio of the gels was calculated as:

$$q = \frac{(W_s - W_d)}{W_d} \cdot 100 \quad (1)$$

where W_s is the weight of the swollen sample and W_d is the weight of the dry sample.

H.2.3 Protein microarray construction

Laminin and fribronectin protein solutions (Sigma) were resuspended in the spotting buffer at the final concentration of 50ng/µl. The deposition buffer contained 1.5 w/w % glycerol and 1X (PBS). We used the Microgrid II (Biorobotics) contact microarrayer with the TeleChem solid pins to construct the protein array. The humidity and temperature in the array chamber were maintained at 50-55% and 25°C respectively, in order to avoid protein solution evaporation and gelification. Pins were cleaned between each different protein deposition to avoid the stock solution contaminations and to ensure specificity in protein deposition.

H.2.4 Cell culture

The murine skeletal muscle immortalized cell line C2C12 was obtained from the American Type Culture Collection (ATCC). These cells were cultured in DMEM (Sigma-Aldrich) supplemented with 10% foetal bovine serum (FBS, Gibco-Invitrogen), 1% penicillin-streptomycin and 1% L-glutamine (all from Invitrogen) on standard 100mm Petri dishes in a 95% humidified and 5% CO2 atmosphere at 37ºC and maintained at low confluence.

80%-confluent C2C12 plates were detached using trypsin/EDTA (Sigma-Aldrich), pelleted by centrifugation for 5 min at 200g and counted. The desired number of cells was resuspended in 150µL of supplemented DMEM culture medium and seeded deposing the suspension over each circular film. The cellular concentration of the suspension varied depending on the desired degree of confluence on the microarray spots. The combination of the hydrophilicity of the hydrogel and the hydrophobicity of the glass surface allowed confinement of the fluid over the polymeric film forming three independent bubbles in each slide. After 2 hours of incubation, unattached cells were removed through repeated washing carried out by adding and immediately removing a 150µL aliquot of DMEM. Cellular microarrays were then maintained in a static or perfused culture.

H.2.5 Immunostaining analyses

C2C12-desmin

At the end of the culture, cellular microarrays on hydrogel films were fixed with paraformaldehyde (PFA) 2% for 7min. After permeabilization with a 0.5% Triton X-100 solution (Sigma) for 8min, the samples were blocked with a 10% FBS/PBS solution for 45 minutes; all these steps were carried out at room temperature. Cells on hydrogel were then treated with primary antibody to desmin, rabbit polyclonal, (AbCam) diluted 1:100 in a 3% BSA/PBS solution for 1 hour at 37°C, and then, with a secondary antibody Cy™3-conjugated anti-rabbit IgG (Jackson) diluted 1:200 in a 3% PBS/BSA solution for 45 minutes at 37°C. A 10 minutes incubation at room temperature with DAPI (Sigma-Aldrich) solution diluted 1:1000 in PBS was used to detect the nuclei. At the end samples were mounted with Elvanol® and analyzed with a fluorescence microscope.

C2C12-BrdU

To evaluate the degree of proliferation after 24 hours of culture, the bubble of medium was changed with a solution of BrdU diluted 1:1000 in DMEM and the slides were incubated for 4 hours. At the end of this treatment, hydrogels were repeatedly washed with PBS and cellular microarrays were fixed in situ with methanol for 10 minutes at -20°C. After rehydration with PBS for 3 minutes, DNA was denatured incubating samples in 1N HCl at 37°C for 1 hour; the acid was then neutralized by immersing slides in 0.1M borate buffer (pH 8.5). The cells were washed again with PBS before an overnight incubation a 4°C with primary antibody to BrdU, mouse monoclonal, (Roche) diluted 1:50 in 0.1% BSA/PBS solution. A secondary antibody FITC-conjugated anti-mouse diluted 1:250 in a 3% BSA/PBS solution was then added and incubated for 45 minutes at 37°C. Cell nuclei were stained for 10 minutes at room temperature with a DAPI solution (Sigma-Aldrich) diluted 1:1000 in PBS. At the end, samples were mounted with Elvanol® and analyzed with a fluorescence microscope

Cell array RNA extraction and amplification

Each of the three different bubble cell arrays from a single slide, was used to extract total RNA from cells cultured in proliferative medium for 1 day and pooled to construct a common reference RNA. On a second slide, the cells of the three arrays were cultured in proliferative medium for 6h and in differentiative medium for 24h and 60h. Total RNA was

extracted using the TRIzol (Invitrogen) method, as specified by the manufacturer, and purified with the Qiagen RNAeasy Columns (Qiagen). RNA was quantized by the NanoDrop ND-1000 spectrophotometer (Thermo Fisher Scientific) and its integrity was evaluated with the Agilent 2100 Bioanalyzer . 400ng good quality total RNA were used to perform a linear amplification using the Eberwine reaction with the MessageAmp^{TM} aRNA amplification kit (Ambion) as specified by the manufacturer. The procedure includes reverse transcription with an oligo-dT primer bearing a T7 promotor using reverse transcriptase to produce the first strand cDNA. After second strand synthesis and clean-up, the cDNA becomes a template for the in vitro transcription technology to generate antisense RNA (aRNA) copies of each mRNA molecule. Modified nucleotides 5-(3-aminoallyl)-UTP (aaUTP) were incorporated into the aRNA during the in vitro transcription reaction. Following purification of aRNA, incorporated aaUTP was coupled to N-hydroxysuccinimidyl ester-derivatized reactive dyes Cy3 or Cy5 (Amersham) to perform microarray experiments.

Microarray and quantitative Real Time PCR analysis

aRNA derived from C2C12 cells grown in proliferative medium was used as a control to detect differentially expressed genes in cells grown in differentiative medium by a genome wide approach. Microarray hybridizations were performed using mouse Operon V1.1 oligonucleotide microarray spotted on a MICROMAX glass slide Superchip I (PerkinElmer) at C.R.I.B.I. microarray facility using the microcontact arrayer Microgrid II (Biorobotics).

The platform used for this publication has been deposited in the NCBI Gene Expression Omnibus (GEO, http://www.ncbi.nlm.nih.gov/geo/) and is accessible through GEO Platform accession number GPL6747. Competitive hybridizations were protracted for 24 hours at 48°C in the specific buffer (25% formamide) in the automatic ArrayBooster (Advalytix) to obtain continuous mixing of the target solution. We performed two replicates for each experiment (the data discussed in this publication have been deposited in the NCBI GEO and are accessible through GEO Series accession number GSE11191). After hybridization, microarray slides were washed once with 1X Sodium Chloride Sodium Citrate (SSC) 1% Sodium dodecyl sulfate (SDS) for 4 min at room temperature (RT) and with 0.1 X SSC 0.1% SDS for 4 min at RT: twice with 0.2 X SSC for 3 min at RT and finally once with 0.1 X SSC for 3 min at RT. After centrifugation dried slides were scanned

using the ScanArray LITE laser scanner (PerkinElmer) producing two tiff format images per microarray. Fluorescence derived from each spot was quantized using ScanArray Express 3.0 software (PerkinElmer) and normalized with the MIDAW tool (Romualdi et al. 2005). Data were normalized using total and lowess normalization methods (Quackenbush 2002) and filtered by considering the values of "empty" control spots in the microarray as outlined in the Supplementary Information of the GEO series. Differentially expressed genes between proliferative and differentiative medium were identified by KMC (K-means clustering) (Soukas et al. 2000) analysis implemented in the TIGR MEV suit (Saeed et al. 2003). Differentially expressed genes were grouped based on their functional category using the Gene Ontology description (Ashburner et al. 2000) implemented in the DAVID database (Dennis et al. 2003) (Database for Annotation, Visualization and Integrated Discovery).

Differentially expressed genes were confirmed by qRT-PCR experiments. 400ng of aRNA were retro-transcribed in triplicate using PM random primers and the Superscript II (Invitrogen) as specified by the manufacturer. The hybrid DNA/RNA was precipitated using the ethanol and salt method and resuspended in ultraPURE™ distilled water DNase, RNase free (Gibco) at a final concentration of 50ng/μL. The purified hybrid DNA/RNA was used to determine different gene expressions for target genes involved in the discrimination between proliferating and differentiated C2C12 cells. The ΔΔCt relative SYBR green method(Pfaffl 2001) was used to determine differentially expressed genes with glyceraldehyde-3-phosphate dehydrogenase (GAPDH) as reference gene. Real Time reaction was performed in triplicate for each gene in a 10μL reaction solution using the DyNAmo™ HS SYBR® Green qPCR kit (Finnzymes) in the 7500 Real time PCR system (Applied Biosystem).

Dynamic apparatus

The dynamic culture system included the bioreactor, a gas exchanger unit and a syringe pump (PHD, Harvard Apparatus, Holliston, MA); connections were made with Tygon tubings (0.8mm ID, 2.4mm OD, Cole Palmer, USA). The bioreactor was composed of two units: a support for the glass slide and a PDMS chamber to isolate the culture system from the external environment and to allow easy set up of the micro injection and suction apparatus for each bubble. The support was a polycarbonate (PC) plate (96x52x6 cm3) with a rectangular hole fitting the glass slide with the seeded hydrogel circles. The chamber,

designed to be perfectly assembled with the glass support and ensure conformal sealing, was molded by pouring 40mL of poly(dimethylsiloxane) (PDMS) over a master. PDMS was chosen for its oxygen permeability, thermal stability and optical transparency, thus allowing image acquisition of the culture. To individually connect every bubble with the dynamic apparatus, we plugged microbore stainless steel tubes (21 gauge, 20mm length) into one end of the Tygon tubing, and vertically drove it into the PDMS creating the inlet and outlet ports for each hydrogel disk. The distances of the tubes from the hydrogel surface were 300µm for the inlet and 400µm for the outlet, fixed so to maintain a 150µl hold up in the bubble. The bioreactor and the gas exchanger unit were kept in the incubator at standard conditions (37°C, 95% humidity, 5% CO2) while the syringe pump was left at room temperature.

The gas exchange unit was made using a tubular non-porous permeable membrane (platinum cured silicone tubing, Vetrotecnica, Padova, Italy); the surface area and the corresponding length were dimensioned to ensure the gas exchange needed for the maintenance of the physiological oxygen and carbon dioxide concentrations and pH value in the culture medium.

Fluid Dynamics modeling

The Navier-Stokes equations for incompressible fluids, numerically solved using the finite elements method implemented in Comsol Multiphysics (Burlington, MA), allowed an estimation of the flow fields and shear stresses that influence the cells. The 3D domain of the bubble was schematized as a semi-ellipsoid with two cylindrical hollows corresponding to the inlet and outlet tubes. A non-structured mesh was then automatically generated with tetrahedron finite elements. Then, to ensure independency of the solution from the spatial discretization, a grid refinement was required near the in/out conduits where the maximum turbulence was located. No-slip boundary conditions were used for the hydrogel surface (bottom plane) and the walls of the tubing, sliding/symmetry for the bubble surface, fixed velocity for the inlet and finally zero pressure for the outlet. The fluid properties' viscosity and density were taken from the literature (Cimetta et al. 2007).

In order to validate the results of the simulations, comparisons between experimental and calculated particle trajectories were carried out. For these experiments, cells devitalized with ethanol were used as tracer-particles and the bioreactor was positioned under the microscope to acquire *in continuum* images of the particles moving in a plane located 50µm

above the hydrogel surface. For fixed positions, restricted to the region where the cell array was confined, phase images of the focal plane were acquired every 5 seconds for 150 seconds. An image analysis program, custom developed using the MATLAB imaging toolbox (The MathWorks, Natick, MA), was used to track the coordinates of all visible particles for each frame and to reconstruct their trajectories.

H.3 Results

H.3.1 Bubble confined cell array

The first steps towards the generation of the cell array involve the choice of the best materials and the compilation of the optimal protocols involved in the substrate fabrication.

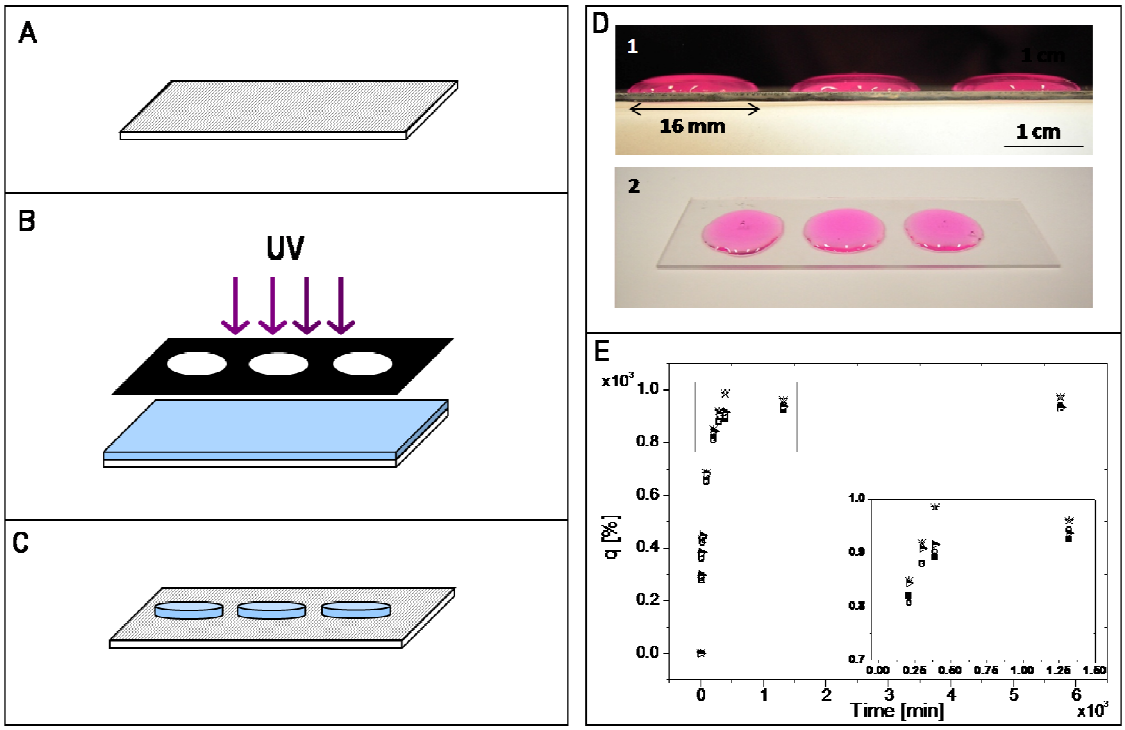

Figure 1. *Development and characterization of the cell array support. A standard microscope slide was functionalized with a hydrophobic layer of methacrylate groups (A), a uniform layer of polyacrylamide-based prepolymer solution was selectively polymerized by UV exposure through a photomask (B), resulting in three independent and highly hydrophilic hydrogel circles (C). Panel D shows the dimensions and shape of the hydrogel circles covered with 150µL of culture medium. Panel E: graph plotting the percentage mass swelling ratio vs time; hydrogels behaved similarly with the different swelling media used: PBS (○), supplemented ( ) and not supplemented DMEM ( ) and ultra pure distilled water (■).*

Figure 1, panels A-C, illustrate the basic steps leading to the formation of the microarray support. A standard microscope slide was functionalized with a hydrophobic layer of methacrylate groups (A) and a uniform layer of polyacrylamide-based prepolymer solution was selectively polymerized by UV exposure through a photomask (B). The final result was represented by three independent and highly hydrophilic hydrogel circles (C). The resulting hydrophobic and hydrophilic characteristics of the glass slide and hydrogel, respectively, allowed precise confinement of the bubble of culture medium. The demonstration is given by pictures in panel D, showing the dimension and shape of the hydrogel circles covered with 150µL of culture medium. The results of the swelling experiments are reported in panel E, with a graph plotting the percentage mass swelling ratio versus time, demonstrating how the hydrogels behave consistently and not showing significant differences with the different swelling media used: PBS, supplemented and not supplemented DMEM and ultra pure distilled water. The fact that swelling behavior is insensitive to the used media is important as it establishes that during culture, the cells will not be influenced by unpredicted mechanical forces induced by gel deformations. Moreover, the swelling media tested represent all of the liquids that will be used with cells, from the culture-related operations to the final immunostaining procedures. Finally, a uniformity in gel behavior is also shown for the phases following the ECM spotting (data not shown), sustaining its elasticity and stability which permitted ECM pattern deposition using a micro-contact arrayer.

The technology employed proved its versatility as it allowed the obtainment of various geometries by simply changing the pins' diameter and/or the deposition scheme of the robotic microarrayer. In particular, we patterned protein arrays characterized by different geometrical arrangements, different spacing between both single and arrays of spots and different diameters of the individual spots themselves. This flexibility allowed us to pattern C2C12 cells in particular orientations favoring their fusion and myotube formation.

The patterns are presented in Figure 2, columns A and B, as fluorescence images obtained by spotting BSA-FITC conjugate protein.

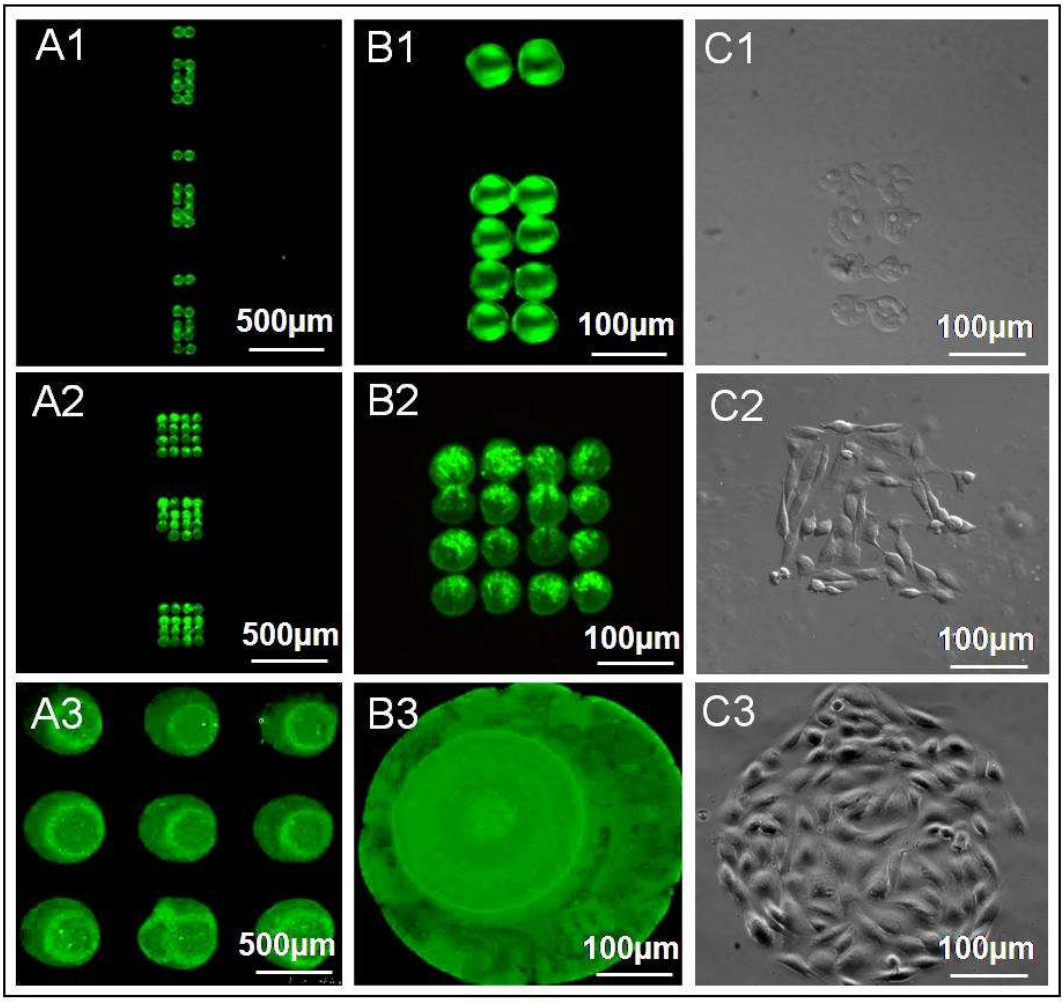

Figure 2. *Spotting versatility and materials properties. In columns A and B: fluorescence images of multiple geometries obtained spotting BSA-FITC conjugate with a robotic DNA microarrayer using pins of different diameter. Column C reports the corresponding pictures of living cells selectively adhering to the protein patterned regions due to the hydrogels non-fouling properties.*

In Figure 2, column 3, we reported the corresponding pictures of living cells selectively adhering to the protein patterned regions. The polyacrylamide hydrogel was a non-fouling material thus preventing cell adhesion to its surface; for this reason, the cells adhered with high selectivity only onto the ECM proteins spotted areas and their migration was prevented, thus allowing a prolonged confinement.

The presented results derive from experiments performed using the following array geometry: two separate 4 by 4 (3x3mm each, 1.5mm spaced) arrays of individual spotted islands with a 480µm average diameter located at the center of the circular hydrogel pad.

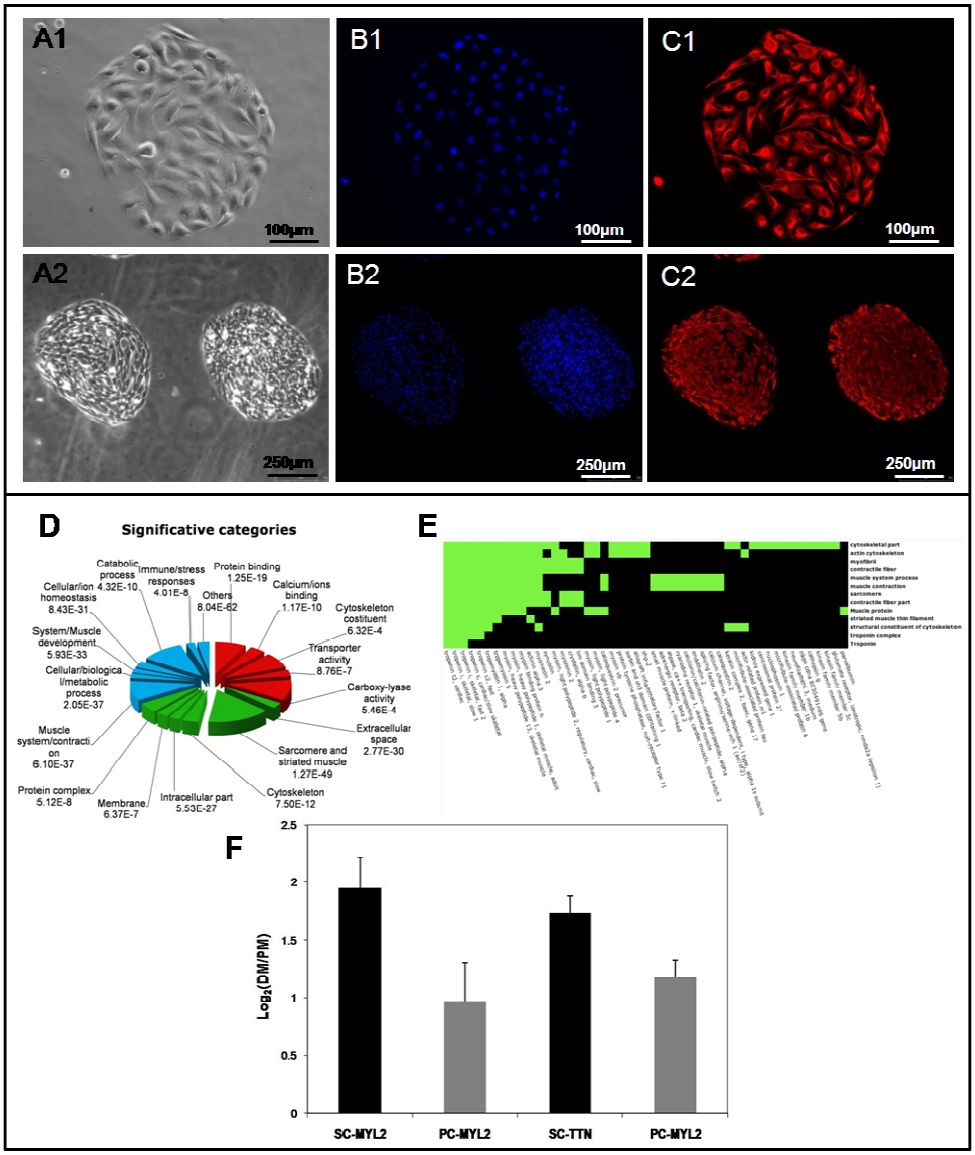

Figure 3. *Biological characterization. Upper panel: C2C12 seeded on hydrogels patterned with 500µm diameter protein islands (Fibronectin, 50µg/mL), demonstrating the selectivity of adhesion. Column A: bright field images; columns B and C: immunofluorescence analyses, DAPI and Desmin respectively, on the same cultures demonstrating the uniform distribution of cells within the spotted islands and the correct and uniform phenotypic expression. Lower panel: genomic analyses. D: gene ontology categorization for up regulated genes in differentiated cells. Significant p values are indicated. E: up-regulated genes in C2C12 differentiated cells. x axis represent the gene, y axis the category. Genes falling in the category are represented by a green box while genes outside the category are represented with a black box. F: histograms represent log2 expression value relative to control gene, obtained by qRT-PCR for the indicated factors. DM: differentiation media, PM: proliferation media; SC: static culture, PC: perfused culture. Up-regulation for myosin light chain 2 (MYL2) and titin (TTN) detected by microarray experiments was confirmed by qRT-PCR. A lower up-regulation of both genes during cell differentiation is detected in PC but the trend is maintained in accordance with C2C12 differentiation events.*

The upper panel of figure 3 presents pictures of C2C12 seeded on a hydrogel pad patterned with 500µm diameter protein islands (Fibronectin, 50ng/µL), further demonstrating the selectivity of adhesion resulting from the utilized and optimized techniques. Column A depicts bright field images while columns B and C show the results of immunofluorescence analyses, DAPI and Desmin respectively, performed on the same cultures demonstrating the uniform distribution of cells within the spotted islands and the correct and uniform phenotypic expression. In addition, we confirmed that our system was compatible with the extraction of integer total RNA from the cultured cells for further enzymatic processing, fundamental to perform molecular studies. Using the well-characterized C2C12 system, we tested differentially expressed genes in cells grown in proliferative medium compared to those grown in differentiative medium (Table 1 supplementary materials). As discussed in previous works(Tomczak et al. 2004, Moran et al. 2002) based on standard cell culture, differentiated C2C12 cells showed an up-regulation for specific genes involved in the striated muscle contraction, its regulation and muscle development (Figure 3D and Table 2 supplementary materials). We demonstrated, using the same technique for the gene expression analysis, that up-regulation for specific muscle genes like myosin light chain 2 (MYL2), myosin heavy chain embryonic or perinatal skeletal muscle or troponins, is correctly maintained in the perfused cell array-bubble system (Figure 3E). This result supports the ability of the system to allow cell growth and differentiation. Up regulation for MYL2 and titin (TTN) genes was confirmed by quantitative real time PCR both in perfused and static cell array-bubble system and for the two culture media used, proliferation and differentiation, evidencing comparable effects in both cultured methods, with a lower up-regulation in perfused cell culture (Figure 3F). This effect could be due to the clearance ability of the liquid movement versus cells not completely attached to the substrate.

H.3.2 Perfusion

The results of the fluidodynamic analyses are reported in Figure 4.

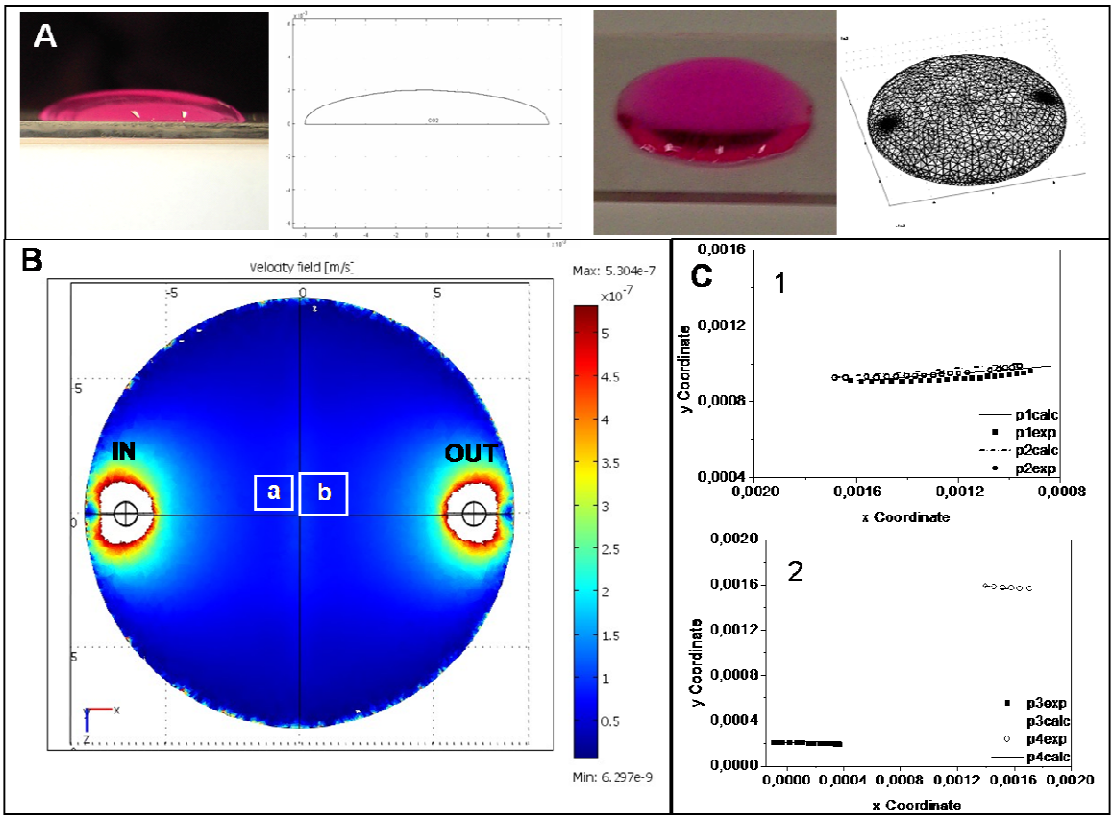

Figure 4. *Fluidodynamic analyses and validation. Upper panel (row A) shows the geometry of the bubble of culture medium and the corresponding modeled images and mesh. Lower panel: B report the results of a simulation performed using a 5µL/min flow rate, generating an uniform velocity field, especially over the cell arrays positioned at the center of the bubble. Turbulence is encountered only in the close proximity of the inner and outer conduits. C: experiments with particle tracers (dotted lines) are in accordance with the modeled trajectories (solid lines). The experiments were performed following the movements of particles in the areas represented by a and b in panel B.*

In the upper panel, pictures show the geometry of the bubble of culture medium and the corresponding modeled images, demonstrating good congruence both in 2 and 3 dimensions. Inner and outer conduits are modeled as cylindrical drilled holes with the same spatial coordinates and dimensions of the stainless steel tubings used for the experiments. The mesh refinement has proven to have little or no effect on the final results of the simulations (data not shown). In the lower panel, the results (B) of a simulation performed using a 5µL/min flow rate demonstrate the uniformity of the velocity field over the entire surface of the bubble and thus over the cell arrays, positioned at the center of the bubble.

Turbulence is encountered only in the close proximity of the inner and outer conduits, but has no effect on the cell arrays positioned in the center of the bubble (around and inside region 1 and 2 in Figure 4 B). In C, the studies performed using devitalized cells as particle tracers (dotted lines) demonstrate accordance with the modeled trajectories (solid lines). The experiments were performed following the movements of particles in the areas represented by a and b in panel B.

In Figure 5, further results deriving from the modeling are reported.

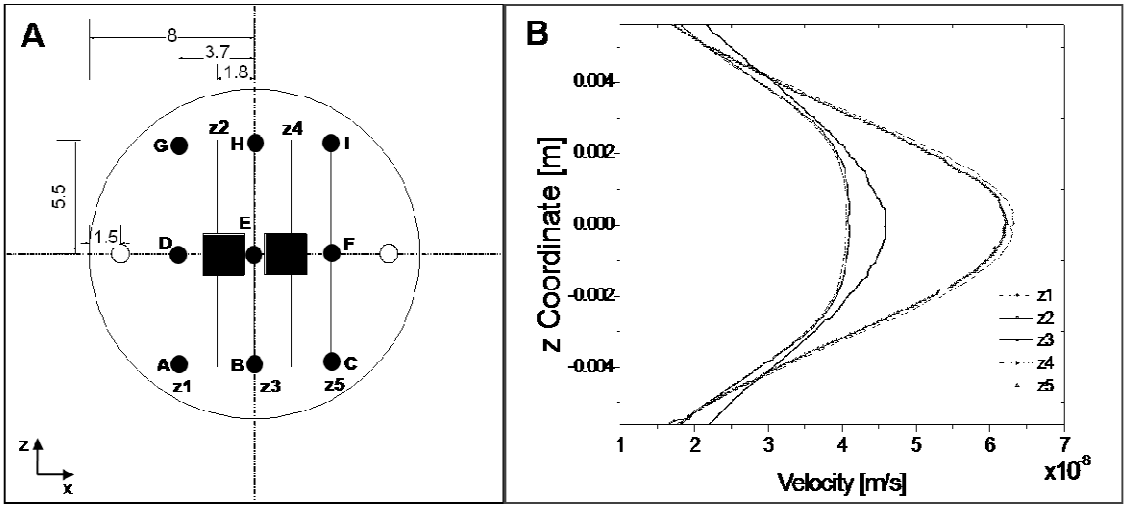

	A	B	C	D	E	F	G	H	I
Velocity [m/s] x10^{-8}	1.72	2.17	1.72	63.2	4.59	62.3	1.75	2.21	1.66
Re x10^{-9}	8.21	10.9	6.88	29.1	15.5	26.6	6.79	12.3	8.07
Shear stress [Pa] x10^{-7}	5.93	8.88	6.56	2.63	19.1	25.9	6.26	9.23	6.34

Figure 5. *Modeling validation and measurements. In A: filled squares identify the areas covered by the cell arrays; open circles locate the inner and outer conduits; vertical lines labeled zi (i=1 to 5) represent the sections were the velocity profiles were calculated and filled circles denoted with capital letters the chosen evaluation points. Represented dimensions are in millimeters. Panel B reports the resulting velocity profiles along xi. The lower table lists the calculated values for velocity, Reynolds number and shear stress on the above mentioned points*

The drawing in A identifies the areas covered by the 2 cell arrays (filled squares) and reports the coordinates of the chosen points of analysis: vertical lines labeled zi (i=1 to 5) for the identification of velocity profiles and filled circles denoted with capital letters for point evaluations. The resulting velocity profiles are reported in panel B, and are clearly

perfectly symmetric with respect to the inner and outer conduit axis. The lower table lists the calculated values for velocity, Reynolds number and shear stress on the above mentioned points. The particular position chosen for the construction of cells array permits cells to be influenced by the same low shear stress evidenced in this table. This avoids eliciting different cell responses influenced by the position in the array during perfused culture.

H.3.3 Biological data and their quality

The ability of the system to generate consistent biological data has also been verified via morphological evaluations and immunochemistry on the cultured cells, and quantification of the obtained outcomes.

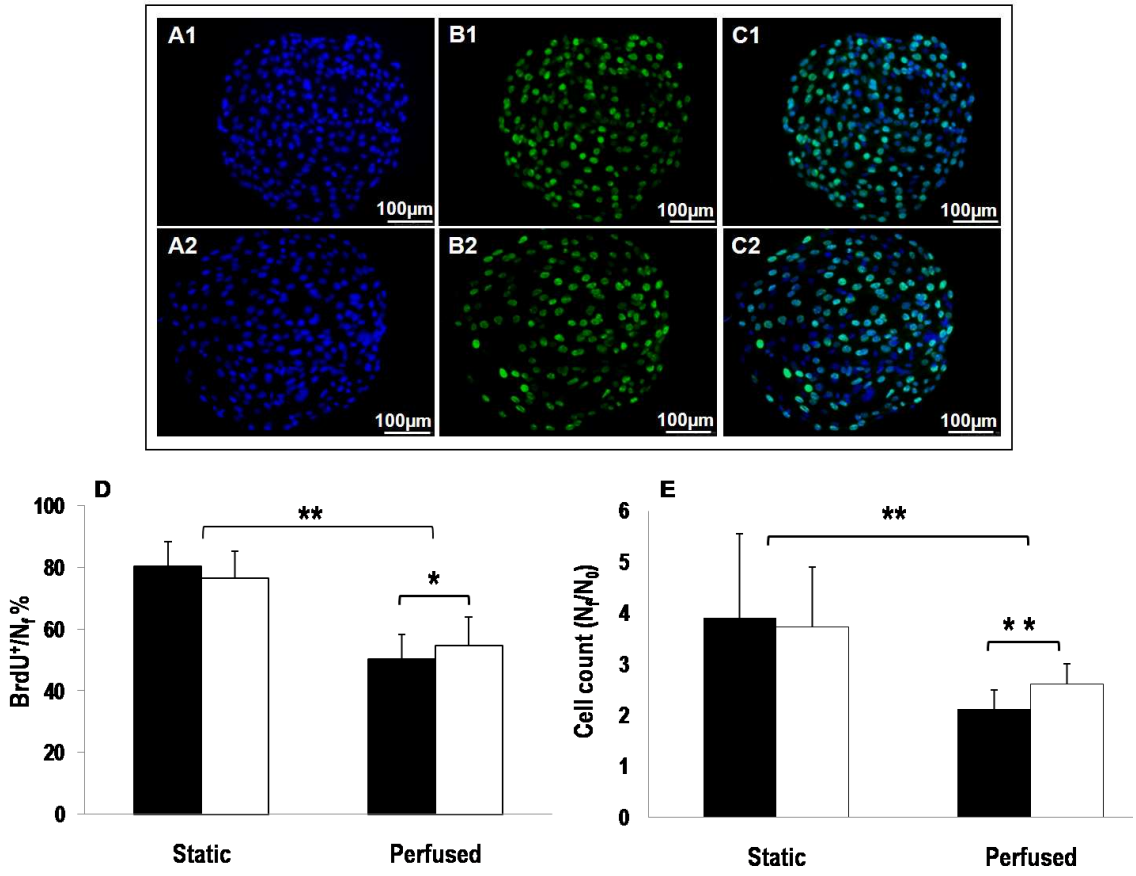

Figure 6. *Biological data. Upper panel: immunofluorescence analyses on individual cell islands forming the array, both after static (A1, B1, C1) and perfused culture (A2, B2, C2). In A nuclei are marked using DAPI, in B BrdU positive cells are stained in green; merged images are reported in column C. Graph D plots the fraction of $BrdU^+$ cells with respect to the total number of cells inside each island for each condition: on fibronectin (■) and laminin (□) and after static and perfused culture. Graph E plots cell counts results (N_f/N_0) in the same conditions. p values were evaluated performing ANOVA tests, (**: $p<0.01$; *: $p<0.05$).*

Upper panel of Figure 6 reports images deriving from individual cell islands forming the array, both after static (row 1) and perfused culture (row 2). In the first column all nuclei are marked using DAPI, while BrdU positive cells are stained in green in the second column; the third column reports the merged images. Data quantification deriving from the fluorescence images allowed us to construct graphs D and E in Figure 6. In D, the fraction of $BrdU^+$ cells with respect to the total number of cells inside each island (N_f) was evaluated and plotted for each condition: on fibronectin and laminin and after static and perfused culture. There are two statistically significant differences: first, static culture results in a higher fraction of $BrdU^+$ cells and second, perfused culture allowed us to capture a different behavior on the two proteins used, which were not in evidence in the static culture method. The same trend is observed in E, with a graph plotting the results of the cell counts N_f/N_0 (being N_0 the number of adhering cells counted 2 hours after seeding). The perfusion of medium and hence the provision of nutrients and oxygen permitted growth and maintenance of the cell array in a more "tissue friendly" condition; though, cell growth is dependent on medium flow rate as this influences mass transfer, shear stress and hydrostatic pressure which may have a negative impact on cell growth. $BrdU^+$ cells and total number of cells were counted for each spot forming the arrays (number of counted spots >100) from fluorescent images obtained with a double staining for BrdU and DAPI.

We used experimental data derived from the immunofluorescence analyses to perform an empirical calculation of the doubling times and fraction of proliferating cells cultured both in static and perfused conditions. The experimental input data were the number of cells counted from the stained nuclei two hours after seeding (N_0) and at the end of the culture (N_f), after 24 hours, inside each individual spot forming the array. We assumed a first-order kinetics for the cells growth so that:

$$N_f/N_0=e^{k\tau} \qquad (2)$$

Where t= 24 hours and k is the reaction constant expressed in $(\text{time})^{-1}$ units. From this equation we calculated the value of the constant k for each culture condition from averages of the ratio N_f/N_0 measured from an elevated number of repeated cells counts (<100). Such values of the constant were used to calculate the doubling time τ from the following equation

$$\tau=ln2/k \qquad (2)$$

An experimental value for τ was evaluated from the ratio $BrdU^+/N_f$ considering a 10 hour time span obtained from the 4 hours of BrdU reagents exposition plus a 6 hour-long S phase in the cell cycle. Experimental and calculated values are in accordance, as demonstrated by the table in figure 6 for both static and perfused conditions.

The results are summarized in the following table.

Table 1.*Experimental data. Experimental data of $BrdU^+$ cells and cell counts are reported in left two columns while the calculated values of the corresponding doubling times are presented in the ones on the right. All conditions were evaluated: static and perfused culture and different spotted proteins. In parentheses, the % errors allows an easier evaluation of the data quality.*

		Experimental data		Calculated doubling times τ [h]	
		$BrdU^+$ cells [%]	**Cell count (N_f/N_0)**	**From $BrdU^+$ data**	**From N_f/N_0 data**
Static	**Fn**	80.4±8.0 (±10%)	3.9±1.7 (±43%)	12.4±1.2 (±31%)	12.2±3.8 (±10%)
	Ln	76.5±8.8 (±12%)	3.7±1.2 (±31%)	13.1±1.5 (±24%)	12.6±3.0 (±12%)
Perfused	**Fn**	50.4±7.9 (±16%)	2.1±0.4 (±18%)	19.8±3.1 (±24%)	22.3±5.3 (±16%)
	Ln	54.9±9.2 (±17%)	2.6±0.4 (±15%)	18.2±3.1 (±16%)	17.3±2.8 (±17%)

H.4 Discussion

In the present study, we produced a cell array and, even though many other examples exist in the literature, our work introduced the novelty of confining the cell array inside a bubble of culture media. Recent papers (Nelson et al. 2005, Peerani et al. 2007) demonstrated an effect on cell proliferation and differentiation due to the size and dimensions of the areas in which the cells are confined to grow; with our technique we were able to obtain cell colonies in different shapes and sizes with versatility and repeatability without noticeably affecting their behavior, as demonstrated by the results of the proliferation and marker expression analyses.

In addition, basing the design of our dynamic system on a previous work (Figallo et al. 2007), we achieved a perfusion system for the bubble-confined cell array using reliable and validated materials and techniques, allowing for precise control of culture conditions.

We then validated our system by performing mathematical modeling of the flow profiles, shear stress levels and mass transport on the entire bubble-volume and the surface of the whole cell array, demonstrating how the conditions were successfully uniform over the entire area covered by the cultured cells and not resulting in harmful shear stresses.

Our system was finally tested using a murine muscle cell line, C2C12, verifying its efficiency in maintaining proper culture conditions and allowing for a precise and effective spatial and temporal control over our arrayed cultures. During our experiments, these cells maintained the ability to express molecular markers of the differentiated status; this is a complex and important response due to the provision of differentiative factors. The possibility of performing a temporal and quantitative modulation of the perfusion allowed us to control this important process.

Working with a bubble allowed us to use small volumes of medium as low as 150µL, but with a working surface of 2cm^2. Soluble factors and metabolites are paramount in ensuring proper culture conditions; with our system we were able to couple the presence of endogenous factors in small volumes, as happens *in vivo*, with the advantages of working with relatively big surface areas. Small volumes, in addition, mean reducing the amounts of costly materials used while big surfaces allow easy access to the cultures facilitating both manual and automated interventions. An observation emerges when comparing our characteristic dimensions with those of traditional multiwell culture plates: similar volumes at play mean choosing 384 well plates, resulting in a 0.136 cm^2 working area, with evident consequences. On the contrary, 96 well plates ensure a similar working area but result in a two-fold increase in liquid volumes. Moreover, we verified that we can extract and purify integer total RNA from the cultured cell array evidencing that the presence of the hydrogel did not alter the stability of the nucleic acid and the possibility of performing enzymatic reactions to detect specific molecular responses.

Our system allowed for an individual evaluation of the effects due to the different ECM proteins tested, specifically fibronectin and laminin. The arraying comprised the creation of distinct and recognizable areas spotted with the two proteins and the subsequent analyses techniques allowed us to separately evaluate the specific responses. Arrayed cells cultured

under perfused conditions had a mean replication time of 19.4±2.2 h (Figure 5) while those kept in static culture duplicated every 12.6±0.4 h, consistent with standard culture in Petri dishes (data not shown). This could be due to 1) an over-estimation of the calculated N_0 value, considering that during perfusion cells that were poorly attached to the surface were washed out and 2) to a different behavior of the cells in a perfused condition with respect to a static condition. For example, one could imagine that cells exposed to a flow regime would need longer times to adapt to the new conditions. The main causes can be attributable to possible dilutions of endogenous factors and, even if extremely low, shear effects. The intrinsic advantages of a dynamic culture system, though, overcome such limitations. First of all, perfusion allows for constant delivery of nutrients and removal of wastes to the cultured cells; in addition such systems offer unique advantages in terms of the possibility of exerting interventions such as medium changes or drugs additions in a repeatable and controllable manner. Moreover, microscaled perfusion systems add the advantage of using small volumes of medium and reagents which results in a cost-effective, more controllable and versatile process.

Concerning the error calculations, it is worth underlining how the sources of errors can be multiple: defects on the staining procedures, on the experiment itself and on the evaluation of the results. While a BrdU staining captures an image representing a particular moment of the experiment, cell counting covers a much longer time-span, thus resulting in un-avoidable higher experimental errors. In addition, both adopted procedures for the calculation of the doubling times (τ) lead to the same values and allowed us to observe how the results deriving from perfused cultures were affected by smaller errors. Perfusion resulted in statistically significant differences in terms of both $BrdU^+$ cells ($BrdU^+/N_f$, $p<0.05$) and cell counts (N_f/N_0, $p<0.01$) with respect to the two proteins used that were not detectable after static culture. One possible explanation derives from the observation that perfusion increases the importance of cell adhesion to the substrate, thus more clearly electing the best adhesion protein for the cultured cells. The significance of this finding is greater with regards to the N_f/N_0 data; this can be explained by considering how these values derive from longer-time span observations, thus resulting in more dramatic effects if compared with the instant by instant outcomes of a BrdU analysis.

H.5 Conclusion

The advantages of having a bubble-confined cell array arise from the needs of dealing with small volumes of media and reagents, easy handling, rapid access to the cultures, and matching with standard culture procedures and protocols. In addition, we emphasized a perfect matching with all of the standard production technologies and techniques, such as from the use of a robotic spotter and standard microscopes. The specifically engineered substrate for culturing the cell array was perfectly compatible with immunostaining and RNA extraction permitting morphological and molecular analyses. This aspect is extremely important for understanding the response to external stimuli like drug subministration, which cannot easily be detectable by the microscope observation alone. Importantly, we were able to culture cells in a more “tissue-friendly” microenvironment mimicked through a constant perfusion of the culture medium. The mathematical modeling assisted the experimental phases, which demonstrated the maintenance of the correct operative values in the cell array region.

Our technology allowed us to gain increased information-density, resulting in a savings of time and reagents. In addition, the multiple datapoints coming from individual batches possess inherent consistency and higher quality. We thus provided a tool to match existing cell array technologies with the advantage of spatio-temporal controlling the soluble micro-environment for high-throughput biological studies or drug screening tests.

H.6 Acknowledgement

We gratefully acknowledge MIUR, University of Padova, Fondazione Cassa di Risparmio di Padova e Rovigo, Regione Veneto Azione biotech III.

H.7 References

T. Peterbauer, J. Heitz, M. Olbrich and S. Hering, Simple and versatile methods for the fabrication of arrays of live mammalian cells. *Lab on a Chip*, 2006, **6**, 857-863.
O. E. Beske and S. Goldbard, High-throughput cell analysis using multiplexed array technologies. *Drug Discovery Today*, 2002, **7**, 131-135.
C. S. Chen, M. Mrksich, S. Huang, G. M. Whitesides and D. E. Ingber, Micropatterned Surfaces for Control of Cell Shape, Position, and Function
Biotechnology Progress, 1998, **14**, 356-363.
C. M. Nelson, R. P. Jean, J. L. Tan, W. F. Liu, N. J. Sniadecki, A. A. Spector and C. S. Chen, Emergent patterns of growth controlled by multicellular form and mechanics. *PNAS*, 2005, **102**, 11594-11599.
K. Bhadriraju and C. S. Chen, Engineering cellular microenvironments to improve cell-based drug testing. *Drug Discovery Today*, 2002, **7**, 612-620.
K. R. King, S. Wang, D. Irimia, A. Jayaraman, M. Toner and M. L. Yarmush, A high-throughput microfluidic real-time gene expression living cell array. *Lab on a Chip*, 2007, **7**, 77-85.
J. Y. Lee, C. Jones, M. A. Zern and A. Revzin, Analysis of Local Tissue-Specific Gene Expression in Cellular Micropatterns. *analitical Chemistry*, 2006, **78**, 8305-8312.
K. Powell, Stem-cell niches: It's the ecology, stupid! *Nature*, 2005, 268-270.
M. R. Burnham, J. N. Turner, D. Szarowski and D. L. Martin, Biological functionalization and surface micropatterning of polyacrylamide hydrogels. *Biomaterials*, 2006, **27**, 5883-5891.
J. Burdick, M. Ward, E. Liang, M. Young and R. Langer, Stimulation of neurite outgrowth by neurotrophins delivered from degradable hydrogels. *Biomaterials* 2005, **27**, 452-9.
P. Angenendt, J. Glokler, J. Sobek, H. Lehrach and D. J. Cahill, Next generation of protein microarray support materials: Evaluation for protein and antibody microarray applications. *Journal of Chromatography A*, 2003, **1009**, 97–104.
D. E. Discher, P. Janmey and Y.-L. Wang, Tissue Cells Feel and Respond to the Stiffness of Their Substrate. *Science*, 2005, **310**, 1139-1143.
A. J. Engler, M. A. Griffin, S. Sen, C. G. Bönnemann, H. L. Sweeney and D. E. Discher, Myotubes differentiate optimally on substrates with tissue-like stiffness: pathological implications for soft or stiff microenvironments. *The Journal of Cell Biology*, 2004, **166**, 877-887.
P. C. Georges and P. A. Janmey, Cell type-specific response to growth on soft materials. *Journal of Applied Physiology*, 2005, **98**, 1547-1553.
D. Falconnet, G. Csucs, H. M. Grandin and M. Textor, Surface engineering approaches to micropattern surfaces for cell-based assays. *Biomat* 2006, **27**, 3044-3063.
S. A. Ruizab and C. S. Chen, Microcontact printing: A tool to pattern
Soft Matter, 2007, **3**, 1-11.
A. Revzin, P. Rajagopalan, A. W. Tilles, F. Berthiaume, M. L. Yarmush and M. Toner, Designing a Hepatocellular Microenvironment with Protein Microarraying and Poly(ethylene glycol) Photolithography. *Langmuir*, 2004, **20**, 2999-3005.
C. J. Flaim, S. Chien and S. N. Bhatia, An extracellular matrix microarray for probing cellular differentiation. *Nature Methods*, 2005, **2**, 119-125.
L. Kim, Y.-C. Toh, J. Voldman and H. Yu, A practical guide to microfluidic perfusion culture of adherent mammalian cells. *Lab on a Chip*, 2007, **7**, 681–694.
C. Romualdi, N. Vitulo, M. D. Favero and G. Lanfranchi, MIDAW: a web tool for statistical analysis of microarray data. *Nucleic Acids Res.*, 2005, W644–W649.

J. Quackenbush, Microarray data normalization and transformation. *Nat Genet*, 2002, **32**, 496-501.
A. Soukas, P. Cohen, N. D. Socci and J. M. Friedman, Leptin-specific patterns of gene expression in white adipose tissue. *Genes and Development*, 2000, **14**, 963-980.
A. I. Saeed, V. Sharov, J. White, J. Li, W. Liang, N. Bhagabati, J. Braisted, M. Klapa, T. Currier, M. Thiagarajan, A. Sturn, M. Snuffin, A. Rezantsev, D. Popov, A. Ryltsov, E. Kostukovich, I. Borisovsky, Z. Liu, A. Vinsavich, V. Trush and J. Quackenbush, A Free, Open-Source System for Microarray Data Management and Analysis. *BioTechniques*, 2003, **34**, 374-378.
M. Ashburner, C. A. Ball, J. A. Blake, D. Botstein, H. Butler, J. M. Cherry, A. P. Davis, K. Dolinski, S. S. Dwight, J. T. Eppig, M. A. Harris, D. P. Hill, L. Issel-Tarver, A. Kasarskis, S. Lewis, J. C. Matese, J. E. Richardson, M. Ringwald, G. M. Rubin and G. Sherlock, Gene Ontology: tool for the unification of biology. *Nature Genetics*, 2000, **25**, 25 – 29.
G. Dennis, B. T. Sherman, D. A. Hosack, J. Yang, W. Gao, H. C. Lane and R. A. Lempicki, DAVID: Database for Annotation, Visualization, and Integrated Discovery. *Genome Biology*, 2003, **4**, P3.
M. Pfaffl, A new mathematical model for relative quantification in real-time RT-PCR. *Nucleic Acids res*, 2001, **29**, e45.
E. Cimetta, M. Flaibani, M. Mella, E. Serena, L. Boldrin, P. D. Coppi and N. Elvassore, Enhancement of viability of muscle precursor cells on 3D scaffold in a perfusion bioreactor. *The International Journal of Artificial Organs*, 2007, **30**, 220-226.
K. Tomczak, V. Marinescu, M. Ramoni, D. Sanoudou, F. Montanaro, M. Han, L. Kunkel, I. Kohane and A. Beggs, Expression profiling and identification of novel genes involved in myogenic differentiation. *FASEB J.*, 2004, **18**, 403-5.
J. L. Moran, Y. Li, A. A. Hill, W. M. Mounts and C. P. Miller, Gene expression changes during mouse skeletal myoblast differentiation revealed by transcriptional profiling. *Physiological Genomics*, 2002, **10**, 103-111.
R. Peerani, B. M. Rao, C. Bauwens, T. Yin, G. Wood, A Nagy, E. Kumacheva and P. W. Zandstra, Niche-mediated control of human embryonic stem cell self-renewal and differentiation. *The EMBO Journal*, 2007, **26**, 4744–4755.
E. Figallo, C. Cannizzaro, S. Gerecht, J. A. Burdick, R. Langer, N. Elvassore and G. Vunjak-Novakovic, Micro-bioreactor array for controlling cellular microenvironments. *Lab on a Chip*, 2007, 710–719.

Appendix I

3rd Italian National Congress of the Group of Italian Researchers on Embryonic Stem Cells (IES Group)

"Financing for research on embryonic stem cells: The situation in Italy and its origins"

Rome, 1st July 2008

Report by Serena Elena, Cimetta Elisa and Zagallo Monica (University of Padua)

Published on:

"Notizie di Politeia. Rivista di Etica e Scelte Pubbliche Politeia"

91/Anno XXIV, 2008, pp. 110-113

"Opened up to this vast and most excellent science, of which my work is mere the beginning, ways and means by which other minds more acute than mine will explore in remotest corners".

These are the words of Italian astronomer and physicist Galileo Galilei, who was sentenced to indefinite prison in San Macuto Palace, on which site the Group of Italian Researchers on Embryonic Stem Cells (IES Group) organized its 3rd National Congress on "Research on Embryonic Stem Cells" (1 July 2008). These scientists strongly believe in the potential of human embryonic stem cells (hESCs), which are already the main focus of their research. A parallel thus emerges, as innovative and revolutionary scientific issues are discussed once again in this place.

In the magnificent structure of the Refectory Room of the Chamber of Deputies, IES scientists presented their research and discussed ethical aspects of its implications.

The main aim of the Congress was to highlight the need for an immediate and tangible opening to research on hESC in Italy. In fact, even while it is legally allowed to work on established hESC lines, it is prohibited to derive new lines from embryos; and even more limiting is the lack of funding from the Government. Consequently, a first and most crucial step is to improve the dialogue between science and both society and politics, in order to make known the potential, in terms of therapeutic outcomes, of hESC research.

Opening speakers of the congress were Elena Cattaneo, pioneer of hESC research in Italy, and Andrew Smith, project manager from ESTOOLS. Cattaneo's speech highlighted the main aims of the meeting, to identify the role of the IES group and to inform the audience on the research carried by its members. Since 2002, the interest of the international scientific community in hESCs has strongly increased, shown by the augmented financial investment and by the number of participants at specific conferences. In this scenario, IES scientists must create a solid network in order to facilitate financial and practical aspects of their research (training of personnel, development of protocols, reporting of results, etc) and to sensitize the public towards the relevant ethical aspects of their research. In underlining the tremendous potential of hESCs as tools for studying human physiology, disease and new therapies development, she stated that IES researchers do not exclusively work on embryonic but also believe in the potential of adult stem cells. Prof. Cattaneo focused the attention on the nr.1 scientific discovery of 2007 (according to The Times): induced pluripotent stem cells (iPS, Takahashi et al., Cell, 2007), now receiving much interest by

some Italian laboratories. This discovery, overcoming the ethical issues involving the use of embryos, would have never been possible without preceding research on hESCs.

Last but not least she expounded the chronic problem of fund-raising in Italy and Europe, and of the long and laborious *iter* leading to a project approval by the EU.

Taking a look outside academia, Andrew Smith described how the ESTOOLS consortium endorses lab research but at the same time tries to make it accessible to the public. Rescaled on an European level, with their 21 labs in 10 countries, the main targets of ESTOOLS resemble those listed by Cattaneo with regard to IES. In particular, ESTOOLS focuses on four different areas of activity: research and technology development (integration of funding and projects), dissemination of results (website, international public symposia), training (fellowships, lab staff exchanges, videos of lab techniques, and media training) and outreach (newsletters, trans-Europe telescope, ethic workshops). Most importantly, ESTOOLS promotes the development of integrated projects involving both academics and industrial partners: successful scientists should thus possess the skills of a good researcher and a good manager, be able to communicate with the public, be open minded and flexible.

After the welcome note of Carlo Flamigni, chairman of the session, Marisa Jaconi and Tiziano Barberi, top Italian scientists working on hESC outside Italy presented the results of their research on cardiac and skeletal muscle, respectively. Jaconi (University of Geneve, Switzerland), in particular, is working to develop animal free protocols and GMP-grade cell lines and to understand and control hES differentiation process for possible clinical applications. She also pointed put the pros and cons of iPS: no embryos are involved and no immune response is elicited but, on the contrary, a strong teratogenic effect would be possible due to their derivation through viral infection. Barberi (Beckman Research Institute of the City of Hope, Duarte, California) works on mesodermal progenitors isolation from pluripotent stem cells; he reported his latest achievements that follow his previous results on skeletal muscle (Barberi et al., Nature Medicine, 2007). The major efforts of his lab are directed on the development of more solid and reproducible protocols in order to take a step further towards clinical applications in general.

I.1 Research activities inside the IES

Research on hESC is applied in three different directions: studying embryonic development, controlling the differentiation in specific lineages, and clinical applications (e.g. drug screening and therapy development). All these research themes are equally important and tightly related, each of them needing the knowledge derived from the others to proceed; the IES group has competencies to cover them all.

I.1.1 IES new members

During the last year, four more research labs (Elvassore, Bianco, Gambari, Mantovani) joined the IES ranks and thus had the chance to present their projects to the audience and to the other members.

Nicola Elvassore, Chemical Engineer from Padova University, supported the idea of coupling engineering and biotechnology skills to develop technologies serving biology. His laboratory already established hESC culture, and is currently developing devices (e.g. substrates, micro and macro-scaled bioreactors, ..) for the control of the culture microenvironment and thus of the cellular differentiation process.

Bianco and Gambari's labs are studying two specific genetic diseases: McCune-Albright syndrome and β-Thalassemia respectively. In particular, Riminucci (Bianco's lab) explained that such syndrome is caused by a mutation occurring in embryonic cells and Gambari underlined the importance of studying the activation of fetal γ-globin in thalassemic patients. For these reasons, they now both aim at using hESC for developing therapeutic strategies as they represent the closest in vitro human model.

Mantovani, studying the transcription factors regulating stemness, recognizes how this research would greatly benefit from the use of hESC.

I.1.2 IES senior members

Cardiac differentiation is the leading theme for research by Condorelli and Cerbai. The first aims at reproducing the protocols for cardiomyocytes derivation from hESCs developed by Keller (Yang et al. Nature, 2008) and showed interest in adopting iPS cells cultures. The second is studying cardiac functionality and physiology in diseased heart *in vitro*, *in vivo* and *in silico*, using hESC as a cellular model.

The teams led by Brevini and Oliviero focus on deriving new cell lines not originating from human embryos and thus overcoming the possible ethical issues. Brevini's group works on human parthenogenetic stem cell, which possess all of the main features of hESC but their potential for clinical application has yet to be tested. Riding the clamor of iPS cells, Oliviero succeeded in inducing iPS and obtaining a 100-fold increased yield by adding myc transcription factor to the original Yamanaka recipe (Takahashi et al., Cell, 2007).

Another important application of hESC is gene therapy; the Sangiuolo group works on this application with regards to spinal muscular atrophy and cystic fibrosis.

Elena Cattaneo and her prominent team working on neural differentiation have derived a population of neural crest precursors from hESC and are currently testing its differentiation potential, in vitro and in vivo, with a view to possible clinical application.

Italian scientists here gathered, unequivocally demonstrated how their research hold an enormous social relevance and all expressed hope in the future possibilities deriving from their integration within the IES and in the common efforts in remodeling the Italian scenario.

I.2 Round table discussion: financing research on hESC

Why use embryos and why finance hESC-based research? These two major issues emerged during the meeting and the final discussion.

In the near future there may no longer be the need for to discuss the rightness of using embryos for progressing science and research, said Neri, followed by Corbellini who underlined that it would be desirable that prejudices should not hinder successful research.

In addition, besides the lack of funding for research in general and on hESCs in particular, it is clear that Italy needs deeply to reform its financing mechanisms. Even Senator Ignazio Marino, Deputy at the Italian Parliament and invited participant to the meeting, expressed his opinion firmly in these terms. It is unfortunately clear that government does not recognize science as crucial for the future of the country's economy. Mindful of his past experience as a scientist in the US, Senator Marino affirmed how Italy should not pose any

ideological barrier to scientific research and, most important, should adopt absolutely new project-evaluation criteria.

To date, only 10% of the research investments are allocated through peer review; the remaining 90% through unclear top-down methods. A reform of the entire system must thus be done, basing the entire distribution of funding on the mechanism of peer review in order to enhance meritocracy and transparency in the selection of projects.

Barberi, active participant in the discussion, finally stated that there's no need for further speculation on the validity of peer review as it must be the sole and only method for a meritocratic evaluation of research projects.

With a favourable legislative and financial environment supporting all areas of human embryonic stem cell research, the future promises to be very exciting for scientists interested in this field, and crucial for progress in clinical applications.

I.3 References

Takahashi K, Tanabe K, Ohnuki M, Narita M, Ichisaka T, Tomoda K, Yamanaka S. "Induction of pluripotent stem cells from adult human fibroblasts by defined factors". Cell. 2007 Nov 30;131(5):861-72.

Barberi T, Bradbury M, Dincer Z, Panagiotakos G, Socci ND, Studer L. "Derivation of engraftable skeletal myoblasts from human embryonic stem cells". Nat Med. 2007 May;13(5):642-8.

Yang L, Soonpaa MH, Adler ED, Roepke TK, Kattman SJ, Kennedy M, Henckaerts E, Bonham K, Abbott GW, Linden RM, Field LJ, Keller GM. "Human cardiovascular progenitor cells develop from a KDR+ embryonic-stem-cell-derived population". Nature. 2008 May 22;453(7194):524-8.